frontiers | Research Topics

Applied neuroimaging for the diagnosis and prognosis of cerebrovascular disease

Edited by
Mingming Lu, Jianming Cai and Jieqiong Wang

Published in
Frontiers in Neurology

ISSN 1664-8714
ISBN 978-2-8325-7077-7
DOI 10.3389/978-2-8325-7077-7

Generative AI statement
Any alternative text (Alt text) provided alongside figures in the articles in this ebook has been generated by Frontiers with the support of artificial intelligence and reasonable efforts have been made to ensure accuracy, including review by the authors wherever possible. If you identify any issues, please contact us.

About Frontiers

Frontiers is more than just an open access publisher of scholarly articles: it is a pioneering approach to the world of academia, radically improving the way scholarly research is managed. The grand vision of Frontiers is a world where all people have an equal opportunity to seek, share and generate knowledge. Frontiers provides immediate and permanent online open access to all its publications, but this alone is not enough to realize our grand goals.

Frontiers journal series

The Frontiers journal series is a multi-tier and interdisciplinary set of open-access, online journals, promising a paradigm shift from the current review, selection and dissemination processes in academic publishing. All Frontiers journals are driven by researchers for researchers; therefore, they constitute a service to the scholarly community. At the same time, the *Frontiers journal series* operates on a revolutionary invention, the tiered publishing system, initially addressing specific communities of scholars, and gradually climbing up to broader public understanding, thus serving the interests of the lay society, too.

Dedication to quality

Each Frontiers article is a landmark of the highest quality, thanks to genuinely collaborative interactions between authors and review editors, who include some of the world's best academicians. Research must be certified by peers before entering a stream of knowledge that may eventually reach the public - and shape society; therefore, Frontiers only applies the most rigorous and unbiased reviews. Frontiers revolutionizes research publishing by freely delivering the most outstanding research, evaluated with no bias from both the academic and social point of view. By applying the most advanced information technologies, Frontiers is catapulting scholarly publishing into a new generation.

What are Frontiers Research Topics?

Frontiers Research Topics are very popular trademarks of the *Frontiers journals series*: they are collections of at least ten articles, all centered on a particular subject. With their unique mix of varied contributions from Original Research to Review Articles, Frontiers Research Topics unify the most influential researchers, the latest key findings and historical advances in a hot research area.

Find out more on how to host your own Frontiers Research Topic or contribute to one as an author by contacting the Frontiers editorial office: frontiersin.org/about/contact

Applied neuroimaging for the diagnosis and prognosis of cerebrovascular disease

Topic editors

Mingming Lu — Characteristic Medical Center of Chinese People's Armed Police Force, China

Jianming Cai — People's Liberation Army General Hospital, China

Jieqiong Wang — Institute of Automation, Chinese Academy of Sciences, China

Citation

Lu, M., Cai, J., Wang, J., eds. (2025). *Applied neuroimaging for the diagnosis and prognosis of cerebrovascular disease*. Lausanne: Frontiers Media SA.

doi: 10.3389/978-2-8325-7077-7

Table of contents

frontiers | Frontiers in Neurology

TYPE Editorial
PUBLISHED 15 October 2025
DOI 10.3389/fneur.2025.1714644

OPEN ACCESS

EDITED AND REVIEWED BY
Jan Kassubek,
University of Ulm, Germany

*CORRESPONDENCE
Mingming Lu
andy_lu_ok@126.com

RECEIVED 28 September 2025
ACCEPTED 29 September 2025
PUBLISHED 15 October 2025

CITATION
Lu M, Wang J and Cai J (2025) Editorial: Applied neuroimaging for the diagnosis and prognosis of cerebrovascular disease. *Front. Neurol.* 16:1714644. doi: 10.3389/fneur.2025.1714644

Editorial: Applied neuroimaging for the diagnosis and prognosis of cerebrovascular disease

Mingming Lu[1]*, Jieqiong Wang[2] and Jianming Cai[3]

[1]Department of Radiology, Pingjin Hospital, Characteristic Medical Center of Chinese People's Armed Police Force, Tianjin, China, [2]Department of Neurological Sciences, University of Nebraska Medical Center, Omaha, NE, United States, [3]Department of Radiology, The Fifth Medical Center of Chinese People's Liberation Army of China (PLA) General Hospital, Beijing, China

KEYWORDS

neuroimaging, cerebrovascular diseases, diagnosis, prognosis, stroke

Editorial on the Research Topic
Applied neuroimaging for the diagnosis and prognosis of cerebrovascular disease

Neuroimaging plays a crucial role in the diagnosis and prognosis of cerebrovascular diseases. By using advanced imaging techniques, neuroimaging can reveal the anatomical structure and function of the brain, providing important evidence for diagnosing and treating these conditions. This Research Topic summarizes 14 recent original research studies that explore the application of advanced imaging techniques to evaluate and predict the outcomes of key neurological disorders, including intracranial arterial disease (ICAD)-related ischemic stroke, acute ischemic stroke (AIS) post-mechanical thrombectomy, transient ischemic attack (TIA), aneurysmal subarachnoid hemorrhage (aSAH), and heart failure. The studies highlight how imaging modalities such as computed tomography (CT), multimodal magnetic resonance imaging (MRI), high-resolution vessel wall imaging (HR-VWI), and arterial spin labeling (ASL) can provide critical insights into disease pathophysiology, temporal dynamics, and prognosis, offering valuable tools for clinical decision-making.

CT and CTA are foundational in vascular neurological assessments due to their speed and accessibility. CTA was used in the ANTIQUE study (Pakizer et al.) to classify carotid plaque calcification in extracranial carotid artery disease into spotty (<3 mm) and large (>3 mm) types. The authors found that spotty calcification correlated with male sex and heavy smoking ($p = 0.014$), while large calcification was associated with older age, coronary heart disease, and atrial fibrillation ($p = 0.025$). In acute stroke, CTA assesses stenosis severity and plaque morphology. Chen et al. showed that acute stroke patients have higher systolic blood pressure, thicker plaques, and more severe stenosis on CTA compared to non-acute patients. CTA—derived perivascular fat density (PFD) was found to be a strong predictor of acute ischemia, with symptomatic-side PFD outperforming contralateral PFD. Kim, Kim et al. retrospectively analyzed 114 aSAH patients to explore the clinical significance of mastoid effusion (ME)—defined as opacification/air-fluid levels in the mastoid air cells on CT/MRI within 14 days of aSAH. Multivariate analysis showed that ME was independently associated with tracheostomy, radiologic vasospasm, higher APACHE II scores, and poor outcomes (90-day mRS > 2, OR = 4.289, $p = 0.041$). Wei et al. investigated the prognostic value of the gray-to-white matter ratio (GWR) on cranial CT scans in 86 heat stroke patients (derivation cohort) and 42 patients (validation cohort),

respectively. All GWR parameters were lower in the poor outcome group. GWR basal ganglia showed the highest sensitivity (80.95%) at 90.77% specificity (cut-off = 1.21) in the derivation cohort, with an AUC of 0.852. Combining GWR basal ganglia with qSOFA (quick Sequential Organ Failure Assessment) significantly improved sensitivity and the AUC (0.958 vs. 0.852 for GWR alone, $p = 0.034$). This study establishes GWR as an objective, early predictor of poor neurological outcomes in heat stroke.

Conventional magnetic resonance imaging (MRI) sequences, such as T1— weighted, T2—weighted, FLAIR, and diffusion-weighted imaging (DWI), provide detailed insights into brain structure and function. In heart failure with preserved ejection fraction (HFpEF), Yu et al. used voxel-based morphometry (VBM) on 3D T1—weighted images and found reduced gray matter volume (GMV) in the bilateral cerebellar hemispheres, right posterior cingulate gyrus, and right inferior frontal gyrus in HFpEF patients. These GMV reductions correlated negatively with NT-proBNP levels and MoCA scores, linking cardiac dysfunction to cognitive impairment and structural brain changes. For AIS prognosis, Pei et al. integrated multimodal MRI with radiomics and deep learning. The authors extracted 1,197 radiomic features, selected 16 via LASSO regression, and developed a CRD (Clinic-Radiomics-Deep Learning) model. The CRD model achieved an AUC of 0.908 in the validation cohort, outperforming clinical (AUC = 0.874) and radiomics (AUC = 0.805) models alone. This highlights the role of MRI in capturing subtle pathological features for personalized prognosis. Almeida et al. explored the link between PCS symptoms (e.g., chronic fatigue, headaches) and T2-hyperintense white matter lesions using MRI in 96 Swiss patients. The majority of patients were women (73%, average age 46), with a high prevalence of chronic fatigue (90%), headaches (57%), and sleep disorders (51%). Brain MRIs showed lesions in 72% of patients, while spinal MRIs showed lesions in 16% of subjects. However, there was no significant correlation between lesions and fatigue ($p = 0.815$) or headaches ($p = 0.178$). This suggests that T2-hyperintense lesions may not be the cause of these PCS symptoms.

This Research Topic included two studies evaluating the application of high-resolution vessel wall imaging (HR-VWI) in treating cerebrovascular diseases. Kang et al. conducted a longitudinal HR-VWI study on 208 ICAD patients and found that arterial dissection led to faster stenosis reduction and an enhancing proportion decline compared to atherosclerosis. Atherosclerosis, however, showed a decreasing enhancement ratio. Thus, HR-VWI aids in monitoring disease progression and guiding treatment. Bao et al. reported a rare case of right type II persistent proatlantal intersegmental artery (PPIA) dissection that caused embolic showers (ES) in a 53-year-old man with hypoplasia of the left vertebral artery. DSA and HRMR-VWI identified aneurysmal dilation in the PPIA's false lumen, and a risk of thrombus dislodgement. Pipeline embolization device (PED)-assisted angioplasty resolved the issue, with no recurrent strokes post-operatively, highlighting the value of PEDs in managing rare vascular variants.

Functional neuroimaging techniques, such as arterial spin labeling (ASL), resting-state functional MRI (rs-fMRI), and electroencephalography (EEG), provide more information for evaluating the diagnosis and prognosis of cerebrovascular disease. Zeng et al. used dual post-label delays (PLD: 1,525 and 2,525 ms) in TIA patients with large artery stenosis/occlusion. FLAIR vascular hyperintensity (FVH)—positive patients had lower CBF on the affected side at both PLDs and a smaller CBF increase than FVH-negative patients. ΔCBF correlated negatively with ABCD2 scores, establishing FVH as a marker for hemodynamic impairment. In OLE, Kim, Ah et al. used diffusion tensor imaging (DTI)—derived peak width of skeletonized mean diffusivity (PSMD), an EEG-related marker. OLE patients had higher PSMD than controls, indicating small vessel disease-related white matter damage. PSMD also correlated with age, positioning it as a novel marker for OLE-associated microvascular changes. Huai et al. assessed the effect of enriched rehabilitation (ER) on post-stroke cognitive impairment (PSCI). Forty PSCI patients were randomly divided into a conventional medical rehabilitation (CMR) group and an ER group, along with 20 healthy controls. The functional connectivity (FC) analysis in the ER group revealed strengthened positive FC between the right dorsolateral prefrontal cortex (DLPFC) and the left superior frontal gyrus (SFG) and left anterior cingulate gyrus (ACG), and decreased FC between the right DLPFC and the right superior temporal gyrus (STG) and right precentral gyrus. ER intervention is more effective than conventional rehabilitation, possibly by reshaping brain functional connectivity. EEG is vital for assessing neural activity and epilepsy. Liao et al. conducted a bibliometric analysis showing a surge in EEG stroke research post-2017, with focus areas including seizure detection, consciousness assessment, and brain-computer interfaces (BCI). Additionally, a bibliometric analysis was conducted by Lou et al. to examine the focal areas of research in the early diagnosis of stroke through machine learning identification of magnetic resonance imaging characteristics from 2004 to 2023. The researchers found that the application of machine learning to the early prediction of stroke and to personalized medical plans for patients using neuroimaging characteristics offers significant value.

In conclusion, multimodal neuroimaging collectively enhances the diagnosis, prognosis, and treatment of neurological disorders. Future research should standardize protocols, validate findings in multicenter cohorts, and integrate multimodal data for more precise clinical care.

Author contributions

ML: Writing – original draft, Writing – review & editing. JW: Writing – review & editing. JC: Writing – review & editing.

Conflict of interest

The authors declare that the research was conducted in the absence of any commercial or financial relationships that could be construed as a potential conflict of interest.

Generative AI statement

The author(s) declare that no Gen AI was used in the creation of this manuscript.

Any alternative text (alt text) provided alongside figures in this article has been generated by Frontiers with the support of artificial intelligence and reasonable efforts have been made to ensure accuracy, including review by the authors wherever possible. If you identify any issues, please contact us.

Publisher's note

frontiers | Frontiers in Neurology

TYPE Original Research
PUBLISHED 07 January 2025
DOI 10.3389/fneur.2024.1503737

OPEN ACCESS

EDITED BY
Mingming Lu,
Characteristic Medical Center of Chinese People's Armed Police Force, China

REVIEWED BY
Luoyu Wang,
Hangzhou First People's Hospital, China
Shangjie Chen,
Shenzhen Baoan People's Hospital, China

*CORRESPONDENCE
Jibing Wang
✉ jibingwang123456@sina.com
Xin Wang
✉ wx000805qm@yeah.net

†These authors have contributed equally to this work and share first authorship

RECEIVED 10 October 2024
ACCEPTED 18 December 2024
PUBLISHED 07 January 2025

CITATION
Huai Y, Yang W, Lv Y, Wang K, Zhou H, Lu Y, Zhang X, Wang Y, Wang J and Wang X (2025) Enriched rehabilitation on brain functional connectivity in patients with post-stroke cognitive impairment. *Front. Neurol.* 15:1503737. doi: 10.3389/fneur.2024.1503737

Enriched rehabilitation on brain functional connectivity in patients with post-stroke cognitive impairment

Yaping Huai[1†], Weiwei Yang[1†], Yichen Lv[2], Kui Wang[2], Hongyu Zhou[2], Yiqing Lu[1], Xiaoyun Zhang[1], Yaze Wang[1], Jibing Wang[2*] and Xin Wang[2*]

[1]Department of Rehabilitation Medicine, Shenzhen Longhua District Central Hospital, Shenzhen, Guangdong, China, [2]Department of Rehabilitation Medicine, Northern Jiangsu People's Hospital, Yangzhou, China

Objective: This study aims to observe the effect of enrichment rehabilitation (ER) on cognitive function in post-stroke patients and to clarify its underlying mechanism.

Methods: Forty patients with post-stroke cognitive impairment (PSCI) meeting the inclusion criteria were randomly assigned to two groups: conventional medical rehabilitation (CM group) and ER intervention (ER group). All patients underwent assessments of overall cognitive function, attention function, and executive function within 24 h before the start of training and within 24 h after the 8 weeks of training. We investigated the altered resting-state functional connectivity (RSFC) with the right dorsolateral prefrontal cortex (DLPFC) in patients with PSCI following ER training through functional magnetic resonance imaging (fMRI). Additionally, twenty people undergoing routine physical examinations in the outpatient department of our hospital were selected as the healthy control (HC) group.

Results: Before training, both groups of PSCI patients exhibited significant impairment in overall cognitive function, attention function, and executive function compared to the HC group. However, there was no significant difference between the two PSCI patient groups. Following 8 weeks of treatment, both PSCI patient groups demonstrated substantial improvement in overall cognitive function, attention function, and executive function. Moreover, the ER group exhibited greater improvement after training compared to the CM group. Despite the improvements, the cognitive behavioral performance assessment scores of both PSCI patient groups remained lower than those of the HC group. RSFC analysis in the ER group revealed strengthened positive functional connectivity between the right DLPFC and the left superior frontal gyrus (SFG) and left anterior cingulate gyrus (ACG), along with decreased functional connectivity between the right DLPFC and the right superior temporal gyrus (STG) and right precentral gyrus post-ER intervention.

Conclusion: ER intervention is more effective than conventional medical rehabilitation in improving the cognitive function of PSCI patients, potentially by augmenting the FC between the right DLPFC and dominant cognitive brain regions, such as the left SFG and left ACG while attenuating the FC between the right DLPFC and non-dominant hemisphere areas including the STG and precentral gyrus within the right hemisphere.

KEYWORDS

enriched rehabilitation, post-stroke cognitive impairment, dorsolateral prefrontal cortex, functional connectivity, dominant hemisphere

1 Introduction

Post-stroke cognitive impairment (PSCI) is one of the most common sequelae of stroke (1). The cognitive challenges experienced by patients often manifest in various sub-domains such as attention, executive function, and memory, among others, contributing to difficulties in perceiving and adapting to the external environment (2, 3). These impairments not only hinder the patient's comprehension of the rehabilitation therapist's language but also impede the accurate execution of given instructions, significantly diminishing the efficacy of rehabilitation for limb dysfunction, swallowing issues, and other related impairments (3). Further, these cognitive deficits can lead to a decline in self-care and work capabilities, social function impairment, and mental health issues (4, 5). Studies have demonstrated a strong correlation between PSCI and an elevated risk of stroke recurrence, along with a heightened prevalence of post-stroke depression (6, 7). In addition, individuals with PSCI pose an added burden on their family members. Caregivers of PSCI patients are reported to be more susceptible to symptoms of depression or anxiety compared to those caring for stroke patients without cognitive decline. Within five years of the stroke incident, 20% of caregivers experience symptoms of anxiety, and 25% develop symptoms of depression, intensifying the burden on both the family and society at large (8, 9). Therefore, tackling the urgent requirement for effective rehabilitation training for PSCI remains a significant challenge in clinical practice.

Enrichment rehabilitation (ER) intervention represents a comprehensive rehabilitation approach that integrates environmental enrichment with task-oriented exercises (10). ER training could increase the level of sensory stimulation, cognitive activity, and organic motor function by placing subjects in more complex existential and social interaction scenarios, utilizing the novelty and complexity of the environment and multiple activities (11). This training strategy aims to enhance positive feedback and input to the central nervous system by creating a diverse and varied environment. It employs task-oriented training methods encompassing motor and sensory stimulation, cognitive activities, and social interactions. Studies have shown that ER interventions can enhance the secretion of nerve growth factor, brain-derived neurotrophic factor, nerve regeneration-related protein, etc., resulting in a long-term potentiation effect, enhancing the proliferation of neural stem cells, increasing the number of dendritic spines, realizing the reorganization of neuronal structure and function, and promoting the recovery of motor, sensory and cognitive functions (12–15). Some studies have proved that the theoretical basis of ER training is to foster the change of functional brain areas, enhance neuroplasticity, and ameliorate impaired functions (10, 16). Several recent studies have further demonstrated the rehabilitative potential of ER in improving both motor and cognitive dysfunction associated with various central nervous system conditions, including stroke, Parkinson's disease, and others (17–19).

The resting-state network (RSN) is acknowledged as a structured system promoting the transmission of brain information, facilitating efficient information processing within and between relevant functional regions of the brain (20, 21). The statistical dependence between brain functional resting-state networks can be quantified using functional connectivity (FC), which also allows for the assessment of the organizational pattern and alterations in specific connections within these networks in the context of disease (21). Network-based statistical analysis revealed that post-stroke cognitive impairment was linked to whole-brain network dysfunction, involving 167 regions and 178 connections (22). This dysfunction resulted in a functional disconnection of brain regions associated with cognitive function, such as the frontal lobe and temporal lobe (22).

However, there is limited literature on the impact of ER intervention on brain FC in patients with PSCI. This study aims to examine the influence of ER on cognitive function and brain FC in PSCI patients and to provide clinical experimental evidence supporting the application of ER in cognitive rehabilitation.

2 Materials and methods

2.1 Ethical approval

The study protocol was approved by the Ethics Committee of Northern Jiangsu People's Hospital Affiliated to Yangzhou University (approval no. 2018021). All participants provided written informed consent before study enrollment.

2.2 Participants recruitment

Forty patients diagnosed with PSCI and treated at the Northern Jiangsu People's Hospital Affiliated to Yangzhou University from January 2020 to December 2021 were randomly allocated into two groups: a conventional medical treatment (CM) group ($n = 20$) and an ER group ($n = 20$). Utilizing the digital random method, 20 healthy subjects undergoing routine physical examinations in the outpatient department of the same hospital during the corresponding period were chosen to constitute the healthy control (HC) group. The general information of the three groups is presented in Table 1. The selection of sixty subjects adhered to specific inclusion and exclusion criteria:

Inclusion criteria for PSCI patients: All patients with cerebral infarction met the diagnostic criteria of cognitive impairment following cerebral infarction as outlined in the diagnostic criteria for cerebrovascular disease (23) and were assessed for enrollment in the study based on the following inclusion criteria (24): patients with right-handedness who experienced their first-ever ischemic cerebrovascular stroke (lesion in the left internal carotid artery system confirmed by MRI); initiation of rehabilitation treatment 1 to 2 months after the onset of stroke, with a Chinese version of the Montreal Cognitive Assessment (MoCA) score ranging from 20 to 23 within 24 h before treatment; ability of the patient to at least complete the basic activities and communication of ER with assistance; aged between 46 and 55 years with a minimum of 12 years of education.

TABLE 1 Demographics and main baseline characteristics of subjects categorized by study group.

Group	Number of cases	Age (years)	Gender	
			Male (*n*)	Female (*n*)
HC	20	51.67 ± 3.14	12	8
CM	20	50.98 ± 3.28	12	8
ER	20	51.02 ± 3.35	12	8

HC, Healthy Control; CM, Conventional; ER, Enriched Rehabilitation; N, Number.

Exclusion criteria for PSCI patients: Patients with a history of multiple strokes or other psychiatric and neurological conditions, including but not limited to brain trauma, Parkinson's disease, mental disorders, hearing impairment, visual impairment, and severe cognitive impairment, were excluded. Additionally, individuals with a history of alcohol and substance abuse, poor adherence, and those unable to move autonomously, along with other medical conditions that could impede the effective implementation of ER intervention, were also excluded.

Inclusion criteria for healthy subjects: Twenty healthy subjects fulfilled the following inclusion criteria: participants must be conscious and have no history of mental illness or diseases of the nervous system; aged between 46 and 55 years with a minimum of 12 years of education. MoCA score within 24 h of the physical examination ranging from 28 to 30 points.

Exclusion criteria for healthy subjects: All healthy participants were required to be free from any neurological disorders as determined by a thorough physical examination. Additionally, they were expected to have no serious heart and kidney diseases, malignant tumors, or other conditions affecting cognitive and emotional functioning.

2.3 Basic demographic information

As shown in Table 1, no statistically significant differences were observed among the three groups concerning age and gender ($P>0.05$). Each group consisted of 12 males and 8 females. The age distribution was as follows: the average age of the HC group was 51.67 ± 3.14 years, the CM group was 50.98 ± 3.28 years, and the ER group was 51.02 ± 3.35 years.

2.4 Study schedule

The treatment protocol for all PSCI patients involved the administration of conventional medications, including antihypertensive agents, lipid-lowering drugs, and cognitive enhancers. In addition to these medications, the patients in CM group received one hour of routine rehabilitation training in the morning and afternoon each day, whereas the ER group received one hour of enriched rehabilitation training in the morning and afternoon each day. Both groups received rehabilitation training 6 days a week for 8 weeks.

The content of conventional cognitive rehabilitation training primarily encompasses attention, memory, logical thinking, calculation ability, executive function, and other cognitive sub-domains (24). The training comprised individualized single or multi-module integration tailored to patients following a cognitive assessment by the therapist. For instance, attention training involved promptly identifying two similar images or texts with differences. In auxiliary exercises, patients were guided to organize their daily activity plan execution or the sequence of specific tasks. Additionally, logical thinking training included tasks such as sequencing pictures in the correct story order and more.

In the ER group, therapists were required to create a diverse and dynamic environment, utilizing multi-sensory stimulation, cognitive activities, social engagements, and task-oriented training for comprehensive rehabilitation. The approach included the following components:

Enriched Environmental Stimulation: Utilizing multimedia equipment such as computers with internet connection and virtual reality technology, as well as other relevant equipment to design a variety of visual, auditory, olfactory, tactile and other multi-sensory stimulation projects. This allowed patients to experience various sensory stimuli triggered by differences in colors, smells, hardness, and more. For instance: ①Olfactory stimulation: Participants engaged in a 5-min odor identification task, involving the sniffing of two bottles of perfume with distinct scents, aiming to accurately name them. ②Auditory stimulation: Virtual reality equipment generated a variety of sounds, including animal calls and traffic horns. Participants were instructed to participate in blind listening, closing their eyes to accurately identify the source or describe the characteristics of each sound.

Cognitive Function Training: With the assistance of therapists, patients engaged in cognitive-related activities indoors using personal devices. Activities included reading books, listening to or humming music, browsing web pages of interest, playing regular card games, et al.

Task-oriented Exercise Training: ①Specific occupational therapy tasks were employed to strengthen the patient's cognitive training for daily living. For example, patients were tasked with using the affected hand to select a specified color of water glass from three different colored glasses or filling a specific pattern with a designated color brush. ②To make physiotherapy more engaging and enhance functional motor training of the lower extremity, competitive elements were introduced among multiple patients during hip bridge exercises. Additionally, incorporating specific power bicycle training intensities based on different music rhythms can also be beneficial.

Social Activities: ①Patients and their family members went to the supermarket together. Once inside, patients independently selected and purchased the prescribed brand and quantity of goods, and settled the bill. ②Ensuring their safety, patients designed a route, with family members guiding them to take a bus to a designated city location, and then returning the same way. ③Participation in multiplayer games such as cards, board games, or table tennis, as well as engaging in group discussions with other patients or family members. ④Involvement in any other activities that patients enjoy doing with friends or family, such as watching movies or dancing, et al. In these activities, patients had the flexibility to choose and alternate between 2–3 items each week.

All patients underwent cognitive function tests within 24 h before the start of formal treatment and within 24 h after the completion of

all treatment sessions. In addition, patients in the ER group underwent rs-fMRI examination both before and after the training period. The HC group completed the cognitive function test within 24 h after the physical examination.

2.5 MRI data preprocessing and analysis

Structural MRI and rs-fMRI were performed in the ER group before and after the intervention using a GE3.0 T MRI scanner. During scanning, all subjects were instructed to remain awake, keep their eyes closed, maintain a fixed head position, and rest without focusing on any specific thoughts. High-resolution structural images were acquired by employing a magnetization-prepared rapid gradient echo (MP-RAGE) sequence (25, 26): TR/TE/TI 1900/3.39/1100 ms, 7° flip angle, 240 mm × 240 mm mm field of view (FOV), 256 × 256 matrix, 176 axial slices, 0.9375 mm thickness, with an acquisition time lasting 4 min. The rs-fMRI scans were obtained using a gradient echo-echo-plane imaging sequence: 31 axial slices, 4 mm thickness, TR/TE 2000/30 ms, 90° flip angle, 240 mm (2) FOV, 64 × 64 matrix, with an acquisition time lasting 8 min.

Statistical Parametric Mapping[1] and the RESTPLUS software[2] were employed for preprocessing the resting-state functional MRI (rs-fMRI) data. Initially, we discarded the first 15 images for each subject to guarantee data stability. Subsequently, we corrected slice timing for the remaining images. Following this, we corrected for motion by aligning each volume to the average of all volumes. After assessing head motion parameters, we ensured that head displacement did not surpass 3 mm and the rotation angle did not exceed 3° for any patient. Then, we utilized Advanced Normalization Tools software for spatial normalization. Initially, we registered each subject's T1 structural images to their mean functional image and mapped corresponding lesions onto it. Next, we registered the T1 structural image to the Montreal Neurological Institute and Hospital (MNI) standard space. Afterward, we applied the nonlinear transformation parameters acquired from the previous step to each motion-corrected volume, yielding each subject's functional image in MNI standard space, and then resampled the spatially normalized functional image to a voxel size of 3 mm × 3 mm × 3 mm. Ultimately, we applied Gaussian smoothing with a full width at half maximum of 6 mm to all voxels. Additional denoising steps were carried out, including detrending and regressing out noise covariates such as motion-related parameters (i.e., Friston-24 model), white matter signals, cerebrospinal fluid signals, and other confounding variables. The data was filtered within a frequency range of 0.01 to 0.08 Hz.

3 Outcome measurement

3.1 Cognitive function measurement

The MoCA was used to assess the overall cognitive function, which involves the evaluation of attention, memory, execution, calculation, and other cognitive functions (24). The maximum score of the test was 30 points, with a score of ≥26 points considered normal in the general population.

The Trail Making Test (TMT) was used to evaluate executive function (27). In this study, the time required to complete TMT-A and TMT-B served as the evaluation indices. Attention function was estimated through the Symbol Digit Modalities Test (SDMT) (28), where the final score was determined by the number of correct modalities filled in within 90 s, excluding those filled in during practice.

4 Statistical analysis

The SPSS 22.0 statistical software package was used for data sorting and analysis. Quantitative data with a normal distribution were represented as mean ± standard deviation ($\overline{x} + s$), while measurement data with a skewed distribution were represented using the median and interquartile range. Qualitative data (gender composition ratio) were compared between groups using a corrected chi-square test. Differences in age and cognitive function levels among the three groups were compared using one-way ANOVA. Paired *t*-test was used to compare the cognitive function of PSCI patients before and after treatment. *p* values less than 0.05 were considered to denote significant statistical differences (significance level: $\alpha = 0.05$).

Statistical Parametric Mapping (SPM8) was utilized to process the rs-fMRI data. Participants with greater than 3.0 mm of translation or 3.0 degree of rotation in any direction were excluded. Following the normalization of anatomical images using Montreal Neurological Institute (MNI) templates, FC analysis was conducted using the Resting-State fMRI Data Analysis Toolkit (REST) (29).

The right DLPFC (coordinates: x = 45, y = 36, z = 21, with the mean signal of each voxel within the 6 mm radius sphere computed) was selected as the seed point and the region of interest (ROI). A voxel-wise FC analysis of each voxel was then performed for the fMRI data. The FC of each subject between each seed region and ROI was calculated and converted into Z-maps. Inter-group analysis involved individual single-sample *t*-tests for each group, followed by merging the results of each group into a mask. Subsequently, a two-sample *t*-test was performed between the two groups within the mask. The selected areas were considered statistically significant after correction ($p < 0.05$, voxel >228) (30). All test methods were two-tailed.

5 Results

5.1 Comparison of cognitive function before and after intervention

Before treatment, the cognitive function scores of both PSCI patient groups were significantly lower compared to those of the HC group ($p < 0.05$). However, there was no significant difference between the CM group and the ER group. After 8 weeks of intervention, this difference persisted in the HC group and both PSCI groups ($p < 0.05$). Although both CM and ER groups exhibited significant improvement in cognitive function post-treatment ($p < 0.05$), the improvement in the ER group was more pronounced than that in the CM group ($p < 0.05$). Specific data are presented in Table 2.

1 Version 12; accessible at http://www.fil.ion.ucl.ac.uk/spm on May 1, 2023.

2 Version 6.1; available at http://restfmri.net/forum/restplus on January 1, 2022.

TABLE 2 Comparison of cognitive function between three groups.

		HC group	CM group	ER group
MoCA	Pre-intervention	29.25 ± 0.75[cd]	21.75 ± 1.29[a]	21.80 ± 1.28[a]
	Post-intervention	-	23.85 ± 1.78[ab]	26.20 ± 1.64[abd]
SDMT	Pre-intervention	76.60 ± 5.75[cd]	46.90 ± 8.07[a]	46.95 ± 8.81[a]
	Post-intervention	-	57.05 ± 8.71[ab]	64.15 ± 10.11[abd]
TMT-A(s)	Pre-intervention	48.11 ± 9.04[cd]	73.25 ± 17.11[a]	73.53 ± 16.78[a]
	Post-intervention	-	72.39 ± 17.64[a]	71.76 ± 16.15[a]
TMT-B(s)	Pre-intervention	91.55 ± 20.67[cd]	149.69 ± 33.81[a]	146.85 ± 36.51[a]
	Post-intervention	-	129.71 ± 27.24[ab]	110.85 ± 17.79[abd]

[a]Compared with the HC group, $p < 0.05$.
[b]Compared with pre-intervention of the same group, $p < 0.05$.
[c]Compared with the CM group pre-intervention, $p < 0.05$. [d]Compared with the CM group post-intervention, $p < 0.05$.

5.2 Comparison of brain function connectivity (FC) in the ER group before and after intervention

As illustrated in Figure 1A and detailed in Table 3, the FC map of the ER group before intervention revealed that the significant functional connectivity with the right DLPFC mainly encompassed the bilateral middle frontal gyrus (MFG), right middle temporal gyrus (MTG), right precentral gyrus, left inferior frontal gyrus (IFG), left parietal inferior angular gyrus, and left inferior temporal gyrus (ITG) ($p < 0.05$, voxel>228).

After the intervention, the ER group exhibited significant FC in the left anterior cingulate gyrus (ACG), right inferior temporal gyrus (ITG), bilateral middle frontal gyrus (MFG), bilateral parietal inferior angular gyrus, and the right DLPFC in the ER group ($p < 0.05$, voxel>228). These findings are illustrated in Figure 1B and detailed in Table 4.

Figure 1C and Table 5 demonstrate that the FC map of the ER group between the right DLPFC and deep brain regions, including the left superior frontal gyrus (SFG) and the left anterior cingulated gyrus (ACG) post-treatment, was stronger post ER compared with pre-ER ($p < 0.05$, voxel>228). Conversely, compared with pre-ER, the FC of post ER between the right DLPFC and the right superior temporal gyrus (STG) and the right precentral gyrus was significantly weaker ($p < 0.05$, voxel>228).

6 Discussion

The present findings indicate that the implementation of ER intervention yields a notable improvement in cognitive functioning among post-stroke patients, particularly in overall cognitive function and attention executive function. This improvement is attributed to the ER intervention's capability to enhance the FC of cognitive-related brain areas, such as the frontal cortex and anterior cingulate cortex, with the dominant hemisphere. Simultaneously, it weakens the FC with the non-dominant hemisphere, restoring the balance between bilateral hemispheres in PSCI patients. Ultimately, this fosters the establishment of a brain remodeling mechanism for cognitive function.

The behavioral findings demonstrated a significant advancement in cognitive function among post-stroke patients undergoing ER intervention, surpassing the results of conventional cognitive rehabilitation training. This improvement was particularly pronounced in attention and executive function. Concurrently, the imaging results of this study revealed alterations in brain functional network connectivity post-treatment for patients in the ER group compared to their pre-treatment conditions. Specifically, an increase in FC was observed between the right DLPFC and the left SFG as well as the left ACG, which are closely associated with attention and executive function. The rationale behind the cognitive function improvement can be attributed to the potential of ER intervention in restructuring the brain's functional network in stroke patient (31, 32).

ER intervention, as a comprehensive training method based on an enriched environment, plays an important role in enhancing both brain plasticity and behavior (33). The research group employed a combination of multi-sensory stimulation, cognitive function training, task-oriented training, and social training to augment the rehabilitation program for ER patients. As a result, there was a significant improvement in the overall cognitive function of the patients. This improvement can be attributed to several factors. The diverse array of multi-sensory stimuli, including visual, auditory, olfactory, and tactile inputs, significantly enhances individuals' ability to perceive and engage with their physical and social surroundings. Moreover, it also promotes neuroplasticity in the brain (33, 34). For instance, visual stimulation can facilitate the establishment of novel neural circuits for information processing and analysis, expedite the reorganization of neural function, and contribute to circuit reconstruction, thereby enhancing individuals' adaptability to complex and dynamic environments. Furthermore, some studies have also demonstrated that visual stimulation can elicit hippocampal neurogenesis, further augmenting cognitive function (35). Cognitive function training strategically assigns appropriate cognitive tasks to patients systematically and comprehensively. Diverging from conventional cognitive rehabilitation training, ER intervention tailors cognitive rehabilitation tasks to be patient-oriented, integrating multiple cognitive functions simultaneously instead of conducting targeted independent training in isolated domains. This approach is more conducive to the comprehensive improvement of patients' diverse cognitive functions. Concurrently, task-oriented training integrates motor and cognitive functions, activating the motor control and attention executive function networks simultaneously, thereby benefiting the enhancement of patients' attention function, planning, and logic (36). In contrast, social training activities such as recitation, shopping, and competitive events (e.g., playing chess) contribute to the improvement of memory and other cognitive functions (37).

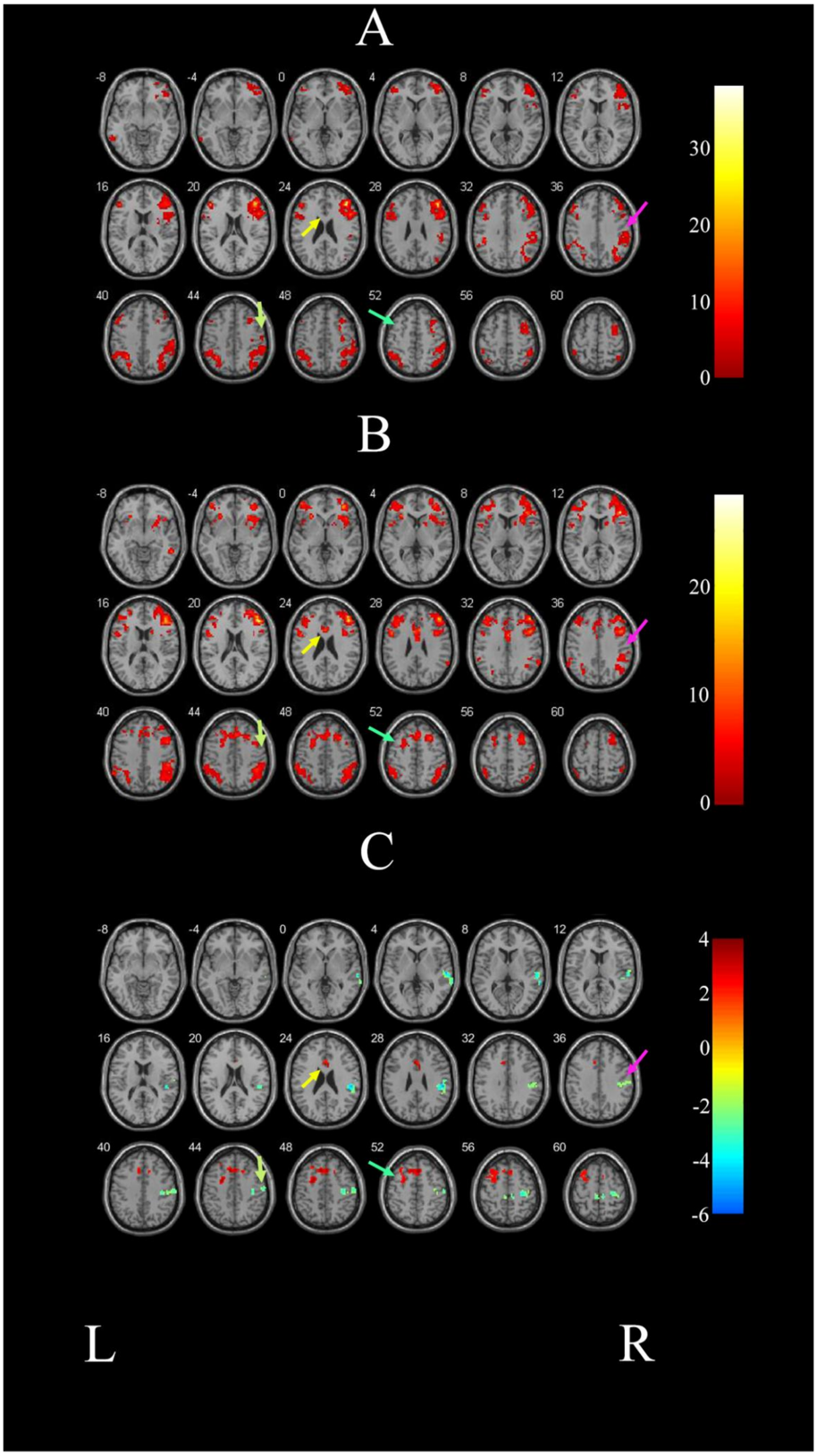

FIGURE 1
Comparison of brain FC before and after intervention in the ER group. **(A)** Illustrated the change of brain regions with FC with the right DLPFC in PSCI patients before ER intervention. **(B)** Depicts the change of brain areas exhibiting FC with the right DLPFC in the ER group after training. **(C)** Demonstrates the difference in FC before and after treatment in the ER group. The right STG is indicated by the pink arrow; the right precentral gyrus is indicated by the grassy green arrow; the left SFG is indicated by the blue-green arrow; and the left ACG is indicated by the yellow arrow. L and R represent the left and right hemispheres, respectively.

TABLE 3 FC of patients in the ER group before intervention.

Region	BA	MNI coordinates			T	VOX
		x	y	z		
Right MFG	45	45	36	21	37.61	1,025
Right MTG	20	57	−39	−12	5.00	384
Right precentral gyrus	6	33	−24	66	7.12	281
Left MFG	44	−51	24	36	12.24	510
Left IFG	45	−45	33	18	22.31	320
Left parietal inferior angular gyrus	40	−30	−54	39	15.91	958
Left ITG	37	−66	−54	−3	7.73	331

MFG, Middle Frontal Gyrus; MTG, Middle Temporal Gyrus; IFG, Inferior Frontal Gyrus; ITG, Inferior Temporal Gyrus; BA, Brodmann Area; T, T value; VOX, Voxel.

TABLE 4 FC of patients in the ER group after intervention.

Region	BA	MNI coordinates			T	VOX
		x	y	z		
Right ITG	20	57	−45	−18	11.99	258
Left MFG	46	−36	36	30	19.53	1,050
Right MFG	45	45	33	12	28.33	1,541
Right parietal inferior angular gyrus	48	66	−48	30	14.03	999
Left parietal inferior angular gyrus	40	−57	−54	39	6.88	698
Left ACG	24	−3	12	27	14.00	173[a]

ITG, Inferior Temporal Gyrus; MFG, Middle Frontal Gyrus; ACG, Anterior Cingulate Gyrus; BA, Brodmann Area; T, T value; VOX, Voxel.
[a]The left ACG was connected to the left MFG.

TABLE 5 Brain regions with differences in FC before and after treatment in the ER group.

Region	BA	MNI coordinates			T	VOX
		x	y	z		
Right STG	22	69	−39	6	−6.05	538
Right precentral gyrus	6	42	3	42	−2.34	131[a]
Left SFG	8	6	21	54	4.01	318
Left ACG	24	−3	18	27	3.09	93[b]

STG, Superior Temporal Gyrus; SFG, Superior Frontal Gyrus; ACG, Anterior Cingulate Gyrus; BA, Brodmann Area; T, T value; VOX, Voxel.
[a]The right precentral gyrus was connected to the right STG.
[b]The left SFG was connected to the left ACG.

Studies have demonstrated that the change of cognitive function is inevitably accompanied by the remodeling of brain function (18). To explore alterations in brain regions associated with cognitive function, this study employed a relatively safe and reliable method rs-fMRI, widely acknowledged for investigating the mechanisms of brain function remodeling in stroke patients (38). In this study, the right DLPFC was chosen as the seed voxel for whole-brain FC. The selection of the DLPFC as the seed region is grounded in its significance for cognitive function, encompassing attention, working memory, executive function, and various other cognitive functions (39). Furthermore, the right DLPFC was specifically designated as the seed voxel due to the subjects' left hemisphere stroke, which resulted in the compromised functional network of the left hemisphere. In some instances, both the structure and function of the DLPFC may have been impaired as a consequence.

The present study identified a robust connection between the right DLPFC and the frontal cortex in patients with PSCI, both before and after ER intervention. The frontal cortex, known for high-level cognitive control and sensorimotor integration, is closely related to attention and executive function. Therefore, even before ER intervention, the DLPFC exhibited FC with the frontal cortex, including the bilateral MFG and the right precentral gyrus of the non-dominant hemisphere (40–42). Radiographic results of this study revealed a significant improvement in FC between the DLPFC and the frontal cortex of the dominant hemisphere following ER intervention. We posit that this enhancement can be attributed to the ER intervention involving concentration,

simulation, planning of relevant motor behaviors, among other factors, fully activating the functional activity of cognitive brain areas (24, 32).

The ACG is recognized as part of the limbic system, closely associated with attention and executive function (43, 44). Groups with a well-developed ACG are more adept at maintaining focus, filtering out external distractions, and transitioning quickly and orderly between different tasks (45, 46). Research indicates that the ACG can implement directional behavior monitoring for ongoing tasks, promptly signaling responses in the event of a conflict or error to adjust and allocate attention resources accordingly (47). Consistent with previous studies, there was no significant FC observed between the right DLPFC and ACG before ER intervention. However, following the intervention, there was a notable enhancement in the FC between the two regions. Furthermore, the patients' test scores for attention and executive function demonstrated improvement, reinforcing the notion that ER training has the potential to optimize the FC of the attention and executive function network post-stroke.

Additionally, this study revealed that following ER intervention, there was an enhancement in the connectivity of DLPFC brain areas associated with cognitive function in the dominant hemisphere (left frontal cortex and left ACG). Simultaneously, a significant decrease was observed in the FC of cognitive-related brain areas (STG and precentral gyrus) in the non-dominant hemisphere, indicating a shift toward cognitive processing favoring the dominant hemisphere. In this study, we found that for patients with moderate PSCI, the core cognitive region DLPFC needed to enhance its FC with non-cognitive brain regions (such as the temporal cortex and precentral gyrus in the non-dominant hemisphere) to sustain cognitive activity before training. The temporal cortex is mainly related to long-term memory, while the precentral gyrus is primarily related to motor function (48, 49). The disruption of interhemispheric connectivity occurs simultaneously with stroke in the dominant hemisphere, resulting in an increased reliance on the non-dominant hemisphere for executive attention and FC (50, 51). Nevertheless, the behavioral test results suggest that the impact of this change in FC is suboptimal, indicating poor remodeling of the brain's functional network in PSCI patients. The transformed FC is insufficient to suppress interference caused by the functional network connectivity unrelated to cognition, nor can it effectively activate the brain's functional network involved in cognitive tasks. Following ER intervention, the cognitive function-related brain areas in the dominant hemisphere can be restored, facilitating the reestablishment of interhemispheric connection and gradual normalization of connectivity within the attention and executive brain function network. However, it was observed that the FC between DLPFC, the core region of the executive attention network, and non-dominant cognitive brain regions (such as the temporal lobe and precentral gyrus of the non-dominant hemisphere) gradually weakens. Consequently, there is a gradual shift of responsibility for cognitive functions, particularly attention and executive functioning, back to the dominant hemisphere along with notable improvements in cognitive function test scores.

The present study also has certain limitations. First of all, the absence of imaging examination for subjects in both the HC group and CM group resulted in a lack of statistical analysis and comparison concerning brain FC before and after training across these three groups of subjects. To address this limitation, the research team plans to enhance imaging examinations for subjects in each group in the subsequent experiments, aiming to investigate the similarities and differences in brain FC between PSCI patients and normal individuals before and after ER intervention. And in the follow-up study, we will continue to explore the differences between ER training and traditional training for altering functional brain connectivity, so as to provide a better basis in clinical work. Additionally, In previous studies, it has been demonstrated that hemodynamic lag interferes with FC measurements (52, 53). The disadvantage of this study is that no imaging correction was performed, thus the effect of hemodynamic lag and intrinsic cerebrovascular reactivity on functional connectivity after stroke could not be ignored, and there was some discrepancy in temporal sensitivity, which will be compensated for by combining functional near-infrared spectroscopy (fNIRS) in the follow-up study to correlate real-time functional connectivity with behavioral assessment. Furthermore, the limited conditions such as stroke location, degree of cognitive impairment, and timing of rehabilitation intervention resulted in a small sample size for each of the three experimental groups. As a result, the comprehensive exploration of the effect of ER intervention on PSCI patients was hindered. Future research endeavors should aim to expand the sample size to enhance the robustness of the study. Finally, this study did not conduct a follow-up to observe the long-term effect. In future research, the follow-up duration for patients will be extended to comprehensively assess sustained efficacy and dynamic changes in fMRI, thereby providing a more robust theoretical foundation for understanding brain remodeling mechanisms following stroke.

7 Conclusion

ER intervention is more effective than conventional medical rehabilitation in improving the cognitive function of PSCI patients. ER intervention has the capacity to enhance the FC between the right DLPFC and dominant cognitive brain regions, such as the left SFG and left ACG, while diminishing the FC between the DLPFC and areas of the non-dominant hemisphere, such as the STG and precentral gyrus within the right hemisphere. This reshaping of the cognitive function network contributes to a discernible improvement in cognitive function among PSCI patients.

Data availability statement

The original contributions presented in the study are included in the article/supplementary material, further inquiries can be directed to the corresponding authors.

Ethics statement

The studies involving humans were approved by the Ethics Committee of Northern Jiangsu People's Hospital Affiliated to Yangzhou University (approval no. 2018021). The studies were conducted in accordance with the local legislation and institutional requirements. The participants provided their written informed consent to participate in this study.

Author contributions

YH: Writing – review & editing, Resources. WY: Visualization, Writing – original draft, Writing – review & editing. YLv: Software,

Writing – original draft. KW: Investigation, Writing – original draft. HZ: Methodology, Writing – original draft. YLu: Supervision, Writing – original draft. XZ: Data curation, Writing – original draft. YW: Formal analysis, Writing – original draft. JW: Validation, Writing – review & editing. XW: Supervision, Writing – review & editing.

Funding

The author(s) declare that financial support was received for the research, authorship, and/or publication of this article. The research was supported by Shenzhen Science and Technology Program (JCYJ20210324123414039), the Scientific Research Projects of Medical and Health Institutions of Longhua District, Shenzhen (2022027 and 2022031), the Natural Science Foundation of China (NSFC, nos.82072533), Six One Project of scientific research project for high-level health talents of Jiangsu province (LGY2018027) and Yangzhou Science and Technology Development Plan Project (YZ2022203).

Conflict of interest

The authors declare that the research was conducted in the absence of any commercial or financial relationships that could be construed as a potential conflict of interest.

Generative AI statement

The authors declare that no Gen AI was used in the creation of this manuscript.

Publisher's note

References

1. Huang YY, Chen SD, Leng XY, Kuo K, Wang ZT, Cui M, et al. Post-stroke cognitive impairment: epidemiology, risk factors, and management. *J Alzheimers Dis*. (2022) 86:983–99. doi: 10.3233/JAD-215644

2. Sun R, Li X, Zhu Z, Li T, Li W, Huang P, et al. Effects of combined cognitive and exercise interventions on Poststroke cognitive function: a systematic review and Meta-analysis. *Biomed Res Int*. (2021) 2021:4558279. doi: 10.1155/2021/4558279

3. Zhang YX, Wei QY, Wang YT, Zeng LP, Sun SY, Wu YF, et al. A postpartum enriched environment rescues impaired cognition and oxidative markers in aged mice with gestational inflammation. *Brain Behav*. (2022) 12:e2817. doi: 10.1002/brb3.2817

4. Jeffares I, Rohde D, Doyle F, Horgan F, Hickey A. The impact of stroke, cognitive function and post-stroke cognitive impairment (PSCI) on healthcare utilisation in Ireland: a cross-sectional nationally representative study. *BMC Health Serv Res*. (2022) 22:414. doi: 10.1186/s12913-022-07837-2

5. Karssemeijer EGA, Aaronson JA, Bossers WJ, Smits T, Olde Rikkert MGM, Kessels RPC. Positive effects of combined cognitive and physical exercise training on cognitive function in older adults with mild cognitive impairment or dementia: a meta-analysis. *Ageing Res Rev*. (2017) 40:75–83. doi: 10.1016/j.arr.2017.09.003

6. Kwon HS, Lee D, Lee MH, Yu S, Lim JS, Yu KH, et al. Post-stroke cognitive impairment as an independent predictor of ischemic stroke recurrence: PICASSO sub-study. *J Neurol*. (2020) 267:688–93. doi: 10.1007/s00415-019-09630-4

7. Terroni L, Sobreiro MFM, Conforto AB, Adda CC, Guajardo VD, de Lucia MCS, et al. Association among depression, cognitive impairment and executive dysfunction after stroke. *Dement Neuropsychol*. (2012) 6:152–7. doi: 10.1590/S1980-57642012DN06030007

8. Rohde D, Gaynor E, Large M, Mellon L, Hall P, Brewer L, et al. The impact of cognitive impairment on Poststroke outcomes: a 5-year follow-up. *J Geriatr Psychiatry Neurol*. (2019) 32:275–81. doi: 10.1177/0891988719853044

9. Rohde D, Gaynor E, Large M, Conway O, Bennett K, Williams DJ, et al. Stroke survivor cognitive decline and psychological wellbeing of family caregivers five years post-stroke: a cross-sectional analysis. *Top Stroke Rehabil*. (2019) 26:180–6. doi: 10.1080/10749357.2019.1590972

10. Kempermann G. Environmental enrichment, new neurons and the neurobiology of individuality. *Nat Rev Neurosci*. (2019) 20:235–45. doi: 10.1038/s41583-019-0120-x

11. Hannan AJ. Environmental enrichment and brain repair: harnessing the therapeutic effects of cognitive stimulation and physical activity to enhance experience-dependent plasticity. *Neuropathol Appl Neurobiol*. (2014) 40:13–25. doi: 10.1111/nan.12102

12. Stamenkovic V, Stamenkovic S, Jaworski T, Gawlak M, Jovanovic M, Jakovcevski I, et al. The extracellular matrix glycoprotein tenascin-C and matrix metalloproteinases modify cerebellar structural plasticity by exposure to an enriched environment. *Brain Struct Funct*. (2017) 222:393–415. doi: 10.1007/s00429-016-1224-y

13. Lisman J, Yasuda R, Raghavachari S. Mechanisms of CaMKII action in long-term potentiation. *Nat Rev Neurosci*. (2012) 13:169–82. doi: 10.1038/nrn3192

14. Hirata K, Kuge Y, Yokota C, Harada A, Kokame K, Inoue H, et al. Gene and protein analysis of brain derived neurotrophic factor expression in relation to neurological recovery induced by an enriched environment in a rat stroke model. *Neurosci Lett*. (2011) 495:210–5. doi: 10.1016/j.neulet.2011.03.068

15. Bayat M, Sharifi MD, Haghani M, Shabani M. Enriched environment improves synaptic plasticity and cognitive deficiency in chronic cerebral hypoperfused rats. *Brain Res Bull*. (2015) 119:34–40. doi: 10.1016/j.brainresbull.2015.10.001

16. Sihvonen AJ, Soinila S, Särkämö T. Post-stroke enriched auditory environment induces structural connectome plasticity: secondary analysis from a randomized controlled trial. *Brain Imaging Behav*. (2022) 16:1813–22. doi: 10.1007/s11682-022-00661-6

17. Gabriel P, Mastracchio TA, Bordner K, Jeffrey R. Impact of enriched environment during adolescence on adult social behavior, hippocampal synaptic density and dopamine D2 receptor expression in rats. *Physiol Behav*. (2020) 226:113133. doi: 10.1016/j.physbeh.2020.113133

18. Janssen H, Ada L, Bernhardt J, McElduff P, Pollack M, Nilsson M, et al. An enriched environment increases activity in stroke patients undergoing rehabilitation in a mixed rehabilitation unit: a pilot non-randomized controlled trial. *Disabil Rehabil*. (2014) 36:255–62. doi: 10.3109/09638288.2013.788218

19. Khan F, Amatya B, Elmalik A, Lowe M, Ng L, Reid I, et al. An enriched environmental programme during inpatient neuro-rehabilitation: a randomized controlled trial. *J Rehabil Med*. (2016) 48:417–25. doi: 10.2340/16501977-2081

20. Lopes R, Bournonville C, Kuchcinski G, Dondaine T, Mendyk AM, Viard R, et al. Prediction of long-term cognitive function after minor stroke using functional connectivity. *Neurology*. (2021) 96:e1167–79. doi: 10.1212/WNL.0000000000011452

21. Kong Y, Peng W, Li J, Zhu C, Zhang C, Fan Y. Alteration in brain functional connectivity in patients with post-stroke cognitive impairment during memory task: a fNIRS study. *J Stroke Cerebrovasc Dis*. (2023) 32:107280. doi: 10.1016/j.jstrokecerebrovasdis.2023.107280

22. Burton L, Tyson SF. Screening for cognitive impairment after stroke: a systematic review of psychometric properties and clinical utility. *J Rehabil Med*. (2015) 47:193–203. doi: 10.2340/16501977-1930

23. Kleindorfer DO, Towfighi A, Chaturvedi S, Cockroft KM, Gutierrez J, Lombardi-Hill D, et al. 2021 guideline for the prevention of stroke in patients with stroke and transient ischemic attack: a guideline from the American Heart Association/American Stroke Association. *Stroke*. (2021) 52:e364–467. doi: 10.1161/STR.0000000000000375

24. Wang X, Peng Y, Zhou H, Du W, Wang J, Wang J, et al. The effects of enriched rehabilitation on cognitive function and serum glutamate levels post-stroke. *Front Neurol*. (2022) 13:829090. doi: 10.3389/fneur.2022.1065942

25. Yin M, Liu Y, Zhang L, Zheng H, Peng L, Ai Y, et al. Effects of rTMS treatment on cognitive impairment and resting-state brain activity in stroke patients: a randomized clinical trial. *Front Neural Circuits*. (2020) 14:563777. doi: 10.3389/fncir.2020.563777

26. Zhang J, Buchsbaum MS, Chu KW, Hazlett EA. A manual, semi-automated and automated ROI study of fMRI hemodynamic response. *Stud Health Technol Inform*. (2013) 192:921. doi: 10.4172/2167-7964.1000150

27. Farias ST, Weakley A, Harvey D, Chandler J, Huss O, Mungas D. The measurement of everyday cognition (ECog): revisions and updates. *Alzheimer Dis Assoc Disord*. (2021) 35:258–64. doi: 10.1097/WAD.0000000000000450

28. Costa SL, Schwizer Ashkenazi S, Strober LB, Chiaravalloti ND, Vakil E. The adapted symbol digit modalities test: examining the impact of response modality. *NeuroRehabilitation*. (2021) 49:215–20. doi: 10.3233/NRE-218021

29. Lee K, Khoo HM, Fourcade C, Gotman J, Grova C. Automatic classification and removal of structured physiological noise for resting state functional connectivity MRI analysis. *Magn Reson Imaging*. (2019) 58:97–107. doi: 10.1016/j.mri.2019.01.019

30. Forman SD, Cohen JD, Fitzgerald M, Eddy WF, Mintun MA, Noll DC. Improved assessment of significant activation in functional magnetic resonance imaging (fMRI): use of a cluster-size threshold. *Magn Reson Med*. (1995) 33:636–47. doi: 10.1002/mrm.1910330508

31. Miguel PM, Pereira LO, Silveira PP, Meaney MJ. Early environmental influences on the development of children's brain structure and function. *Dev Med Child Neurol*. (2019) 61:1127–33. doi: 10.1111/dmcn.14182

32. Manno FAM, An Z, Kumar R, Su J, Liu J, Wu EX, et al. Environmental enrichment leads to behavioral circadian shifts enhancing brain-wide functional connectivity between sensory cortices and eliciting increased hippocampal spiking. *NeuroImage*. (2022) 252:119016. doi: 10.1016/j.neuroimage.2022.119016

33. Delanogare E, de Souza RM, Rosa GK, Guanabara FG, Rafacho A, Moreira E. Enriched environment ameliorates dexamethasone effects on emotional reactivity and metabolic parameters in mice. *Stress*. (2020) 23:466–73. doi: 10.1080/10253890.2020.1735344

34. Ohline SM, Abraham WC. Environmental enrichment effects on synaptic and cellular physiology of hippocampal neurons. *Neuropharmacology*. (2019) 145:3–12. doi: 10.1016/j.neuropharm.2018.04.007

35. Lee M, Pyun SB, Chung J, Kim J, Eun SD, Yoon B. A further step to develop patient-friendly implementation strategies for virtual reality-based rehabilitation in patients with acute stroke. *Phys Ther*. (2016) 96:1554–64. doi: 10.2522/ptj.20150271

36. Almhdawi KA, Mathiowetz VG, White M, delMas RC. Efficacy of occupational therapy task-oriented approach in upper extremity post-stroke rehabilitation. *Occup Ther Int*. (2016) 23:444–56. doi: 10.1002/oti.1447

37. Frih B, Mkacher W, Bouzguenda A, Jaafar H, ALkandari S, Ben Z, et al. Effects of listening to holy Qur'an recitation and physical training on dialysis efficacy, functional capacity, and psychosocial outcomes in elderly patients undergoing haemodialysis. Libyan. *J Med*. (2017) 12:1372032. doi: 10.1080/19932820.2017.1372032

38. Wang C, Van Dyk K, Cho N, Raymond C, Choi J, Salamon N, et al. Characterization of cognitive function in survivors of diffuse gliomas using resting-state functional MRI (rs-fMRI). *Brain Imaging Behav*. (2022) 16:239–51. doi: 10.1007/s11682-021-00497-6

39. Jones DT, Graff-Radford J. Executive dysfunction and the prefrontal cortex. *Continuum (Minneap Minn)*. (2021) 27:1586–601. doi: 10.1212/CON.0000000000001009

40. Henri-Bhargava A, Stuss DT, Freedman M. Clinical assessment of prefrontal lobe functions. *Continuum (Minneap Minn)*. (2018) 24:704–26. doi: 10.1212/CON.0000000000000609

41. Catani M. The anatomy of the human frontal lobe. *Handb Clin Neurol*. (2019) 163:95–122. doi: 10.1016/B978-0-12-804281-6.00006-9

42. Boespflug EL, Eliassen JC, Dudley JA, Shidler MD, Kalt W, Summer SS, et al. Enhanced neural activation with blueberry supplementation in mild cognitive impairment. *Nutr Neurosci*. (2018) 21:297–305. doi: 10.1080/1028415X.2017.1287833

43. Rolls ET. The cingulate cortex and limbic systems for emotion, action, and memory. *Brain Struct Funct*. (2019) 224:3001–18. doi: 10.1007/s00429-019-01945-2

44. Hopfinger JB, Slotnick SD. Attentional control and executive function. *Cogn Neurosci*. (2020) 11:1–4. doi: 10.1080/17588928.2019.1682985

45. Schneider KN, Sciarillo XA, Nudelman JL, Cheer JF, Roesch MR. Anterior cingulate cortex signals attention in a social paradigm that manipulates reward and shock. *Curr Biol*. (2020) 30:3724–3735.e2. doi: 10.1016/j.cub.2020.07.039

46. Lockwood PL, Wittmann MK. Ventral anterior cingulate cortex and social decision-making. *Neurosci Biobehav Rev*. (2018) 92:187–91. doi: 10.1016/j.neubiorev.2018.05.030

47. Carlson JM, Fang L, Koster EHW, Andrzejewski JA, Gilbertson H, Elwell KA, et al. Neuroplastic changes in anterior cingulate cortex gray matter volume and functional connectivity following attention bias modification in high trait anxious individuals. *Biol Psychol*. (2022) 172:108353. doi: 10.1016/j.biopsycho.2022.108353

48. Jeneson A, Squire LR. Working memory, long-term memory, and medial temporal lobe function. *Learn Mem*. (2012) 19:15–25. doi: 10.1101/lm.024018.111

49. Koch PJ, Park CH, Girard G, Beanato E, Egger P, Evangelista GG, et al. The structural connectome and motor recovery after stroke: predicting natural recovery. *Brain*. (2021) 144:2107–19. doi: 10.1093/brain/awab082

50. Ten Brink AF, Biesbroek JM, Kuijf HJ, Van der Stigchel S, Oort Q, Visser-Meily JM, et al. The right hemisphere is dominant in organization of visual search-a study in stroke patients. *Behav Brain Res*. (2016) 304:71–9. doi: 10.1016/j.bbr.2016.02.004

51. Jang SH, Cho IT, Lim JW. Recovery of aphasia and change of injured arcuate fasciculus in the dominant hemisphere in stroke patients. *NeuroRehabilitation*. (2017) 41:759–64. doi: 10.3233/NRE-172167

52. Siegel JS, Snyder AZ, Ramsey L, Shulman GL, Corbetta M. The effects of hemodynamic lag on functional connectivity and behavior after stroke. *J Cereb Blood Flow Metab*. (2016) 36:2162–76. doi: 10.1177/0271678X15614846

53. Wang L, Wu X, Song J, Fu Y, Ma Z, Wu X, et al. Unraveling the influences of hemodynamic lag and intrinsic cerebrovascular reactivity on functional metrics in ischemic stroke. *NeuroImage*. (2024) 303:120920. doi: 10.1016/j.neuroimage.2024.120920

frontiers | Frontiers in Neurology

TYPE Original Research
PUBLISHED 22 January 2025
DOI 10.3389/fneur.2024.1526130

OPEN ACCESS

EDITED BY
Jieqiong Wang,
Chinese Academy of Sciences, China

REVIEWED BY
Xiang Li,
Washington University in St. Louis, United States
Mohamed Azzam,
University of Nebraska Medical Center, United States

*CORRESPONDENCE
Gonçalo G. Almeida
✉ goncalo.gg.almeida@gmail.com

†These authors share last authorship

RECEIVED 11 November 2024
ACCEPTED 27 December 2024
PUBLISHED 22 January 2025

CITATION
Almeida GG, Alkan S, Hoepner R, Euler A, Diem L and Wagner F (2025) Chronic fatigue and headache in post-COVID-19 syndrome: a radiological and clinical evaluation. *Front. Neurol.* 15:1526130. doi: 10.3389/fneur.2024.1526130

Chronic fatigue and headache in post-COVID-19 syndrome: a radiological and clinical evaluation

Gonçalo G. Almeida[1,2]*, Saide Alkan[3,4], Robert Hoepner[5], André Euler[1,2], Lara Diem[6†] and Franca Wagner[4†]

[1]Department of Radiology, Kantonsspital Baden, Baden, Switzerland, [2]Affiliated Hospital for Research and Teaching of the Faculty of Medicine of the University of Zurich, Zurich, Switzerland, [3]Switzerland Center for Neuroradiology, Klinik Hirslanden, Zurich, Switzerland, [4]University Institute of Diagnostic and Interventional Neuroradiology, Inselspital, Bern University Hospital, University of Bern, Bern, Switzerland, [5]Department of Neurology, Inselspital, Bern University Hospital, University of Bern, Bern, Switzerland, [6]Department of Neurology, Cantonal Hospital Lucerne, Lucerne, Switzerland

Introduction: The coronavirus disease 2019 (COVID-19) pandemic has caused millions of infections and deaths globally. Post-COVID-19 syndrome, or long COVID is characterized by lingering symptoms such as chronic fatigue, headaches, and sleep disturbances. This study aimed to investigate the correlation between these symptoms and T2-hyperintense white matter lesions detected on magnetic resonance imaging (MRI) of the brain and spine in patients with post-COVID-19 syndrome.

Methods: This retrospective, single-center study analyzed a sample of 96 patients from Bern University Hospital in Switzerland who presented with suspected post-COVID-19 syndrome between 2020 and 2022. Patients completed self-report questionnaires evaluating fatigue, emotional wellbeing, and daytime sleepiness. Brain and spine MRIs were independently rated by 2 neuroradiologists for T2-hyperintense lesions. The correlation between these lesions and symptoms of fatigue and headache was assessed.

Results: The cohort consisted predominantly of women (73%) with an average age of 46 years. Chronic fatigue (90%), sleep disorders (51%), and headache (57%) were the most prevalent symptoms. The fatigue questionnaires indicated high levels of fatigue. Brain MRI revealed T2-hyperintense lesions in 72% of patients, whereas spine MRI showed these lesions in only 16%. There was no statistically significant correlation between the presence of cerebral T2-hyperintense lesions and symptoms of fatigue ($p = 0.815$) or headaches ($p = 0.178$). Similarly, no significant correlation was found when considering numbers of pathological brain lesions (fatigue: $p = 0.557$; headaches: $p = 0.820$).

Conclusion: While T2-hyperintense lesions are common in patients with post-COVID-19 syndrome, their presence does not correlate significantly with symptoms of fatigue or headaches. These findings suggest that T2-hyperintense brain lesions may not be directly related to the subjective experience of these symptoms. Further research with larger sample sizes and adjustment for potential confounding factors is necessary to better understand the relationship between MRI findings and post-COVID-19 syndrome symptoms.

KEYWORDS

post-COVID-19 syndrome, MRI, white matter lesions, brain, spine, fatigue, headache, sleep disturbance

1 Introduction

The coronavirus disease 2019 (SARS-CoV-2) is a viral strain first reported in China in 2019, which rapidly evolved into a global pandemic responsible for more than 700 million infections and more than 7 million deaths reported worldwide as of April 2024 (1, 2). Infection-associated symptoms are multisystemic, possibly affecting the respiratory, cardiovascular, gastrointestinal, musculoskeletal, and neurologic systems. Most infected patients exhibit mild symptoms not requiring hospitalization (3). Although symptoms fully resolve in most cases, in over 10% of cases patients will experience lingering complications of infection, such as chronic fatigue and headaches, months after the initial infection (4–6). The finding of post-COVID-19 syndrome has been defined as "persistent, new, or recurrent symptoms and conditions more than 4 weeks after initial COVID-19 diagnosis" (7, 8).

Neurologic effects of COVID-19 on the central nervous system (CNS) have been reported since the start of the pandemic (9) and may be related to various mechanisms such as underlying systemic disease, immune dysfunction, vasculopathy, and complications of prolonged illness or hospitalization (6, 10, 11). The most common sequelae include chronic fatigue, headaches, sleep disorders, and depression (12, 13). A number of questionnaires have been validated for the clinical evaluation of these conditions, including the Fatigue Severity Scale (FSS), the Fatigue Scale for Motor and Cognitive Functions (FSMC) (14, 15), the Epworth Sleepiness Scale (ESS) (16, 17) and the Beck Depression Inventory (BDI-II) (18, 19). Some of these have also been applied to patients diagnosed with post-COVID-19 syndrome (20).

Overall, post-COVID-19 syndrome is associated with more than 60 heterogeneous physical and psychological symptoms affecting multiple organ systems (21). This heterogeneity has led to controversial and confusing findings in medical imaging research. In a large longitudinal brain imaging study, significant effects of SARS-CoV-2 infection, including a reduction in gray matter thickness and global brain size were reported (22). In contrast, Yiping et al. reported higher bilateral gray matter volume with no significant change in white matter volume in COVID-positive patients (23). Imaging findings tend to be nonspecific and are often seen as T2-hyperintense white matter lesions or supratentorial susceptibility abnormalities suggestive of microvascular pathology (24, 25). T2-hyperintense lesions are associated with small vessel disease, inflammatory processes and post-infectious sequelae, which may play a role in the pathophysiology of post-COVID-19 syndrome (26, 27). Despite conflicting reports in the literature, such as differences in lesion prevalence and significance in symptomatic patients (28), these lesions remain a widely studied marker of neurological abnormalities in post-viral syndromes.

The McDonald diagnostic criteria are commonly used in clinical practice as a way to standardize and provide diagnostic accuracy in the identification of multiple sclerosis (MS) (29). The revised McDonald criteria (2024) are expected to place more emphasis on early diagnosis. This will be achieved through advanced imaging techniques such as susceptibility-weighted imaging (SWI) and diffusion-weighted imaging (DWI), as well as certain imaging and laboratory biomarkers, such as the central vein sign (CVS) and paramagnetic rim lesions, among others (30, 31). The CVS represents the imaging manifestation of the perivenular nature of demyelinating plaques and has been defined as a hypointensity appearing at the center of a surrounding hyperintense lesion in at least 2 of 3 orthogonal planes. Although not pathognomonic for MS, the CVS can help differentiate between MS and other demyelinating diseases of the CNS (32, 33).

The exact relationship between these imaging findings and different post-COVID-19 syndrome symptoms remains unclear. The aim of this study was therefore to compare the number of T2-hyperintense white matter lesions in the brain and within the spinal cord among patients with post-COVID-19 syndrome exhibiting either chronic fatigue and/or headaches after initial infection.

2 Materials and methods

2.1 Ethics

We retrospectively evaluated clinical and paraclinical data on patients with post-COVID-19 syndrome included in the neuroimmunological registry (registration no. KEK-BE 2017–01369), treated at the neuroimmunological outpatient department of the Inselspital, University Hospital Bern, a tertiary care hospital. We analyzed the medical records of all patients with post-COVID-19 syndrome who had given informed consent. Only patients with MRIs performed in our neuroradiology department were included to ensure comparability of the images and availability of the necessary MRI sequences.

2.2 Materials

This retrospective, single-center study analyzed a sample of 96 patients from Bern University Hospital in Switzerland, who presented following COVID-19 infection between November 2020 and May 2022. All patients were confirmed to have had acute COVID-19 infection and persistent symptoms consistent with post-COVID-19 syndrome and presented at the neurology department for post-COVID-19 consultation.

2.3 Methods

Patients were selected based on their presentation to the Post-COVID-19 clinic with neurological symptoms such as fatigue and headache. Inclusion criteria required MRI imaging of the brain and/or spine and completion of validated symptom questionnaires. Imaging was performed on a 3T MRI scanner using standardized protocols, including for all patients an axial diffusion-weighted imaging sequences (DWI) with a slice thickness (ST) of 4 mm, an axial T2-weighted image sequence (ST 4 mm), a native T1-weighted MPR (ST 1 mm) and an axial susceptibility weighted imaging (SWI) sequence (ST 1.2 mm). After contrast application a 3D FLAIR sequence (ST 1 mm), an axial T1-weighted TSE (ST 4 mm) and a 3D T1-weighted MPR were acquired. If the patient presented with visual disturbances a native coronal T2-weighted fad suppressed sequence covering the orbits was added and after contrast application additional coronal T1- and T2-weighted sequences with fad suppression over the orbits were acquired. The standard spine protocol included the following sequences, covering the whole spine: coronal STIR, native

sagittal T1- and T2-weighted imaging sequences and post contrast sagittal T1- and PD-weighted imaging sequences. In case of a pathological finding dedicated axial T2-weighted sequences and post contrast axial T1-weighted images were added. Table 1 shows the imaging protocols.

During the first consultation, a clinical history was taken detailing the reported symptoms during the acute phase of COVID-19 infection, as well as the current symptoms. Patients completed questionnaires on fatigue (Fatigue Severity Scale [FSS]), the impact of fatigue on motor and cognitive function (Fatigue Scale for Motor and Cognitive Functions [FSMC]), emotional wellbeing (Beck Depression Inventory II [BDI-II]), and daytime sleepiness (Epworth Sleepiness Scale [ESS]). Laboratory parameters such as C-reactive protein and ferritin were also analyzed to exclude possible secondary causes for fatigue.

Brain and spine MRIs performed in the setting of post-COVID-19 syndrome were independently rated by one board-certified radiologists with 5 years' experience and by one board certified neuroradiologist with over 15 years' experience, for the presence, number, and location of T2-hyperintense lesions in the brain and the spinal cord. The incidence of lesions with CVS and paramagnetic rim was also assessed. Both readers were blinded to clinical history and patients symptoms including questionnaire results to reduce observer bias. Discrepancies in lesion counts between the two raters were resolved through a consensus reading.

2.4 Statistical analysis

Data are presented as mean with 95% confidence interval (95% CI) and comparative statistics (Mann–Whitney U test (MWU) and chi-squared test, respectively) were used. A p-value of 0.05 was assumed to be statistically significant.

2.5 Data sharing statement

In compliance with an open data approach, anonymized data of the cohort are available on request from the corresponding author.

TABLE 1 Brain and spine MRI protocols.

Spine MRI		Brain MRI	
Native sequence	sag T2 sag T1 cor STIR	Native sequence	ax DWI ax T2 + PD sag 3D T1 MPRAGE ax SWI cor T2 fs Orbita
Contrast medium (mmol/kg)	0.1	Contrast medium (mmol/kg)	0.1
Contrast medium sequences	sag PD ax T2 sag T1 ax T1	Contrast medium sequences	sag 3D T1 MPRAGE ax T1 TSE sag 3D FLAIR cor T2 fs Orbita cor T1 KM fs Orbita

MRI, magnetic resonance imaging; sag, sagittal; ax, axial; cor, coronal; fs, fat suppression.

3 Results

3.1 Cohort

The average age of the study population was 46.0 years (95% confidence interval (CI): 42.8–49.1) and 73% were female (70/96). The patients had their first consultation a mean of 35.8 days after the onset of acute infection (95% CI: 31.4–40.2). Ninety-one tested positive with the PCR/antigen test (95%) and only 2 tested positive for antibodies (2%). For 3 patients no information about the testing method was available. The sample was further categorized according to the associated comorbidities. Asthma was the most prevalent (8 out of 96 patients; 8%), followed by 7 reports of depression (7%). The data are summarized in Table 2.

3.2 COVID-19 infection symptoms—acute phase

Most of the patients reported fever (n = 57, 59%), followed by headache (n = 55, 57%), anosmia (n = 55, 57%), fatigue (n = 54, 56%), and cough (n = 52, 54%). Intubation was the rarest consequence of COVID-19 infection observed in this sample, reported in only one case (1%). All reported symptoms are listed in Table 3.

3.3 Post-COVID-19 symptoms—first consultation

The first follow-up consultation post-COVID-19 infection aimed at the assessment of lingering symptoms, analysis of various laboratory parameters, and completion of self-report questionnaires. Fatigue was to the most reported symptom during the acute phase of COVID-19 infection and still affected the majority of patients (n = 86, 90%) at the first post-COVID appointment. Fifty-five patients reported recurrent headaches (57%) and 49 sleep disorders (51%).

Of the 82 patients assessed for depressive symptoms following COVID-19 infection, 23 (28%) reported depression. When asked about daytime sleepiness, 29 patients (36%) reported feeling sleepy during the day. A full list of the prevailing symptoms post-COVID-19 infection is provided in Table 4.

3.4 Self-report questionnaire scores

The FSS was completed by 81 patients of the original patient sample of 96 to assess self-reported fatigue severity in daily activities. The mean score was 5.2 for a cut-off defined at 4.0 (95% CI: 66.2–74.9). The impact of these fatigue levels on daily performance was measured using the FSMC, with 79 patients averaging 70.5 (43.0 cut-off; 95% CI: 66.2–74.9).

Eighty patients completed the ESS, scoring a mean average of 9.2 (10.0 cut-off; 95% CI: 66.2–74.9). The BDI-II was filled in by 82 patients who scored an average of 16.6 (14.0 cut-off; 95% CI: 14.7–18.5). The results are given in Table 5.

TABLE 2 Patient characteristics at first consultation.

Age, years, mean (95% CI), *n*	46.0 (42.8–49.1), 96
Female, *n* (%)	70/96 (73%)
Time between onset of acute infection and first consultation, weeks, mean (95% CI), *n*	35.8 (31.4–40.2), 96
Positive PCR/antigen test, *n* (%)	91/96 (95%)
Positive antibody test, *n* (%)	2/96 (2%)
Comorbidities	
Arterial hypertonia, *n* (%)	4/96 (4%)
Metabolic syndrome, *n* (%)	2/96 (2%)
Sleep apnea syndrome, *n* (%)	1/96 (1%)
Depression, *n* (%)	7/96 (7%)
Rheumatological disorders, *n* (%)	2/96 (2%)
Multiple sclerosis, *n* (%)	4/96 (4%)
Hashimoto thyroiditis, *n* (%)	2/96 (2%)
Asthma, *n* (%)	8/96 (8%)
Neurodermatitis, *n* (%)	2/96 (2%)

TABLE 3 Symptoms of acute COVID-19, *n* (%).

Headache, *n* (%)	55/96 (57%)
Fever, *n* (%)	57/96 (59%)
Anosmia, *n* (%)	55/96 (57%)
Dyspnea, n (%)	34/96 (35%)
Cough, *n* (%)	52/96 (54%)
Cold, *n* (%)	43/96 (45%)
Pain, *n* (%)	47/96 (49%)
Gastrointestinal symptoms, *n* (%)	17/96 (18%)
Fatigue, *n* (%)	54/96 (56%)
Sleep disturbance, *n* (%)	25/96 (26%)
Hospitalization, *n* (%)	15/96 (16%)
Intubation, *n* (%)	1/96 (1%)

3.5 Brain MRI

Of the 96 patients, 88 underwent a brain MRI after COVID-19 diagnosis. A total of 5 patients had a known demyelinating disease such as MS and were excluded from further analysis. The time between COVID-19 infection and brain imaging averaged 37.8 weeks (95% CI: 32.5–43.1) for the remaining 83 patients. Although post-COVID-19 syndrome shows a clear female predominance, we found no sex-specific differences in MRI findings.

The subsequent analysis of the MRIs was conducted independently by 2 radiologists. The first rater identified 64 patients with T2-hyperintense lesions, whereas the second identified 56. Both examiners then grouped the findings according to the total number and location of T2-hyperintense lesions as well as the number of lesions displaying a CVS. According to Rater 1 most patients (36%) had between 1 and 5 hyperintense lesions; 17 patients (27%) had more than 15 lesions; 16 (25%) had between 6 and 10 lesions and 8 patients (13%) had 11–15 T2-hyperintense lesions. Rater 2 reported that most

TABLE 4 Post-COVID-19 symptoms at first consultation.

Fatigue, *n* (%)		86/96 (90%)
Sleep disorders, *n* (%)		49/96 (51%)
Headache, *n* (%)		55/96 (57%)
Pain, *n* (%)		39/96 (40%)
Paresthesia, *n* (%)		17/96 (18%)
Dyspnea, *n* (%)		32/96 (33%)
Anosmia/Ageusia, *n* (%)		28/96 (29%)
Cough, *n* (%)		3/96 (3%)
Dizziness, *n* (%)		31/96 (32%)
Autonomic dysfunction, *n* (%)		18/96 (19%)
Dermatological symptoms, *n* (%)		8/86 (9%)
Gastroenterological symptoms, *n* (%)		11/96 (11%)
Tinnitus, *n* (%)		5/96 (5%)
Visual symptoms, *n* (%)		3/96 (3%)
	Depression, *n* (%)	23/82 (28%)
	Daytime sleepiness, *n* (%)	29/80 (36%)

TABLE 5 Scores of self-reported questionnaires at first consultation.

FSS, mean (95% CI), *n*	5.2 (4.9–5.5), 81
FSMC total, mean (95% CI), *n*	70.5 (66.2–74.9), 79
ESS, mean (95% CI)	9.2 (8.0–10.3), 80
BDI-II, mean (95% CI)	16.6 (14.7–18.5), 82

FSS, Fatigue Severity Scale; FSMC, Fatigue Scale for Motor and Cognitive Functions; ESS the Epworth Sleepiness Scale, BDI-II Beck Depression Inventory.

patients (27; 48%) had more than 15 lesions, whereas only 4% had between 11 and 15 T2-hyperintense lesions. Neither of the raters found enhancing lesions or lesions with a paramagnetic rim. In the majority of cases no CVS was reported by either of the radiologists (Rater 1–75%; Rater 2–63%) with a decrease in incidence of patients displaying a higher number of lesions with CVS. As for the location of T2-hyperintense lesions, the first rater identified most lesions in the subcortical and periventricular areas (34 patients—53%), as well as 16 patients (25%) with only subcortical lesions. Rater 2 reported more patients showing sub- and juxtacortical lesions (20 patients—36%) and fewer with subcortical and periventricular lesions (14 patients—25%). Fifteen patients were reported by the second rater as having only subcortical T2-hyperintense lesions (25%). The results are shown in Table 6 and summarized in Figure 1.

3.6 Spine MRI

A collection of spine MRIs was analyzed in a similar way to the brain MRIs. Of 95 patients, 19 had undergone spine MRI following infection with SARS-CoV-2. For 19 of 95 patients, no demyelinating CNS disorders were identified. The average time elapsed between COVID-19 infection and spine imaging was 36.1 weeks (95% CI: 19.9–52.3).

The same 2 raters conducted the evaluation of the spine MRIs. Both raters recorded a similar number of lesions across all spine regions with one third of patients showing between 1 and 3 lesions,

TABLE 6 Findings of brain MRIs conducted in patients post-COVID-19 infection.

Cerebral MRI		
Number of patients with brain MRI after SARS-CoV-2 infection, *n* (%)	88/96 (92%)	
Number of patients with brain MRI and without demyelinating CNS disorders (e.g., multiple sclerosis) *n* (%)	83/96 (86%)	
Time between COVID-19 and brain MRI, weeks, mean (95% CI)	37.8 (32.5–43.1)	
Patients with T2-hyperintense lesions, *n* (%)	Rater 1	Rater 2
	64/83 (77%)	56/83 (67%)
Number of T2-hyperintense lesions, *n* (%)		
1–5	23/64 (36%)	13/56 (23%)
6–10	16/64 (25%)	14/56 (25%)
11–15	8/64 (13%)	2/56 (4%)
>15	17/64 (27%)	27/56 (48%)
Enhancing lesions	0/64 (0%)	0/56 (0%)
Lesions with paramagnetic rim	0/64 (0%)	0/56 (0%)
Lesions with CVS, *n* (%)		
None	48/64 (75%)	35/56 (63%)
1–2	10/64 (16%)	12/56 (21%)
3–4	6/64 (9%)	7/56 (13%)
5–6	0/64 (0%)	2/56 (4%)
T2-hyperintense lesions by location, *n* (%)		
Only subcortical	16/64 (25%)	14/56 (25%)
Only juxtacortical	0/64 (0%)	0/56 (0%)
Only periventricular	1/64 (2%)	0/56 (0%)
Only infratentorial	0/64 (0%)	0/56 (0%)
Sub- and juxtacortical	5/64 (8%)	6/56 (11%)
Subcortical and periventricular	34/64 (53%)	14/56 (25%)
Sub- and juxtacortical and periventricular	6/64 (9%)	20/56 (36%)
Subcortical, periventricular, infratentorial	2/64 (3%)	0/56 (0%)
All locations	0/64 (0%)	2/56 (4%)
Black holes	0/83 (0%)	0/83 (0%)
Leptomeningeal enhancement	1/79 (1%)	1/79 (1%)
Diffusion restriction	0/81 (0%)	0/81(0%)
Orbital/optic nerve pathologies	0/81 (0%)	0/81 (0%)
Only subcortical	16/64 (25%)	14/56 (25%)

MRI, magnetic resonance imaging; CNS, central nervous system; CVS central vein sign.

most of which (67%) were in the cervical spine. All enhancing spine lesions appeared at the thoracic level. Table 7 summarizes the findings.

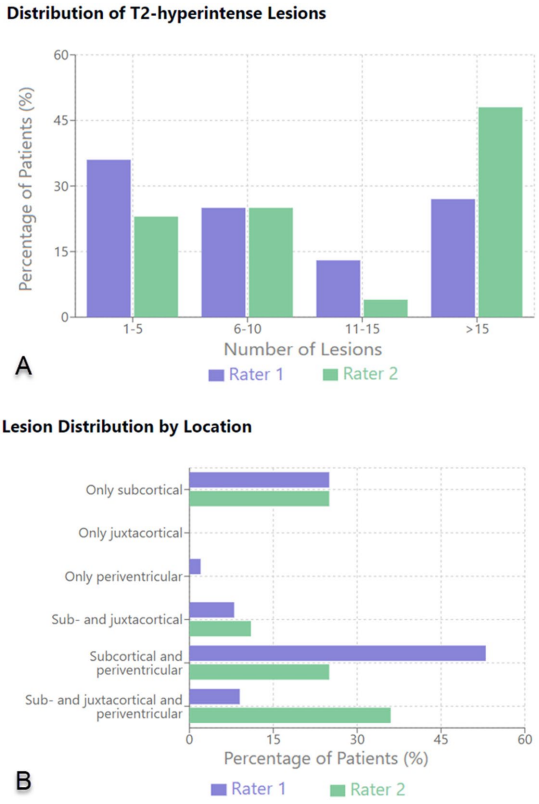

FIGURE 1
Distribution of T2-hyperintense lesions **(A)** and lesion distribution by location **(B)** on brain MRI.

4 Correlation between symptoms and brain MRI

This study considered the 2 most reported symptoms persisting after SARS-CoV-2 infection—headache and fatigue—and tried to determine the relationship between the prevalence of these symptoms and the number and location of T2-hyperintense lesions identified on brain MRI in this cohort of patients. The statistical analysis is depicted in Table 8.

Due to the small number of patients with T2-hyperintense lesions identified on spine MRI, a similar statistical analysis was not possible for these data.

4.1 Headaches in patients with post-COVID-19 syndrome

For the 41 patients presenting with no headache, 31 had T2-lesions identified on brain MRI with a mean value of 7.4 (95% CI: 5.3–9.6), whereas for the 55 subjects presenting with headaches, the mean value was 5.9 (95% CI: 4.3–7.5, *p*-value 0.557). Of the 31 patients presenting with headaches and having T2-lesions identified on brain MRI, 13 showed a pathological number of T2-lesions according to age. In the "no headache" group of 31 individuals with T2-lesions, 24 were observed to have a pathological number of lesions for their age group (*p*-value 0.820).

TABLE 7 Findings of spine MRIs conducted in patients post-COVID-19 infection.

Spine MRI		
Number of patients with spine MRI after SARS-CoV-2 infection, *n* (%)	19/95 (20%)	
Number of patients with spine MRI and without demyelinating CNS disorders (e.g., multiple sclerosis), *n* (%)	19/90 (20%)	
Time between COVID-19 and spine MRI, weeks, mean (95% CI)	36.1 (19.9–52.3)	
T2-hyperintense lesions, *n* (%)	Rater 1	Rater 2
	3/19 (16%)	3/19 (16%)
Number of T2-hyperintense lesions, *n* (%)		
1	1/3 (33%)	1/3 (33%)
2	1/3 (33%)	1/3 (33%)
3	1/3 (33%)	1/3 (33%)
T2-hypertintense lesions by location, *n* (%)		
Cervical spine	2/3 (67%)	2/3 (67%)
Thoracic spine	1/3 (33%)	1/3 (33%)
Enhanced lesions (thoracic spine)	1/3 (33%)	1/3 (33%)

MRI, magnetic resonance imaging; CNS, central nervous system.

TABLE 8 Statistical analysis comparing the number of T2-lesions in the brain between patients reported as having headaches or who were assessed as having chronic fatigue after COVID-19 infection.

	Patients without fatigue (FSS < 4.0)	Patients with fatigue (FSS > 4.0)	*p*-value
Number of T2-lesions in brain MRI, mean (95% CI)	6.7 (3.1–10.4), 14	6.4 (4.9–7.9), 59	0.815
	Patients without headache	Patients with headache	
Number of T2-lesions in brain MRI, mean (95% CI)	7.4 (5.3–9.6), 31	5.9 (4.3–7.5), 53	0.178
	Patients without fatigue (FSS < 4.0)	Patients with fatigue (FSS > 4.0)	*p*-value
Patients with pathological number of T2 lesions for age, *n* (%)	5/14 (35%)	27/59 (46%)	0.557
	Patients without headache	Patients with headache	
Patients with pathological number of T2 lesions for age, *n* (%)	13/31 (42%)	24/53 (45%)	0.820

FSS, Fatigue Severity Scale.

4.2 Fatigue in patients with post-COVID-19 syndrome

For the 14 patients presenting with no fatigue (FSS < 4.0), a mean of 6.7 (95% CI: 3.1–10.4) T2-lesions were identified in brain MRI. The subjects identified as having fatigue (FSS ≥ 4.0) had a mean of 6.4 T2-lesions (95% CI: 4.9–7.9, *p*-value 0.815). Of the 14 individuals with no fatigue, 5 were diagnosed with a pathological number of T2-lesions for their age whereas, of the 59 patients with fatigue, 27 had a pathological number of lesions for their age (p-value 0.557).

5 Discussion

This study focused on radiological evaluation with brain/spine MRI in participants with post-COVID-19 syndrome in single-center cohort in Switzerland. In our cohort, the majority of patients suffering from Post-COVID-19 Syndrome were female (73%; 70/96). This gender predominance aligns with findings from previous studies on long COVID, which have shown that women are disproportionately affected by persistent symptoms (34). Several factors may contribute to this gender disparity: biological differences, such as sex-specific variations in immune response are well-documented with women tending to have stronger immune responses making them more prone to immune-mediated conditions, which could influence susceptibility to long COVID (35). Additionally, hormonal differences, particularly the modulatory effects of estrogen on immune and vascular function, may play a role in the manifestation of chronic post-viral symptoms (35). Beyond biological factors, gender-specific reporting and healthcare-seeking behaviors may further contribute to the observed differences, as women may be more likely to report symptoms and seek medical attention for chronic conditions like Post-COVID-19 Syndrome (36). These considerations underscore the need to account for gender differences when interpreting findings and developing management strategies for long COVID.

Our study underscores the complexity of interpreting radiological findings in patients with post-COVID-19 syndrome. This is particularly evident with respect to structural brain alterations seen on MRI and their relationship with the most commonly identified symptoms such as chronic fatigue, headaches and depression. MRI is often used to identify possible structural causes for persistent neurological symptoms. The most common finding in brain MRI in our study was the presence of T2-hyperintense lesions in subcortical and periventricular areas, which is in line with the current literature (37). These lesions have previously been reported in patients suffering from persistent fatigue after hospitalization for COVID-19 (26), as well as in those with post-COVID-19 "brain fog" (28). However, these lesions tend to be frequently encountered in other unrelated settings such as post-infectious and inflammatory conditions, as well as in

cases of chronic hypertension and small vessel disease. Advanced MRI techniques, such as diffusion tensor imaging and functional MRI (fMRI) have been shown to help in identifying imaging alterations that seem to be more prevalent in patients exhibiting neurological symptoms in the setting of post-COVID-19 syndrome (23, 38). However, our study did not find a significant correlation between reported radiological abnormalities and the most common symptoms reported by our patient cohort.

Symptoms such as chronic fatigue could be influenced by a range of physiological and psychological factors, including immune dysregulation, hormonal imbalances, and mental health conditions like depression or anxiety (21). The findings of our study suggest that these complex factors may not manifest as detectable structural changes in the brain, at least not in ways that are visible using conventional MRI protocols. While more complex imaging protocols such as fMRI or advanced diffusion techniques may be more sensitive to subtle brain changes, in our experience their application in clinical practice remains limited. Other options, such as detailed clinical assessments and the use of validated questionnaires for symptom tracking, may be a more effective strategy in guiding therapy for patients presenting with post-COVID-19 syndrome (39), than using MRI as a routine follow-up tool. This could shift the focus of treatment strategies from purely neurological investigations to a more multidisciplinary approach including neuropsychiatric, psychological, and rehabilitative care.

Transverse myelitis, while uncommon, has been documented in the literature as a severe complication of viral infections, including COVID-19 (27). In our study, only 3 patients demonstrated spine lesions consistent with post-infectious myelitis. This low prevalence aligns with current findings that transverse myelitis is a rare but serious post-COVID-19 complication, typically linked to more severe neurological symptoms such as motor weakness and sensory deficits (27). This suggests reserving spine MRI for cases where more specific neurological deficits are present, rather than incorporating it as part of the routine post-COVID-19 workup.

Our findings suggest a need to re-evaluate the role of MRI in managing patients with post-COVID-19 syndrome. The absence of a clear structural correlation with common symptoms such as fatigue and headaches indicates that MRI findings, while useful in excluding structural brain abnormalities, may not provide actionable insights for guiding therapeutic interventions. As such, the nonspecific nature of white matter lesions calls for a cautious approach when attributing patient symptoms to these findings. Instead, functional and neuropsychological assessments, including cognitive testing and fatigue scales, might yield more direct information about the patient's condition and better inform therapeutic strategies.

Our study has some limitations. Firstly, the sample size is relatively small, particularly that for the analysis of spine MRI data, which limits the statistical power of the findings. Secondly, this study is retrospective and single-center, which may limit the generalizability of the results. The subjective nature of self-report questionnaires could introduce bias in the evaluation of symptoms. Additionally, the study did not adjust for other potential confounding factors such as treatment received during acute COVID-19 infection. Furthermore, this study relies on a single time-point for imaging and symptom assessment. Whilst previous studies suggest that some imaging abnormalities, such as those associated with inflammation or microvascular injury, may resolve or change with symptom recovery (38, 39), additional longitudinal studies with repeated imaging at multiple timepoints—such as 1, 3, and 6 months post-infection—are needed to evaluate the progression and resolution of T2-hyperintense lesions over time and to validate our findings.

While T2-hyperintense lesions are commonly observed in patients with post-COVID-19 syndrome, their presence does not seem to significantly correlate with symptoms of fatigue or headaches. These findings suggest that T2-hyperintense lesions may not be directly related to the subjective experience of these symptoms in patients with post-COVID-19 syndrome. Further research with larger sample sizes and adjustment for potential confounding factors is necessary to better understand the relationship between MRI findings and post-COVID-19 syndrome.

Data availability statement

The raw data supporting the conclusions of this article will be made available by the authors, without undue reservation. Requests to access the datasets included in the neuroimmunological registry (registration no. KEK-BE 2017-01369) and treated at the neuroimmunological outpatient department of the Inselspital, University Hospital Bern, should be directed to franca.wagner@insel.ch.

Ethics statement

The studies involving humans were approved by Inselspital Bern University Hospital. The studies were conducted in accordance with the local legislation and institutional requirements. Written informed consent for participation was not required from the participants or the participants' legal guardians/next of kin in accordance with the national legislation and institutional requirements.

Author contributions

GA: Writing – original draft, Writing – review & editing. SA: Data curation, Investigation, Methodology, Writing – review & editing. RH: Data curation, Investigation, Resources, Validation, Writing – review & editing, Project administration, Supervision. AE: Validation, Visualization, Writing – review & editing. LD: Conceptualization, Data curation, Formal analysis, Investigation, Methodology, Project administration, Resources, Software, Supervision, Validation, Visualization, Writing – review & editing. FW: Conceptualization, Data curation, Formal analysis, Investigation, Methodology, Project administration, Resources, Software, Supervision, Validation, Visualization, Writing – review & editing.

Funding

The author(s) declare that financial support was received for the research, authorship, and/or publication of this article. The resources

utilized were supported by the Bern University Hospital as part of its institutional research initiatives.

Acknowledgments

The authors thank Kaplan (certified medical editor; University College London) for the proofreading of the manuscript.

Conflict of interest

The authors declare that the research was conducted in the absence of any commercial or financial relationships that could be construed as a potential conflict of interest.

Generative AI statement

The author(s) declare that no Gen AI was used in the creation of this manuscript.

Publisher's note

All claims expressed in this article are solely those of the authors and do not necessarily represent those of their affiliated organizations, or those of the publisher, the editors and the reviewers. Any product that may be evaluated in this article, or claim that may be made by its manufacturer, is not guaranteed or endorsed by the publisher.

References

1. Natarajan A, Shetty A, Delanerolle G, Zeng Y, Zhang Y, Raymont V, et al. A systematic review and meta-analysis of long COVID symptoms. *Syst Rev*. (2023) 12:88. doi: 10.1186/s13643-023-02250-0

2. Alimetov A. (2024). Dover, Delaware, U.S.A. Available at: Worldometers.info (Accessed July 01, 2024).

3. Carfì A, Bernabei R, Landi Ffor the Gemelli Against COVID-19 Post-Acute Care Study Group. Persistent symptoms in patients after acute COVID-19. *JAMA*. (2020) 324:603. doi: 10.1001/jama.2020.12603

4. Diem L, Fregolente-Gomes L, Warncke JD, Hammer H, Friedli C, Kamber N, et al. Fatigue in post-COVID-19 syndrome: clinical phenomenology, comorbidities and association with initial course of COVID-19. *J Cent Nerv Syst Dis*. (2022) 14:117957352211027. doi: 10.1177/11795735221102727

5. Ballering AV, Van Zon SKR, Olde Hartman TC, Rosmalen JGM. Persistence of somatic symptoms after COVID-19 in the Netherlands: an observational cohort study. *Lancet*. (2022) 400:452–61. doi: 10.1016/S0140-6736(22)01214-4

6. Taruffi L, Muccioli L, Mitolo M, Ferri L, Descovich C, Mazzoni S, et al. Neurological manifestations of long COVID: a single-center one-year experience. *Neuropsychiatr Dis Treat*. (2023) 19:311–9. doi: 10.2147/NDT.S387501

7. Centers for Disease Control and Prevention (2023). Post-COVID conditions: information for healthcare providers. Available at: https://www.cdc.gov/coronavirus/2019-ncov/hcp/clinical-care/post-covid-conditions.html (Accessed July 01, 2024).

8. COVID-19 Treatment Guidelines Panel (2020). Coronavirus Disease 2019 (COVID-19) Treatment Guidelines. National Institutes of Health. Available at https://www.covid19treatmentguidelines.nih.gov/ (Accessed July 01, 2024).

9. Iadecola C, Anrather J, Kamel H. Effects of COVID-19 on the nervous system. *Cell*. (2020) 183:16–27.e1. doi: 10.1016/j.cell.2020.08.028

10. Ellul MA, Benjamin L, Singh B, Lant S, Michael BD, Easton A, et al. Neurological associations of COVID-19. *Lancet Neurol*. (2020) 19:767–83. doi: 10.1016/S1474-4422(20)30221-0

11. Moonis G, Filippi CG, Kirsch CFE, Mohan S, Stein EG, Hirsch JA, et al. The Spectrum of neuroimaging findings on CT and MRI in adults with COVID-19. *Am J Roentgenol*. (2021) 217:959–74. doi: 10.2214/AJR.20.24839

12. Nehme M, Diem L, Bassetti CLA, Guessous I. Swiss recommendations for the diagnosis, management and follow-up of post-COVID condition in primary care medicine (2023). *Swiss Med Wkly*. (2023) 153:3468. doi: 10.57187/s.3468

13. Townsend L, Dyer AH, Jones K, Dunne J, Mooney A, Gaffney F, et al. Persistent fatigue following SARS-CoV-2 infection is common and independent of severity of initial infection. *PLoS One*. (2020) 15:e0240784. doi: 10.1371/journal.pone.0240784

14. Naik H, Shao S, Tran KC, Wong AW, Russell JA, Khor E, et al. Evaluating fatigue in patients recovering from COVID-19: validation of the fatigue severity scale and single item screening questions. *Health Qual Life Outcomes*. (2022) 20:170. doi: 10.1186/s12955-022-02082-x

15. Penner I, Raselli C, Stöcklin M, Opwis K, Kappos L, Calabrese P. The fatigue scale for motor and cognitive functions (FSMC): validation of a new instrument to assess multiple sclerosis-related fatigue. *Mult Scler J*. (2009) 15:1509–17. doi: 10.1177/1352458509348519

16. Babicki M, Piotrowski P, Mastalerz-Migas A. Assessment of insomnia symptoms, quality of life, daytime sleepiness, and psychoactive substance use among polish students: a cross-sectional online survey for years 2016–2021 before and during COVID-19 pandemic. *J Clin Med*. (2022) 11:2106. doi: 10.3390/jcm11082106

17. Lapin BR, Bena JF, Walia HK, Moul DE. The Epworth sleepiness scale: validation of one-dimensional factor structure in a large clinical sample. *J Clin Sleep Med*. (2018) 14:1293–301. doi: 10.5664/jcsm.7258

18. Smarr KL, Keefer AL. Measures of depression and depressive symptoms. *Arthritis Care Res*. (2020) 72:608–29. doi: 10.1002/acr.24191

19. Beck AT. An inventory for measuring depression. *Arch Gen Psychiatry*. (1961) 4:561. doi: 10.1001/archpsyc.1961.01710120031004

20. Weich C, Dettmers C, Saile R, Schleicher L, Vieten M, Joebges M. Prominent fatigue but no motor fatigability in non-hospitalized patients with post-COVID-syndrome. *Front Neurol*. (2022) 13:902502. doi: 10.3389/fneur.2022.902502

21. Davis HE, McCorkell L, Vogel JM, Topol EJ. Long COVID: major findings, mechanisms and recommendations. *Nat Rev Microbiol*. (2023) 21:133–46. doi: 10.1038/s41579-022-00846-2

22. Douaud G, Lee S, Alfaro-Almagro F, Arthofer C, Wang C, McCarthy P, et al. SARS-CoV-2 is associated with changes in brain structure in UK biobank. *Nature*. (2022) 604:697–707. doi: 10.1038/s41586-022-04569-5

23. Lu Y, Li X, Geng D, Mei N, Wu PY, Huang CC, et al. Cerebral Micro-structural changes in COVID-19 patients – an MRI-based 3-month follow-up study. *EClinicalMedicine*. (2020) 25:100484. doi: 10.1016/j.eclinm.2020.100484

24. Elliott P, Ward H, Riley S. Population monitoring of SARS-CoV-2 infections via random sampling during the COVID-19 pandemic. *Am J Public Health*. (2023) 113:514–6. doi: 10.2105/AJPH.2023.307231

25. Radmanesh A, Raz E, Zan E, Derman A, Kaminetzky M. Brain imaging use and findings in COVID-19: a single academic center experience in the epicenter of disease in the United States. *Am J Neuroradiol*. (2020) 41:1179–83. doi: 10.3174/ajnr.A6610

26. Hellgren L, Birberg Thornberg U, Samuelsson K, Levi R, Divanoglou A, Blystad I. Brain MRI and neuropsychological findings at long-term follow-up after COVID-19 hospitalisation: an observational cohort study. *BMJ Open*. (2021) 11:e055164. doi: 10.1136/bmjopen-2021-055164

27. Ahmad SA, Salih KH, Ahmed SF, Kakamad FH, Salh AM, Hassan MN, et al. Post COVID-19 transverse myelitis; a case report with review of literature. *Ann Med Surg*. (2021) 69:69. doi: 10.1016/j.amsu.2021.102749

28. Kotzalidis GD, Ferrara OM, Margoni S, Ieritano V, Restaino A, Bernardi E, et al. Are the post-COVID-19 posttraumatic stress disorder (PTSD) symptoms justified by the effects of COVID-19 on brain structure? A systematic review. *J Pers Med*. (2023) 13:1140. doi: 10.3390/jpm13071140

29. McDonald WI, Compston A, Edan G, Hartung HP, Lublin FD, McFarland HF, et al. Recommended diagnostic criteria for multiple sclerosis: guidelines from the international panel on the diagnosis of multiple sclerosis. *Ann Neurol*. (2001) 50:121–7. doi: 10.1002/ana.1032

30. Filippi M, Preziosa P, Arnold DL, Barkhof F, Harrison DM, Maggi P, et al. Present and future of the diagnostic work-up of multiple sclerosis: the imaging perspective. *J Neurol*. (2023) 270:1286–99. doi: 10.1007/s00415-022-11488-y

31. Sati P, Oh J, Constable RT, Evangelou N, Guttmann CRG, Henry RG, et al. The central vein sign and its clinical evaluation for the diagnosis of multiple sclerosis: a consensus statement from the north American imaging in multiple sclerosis cooperative. *Nat Rev Neurol*. (2016) 12:714–22. doi: 10.1038/nrneurol.2016.166

32. Suh CH, Kim SJ, Jung SC, Choi CG, Kim HS. The "central vein sign" on T2*-weighted images as a diagnostic tool in multiple sclerosis: a systematic review and Meta-analysis using individual patient data. *Sci Rep*. (2019) 9:18188. doi: 10.1038/s41598-019-54583-3

33. Sinnecker T, Clarke MA, Meier D, Enzinger C, Calabrese M, de Stefano N, et al. Evaluation of the central vein sign as a diagnostic imaging biomarker in multiple sclerosis. *JAMA Neurol*. (2019) 76:1446–56. doi: 10.1001/jamaneurol.2019.2478

34. Alwan NA. The road to addressing long Covid. *Science*. (2021) 373:491–3. doi: 10.1126/science.abg7113

35. Klein SL, Flanagan KL. Sex differences in immune responses. *Nat Rev Immunol*. (2016) 16:626–38. doi: 10.1038/nri.2016.90

36. Davis HE, Assaf GS, McCorkell L, Wei H, Low RJ, Re'em Y, et al. Characterizing long COVID in an international cohort: 7 months of symptoms and their impact. *eClinicalMedicine*. (2021) 38:101019. doi: 10.1016/j.eclinm.2021.101019

37. Vasilev Y, Blokhin I, Khoruzhaya A, Kodenko M, Kolyshenkov V, Nanova O, et al. Routine brain MRI findings on the long-term effects of COVID-19: a scoping review. *Diagnostics*. (2023) 13:2533. doi: 10.3390/diagnostics13152533

38. Kim M, Sim S, Yang J, Kim M. Multivariate prediction of long COVID headache in adolescents using gray matter structural MRI features. *Front Hum Neurosci*. (2023) 17:1202103. doi: 10.3389/fnhum.2023.1202103

39. Díez-Cirarda M, Yus M, Gómez-Ruiz N, Polidura C, Gil-Martínez L, Delgado-Alonso C, et al. Multimodal neuroimaging in post-COVID syndrome and correlation with cognition. *Brain*. (2023) 146:2142–52. doi: 10.1093/brain/awac384

frontiers | Frontiers in Neurology

TYPE Original Research
PUBLISHED 29 January 2025
DOI 10.3389/fneur.2025.1532883

OPEN ACCESS

EDITED BY
Jieqiong Wang,
Chinese Academy of Sciences, China

REVIEWED BY
Pui Yeung Lee,
Yale University, United States
Yue Lyu,
University of Texas MD Anderson Cancer Center, United States

*CORRESPONDENCE
David Školoudík
✉ skoloudik@hotmail.com

RECEIVED 22 November 2024
ACCEPTED 03 January 2025
PUBLISHED 29 January 2025

CITATION
Pakizer D, Šalounová D and Školoudík D (2025) Extracranial carotid plaque calcification and its association with risk factors for cerebrovascular events: insights from the ANTIQUE study.
Front. Neurol. 16:1532883.
doi: 10.3389/fneur.2025.1532883

Extracranial carotid plaque calcification and its association with risk factors for cerebrovascular events: insights from the ANTIQUE study

David Pakizer, Dana Šalounová and David Školoudík*on behalf of The ANTIQUE Study Group

Centre for Health Research, Department of Clinical Neurosciences, Faculty of Medicine, University of Ostrava, Ostrava, Czechia

Introduction: Extracranial carotid calcification is a common marker of advanced atherosclerosis. However, its impact on stroke risk is not consistent across studies, and examining the type of calcification and the presence of systemic diseases might be helpful. We aimed to investigate extracranial carotid calcification and its association with risk factors for ischemic cerebrovascular diseases.

Materials and methods: Among 1,863 consecutive patients in the Atherosclerotic Plaque Characteristics Associated with a Progression Rate of the Plaque and a Risk of Stroke in Patients with the Carotid Bifurcation Plaque Study (ANTIQUE), 132 symptomatic or asymptomatic patients (177 carotid plaques) with >30% carotid stenosis examined through computed tomography (CT) and magnetic resonance imaging (MRI) were included. Statistical data were assessed using the χ^2-test, Fisher's exact test, *t*-test, and Mann–Whitney test to investigate the calcification risk factors.

Results: Compared to the absence of calcifications, spotty calcifications were associated with male sex [odds ratio (OR): 3.72, 95% confidence interval (CI): 1.06–13.05], while large calcifications were associated with older patients (OR: 1.60 per 5 years of age, 95% CI: 1.20–2.13). Large calcifications were also strongly associated with coronary heart disease (OR: 4.07, 95% CI: 1.15–14.44) and atrial fibrillation ($p = 0.025$). In comparison between only spotty and large calcifications, spotty calcifications were associated with male sex (OR: 3.72, 95% CI: 1.06–13.05), smoking ($p = 0.020$) in more significant quantities ($p = 0.014$), and lipid plaque ($p < 0.001$), while large calcifications with contralateral stenosis degree ($p = 0.044$). No significant relationship was found between cerebrovascular events and the type of calcification.

Conclusion: Although the presence and type of extracranial carotid calcification were not related to ipsilateral ischemic events, large calcifications were strongly associated with coronary heart disease and atrial fibrillation.

Clinical trial registration: ClinicalTrials.gov, identifier NCT02360137.

KEYWORDS

atherosclerosis, carotid artery disease, calcification, cerebrovascular disease, magnetic resonance imaging, computed tomography

1 Introduction

Carotid artery stenosis caused by atherosclerosis represents a substantial global epidemiological burden, with the prevalence of carotid plaque at 21% among individuals aged 30–79 years (1). Importantly, carotid atherosclerosis accounts for up to 25% of all ischemic strokes, which are among the leading causes of mortality and disability worldwide (2, 3). Extracranial carotid calcification represents a well-known clinical marker of atherosclerosis, which is characteristic of arterial aging. It is present in up to 75% of the population over the age of 75 years (1, 4).

The immediate inflammatory response that results in microcalcifications represents the pathophysiology of carotid calcification, which can be detected by non-invasive imaging methods, such as computed tomography (CT) and magnetic resonance imaging (MRI) (5). While microcalcifications and spotty calcifications indicate active vascular calcification related to inflammation, causing plaque instability, macrocalcification is strongly inversely related to macrophage infiltration, causing plaque stabilization (6). However, the results of the previous studies are not consistent. Several comprehensive studies have shown that carotid plaque calcification is a protective plaque characteristic not associated with stroke (7–9), but some studies found a positive association between calcification and stroke (10–12). Therefore, examining the relationship between extracranial carotid calcification and systemic diseases that play a role in stroke risk might be useful for risk stratification in patients (13). To the best of our knowledge, when considering the calcification type and multiple atherosclerosis-related systematic diseases, there exists a lack of evidence of these types of relationships.

This study aimed to assess the association between extracranial carotid plaque calcification and risk factors for ischemic cerebrovascular diseases in both symptomatic and asymptomatic patients.

2 Materials and methods

2.1 Study design

This study presents a *post hoc* analysis of data from the prospective multicenter observational and cross-sectional Atherosclerotic Plaque Characteristics Associated with a Progression Rate of the Plaque and a Risk of Stroke in Patients with the Carotid Bifurcation Plaque Study (ANTIQUE; ClinicalTrials.gov Identifier: NCT02360137).

2.2 Sample characterization

For the present study, we enrolled all consecutive patients from the ANTIQUE study who has carotid stenosis of at least 30% and underwent clinical and diagnostic (CT and MRI) examinations. The patients were recruited into the comprehensive stroke center between October 2016 and March 2019 from those indicated for neurosonology examination in stroke prevention or acute stroke diagnostics (14, 15). The inclusion criteria were as follows: Patients aged above 30 years; atherosclerotic plaque in the carotid bifurcation or the proximal part of the internal carotid artery with a thickness of ≥2 mm in the transverse plane of the ultrasound B-mode measurement; calcification detected in the mentioned area of carotid bifurcation in CT examination; sufficient image quality from CT and MRI examinations; and patient self-sufficiency (modified Rankin scale score, 0–2 points). A carotid plaque, representing the most stenotic lesion when multiple plaques were present, causing stenosis at least 30% on ultrasound B-mode (transition from laminar to turbulent blood flow) was included and further assessed (16).

The exclusion criteria were as follows: Patients whose CT or MRI of the neck was not performed; insufficient CT and MR image quality of the patients; non-cooperative patients for the examinations; patients detected with carotid artery occlusion; patients undergoing stenting in the carotid bifurcation; and patients after invasive treatment of ipsilateral carotid artery (carotid endarterectomy or stenting).

Symptomatic patients were characterized as those with clinical signs of recent ipsilateral cerebrovascular ischemic events [transient ischemic attack (TIA), stroke, amaurosis fugax, and/or retinal infarction] in the last 90 days (time from symptom onset to imaging), excluding patients with other potential stroke etiologies (cardioembolic, lacunar, arterial dissection, vasculitis, other rare causes of stroke) (17). Both arteries from symptomatic patients were included: the artery ipsilateral to the cerebrovascular event (symptomatic) and the contralateral (asymptomatic). Patients without clinical signs of TIA/stroke in the relevant arterial territory within the last 90 days were classified as asymptomatic.

All patients were examined through CT (first-line modality—as soon as possible after the onset of symptoms or within 30 days of recruitment from the neurosonology laboratory for asymptomatic patients) and MRI within 7 days following the CT examination.

2.3 Computed tomography

All patients were examined by a standard multidetector CT angiography (CTA) of carotid and brain arteries using various machines, with an intravenous iodine contrast agent Iomeron® 400 (Bracco Imaging, Milan, Italy) or Ultravist® 370 (Bayer HealthCare Pharmaceuticals LLC, Berlin, Germany) administered with 50–100-mL doses. Multiplanar axial plane reconstructions (<1-mm slices) and sagittal and coronal maximum intensity projection reconstructions (3–8 mm) were assessed with a uniform window width and center of 700 and 200 Hounsfield units (HU), respectively.

Carotid artery stenosis severity was measured based on the North American Symptomatic Carotid Endarterectomy Trial (NASCET) criteria (18). Plaque morphology was analyzed using density measurement of individual characteristics in HU. Characteristics were classified as lipid (<60 HU), fibrous (60–130 HU), or calcified (>130 HU) based on voxel-level measurements within regions of interest (2–10 pixels per region, covering a minimum of three plaque slices) (19). For overall plaque evaluation (lipid, fibrous, or calcified), the predominant characteristic had to occur in >50% plaque area. Calcifications were divided according to size into spotty (<3 mm in length/width) or large (>3 mm) (20). Additionally, smooth (no irregularities), irregular (minor surface changes), or ulcerated (>1 mm deep excavation in at least two planes) plaque surface was evaluated (19).

2.4 Magnetic resonance imaging

Carotid MRI examination protocol was conducted on different 1.5-Tesla machines with head/neck coil, consisting of the following

sequences: Fat-suppressed T1-weighted_TSE [turbo spin echo; echo time (TE) 19 ms, repetition time (TR) 600 ms; slice thickness 3 mm; duration 3:50 min], 3D_T1-weighted_MPRAGE (magnetization prepared rapid gradient echo; TE 4 ms; TR 670 ms; inversion time 370 ms; 1 mm; 5:49 min), T2-weighted TSE (TE 72 ms; TR 4,580 ms; 4 mm; 3:18 min), and 3D_TOF (time of flight; TE 7 ms; TR 24 ms; 1 mm; 2:43 min).

In the individual plaque characteristics evaluation, differently distributed intraplaque signal intensities were visually compared to sternocleidomastoid muscle intensity. Overall, plaque composition was evaluated by the modified American Heart Association (AHA) plaque classification for MRI (IV–V, VI: unstable soft plaques; VII, VIII: stable hard plaques) (21). Lipid-rich necrotic core (LRNC; TOF: isointense, T1-w: isointense to hyperintense, T2-w: hypointense) and LRNC covering fibrous cap status (thick, thin, or ruptured) were assessed (22). Finally, intraplaque hemorrhage (IPH) categorized into acute (<1 week old; T1-w, TOF: hyperintense, T2-w: iso to hypointense) and subacute (1–6 weeks old; T1-w, T2-w, TOF: hyperintense) was evaluated.

All mentioned CT- and MRI-derived carotid plaque characteristics were evaluated by a single experienced rater (D.P.), blinded to patient medical history and CT results, based on cited major studies and expert consensus (5).

2.5 Demographic and clinical patient data

From the patient anamnestic data, the following atherosclerosis-related risk factors were retrieved: sex, age, arterial hypertension, diabetes mellitus, hyperlipidemia, bronchial asthma, chronic obstructive pulmonary disease, nephropathy, hyperuricemia, cancer, smoking, and alcohol. Daily cigarette and alcohol consumption (1 unit/20 g of alcohol = beer 0.5 L or wine 0.2 L or spirits 0.05 L) in the last year was also recorded. Moreover, data regarding atherosclerosis-related diseases (coronary heart disease, myocardial infarction, atrial fibrillation, and peripheral arterial disease) and cerebrovascular events (ischemic stroke, hemorrhagic stroke, transient ischemic attack, amaurosis fugax, and retinal infarction) were collected.

2.6 Statistical analysis

A statistical study power calculation was carried out. For a medium effect size $w = 0.3$, the significance level 0.05, and the test power 0.8 in the 2×2 table, the total sample size equal to 88 was sufficient. To account for the low quality of data in 25%, 110 patients were considered as a minimum to be recruited for the study.

The baseline characteristics were analyzed using descriptive statistics. Continuous data were noted as means ± standard deviations (SD) or medians and ranges. The categorical data were presented as numbers and percentages. Baseline differences between asymptomatic and symptomatic arteries were analyzed using the χ^2-test of independence for contingency tables for categorical variables. If the assumption that the value of the expected cell counts is 5, or more, in at least 80% of the cells, and no cell has an expected count less than one was violated, Fisher's exact test was used. Differences in continuous variables were assessed using the independent samples' *t*-test for normally distributed variables or Mann–Whitney test otherwise. The normality of data was evaluated through the Shapiro–Wilk test.

Associations between the mentioned risk factors and calcification type (spotty, large) were assessed using the χ^2-test, Fisher's exact test, *t*-test, or Mann–Whitney test. Relationships between calcification type (spotty and large) and other plaque characteristics (CT: plaque type, plaque surface; MRI: AHA type, LRNC, fibrous cap, IPH), side of stenosis (ipsilateral, contralateral) were assessed using χ^2-test or Fisher's exact test with *post hoc* comparisons using adjusted residuals, or Mann–Whitney test. Associations of calcification type (no calcification, spotty, and large) and atherosclerosis-related diseases were evaluated by a χ^2-test or Fisher's exact test with *post hoc* comparisons using adjusted residuals. Detailed tables of the adjusted residuals are provided in Supplementary Tables S1–S5).

As a direct outcome, relationships between the calcification type (none, spotty, and large) and mentioned cerebrovascular events were assessed via the χ^2-test or Fisher's exact test where appropriate. Statistical significance was assumed at a p-value of <0.05. All analyses were performed using IBM-SPSS Statistics version 29.0 for Windows.

3 Results

3.1 Study population

Overall, 132 patients (264 carotid bifurcations) were examined by CT and MRI from 1,863 patients enrolled in the ANTIQUE study. Only a symptomatic artery was included from symptomatic patients (not the contralateral asymptomatic artery) to reach homogeneous groups of plaques. From 264 carotid arteries, 177 plaques (68.9% male individuals; median age of 69 years) were included, and 87 arteries were excluded due to asymptomatic artery of symptomatic patient (60 cases), carotid occlusion (17 cases), and carotid stenosis <30% (10 cases). The study flow chart is presented in Figure 1. Symptomatic patients were significantly more likely to consume alcohol in larger quantities, have hyperuricemia, and have less frequent coronary heart disease compared to asymptomatic patients. All the details about the study population are available in Table 1.

3.2 Risk factors for the presence of different calcification types

When assessing the risk factors regarding absent calcification, spotty calcifications were associated with male sex [crude odds ratio (OR) 3.72, 95% confidence interval (CI) 1.06–13.05; Supplementary Table S6]. For large calcification, logistic regression analysis showed that these patients were significantly older (crude OR 1.60 per 5 years of age, 95% CI 1.20–2.13; Supplementary Table S6). Detailed results are presented in Supplementary Table S6 (crude ORs) and Supplementary Table S7 (adjusted ORs).

In comparison between only spotty and large calcifications, men had more often spotty calcifications, while women had more frequent large calcifications ($p = 0.015$). Higher age was associated with the presence of large calcification ($p = 0.027$). Smoking in more significant quantities was significantly related to spotty calcification ($p = 0.014$).

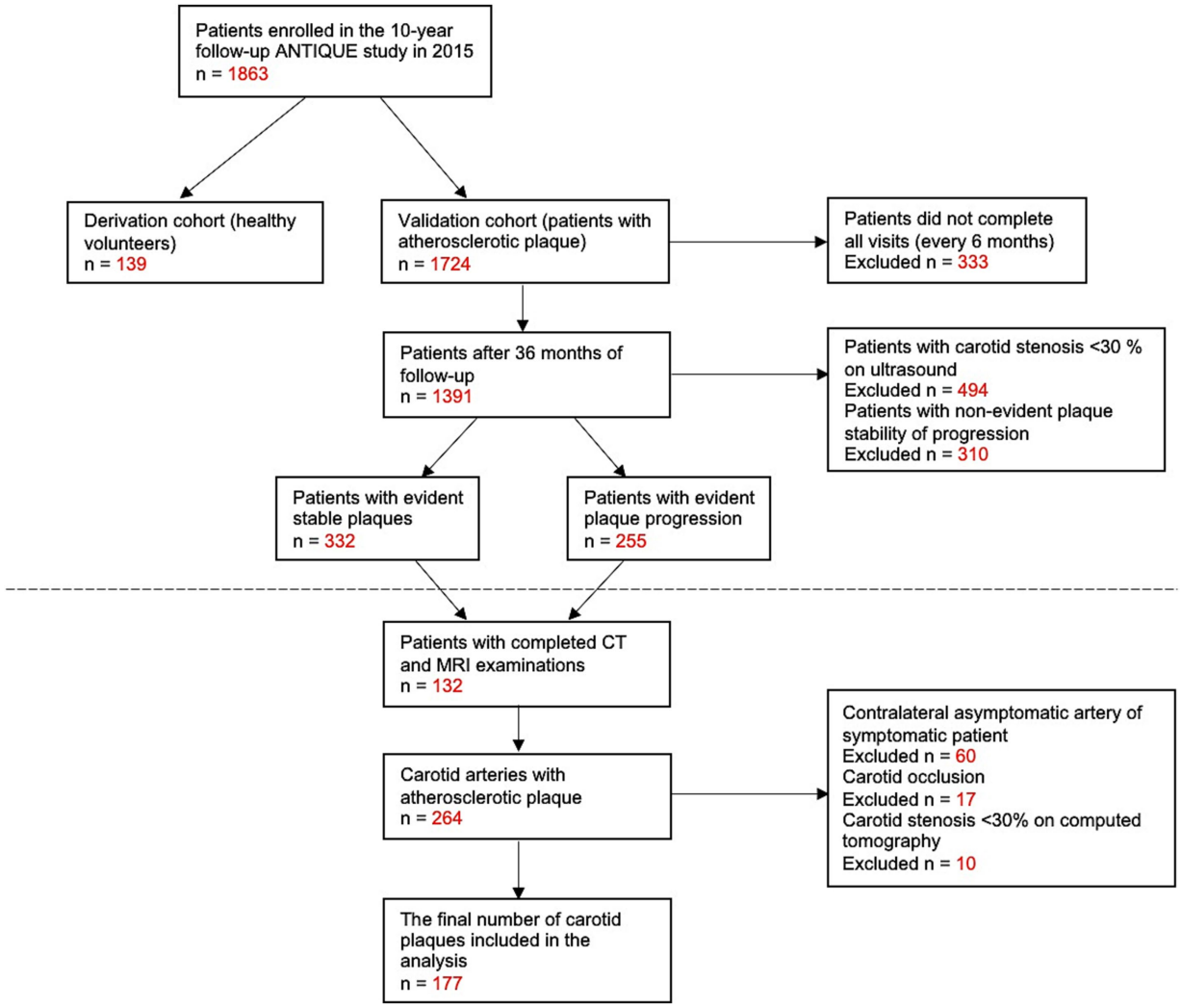

FIGURE 1
Study flowchart diagram.

At the same time, alcohol consumption, along with other atherosclerosis risk factors and chronic diseases, did not differ between the groups. All the above-mentioned results are presented in Table 2.

3.3 Calcification and other plaque characteristics

The calcification type was not related to the degree of ipsilateral stenosis but to contralateral stenosis. Large calcification was associated with a high degree of stenosis contralaterally ($p = 0.044$). Lipid plaque on CT was associated with spotty calcification ($p < 0.001$), while a large calcification was associated with calcified plaque ($p < 0.001$). Spotty calcification showed a non-significant trend toward more frequent presence in plaques with irregular surfaces than large calcification ($p = 0.16$). No significant associations were found between calcification patterns and MRI-derived carotid plaque characteristics. However, non-significant trends suggested spotty calcifications were more common in AHA type IV–V plaques (LRNC surrounded by fibrous tissue with possible calcification), plaques with LRNC, and thin or ruptured fibrous cap; and large calcification were more common in AHA type VII (calcified plaque) and subacute IPH. Detailed results on CT- and MRI-derived plaque characteristics are presented in Table 3.

3.4 Calcification in atherosclerosis-related diseases and cerebrovascular events

No significant relation was found between ipsilateral cerebrovascular events and the presence or type of calcification. However, atrial fibrillation was significantly more often in patients with large calcification within carotid plaque ($p = 0.015$, overall test, Table 4). Large calcifications were associated with coronary heart disease (crude OR 4.07, 95% CI 1.15–14.44; Supplementary Table S8) and atrial fibrillation ($p = 0.025$; Supplementary Table S8) compared to no calcification. Further results are provided in Table 4, and crude and adjusted OR values are given in the Supplementary Tables S8, S9, respectively.

10.3389/fneur.2025.1532883

TABLE 1 Baseline patient characteristics.

	Patients included in the study (n = 132)	Arteries included in analyses		
		All arteries (n = 177)	Only asymptomatic arteries (n = 117)	Only symptomatic arteries (n = 60)
Male sex	93 (70.5)	122 (68.9)	79 (67.5)	43 (71.7)
Patient age (years); median (range) in years	68.5 (44–88)	69 (44–88)	69 (49–86)	68 (44–88)
Atherosclerosis risk factors				
Hypertension	121 (91.7)	164 (92.7)	111 (94.9)	53 (88.3)
Diabetes mellitus	55 (41.7)	75 (42.4)	50 (42.7)	25 (41.7)
Hyperlipidemia	98 (74.2)	133 (75.1)	86 (73.5)	47 (78.3)
Smoking	44 (33.3)	59 (33.3)	35 (29.9)	24 (40)
Number of cigarettes per day; median (range)	0 (0–40)	0 (0–40)	0 (0–40)	0 (0–40)
Alcohol	51 (38.6)	62 (35.0)	28 (23.9)	34 (56.7)[a]
Number of alcohol units per day; median (range)	0.0 (0–3)	0.0 (0–3)	0.0 (0–3)	1.0 (0–3)[c]
Chronic diseases				
Bronchial asthma	2 (1.5)	3 (1.7)	2 (1.7)	1 (1.7)
Obstructive pulmonary disease	10 (7.6)	13 (7.3)	10 (8.5)	3 (5)
Nephropathy	9 (6.8)	10 (5.6)	5 (4.3)	5 (8.3)
Hyperuricemia	11 (8.3)	14 (7.9)	4 (3.4)	10 (16.7)[b]
Cancer	4 (3)	4 (2.3)	1 (0.9)	3 (5)
Atherosclerosis-related diseases				
Coronary heart disease	40 (30.3)	56 (31.6)	43 (36.8)	13 (21.7)[a]
Myocardial infarction	24 (18.2)	32 (18.1)	25 (21.4)	7 (11.7)
Atrial fibrillation	18 (13.6)	24 (13.6)	15 (12.8)	9 (15)
Peripheral arterial disease	20 (15.2)	25 (14.1)	16 (13.7)	9 (15)
Cerebrovascular events				
Ischemic stroke	36 (27.3)	37 (20.9)	0 (0)	37 (61.7)[a]
Hemorrhagic stroke	1 (0.8)	2 (1.1)	0 (0)	2 (3.3)
Transient ischemic attack	13 (9.8)	15 (8.5)	0 (0)	15 (25)[a]
Amaurosis fugax	4 (3)	4 (2.3)	0 (0)	4 (6.7)[b]
Retinal infarction	2 (1.5)	2 (1.1)	0 (0)	2 (3.3)
Extracranial calcifications				
Absent		24 (13.6)	13 (11.1)	11 (18.3)
Spotty only		36 (20.3)	25 (21.4)	11 (18.3)
Large		117 (66.1)	79 (67.5)	38 (63.3)
Plaque type				
Lipid		89 (50.3)	53 (45.3)	36 (60)
Fibrous		47 (26.6)	35 (29.9)	12 (20)
Calcified		41 (23.2)	29 (24.8)	12 (20)

All data are presented as "n (%)," if not specified differently.
[a]Significant difference between asymptomatic and symptomatic patients at the level $p < 0.05$, analyzed using the χ^2-test.
[b]Significant difference between asymptomatic and symptomatic patients at the level $p < 0.05$, analyzed using Fisher's exact test.
[c]Significant difference between asymptomatic and symptomatic patients at the level $p < 0.05$, analyzed using the Mann–Whitney test.

TABLE 2 Risk factors for extracranial carotid plaque calcifications.

	Absent (n = 24)	Spotty calcification only (n = 36)	Large calcification (n = 117)	p-value[a]
Male sex	15 (62.5)	31 (86.1)	76 (65)	0.015[b]
Patient age; mean ± SD (years)	65.0 ± 9.8	68.2 ± 7.9	71.5 ± 7.9	0.027[d]
Atherosclerosis risk factors				
Hypertension	21 (87.5)	35 (97.2)	108 (92.3)	0.45[c]
Diabetes mellitus	8 (33.3)	15 (41.7)	52 (44.4)	0.77[b]
Hyperlipidemia	17 (70.8)	30 (80.3)	86 (73.5)	0.23[b]
Smoking	7 (29.2)	18 (50)	34 (29.1)	0.020[b]
Number of cigarettes per day; median (range)	0 (0–30)	2.5 (0–40)	0 (0–30)	0.014[e]
Alcohol	9 (37.5)	11 (30.6)	42 (35.9)	0.56[b]
Number of alcohol units per day; median (range)	0.0 (0–2)	0.0 (0–2)	0.0 (0–3)	0.41[e]
Chronic disease				
Bronchial asthma	1 (4.2)	1 (2.8)	1 (0.9)	0.42[e]
Obstructive pulmonary disease	1 (4.2)	5 (13.9)	7 (6)	0.16[c]
Nephropathy	1 (4.2)	1 (2.8)	8 (6.8)	0.69[c]
Hyperuricemia	3 (12.5)	4 (11.1)	7 (6)	0.29[c]
Cancer	2 (8.3)	0 (0)	2 (1.7)	>0.99[c]

All data are presented as "n (%)," if not specified differently.
[a]p-values are given for a difference between the groups with spotty calcifications only and large calcifications.
[b]Analyzed using the χ^2-test.
[c]Analyzed using Fisher's exact test where appropriate.
[d]Analyzed using the t-test.
[e]Analyzed using the Mann–Whitney test.

4 Discussion

We could not find an association between the presence and type of plaque calcifications and ipsilateral ischemic events (stroke, TIA, amaurosis fugax, or retinal infarction) in our study population. The presence of large carotid plaque calcification represented the highest association with coronary heart disease and atrial fibrillation, followed by higher patient age and female sex. On the other hand, spotty calcifications were associated with male sex, higher levels of smoking, and a greater prevalence in soft plaques.

While some evidence suggested a positive relationship between extracranial carotid calcification and ipsilateral ischemic events (10–12), particularly for spotty calcifications (23, 24), our study results are in agreement with the two recent comprehensive meta-analyses that identified negative association between carotid calcification and stroke (risk ratio: 0.75, OR: 0.5) (7, 9). In the interventional treatment, a large recent study found that a greater severity of carotid calcification (>50% of the plaque volume) is a significant risk factor for in-hospital stroke or death in 21,860 patients undergoing carotid artery stenting (25). Another study differentiated two calcium salts using dispersive X-ray microanalysis (hydroxyapatite, presented more in unstable plaque, and calcium oxalate, associated with plaque stability), suggesting different implications on plaque biology and subsequent stability (26). The distinction between these two types of calcium salts could have important clinical implications and can be investigated using dual-energy CT scanners to identify differences in tissue chemical composition (27, 28). Large calcifications relate with a gene transcriptional profile typical for stable plaques, repressed inflammation, and extracellular matrix organization (29). However, the association between spotty calcification and inflammatory markers, plaque instability, and accelerated disease progression should be noted (30). Finally, macrophages crucially control the mineralization process from microcalcification to bone-like tissue but are having accelerative and decelerative association with calcification. The bilateral interaction remains rather unexplored and should be studied (31).

Our study results proved the association between large calcification and generalized atherosclerosis manifested in a strong relationship with coronary heart disease, atrial fibrillation, and the severity of contralateral carotid stenosis. Two large population-based studies found the same results regarding the presence and extent of calcification and the risk of coronary heart disease (32, 33). However, a large meta-analysis revealed less prevalent carotid calcification in non-significant compared with significant coronary artery disease and moderate relation between carotid and coronary stenosis (34). Atherosclerosis affects both carotid and coronary systems, although not always in an identical phenotypic manner, so examination of carotid arteries is beneficial whenever coronary artery disease is suspected, mainly when large carotid calcification is detected. Despite the findings that patients with carotid atherosclerosis are at high risk of developing atrial fibrillation or both diseases coexist (35–37), no evidence of an association between carotid calcification and atrial fibrillation was found, which has been investigated in our study. Our

TABLE 3 Extracranial carotid plaque calcification and other plaque characteristics evaluated on computed tomography (CT) and magnetic resonance imaging (MRI).

	Spotty calcification only (n = 36)	Large calcification (n = 117)	p-value
Computed tomography			
Severity of ipsilateral stenosis; mean ± SD %	76.1 ± 15.1	71.4 ± 17.9	0.14[c]
Severity of contralateral stenosis; mean ± SD %	54.4 ± 33.3	68.0 ± 26.3	0.044[c]
Plaque type			
Lipid	26 (72.2)	47 (40.2)	<0.001[a]
Fibrous	9 (25)	30 (25.6)	
Calcified	1 (2.8)	40 (34.2)	
Surface			
Smooth	0 (0)	5 (4.3)	0.16[b]
Irregular	18 (50)	46 (39.3)	
Ulcerated	18 (50)	66 (56.4)	
Magnetic resonance imaging			
AHA plaque type			
IV–V	17 (56.7)	34 (37)	0.076[a]
VI	9 (30)	28 (30.4)	
VII	1 (3.3)	21 (22.8)	
VIII	3 (10)	9 (9.8)	
Lipid-rich necrotic core	26 (86.7)	60 (73.2)	0.13[a]
Intraplaque hemorrhage			
Acute	4 (12.5)	12 (11.1)	0.38[b]
Subacute	1 (3.1)	11 (10.2)	
Fibrous cap			
Thick	10 (33.3)	27 (32.1)	0.16[a]
Thin	7 (23.3)	12 (14.3)	
Ruptured	7 (23.3)	11 (13.1)	

All data are presented as "n (%)," if not specified differently. Note that in 17 plaques assessed through CT, the MRI quality was insufficient to analyze those plaques on MRI, resulting in 199 plaques evaluated by MRI and 216 by CT.
[a]Analyzed using a χ^2-test.
[b]Analyzed using Fisher's exact test.
[c]Analyzed using the Mann–Whitney test.

positive risk association between large carotid calcification and atrial fibrillation was found only in a recent study but significantly after adjustments only in coronary plaques (38). The higher degree of contralateral carotid stenosis associated with carotid calcification demonstrated the presence of generalized atherosclerosis. However, possible overestimation of stenosis severity on CTA due to blooming artifacts from large carotid calcification should be considered (39).

Active smoking or exposure to cigarette smoke is responsible as a catalyst for the formation and development of unstable plaques (40). In particular, carotid calcification is promoted by nicotine (41), but no study was found with evidence of the influence of smoking on spotty calcification. In our study, only spotty calcifications were more often in smokers in greater quantities. The coexistence of spotty carotid calcifications and soft plaque characteristics (LRNC and IPH) (42, 43), typically associated with ipsilateral cerebrovascular events, is suggested in studies even in non-stenosing plaques (24). We found only an association between spotty calcification and lipid plaque but not with IPH or ischemic events. Although spotty calcifications might be at risk of stroke, meta-analyses confirmed that other carotid plaque characteristics are more associated with stroke (44, 45). Male sex was associated with carotid calcification compared to women (46), particularly when looking only at spotty calcification, similar to our study results (47). Calcification growth is mainly associated with increasing age, calcification load, hypertension, or smoking over time (48).

Additionally, extracranial calcification was associated with diabetes mellitus, hypertension (49), or hyperlipidemia (50) in previous studies, but we did not find any difference between them and spotty and large calcification in our study. Regarding the treatment of carotid calcification, high-density lipoprotein appears to benefit vascular calcification (51). Beneficial changes in serum calcification markers were found after ipsilateral carotid artery stenting with intensive lipid-lowering therapy to enhance contralateral carotid plaque stability in patients with bilateral carotid stenosis (52). However, no preferred treatment for extracranial carotid calcification is recommended by current guidelines. To our knowledge, this is the first study that complexly investigated the type of CT-derived extracranial carotid calcification associated with multiple atherosclerotic-related systematic diseases. Large or spotty plaque calcifications were not associated with cerebrovascular events, suggesting an association with plaque stability with no need for acute treatment. However, larger prospective studies and future efforts are warranted to study the effect of, particularly, carotid spotty calcifications on stroke risk.

This study has the following limitations. (1) Approximately 90% of all patients enrolled in the ANTIQUE study were excluded from our analysis due to stenosis degree >30% or mostly because of missing CT and MRI examination together because ultrasound was the first-line imaging modality accompanied by CT if needed or before invasive intervention (MRI underwent only a minority of patients). (2) Laboratory markers were not measured, as our primary focus was on the imaging-based presence of calcification and its relation with various atherosclerosis and stroke risk factors and other diseases. (3) Various CT and MRI devices were utilized due to the multicenter study design, which could introduce minor discrepancies in evaluating calcification and other plaque characteristics. Diagnostic modalities were calibrated using five plaques *in vitro* to minimize this variation.

5 Conclusion

Although the presence and type of extracranial carotid plaque calcification were not related to ipsilateral ischemic events, large

TABLE 4 Extracranial carotid plaque calcification in association with atherosclerosis-related diseases and cerebrovascular events.

	Absent (n = 24)	Spotty calcification only (n = 36)	Large calcification (n = 117)	p-value[a]
Coronary heart disease	3 (12.5)	10 (27.8)	43 (36.8)	0.057[b]
Myocardial infarction	2 (8.3)	6 (16.7)	24 (20.5)	0.36[b]
Atrial fibrillation	0 (0)	4 (11.1)	20 (17.1)	0.015[c]
Peripheral arterial disease	2 (8.3)	8 (22.2)	15 (12.8)	0.25[b]
Ischemic stroke	6 (25)	9 (25)	22 (18.8)	0.63[b]
Hemorrhagic stroke	0 (0)	0 (0)	2 (1.7)	0.43[c]
Transient ischemic attack	4 (16.7)	2 (5.6)	9 (7.7)	0.33[c]
Amaurosis fugax	1 (4.2)	0 (0)	3 (2.6)	0.37[c]
Retinal infarction	0 (0)	0 (0)	2 (1.7)	0.43[c]

All data are presented as "n (%)" if not specified differently. The numbers in the table do not sum to column totals, as patients could have had multiple conditions.
[a]p-value for the overall test.
[b]Analyzed using a χ^2-test.
[c]Analyzed using Fisher's exact test.

calcification was strongly associated with coronary heart disease and atrial fibrillation. Higher levels of smoking was responsible for the presence of spotty calcification associated with male sex and the occurrence of soft plaques.

Data availability statement

The raw data supporting the conclusions of this article will be made available by the authors, without undue reservation.

Ethics statement

This study involving humans was reviewed and approved by the Ethics Committee of the University Hospital Ostrava (July 31, 2014, approval no. 605/2014) and performed according to the Declaration of Helsinki (1964) and its later amendments or comparable ethical standards. All patients gave written informed consent to participate in the study.

Author contributions

DP: Conceptualization, Data curation, Formal analysis, Investigation, Methodology, Visualization, Writing – original draft. DŠa: Conceptualization, Data curation, Methodology, Writing – review & editing, Formal analysis, Visualization, Writing – original draft. DŠk: Conceptualization, Data curation, Methodology, Writing – review & editing, Funding acquisition, Project administration, Supervision.

Group members for The ANTIQUE Study Group

David Netuka, Jiří Vrána, František Charvát (Military University Hospital Prague, Prague), Petra Kešnerová (University Hospital Motol, Prague); Tomáš Hrbáč, Tomáš Jonszta (University of Ostrava and University Hospital Ostrava, Ostrava); Roman Herzig (Charles University and University Hospital Hradec Králové, Hradec Králové).

Funding

The author(s) declare that financial support was received for the research, authorship, and/or publication of this article. This study was supported by the Ministry of Health of the Czech Republic (Grant Nos. NV-19-04-00270, NV-19-08-00362, and NU22-09-00389).

Conflict of interest

The authors declare that the research was conducted in the absence of any commercial or financial relationships that could be construed as a potential conflict of interest.

Generative AI statement

The authors declare that no Gen AI was used in the creation of this manuscript.

Publisher's note

Supplementary material

The Supplementary material for this article can be found online at: https://www.frontiersin.org/articles/10.3389/fneur.2025.1532883/full#supplementary-material

References

1. Song P, Fang Z, Wang H, Cai Y, Rahimi K, Zhu Y, et al. Global and regional prevalence, burden, and risk factors for carotid atherosclerosis: a systematic review, meta-analysis, and modelling study. *Lancet Glob Health*. (2020) 8:e721–9. doi: 10.1016/S2214-109X(20)30117-0

2. Hart RG, Diener HC, Coutts SB, Easton JD, Granger CB, O'Donnell MJ, et al. Embolic strokes of undetermined source: the case for a new clinical construct. *Lancet Neurol*. (2014) 13:429–38. doi: 10.1016/S1474-4422(13)70310-7

3. Martin SS, Aday AW, Almarzooq ZI, Anderson CAM, Arora P, Avery CL, et al. 2024 heart disease and stroke statistics: a report of US and global data from the American Heart Association. *Circulation*. (2024) 149:e347–913. doi: 10.1161/CIR.0000000000001209

4. Tesauro M, Mauriello A, Rovella V, Annicchiarico-Petruzzelli M, Cardillo C, Melino G, et al. Arterial ageing: from endothelial dysfunction to vascular calcification. *J Intern Med*. (2017) 281:471–82. doi: 10.1111/joim.12605

5. Saba L, Loewe C, Weikert T, Williams MC, Galea N, Budde RPJ, et al. State-of-the-art CT and MR imaging and assessment of atherosclerotic carotid artery disease: standardization of scanning protocols and measurements-a consensus document by the European Society of Cardiovascular Radiology (ESCR). *Eur Radiol*. (2023) 33:1063–87. doi: 10.1007/s00330-022-09024-7

6. Ahmed M, McPherson R, Abruzzo A, Thomas SE, Gorantla VR. Carotid artery calcification: what we know so far. *Cureus*. (2021) 13:e18938. doi: 10.7759/cureus.18938

7. Baradaran H, Al-Dasuqi K, Knight-Greenfield A, Giambrone A, Delgado D, Ebani EJ, et al. Association between carotid plaque features on CTA and cerebrovascular ischemia: a systematic review and meta-analysis. *Am J Neuroradiol*. (2017) 38:2321–6. doi: 10.3174/ajnr.A5436

8. Nandalur KR, Hardie AD, Raghavan P, Schipper MJ, Baskurt E, Kramer CM. Composition of the stable carotid plaque: insights from a multidetector computed tomography study of plaque volume. *Stroke*. (2007) 38:935–40. doi: 10.1161/01.STR.0000257995.74834.92

9. Homssi M, Saha A, Delgado D, RoyChoudhury A, Thomas C, Lin M, et al. Extracranial carotid plaque calcification and cerebrovascular ischemia: a systematic review and meta-analysis. *Stroke*. (2023) 54:2621–8. doi: 10.1161/STROKEAHA.123.042807

10. Nandalur KR, Baskurt E, Hagspiel KD, Finch M, Phillips CD, Bollampally SR, et al. Carotid artery calcification on CT may independently predict stroke risk. *Am J Roentgenol*. (2006) 186:547–52. doi: 10.2214/AJR.04.1216

11. Elias-Smale SE, Odink AE, Wieberdink RG, Finch M, Phillips CD, Bollampally SR, et al. Carotid, aortic arch and coronary calcification are related to history of stroke: the Rotterdam study. *Atherosclerosis*. (2010) 212:656–60. doi: 10.1016/j.atherosclerosis.2010.06.037

12. Kan Y, He W, Ning B, Li H, Wei S, Yu T. The correlation between calcification in carotid plaque and stroke: calcification may be a risk factor for stroke. *Int J Clin Exp Pathol*. (2019) 12:750–8.

13. Agacayak KS, Guler R, Sezgin Karatas P. Relation between the incidence of carotid artery calcification and systemic diseases. *Clin Interv Aging*. (2020) 15:821–6. doi: 10.2147/CIA.S256588

14. Školoudík D, Kešnerová P, Hrbáč T, Netuka D, Vomáčka J, Langová K, et al. Visual and digital analysis of the ultrasound image in a stable and progressive carotid atherosclerotic plaque. *Cesk Slov Neurol N*. (2021) 84/117:38–44. doi: 10.48095/cccsnn202138

15. Školoudík D, Kešnerová P, Hrbáč T, Netuka D, Vomáčka J, Langová K, et al. Risk factors for carotid plaque progression after optimising the risk factor treatment: substudy results of the Atherosclerotic Plaque Characteristics Associated with a Progression Rate of the Plaque and a Risk of Stroke in Patients with the carotid Bifurcation Plaque Study (ANTIQUE). *Stroke Vasc Neurol*. (2022) 7:132–9. doi: 10.1136/svn-2021-001068

16. von Reutern GM, von Büdingen HJ. Ultrasound diagnosis of cerebrovascular disease: Doppler sonography of the extra- and intracranial arteries duplex scanning. *2nd* ed. Stuttgart: Thieme (1993).

17. Sacco RL, Kasner SE, Broderick JP, Caplan LR, Connors JJ, Culebras A, et al. An updated definition of stroke for the 21st century: a statement for healthcare professionals from the American Heart Association/American Stroke Association. *Stroke*. (2013) 44:2064–89. doi: 10.1161/STR.0b013e318296aeca

18. HJM B, Taylor DW, Haynes RB, Sackett DL, Peerless SJ, Ferguson GG, et al. Beneficial effect of carotid endarterectomy in symptomatic patients with high-grade carotid stenosis. *N Engl J Med*. (1991) 325:445–53. doi: 10.1056/NEJM199108153250701

19. de Weert TT, Ouhlous M, Meijering E, Zondervan PE, Hendriks JM, van Sambeek MR, et al. *In vivo* characterization and quantification of atherosclerotic carotid plaque components with multidetector computed tomography and histopathological correlation. *Arterioscler Thromb Vasc Biol*. (2006) 26:2366–72. doi: 10.1161/01.ATV.0000240518.90124.57

20. Motoyama S, Sarai M, Harigaya H, Anno H, Inoue K, Hara T, et al. Computed tomographic angiography characteristics of atherosclerotic plaques subsequently resulting in acute coronary syndrome. *J Am Coll Cardiol*. (2009) 54:49–57. doi: 10.1016/j.jacc.2009.02.068

21. Cai JM, Hatsukami TS, Ferguson MS, Small R, Polissar NL, Yuan C. Classification of human carotid atherosclerotic lesions with *in vivo* multicontrast magnetic resonance imaging. *Circulation*. (2002) 106:1368–73. doi: 10.1161/01.cir.0000028591.44554.f9

22. Saam T, Ferguson MS, Yarnykh VL, Takaya N, Xu D, Polissar NL, et al. Quantitative evaluation of carotid plaque composition by *in vivo* MRI. *Arterioscler Thromb Vasc Biol*. (2005) 25:234–9. doi: 10.1161/01.ATV.0000149867.61851.31

23. Zhang F, Yang L, Gan L, Fan Z, Zhou B, Deng Z, et al. Spotty calcium on cervicocerebral computed tomography angiography associates with increased risk of ischemic stroke. *Stroke*. (2019) 50:859–66. doi: 10.1161/STROKEAHA.118.023273

24. Homssi M, Vora A, Zhang C, Baradaran H, Kamel H, Gupta A. Association between spotty calcification in nonstenosing extracranial carotid artery plaque and ipsilateral ischemic stroke. *J Am Heart Assoc*. (2023) 12:e028525. doi: 10.1161/JAHA.122.028525

25. Mota L, Wang SX, Cronenwett JL, Nolan BW, Malas MB, Schermerhorn ML, et al. Association of stroke or death with severity of carotid lesion calcification in patients undergoing carotid artery stenting. *J Vasc Surg*. (2024) 79:305–315.e3. doi: 10.1016/j.jvs.2023.10.046

26. Bischetti S, Scimeca M, Bonanno E, Federici M, Anemona L, Menghini R, et al. Carotid plaque instability is not related to quantity but to elemental composition of calcification. *Nutr Metab Cardiovasc Dis*. (2017) 27:768–74. doi: 10.1016/j.numecd.2017.05.006

27. Manglaviti G, Tresoldi S, Guerrer CS, Di Leo G, Montanari E, Sardanelli F, et al. *In vivo* evaluation of the chemical composition of urinary stones using dual-energy CT. *AJR Am J Roentgenol*. (2011) 197:W76–83. doi: 10.2214/AJR.10.5217

28. Mannelli L, MacDonald L, Mancini M, Ferguson M, Shuman WP, Ragucci M, et al. Dual energy computed tomography quantification of carotid plaques calcification: comparison between monochromatic and polychromatic energies with pathology correlation. *Eur Radiol*. (2015) 25:1238–46. doi: 10.1007/s00330-014-3523-0

29. Karlöf E, Seime T, Dias N, Lengquist M, Witasp A, Almqvvist H, et al. Correlation of computed tomography with carotid plaque transcriptomes associates calcification with lesion-stabilization. *Atherosclerosis*. (2019) 288:175–85. doi: 10.1016/j.atherosclerosis.2019.05.005

30. Joshi NV, Vesey AT, Williams MC, Shah AS, Calvert PA, Craighead FH, et al. ^{18}F-fluoride positron emission tomography for identification of ruptured and high-risk coronary atherosclerotic plaques: a prospective clinical trial. *Lancet*. (2014) 383:705–13. doi: 10.1016/S0140-6736(13)61754-7

31. Waring OJ, Skenteris NT, Biessen EAL, Donners MMPC. Two-faced Janus: the dual role of macrophages in atherosclerotic calcification. *Cardiovasc Res*. (2022) 118:2768–77. doi: 10.1093/cvr/cvab301

32. Mehta A, Rigdon J, Tattersall MC, German CA, Barringer TA 3rd, Joshi PH, et al. Association of carotid artery plaque with cardiovascular events and incident coronary artery calcium in individuals with absent coronary calcification: the MESA. *Circ Cardiovasc Imaging*. (2021) 14:e011701. doi: 10.1161/CIRCIMAGING.120.011701

33. Gepner AD, Young R, Delaney JA, Budoff MJ, Polak JF, Blaha MJ, et al. Comparison of carotid plaque score and coronary artery calcium score for predicting cardiovascular disease events: the multi-ethnic study of atherosclerosis. *J Am Heart Assoc*. (2017) 6:e005179. doi: 10.1161/JAHA.116.005179

34. Bytyçi I, Shenouda R, Wester P, Henein MY. Carotid atherosclerosis in predicting coronary artery disease: a systematic review and meta-analysis. *Arterioscler Thromb Vasc Biol*. (2021) 41:e224–37. doi: 10.1161/ATVBAHA.120.315747

35. Willeit K, Pechlaner R, Egger G, Weger S, Oberhollenzer M, Willeit J, et al. Carotid atherosclerosis and incident atrial fibrillation. *Arterioscler Thromb Vasc Biol*. (2013) 33:2660–5. doi: 10.1161/ATVBAHA.113.302272

36. Heeringa J, van der Kuip DA, Hofman A, Kors JA, van Rooij FJ, Lip GY, et al. Subclinical atherosclerosis and risk of atrial fibrillation: the Rotterdam study. *Arch Intern Med*. (2007) 167:382–7. doi: 10.1001/archinte.167.4.382

37. Noubiap JJ, Agbaedeng TA, Tochie JN, Nkeck JR, Ndoadoumgue AL, Fitzgerald JL, et al. Meta-analysis comparing the frequency of carotid artery stenosis in patients with atrial fibrillation and vice versa. *Am J Cardiol*. (2021) 138:72–9. doi: 10.1016/j.amjcard.2020.10.017

38. Geurts S, Bos MM, van der Toorn JE, Stricker BHC, Ghanbari M, Kors JA, et al. Arteriosclerotic calcification and atrial fibrillation in the general population: the Rotterdam study. *Am J Cardiol*. (2024) 231:62–9. doi: 10.1016/j.amjcard.2024.09.002

39. Pakizer D, Vybíralová A, Jonszta T, Roubec M, Král M, Chovanec V, et al. Peak systolic velocity ratio for evaluation of internal carotid artery stenosis correlated with plaque morphology: substudy results of the ANTIQUE study. *Front Neurol*. (2023) 14:1206483. doi: 10.3389/fneur.2023.1206483

40. Csordas A, Bernhard D. The biology behind the atherothrombotic effects of cigarette smoke. *Nat Rev Cardiol*. (2013) 10:219–30. doi: 10.1038/nrcardio.2013.8

41. Petsophonsakul P, Burgmaier M, Willems B, Heeneman S, Stadler N, Gremse F, et al. Nicotine promotes vascular calcification via intracellular Ca^{2+}-mediated, Nox5-

induced oxidative stress, and extracellular vesicle release in vascular smooth muscle cells. *Cardiovasc Res*. (2022) 118:2196–210. doi: 10.1093/cvr/cvab244

42. van den Bouwhuijsen QJ, Bos D, Ikram MA, Hofman A, Krestin GP, Franco OH, et al. Coexistence of calcification, intraplaque hemorrhage and lipid Core within the asymptomatic atherosclerotic carotid plaque: the Rotterdam study. *Cerebrovasc Dis*. (2015) 39:319–24. doi: 10.1159/000381138

43. Kataoka Y, Puri R, Hammadah M, Duggal B, Uno K, Kapadia SR, et al. Spotty calcification and plaque vulnerability in vivo: frequency-domain optical coherence tomography analysis. *Cardiovasc Diagn Ther*. (2014) 4:460–9. doi: 10.3978/j.issn.2223-3652.2014.11.06

44. Kamtchum-Tatuene J, Noubiap JJ, Wilman AH, Saqqur M, Shuaib A, Jickling GC. Prevalence of high-risk plaques and risk of stroke in patients with asymptomatic carotid stenosis: a meta-analysis. *JAMA Neurol*. (2020) 77:1524–35. doi: 10.1001/jamaneurol.2020.2658

45. Zhang Y, Bai Y, Xie J, Wang J, He L, Huang M, et al. Carotid plaque components and other carotid artery features associated with risk of stroke: a systematic review and meta-analysis. *J Stroke Cerebrovasc Dis*. (2022) 31:106857. doi: 10.1016/j.jstrokecerebrovasdis.2022.106857

46. Plank F, Beyer C, Friedrich G, Wildauer M, Feuchtner G. Sex differences in coronary artery plaque composition detected by coronary computed tomography: quantitative and qualitative analysis. *Neth Heart J*. (2019) 27:272–80. doi: 10.1007/s12471-019-1234-5

47. Kataoka Y, Wolski K, Uno K, Puri R, Tuzcu EM, Nissen SE, et al. Spotty calcification as a marker of accelerated progression of coronary atherosclerosis: insights from serial intravascular ultrasound. *J Am Coll Cardiol*. (2012) 59:1592–7. doi: 10.1016/j.jacc.2012.03.012

48. van Gils MJ, Bodde MC, Cremers LG, Dippel DW, van der Lugt A. Determinants of calcification growth in atherosclerotic carotid arteries; a serial multi-detector CT angiography study. *Atherosclerosis*. (2013) 227:95–9. doi: 10.1016/j.atherosclerosis.2012.12.017

49. Gao X, Song J, Watase H, Hippe DS, Zhao X, Canton G, et al. Differences in carotid plaques between symptomatic patients with and without diabetes mellitus. *Arterioscler Thromb Vasc Biol*. (2019) 39:1234–9. doi: 10.1161/ATVBAHA.118.312092

50. Odink AE, van der Lugt A, Hofman A, Hunink MG, Breteler MM, Krestin GP, et al. Risk factors for coronary, aortic arch and carotid calcification; the Rotterdam study. *J Hum Hypertens*. (2010) 24:86–92. doi: 10.1038/jhh.2009.42

51. Pletsch-Borba L, Selwaness M, van der Lugt A, Hofman A, Franco OH, Vernooij MW. Change in carotid plaque components: a 4-year follow-up study with serial MR imaging. *JACC Cardiovasc Imaging*. (2018) 11:184–92. doi: 10.1016/j.jcmg.2016.12.026

52. Akers EJ, Nicholls SJ, Di Bartolo BA. Plaque calcification: Do lipoproteins have a role? *Arterioscler Thromb Vasc Biol*. (2019) 39:1902–10. doi: 10.1161/ATVBAHA.119.311574

frontiers | Frontiers in Neurology

TYPE Brief Research Report
PUBLISHED 04 February 2025
DOI 10.3389/fneur.2025.1490799

OPEN ACCESS

EDITED BY
Faheem G. Sheriff,
Texas Tech University Health Science Center, United States

REVIEWED BY
Eugene Lin,
St. Vincent Mercy Medical Center, United States
Rashid Ahmed,
Massachusetts General Hospital and Harvard Medical School, United States

*CORRESPONDENCE
Shuang He
67105704@qq.com

RECEIVED 03 September 2024
ACCEPTED 13 January 2025
PUBLISHED 04 February 2025

CITATION
Bao L, Pan Z, Ji H and He S (2025) Pipeline embolization device-assisted angioplasty for type II proatlantal intersegmental artery dissection inducing an embolic shower. *Front. Neurol.* 16:1490799. doi: 10.3389/fneur.2025.1490799

Pipeline embolization device-assisted angioplasty for type II proatlantal intersegmental artery dissection inducing an embolic shower

Li Bao[1,2], Zhenguo Pan[3], Haifeng Ji[3] and Shuang He[1]*

[1]Department of Stroke Center, Affiliated Hospital of Nantong University, Nantong, China, [2]Medical College of Nantong University, Nantong, China, [3]Department of Neurology, Xiangshui People's Hospital, Yancheng, China

The proatlantal intersegmental artery (PIA) plays a crucial role in blood supply during embryonic development, and failure of its closure can lead to the persistent proatlantal intersegmental artery (PPIA), which may result in pathological changes such as dissection and aneurysms. We present a case of a patient with right type II PPIA dissection inducing an embolic shower, accompanied by left vertebral artery hypoplasia (VAH). Digital subtraction angiography (DSA) and high-resolution magnetic resonance vascular wall imaging (HRMR-VWI) showed the aneurysmal dilation of the false lumen in the right PPIA dissection and indicated the high risk of mural thrombosis and dislodgement. Following a comprehensive evaluation of the patient's condition, we conducted pipeline embolization device (PED)-assisted angioplasty to treat the PPIA dissection and mitigate the risk of recurrent strokes. Postoperative follow-up indicated that the patient recovered smoothly, with no signs of recurrent stroke. This case highlights the critical need for prompt recognition and intervention in cases of rare vascular variants. The flow diverter implantation can greatly enhance patient outcomes and lower the risk of recurrent strokes, offering important insights for the clinical management of similar cases. Additional research is necessary to investigate the underlying pathological mechanisms of PPIA and its connection to stroke occurrence, which will help refine treatment strategies in the future.

KEYWORDS

proatlantal intersegmental artery, pipeline embolization device, dissection, stroke, angioplasty, HR-VWI

Introduction

In embryonic development, the primitive carotid-vertebrobasilar anastomoses facilitate blood flow from the primitive internal carotid artery (ICA) to the posterior circulation. There are four types of carotid-vertebrobasilar anastomoses: the primitive trigeminal, otic, hypoglossal and proatlantal intersegmental artery (PIA) (1). The regression of these anastomotic channels begins as the embryo reaches a size of 7 to 12 mm, with the PIA being the last one (1, 2). In cases where anastomotic closure does not occur, these vessels persist into adulthood (2, 3). Among these, the persistent proatlantal intersegmental artery (PPIA) represents the rarest type of persistent carotid-vertebrobasilar anastomosis in adults, often identified incidentally (4). The PPIA originates from the common carotid artery (CCA),

external carotid artery (ECA), or ICA, and penetrates the cranial cavity via the foramen magnum of the occipital bone, converging with the V3 segment of the vertebral artery (VA). There are two primary variants of PPIA: type I, originating from the ICA, and type II, more frequently arising from the ECA (5, 6).

This report examines a rare instance of a right type II PPIA dissection, which repeatedly inducing an embolic shower (ES). We determined that the ES were caused by thrombus dislodgement from the false lumen of the PPIA dissection. Given the ineffectiveness of pharmacological treatment, we performed PPIA angioplasty using a pipeline embolization device (PED), aiming to prevent ES caused by thrombus dislodgement.

Case

A 53-year-old male with a history of paroxysmal dizziness and hypertension experienced a sudden exacerbation of dizziness and onset of left hemiparesis. Initial evaluation at a local hospital showed stable vital signs and unremarkable laboratory findings. Cranial magnetic resonance imaging (MRI) revealed an acute infarction in the right brainstem and right cerebellum, with encephalomalacia in the right thalamus (Supplementary Figures S1A–C). Magnetic resonance angiography (MRA) indicated left VA agenesis (Supplementary Figure S1D). The patient was diagnosed with multiple lacunar strokes (LS) and received conservative treatment including dual antiplatelet therapy (aspirin and clopidogrel), lipid-lowering agents (statins), and neuroprotective medications (edaravone and N-butylphthalide). Computed tomography (CT) 1 week later revealed a hypodense lesion in the right cerebellum (Supplementary Figure S1E).

Despite ongoing antiplatelet therapy, 2.5 months after initial stroke the patient developed symptoms of stroke, including bilateral blurred vision, facial asymmetry, and unsteady gait, after waking from a nap on the morning. CT scan revealed lacunar infarction and encephalomalacia in the right cerebellum and right thalamus (Supplementary Figures S2A,B). MRI suggested new infarct foci in the right cerebellum and left thalamus, alongside the earlier encephalomalacia in the right cerebellum and right brainstem (Supplementary Figures S2D–F). MRA once again confirmed left VA agenesis (Supplementary Figure S2C). Given the contraindication for intravenous thrombolysis owing to the patient's recent stroke history, the treating team opted to continue with conservative management.

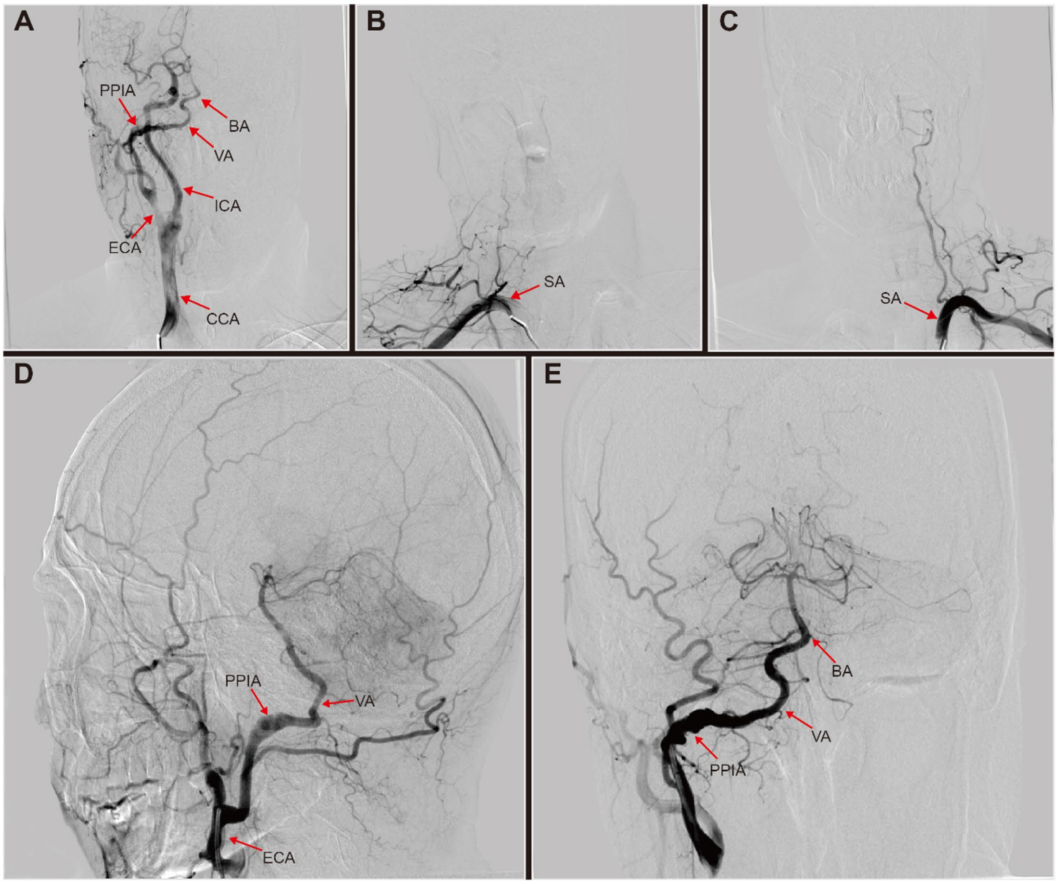

FIGURE 1
Digital subtraction angiography (DSA) of this patient with right persistent proatlantal intersegmental artery (PPIA) dissection. **(A)** Right common carotid artery (CCA) injection revealed a prominent type II PPIA branching off from the right external carotid artery (ECA). This artery connected to the ipsilateral vertebral artery (VA), supplying basilar artery (BA). **(B)** Right subclavian artery (SA) injection showed no origin of the right VA from the SA. **(C)** Left SA injection revealed left VA hypoplasia with no visualization of BA. **(D,E)** Right ECA injection revealed a right PPIA with dissection aneurysmal dilatated, which connected to the right VA to supply the BA.

Following stabilization, the patient was transferred to our institution 19 days after second stroke to elucidate the etiology of recurrent LS and to improve his prognosis. A digital subtraction angiogram (DSA) was performed to assess the cerebral vasculature. The DSA revealed a branch from the right external carotid artery (ECA) merging into the ipsilateral vertebral artery (VA), absent VA branching from the right subclavian artery, and left vertebral artery hypoplasia (VAH) with no significant abnormalities in the remaining vessels (Figures 1A–E). Further review of DSA led to the diagnosis of a right type II persistent proatlantal intersegmental artery (PPIA) dissection with an aneurysmal dilatation in the false lumen, alongside left VAH. After ruling out atrial fibrillation by 24-h ambulatory electrocardiographic monitoring, we hypothesized that mural thrombus dislodgement from the PPIA dissection was the probable cause of the ES observed in this patient.

To confirm this diagnosis, high-resolution magnetic resonance imaging (HRMRI) was performed, which indicated infarct and encephalomalacia in the right cerebellum, right brainstem, and right thalamus (Figures 2A–C). MRA corroborated the presence of a right type II PPIA dissection with contralateral VAH, consistent with DSA findings (Figure 2D). High-resolution magnetic resonance vascular wall imaging (HRMR-VWI) displayed a subacute intramural hematoma and intimal flap thickening in the dissection's false lumen, which were considered high-risk factors for mural thrombosis and dislodgement (Figures 2E,F).

Given the patient's history and HRMR-VWI results, we concluded that addressing the right type II PPIA dissection could mitigate the risk of the recurrent ES. Given that the true lumen stenosis at the site of the dissection is not severe, we chose to perform simple PED implantation for PPIA angioplasty. The PED (4.5 mm × 30 mm; Flex, Medtronic, United States) was successfully delivered and deployed under the guidance of the microcatheter (Phenom27, Medtronic, United States) and microwire (Synchro2, Stryker, United States) after the guide catheter (Envoy, Codman, United States) was in position (Figure 3E). Postoperatively, three-dimensional reconstructions of the DSA images demonstrated the PED effectively reshaping the PPIA, isolating the aneurysmal dilated false lumen, and securing posterior circulation blood flow (Figures 3A–I).

One month post-procedure, the patient reported no new symptoms. A repeat cranial CTA demonstrated significant reduction

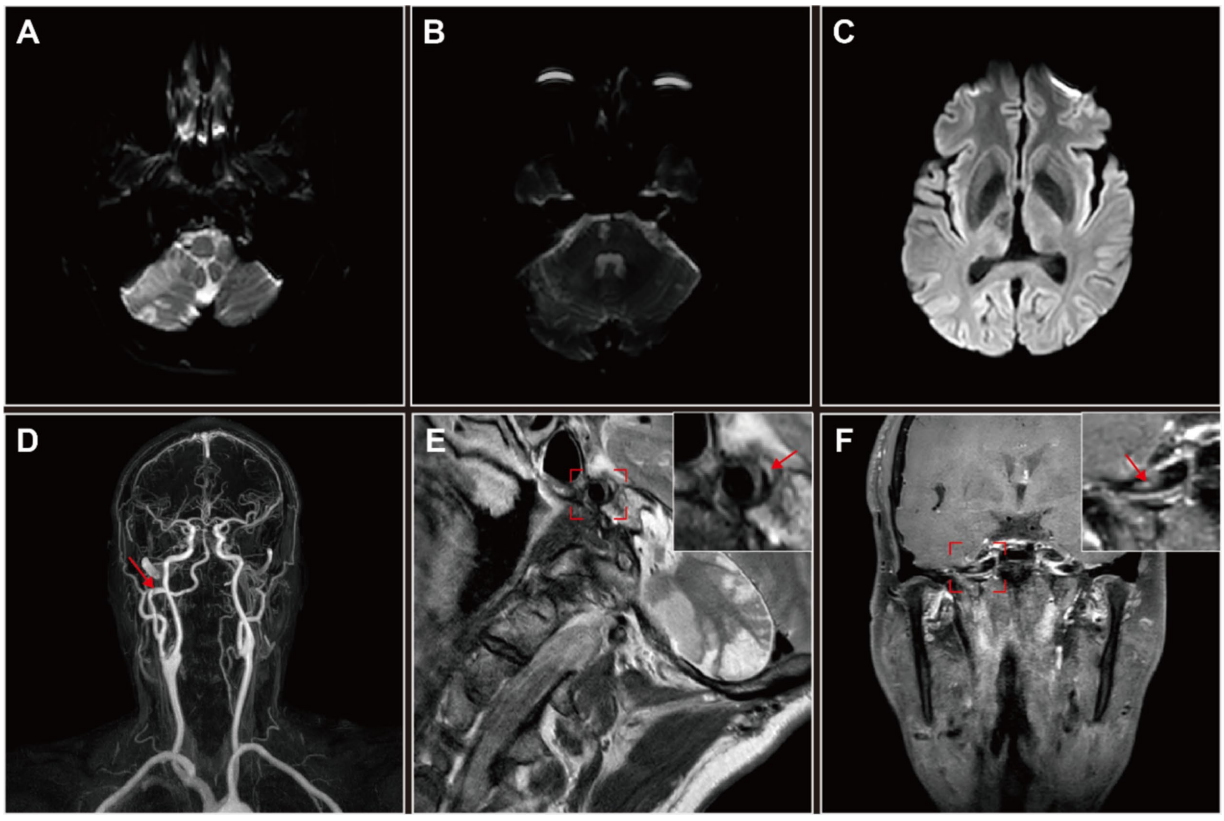

FIGURE 2
High-resolution magnetic resonance imaging (HRMRI) of the head and neck in this patient with right persistent proatlantal intersegmental artery (PPIA) dissection. **(A–C)** Diffusion weighted imaging (DWI) revealed multiple infarct foci and encephalomalacia across various cerebral regions: the right cerebellum **(A)**, right brainstem **(B)** and right thalamus **(C)**. **(D)** MRA suggested an dissection aneurysmal dilatation of the right PPIA, which is the exclusive supplier to the vertebrobasilar artery system. **(E,F)** High-resolution magnetic resonance vascular wall imaging (HRMR-VWI). **(E)** Sagittal contrast-enhanced T2-weighted imaging revealed eccentric thickening of the PPIA arterial wall accompanied by a crescent-shaped subacute-phase intramural hematoma (arrow) in the thickened lumen wall. The detailed sagittal profile of the PPIA, highlighted in a red frame, is positioned in the upper right corner. **(F)** Coronal contrast-enhanced T1-weighted imaging revealed inhomogeneous thickening of the intimal flap of the PPIA dissection (arrow), suggesting irregular attachment of fibrous tissue. The detailed coronal profile of the PPIA, encased in a red frame, is situated in the upper right corner. Both coronal and sagittal HRMR-VWI indicated a right PPIA dissection aneurysmal dilatation and a high risk of mural thrombosis and dislodgement.

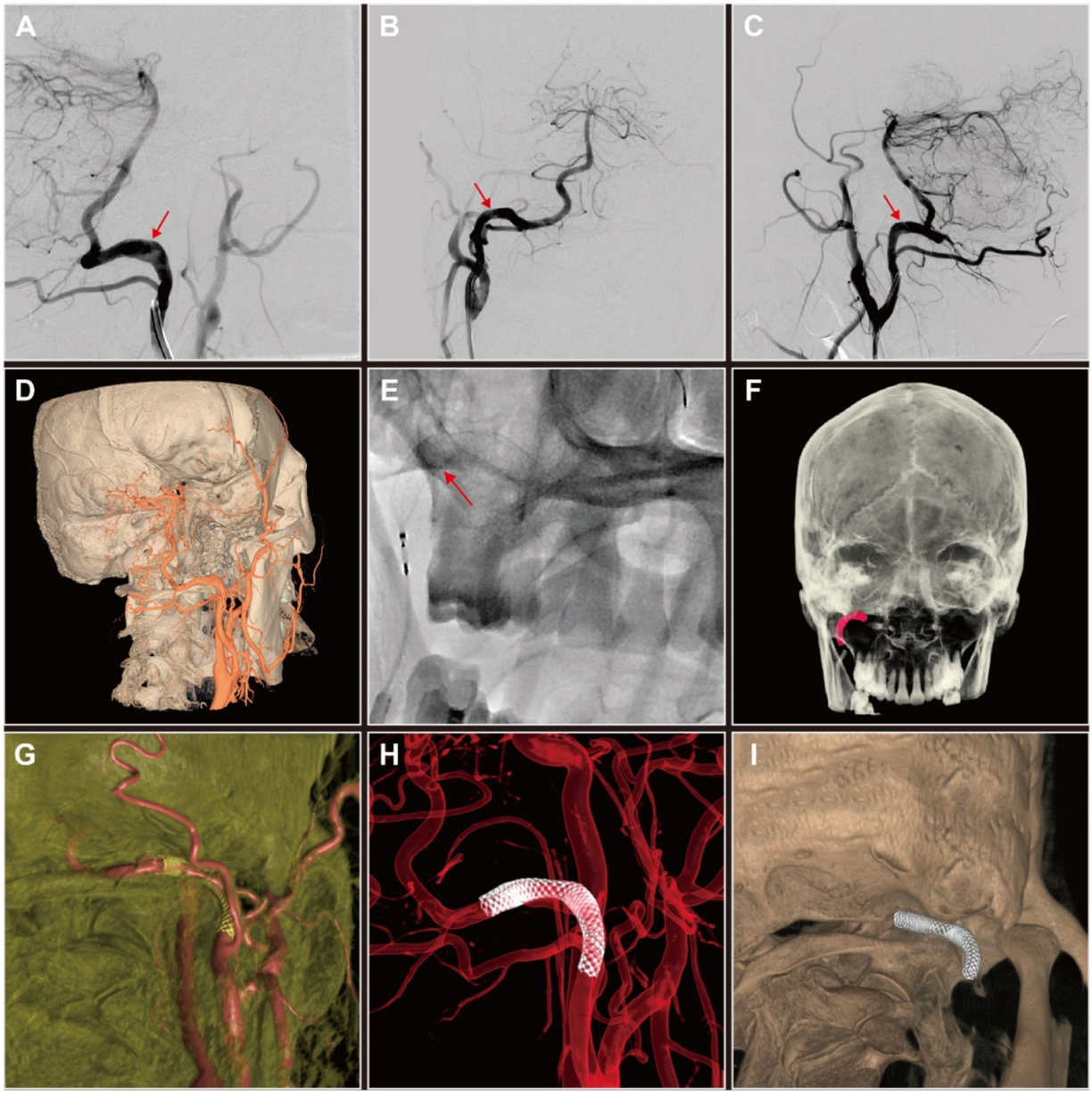

FIGURE 3
Digital subtraction angiography (DSA) and three-dimensional (3D) reconstruction of persistent proatlantal intersegmental artery (PPIA) angioplasty with flow diverter implantation of this patient with right PPIA dissection. **(A–C)** Comparative DSA images of the right PPIA dissection (arrow) pre-implantation **(A)** and post-implantation **(B,C)** of pipeline embolization device (PED). **(D)** DSA-based 3D reconstruction of PPIA dissection prior to PED implantation. **(E)** Release of PED. **(F–I)** Post-implantation DSA-based 3D reconstruction of PED in the PPIA highlighted the improvements in vascular architecture and the therapeutic benefits of the intervention.

in the aneurysmal dilatation of the right PPIA dissection and optimal remodeling of the PPIA, compared to previous images (Figure 4).

Discussion

By the end of the sixth week of gestation, when the embryo has developed to 12–14 mm, the PIA physiologically regresses completely, leading to the formation of the VA (7). However, poor anastomotic closure can result in persistent patency of the primitive PIA, transforming into a PPIA, and hypoplasia of the ipsilateral VA (3). Embryologically, VA is constructed through the fusion of multiple longitudinal anastomoses between neighboring cervical intersegmental arteries (8). Difficulty in fusion between any of the segments of the VA under the influence of various congenital or acquired factors that impede VA formation could also lead to persistent opening of the ipsilateral PIA to ensure posterior circulatory blood supply. A notable case report by Zuflacht et al. (9) illustrated a unique unilateral type II PPIA functioning in conjunction with the ipsilateral CCA to sustain whole brain blood flow.

PPIA has been implicated in a variety of vascular pathologies, albeit infrequently. It has been reported that type I PPIA could cause top of the basilar syndrome (10), pontine infarction (11), cerebral watershed and posterior circulation infarction (12). Type II PPIA

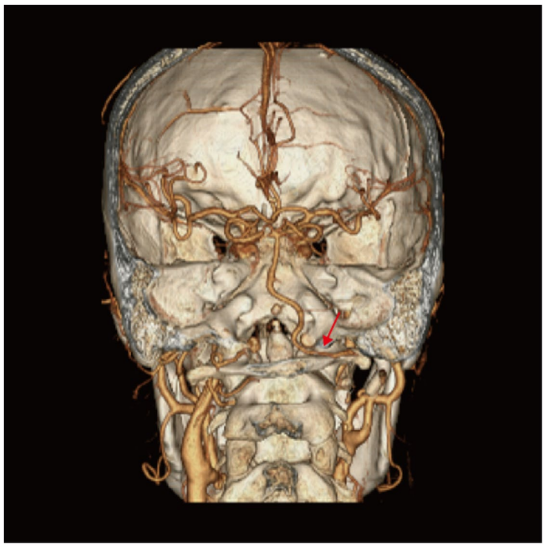

FIGURE 4
Computed tomography angiography (CTA) of the patient 1 month after persistent proatlantal inter-segmental artery (PPIA) angioplasty with flow diverter implantation. Right PPIA (arrow) aneurysmal dilatation was significantly improved compared to the pre-intervention images.

could cause dizziness and syncope (13), transient hand weakness and amaurosis fugax when occurring with severe ICA stenosis (14). The linkage between PPIA, VAH, and intracranial aneurysms has been extensively documented, highlighting a prevalent association with vascular anomalies (5, 15, 16).

In the present case, diagnostic exclusions were made for atherosclerotic and cardioembolic cerebral infarction based on an infarct diameter of less than 1.5 cm, absence of atherosclerotic vulnerable plaques and vessels with no greater than 50% stenosis on DSA and HRMR-VWI, as well as the absence of atrial fibrillation in this patient (17). A right type II PPIA with a dissection characterized by aneurysmal dilatation of the false lumen, elevating the risk of mural thrombosis. This pathology was identified as the primary cause of the ES in a 53-year-old patient. Given the high-risk nature of the pathology, characterized by subacute intramural hematoma and extensive fibrous tissue attachment to the intimal flap, and the ineffectiveness of conservative drug treatments, we preferred PED implantation to avoid thrombus formation and dislodgement. Follow-up neurologic function assessment, CTA and CT Perfusion (CTP) showed that the PED effectively maintained posterior circulation, and the patient experienced no recurrent ischemic strokes.

This case is the first documented instance of a type II PPIA dissection leading to an ES. The type II PPIA dissection was initially identified on DSA as originating from the ECA and displayed aneurysmal dilatation changes before traversing the occipital foramen. Although intravascular imaging techniques such as MRA and DSA are adept at visualizing lumen morphology, they fall short in detecting dissection lesions with normal vessel diameters or fully delineating the aneurysmal wall. The unique capabilities of HRMR-VWI allowed for the detection of likely thrombosis formation and dislodgement within the dissected PPIA, confirming its role as the causative lesion.

In general, early and precise identification of vascular variants like PPIA is crucial in clarifying the clinical diagnoses, underlying etiologies, and therapeutic options. While PPIA is often linked with serious posterior circulation strokes and other cerebrovascular pathologies, it can also facilitate critical interventions such as stent thrombectomy (18), angioplasty (19), and reflux compensation (20), occasionally proving to be lifesaving.

Data availability statement

The original contributions presented in the study are included in the article/Supplementary material, further inquiries can be directed to the corresponding author.

Ethics statement

Written informed consent was obtained from the individual(s) for the publication of any potentially identifiable images or data included in this article.

Author contributions

LB: Conceptualization, Data curation, Formal analysis, Funding acquisition, Investigation, Methodology, Project administration, Resources, Software, Supervision, Validation, Visualization, Writing – original draft, Writing – review & editing. ZP: Conceptualization, Data curation, Writing – review & editing. HJ: Writing – review & editing. SH: Resources, Supervision, Writing – review & editing.

Funding

The author(s) declare that no financial support was received for the research, authorship, and/or publication of this article.

Conflict of interest

The authors declare that the research was conducted in the absence of any commercial or financial relationships that could be construed as a potential conflict of interest.

Publisher's note

Supplementary material

The Supplementary material for this article can be found online at: https://www.frontiersin.org/articles/10.3389/fneur.2025.1490799/full#supplementary-material

References

1. Vasović L, Mojsilović M, Anđelković Z, Jovanović I, Arsić S, Vlajković S, et al. Proatlantal intersegmental artery: a review of normal and pathological features. *Childs Nerv Syst*. (2009) 25:411–21. doi: 10.1007/s00381-008-0765-7

2. Purkayastha S, Gupta AK, Varma R, Kapilamoorthy TR. Proatlantal intersegmental arteries of external carotid artery origin associated with Galen's vein malformation. *AJNR Am J Neuroradiol*. (2005) 26:2378–83.

3. Luh GY, Dean BL, Tomsick TA, Wallace RC. The persistent fetal carotid-vertebrobasilar anastomoses. *AJR Am J Roentgenol*. (1999) 172:1427–32. doi: 10.2214/ajr.172.5.10227532

4. Dimmick SJ, Faulder KC. Normal variants of the cerebral circulation at multidetector CT angiography. *Radiographics*. (2009) 29:1027–43. doi: 10.1148/rg.294085730

5. Dimitriade A, Stănciulescu R, Dorobăţ B, Iana G. A symptomatic presentation of a rare type of proatlantal artery. *Diagn Interv Imaging*. (2016) 97:371–2. doi: 10.1016/j.diii.2015.11.002

6. Zarghouni M, Marichal D. Persistent bilateral proatlantal type II artery. *Proc (Bayl Univ Med Cent)*. (2013) 26:50–1. doi: 10.1080/08998280.2013.11928918

7. Yilmaz E, Ilgit E, Taner D. Primitive persistent carotid-basilar and carotid-vertebral anastomoses: a report of seven gases and a review of the literature. *J Neurosurg*. (1995) 8:36–43. doi: 10.1002/ca.980080107

8. Padget DH. Designation of the embryonic intersegmental arteries in reference to the vertebral artery and subclavian stem. *Anat Rec*. (1954) 119:349–56. doi: 10.1002/ar.1091190306

9. Zuflacht JP, Liang C, Burkhardt JK, Favilla CG. Whole-brain perfusion via right common carotid artery with type 2 proatlantal intersegmental artery. *Stroke*. (2022) 53:e481–2. doi: 10.1161/strokeaha.122.040239

10. Bahşi YZ, Uysal H, Peker S, Yurdakul M. Persistent primitive proatlantal intersegmental artery (proatlantal artery I) results in 'top of the basilar' syndrome. *Stroke*. (1993) 24:2114–7. doi: 10.1161/01.str.24.12.2114

11. Ikeda M, Okamoto K, Hirai S, Amari M, Takatama M. A case of pontine infarction with persistent primitive proatlantal artery. *Rinsho Shinkeigaku*. (1993) 33:976–9.

12. Schoof J, Skalej M, Halloul Z, Wunderlich MT. Carotid endarterectomy in a patient with persistent proatlantal artery. *Cerebrovasc Dis*. (2007) 23:458–9. doi: 10.1159/000101748

13. Gocer GC, Ogul H. Unusual vascular cause of syncope in an adult patient: type 2 proatlantal intersegmental artery. *Acta Neurol Belg*. (2024) 124:1671–3. doi: 10.1007/s13760-024-02538-5

14. Liechty JM, Weddle RJ, Shutze WP, Smith BL. Occurrence of a type 2 proatlantal intersegmental artery during carotid endarterectomy for symptomatic stenosis. *J Vasc Surg*. (2016) 64:807–8. doi: 10.1016/j.jvs.2014.10.100

15. Kolbinger R, Heindel W, Pawlik G, Erasmi-Körber H. Right proatlantal artery type I, right internal carotid occlusion, and left internal carotid stenosis: case report and review of the literature. *J Neurol Sci*. (1993) 117:232–9. doi: 10.1016/0022-510x(93)90178-2

16. Nonaka Y, Nakatani K, Tanigawara T, Hattori T, Ohkuma A, Kaku Y, et al. A case of a persistent primitive proatlantal intersegmental artery with a ruptured basilar bifurcation aneurysm. *No Shinkei Geka*. (2001) 29:775–9.

17. Neurology Society of Chinese Medical Association. Diagnostic criteria of cerebrovascular diseases in China. *Chin J Neurol*. (2019) 52:710–5. doi: 10.3760/cma.j.issn.1006-7876.2019.09.003

18. Zhao L, Yang L, Liu X, Wang X, Zhang G, Wu J. Case report: Stent retriever thrombectomy of acute basilar artery occlusion via the type 1 proatlantal intersegmental artery. *Front Neurol*. (2022) 13:812458. doi: 10.3389/fneur.2022.812458

19. Babici D, Johansen PM, Sial N, Snelling B. Intracranial angioplasty via type II proatlantal intersegmental artery. *Cureus*. (2023) 15:e47724. doi: 10.7759/cureus.47724

20. Haiqi Z, Feng L, Cong L. Reflux compensation of persistent proatlantal intersegmental artery: report of one case. *Br J Neurosurg*. (2023) 37:1154–6. doi: 10.1080/02688697.2020.1850639

frontiers | Frontiers in Neurology

TYPE Original Research
PUBLISHED 11 February 2025
DOI 10.3389/fneur.2025.1538598

OPEN ACCESS

EDITED BY
Jieqiong Wang,
Chinese Academy of Sciences, China

REVIEWED BY
Jin-Ming Zhang,
University of Texas Health Science Center at Houston, United States
Hongmiao Yu,
Nationwide Children's Hospital, United States

*CORRESPONDENCE
Kang Min Park
✉ smilepkm@hanmail.net

†These authors have contributed equally to this work

RECEIVED 03 December 2024
ACCEPTED 29 January 2025
PUBLISHED 11 February 2025

CITATION
Kim J, Lee DA, Lee H-J and Park KM (2025) Small-vessel-disease-induced white matter damage in occipital lobe epilepsy.
Front. Neurol. 16:1538598.
doi: 10.3389/fneur.2025.1538598

Small-vessel-disease-induced white matter damage in occipital lobe epilepsy

Jinseung Kim[1†], Dong Ah Lee[2†], Ho-Joon Lee[3] and Kang Min Park[2*]

[1]Department of Family Medicine, Busan Paik Hospital, Inje University College of Medicine, Busan, Republic of Korea, [2]Department of Neurology, Haeundae Paik Hospital, Inje University College of Medicine, Busan, Republic of Korea, [3]Department of Radiology, Haeundae Paik Hospital, Inje University College of Medicine, Busan, Republic of Korea

Background: Peak width of skeletonized mean diffusivity (PSMD) is a novel marker of small vessel disease. This study aimed to investigate the presence of small vessel disease in patients with occipital lobe epilepsy (OLE) using PSMD.

Methods: We enrolled 27 patients newly diagnosed with OLE and included 29 healthy controls. The age and sex of the patients and controls were comparable. Diffusion tensor imaging (DTI) was performed using a 3 T MRI scanner. We measured the PSMD based on DTI in several steps, including preprocessing, skeletonization, application of a custom mask, and histogram analysis, using the FSL program. We compared PSMD between patients with OLE and healthy controls. Additionally, we performed a correlation analysis between PSMD and clinical factors in patients with OLE.

Results: Our findings revealed that the patients with OLE exhibited higher PSMD compared to healthy controls (2.459 vs. 2.079×10^{-4} mm^2/s, $p < 0.001$). In addition, PSMD positively correlated with age ($r = 0.412$, $p = 0.032$). However, the PSMD of the patients with OLE was not associated with other clinical factors such as age at seizure onset and duration of epilepsy.

Conclusion: We demonstrated that patients with OLE had a higher PSMD than healthy controls, indicating evidence of small vessel disease in patients with OLE. This finding also highlights the potential of PSMD as a marker for detecting small vessel diseases in epileptic disorders.

KEYWORDS

epilepsy, diffusion tensor imaging, cerebral small vessel diseases, white matter, neuroimaging

1 Introduction

Occipital lobe epilepsy (OLE) is a relatively uncommon type of focal epilepsy, originating in the occipital lobe and accounting for approximately 2–8% of surgical cases (1). It can result from structural brain abnormalities, such as tumors, strokes, or hemorrhages. However, it also occurs as part of self-limited focal epilepsies in childhood, including self-limited epilepsy with autonomic seizures or childhood occipital visual epilepsy (2).

Diffusion tensor imaging (DTI) is a magnetic resonance imaging (MRI) sequence that measures the diffusion of water molecules in tissues. Traditionally, DTI has been utilized in epilepsy surgery to define surgical margins using tractography (3). It also provides valuable insight into the microstructural integrity of white matter tracts, which cannot be visualized with

conventional brain MRI (4, 5). DTI can facilitate calculations of fractional anisotropy (FA) and mean diffusivity (MD) values, which serve as indicators of white matter microstructure. In patients with focal epilepsy, FA values generally increase, while MD values tend to decrease compared to healthy controls, with more pronounced changes observed on the ipsilateral side than the contralateral side (6). In addition, DTI can be used to investigate the structural connectivity of the brain. In patients with OLE, global integration is reduced, and alterations in local networks beyond the occipital lobe have been observed (7). Recently, DTI has been used to investigate the glymphatic system function of the brain, with dysfunction in this system identified in patients with OLE (8). Therefore, DTI is increasingly being used in both research and clinical practice, particularly for patients with epilepsy, including those with OLE.

Peak width of skeletonized mean diffusivity (PSMD) is a recently proposed neuroimaging marker derived from DTI that serves as an objective index for quantifying white matter damage caused by small vessel disease (9, 10). PSMD can be fully automatically calculated in a short time and has shown a stronger correlation with cognitive impairment than conventional DTI measures such as FA or MD. As a result, active research using PSMD has been conducted in various neurological diseases, such as multiple sclerosis, stroke, cerebral amyloid angiopathy, and dementia (11–15). However, white matter damage due to small vessel disease in patients with epilepsy, particularly OLE, has never been studied using PSMD.

Therefore, in this study, we aimed to investigate the degree of white matter damage due to small vessel disease in patients with OLE compared to healthy controls using PSMD. Additionally, we investigated the volumes of white matter hypointensities, which is another MRI marker for white matter damage based on T1-weighted imaging, in patients with OLE and compared them with healthy controls. We hypothesized that white matter damage in patients with OLE might be associated with small vessel disease than in the healthy control group.

2 Methods

2.1 Participants

This study was approved by the Institutional Review Board, and informed consent was obtained from all participants. We enrolled 27 patients newly diagnosed with OLE according to the ILAE criteria (16, 17). Only patients whose ictal semiology clearly indicated OLE and whose electroencephalography showed ictal or interictal epileptiform discharges originating in the occipital lobe were included in this study. DTI and T1-weighted MRI was performed at the time of OLE diagnosis in the drug-naïve state. We excluded the following participants from this study: (1) those with structural lesions on brain MRI that could influence the results of imaging analysis, (2) those with any neurological diseases other than OLE, (3) those with risk factors for small vessel disease, such as diabetes, hypertension, or dyslipidemia, or (4) those who did not consent to participate in the study. We also enrolled 29 age- and sex-matched healthy controls who had not been diagnosed with any medical or neurological diseases. The healthy controls underwent DTI and T1-weighted MRI, and their brain MRI revealed no structural lesions. Like the patients, the healthy controls did not have the risk factors associated with small vessel disease.

2.2 DTI scan

All DTI and T1-weighted MRI scans were performed using a 3.0 T MRI scanner (AchievaTx; Phillips Healthcare, Best, Netherlands) equipped with a 32-channel head coil for both patients with OLE and healthy controls. The DTI scans utilized spin-echo single-shot echo-planar pulse sequences with 32 different diffusion directions (repetition time/echo time, 8,620/85 ms; flip angle, 90°; slice thickness, 2.25 mm, acquisition matrix, 120 × 120; field of view, 240 × 240 mm^2; and *b*-value, 1,000 s/mm^2). The three-dimensional T1-weighted images were scanned using the following parameters: inversion time = 1,300 ms, repetition time/echo time = 8.6/3.96 ms, flip angle = 8°, and isotropic voxel size = 1 mm^3.

2.3 Obtaining the PSMD

Figure 1 shows the process for obtaining PSMD from DTI using the FSL program installed on a Linux system, involving a total of four steps (9, 10). The first step preprocesses the DTI, which includes motion and eddy current correction, brain

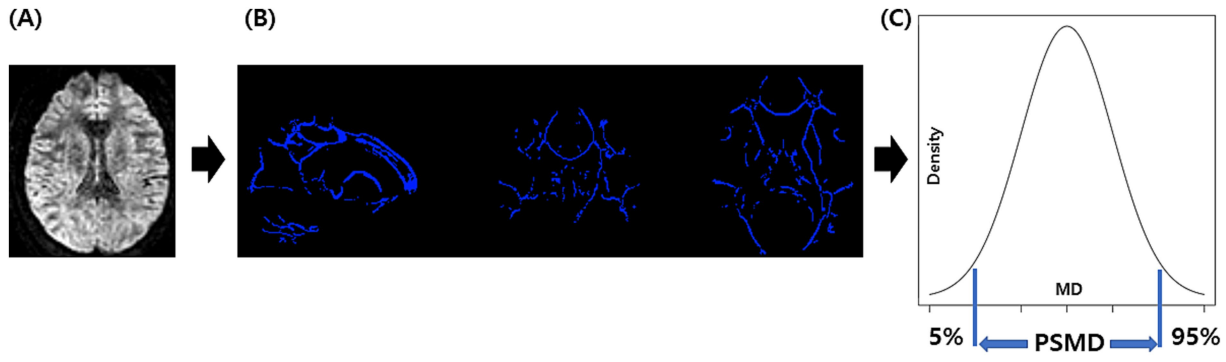

FIGURE 1
The process for obtaining PSMD: we perform DTI acquisition on the participants, followed by preprocessing steps including motion and eddy current correction, brain extraction, and tensor fitting **(A)**. Subsequently, we conducted skeletonization, which included normalization, projection onto the skeleton template, and the application of a custom mask **(B)**. Finally, we performed histogram analysis and calculated PSMD based on the difference between the 95th and 5th percentiles **(C)**. PSMD, peak width of skeletonized mean diffusivity.

extraction, and tensor fitting. The second step is skeletonization, which involves tract-based spatial statistics obtained by registering an FA map to the common space and projecting it onto the skeleton. The same transformation matrices were used for MD data to obtain a skeletonized MD map. The third step was the application of a custom mask using the template thresholded at an FA value of 0.3 and a custom-made mask. The fourth step was histogram analysis, in which the width of the histogram (the difference between 95 and 5) derived from the MD values of all voxels included in the skeleton was obtained.

2.4 White matter hypointensities segmentation

To segment white matter hypointensities from T1-weighted images and acquire the volumes of white matter hypointensities, we used WMH-SynthSeg (18), which provides segmentation for white matter hyper- or hypointensities from scans of any resolution and contrast without retraining, available as module in the development version of Freesurfer.

2.5 Statistical analysis

An independent sample *t*-test was used to compare age and PSMD values between patients with OLE and healthy controls. The Mann–Whitney test was used to compare the volumes of white matter hypointensities between the groups. The chi-square test was used to compare sex differences between the groups. Pearson's correlation test was used for correlation analysis. The performance of the classification was evaluated using the receiver operating characteristic (ROC) curve analysis. Statistical significance was considered when the *p*-value was less at $p < 0.05$. All statistical analyses were performed using MedCalc® Statistical Software version 22.009 (MedCalc Software Ltd., Ostend, Belgium; https://www.medcalc.org; 2023).

3 Results

3.1 Demographic and clinical characteristics of participants

Table 1 shows the demographic data in the participants and clinical characteristics of patients with OLE. There were no significant differences in age or sex between the OLE patients and the healthy control group.

3.2 Difference in the PSMD between the groups

There was a significant difference in the PSMD between patients with OLE and healthy controls. The patients with OLE exhibited higher PSMD compared to healthy controls (2.459 vs. 2.079×10^{-4} mm^2/s, $p < 0.001$) (Figure 2).

TABLE 1 Demographic data in participants and clinical characteristics of patients with OLE.

	Patients with JME (*N* = 27)	Healthy controls (*N* = 29)	*p*-value
Demographic data			
Age, years (SD)	34.2 (15.6)	32.8 (4.1)	0.627
Men, *N* (%)	12 (44.4)	11 (37.9)	0.623
Clinical data			
Age of seizure onset, years (SD)	16.5 (15.9)		
Duration of epilepsy, months (SD)	156.0 (154.4)		
Number of seizures prior to treatment	5 (2.3)		
Initial seizure semiology			
Visual symptoms, *N* (%)	18 (66.6)		
Oculomotor symptoms, *N* (%)	8 (29.6)		
Others, *N* (%)	1 (3.7)		

PSMD, peak width of skeletonized mean diffusivity; OLE, occipital lobe epilepsy; SD, standard deviation.

3.3 Difference in the volumes of white matter hypointensities between the groups

The volumes of white matter hypointensities were higher in patients with OLE than that in the healthy controls [1309.6 (interquartile range, 1165.5–2793.2) vs. 1141.0 (interquartile range, 874.1–1298.9) mm^3, $p = 0.011$].

3.4 ROC curve analysis

ROC curve analysis using PSMD showed an area under curve (AUC) of 0.747 in distinguishing the patients with OLE and healthy controls ($p < 0.001$). Additionally, ROC curve analysis using the volumes of white matter hypointensities revealed an AUC of 0.699 in distinguishing the groups ($p = 0.005$). Although the AUC using PSMD was higher than that of the volumes of white matter hypointensities, there were no significant difference in the comparison of AUC between PSMD and the volumes of white matter hypointensities in distinguishing the groups ($p = 0.602$) (Figure 3).

3.5 Correlation between the PSMD and clinical characteristics

In patients with OLE, a positive correlation was observed between PSMD and age ($r = 0.412$, $p = 0.032$) (Figure 4). However, PSMD was not associated with other clinical factors, such as age at seizure onset

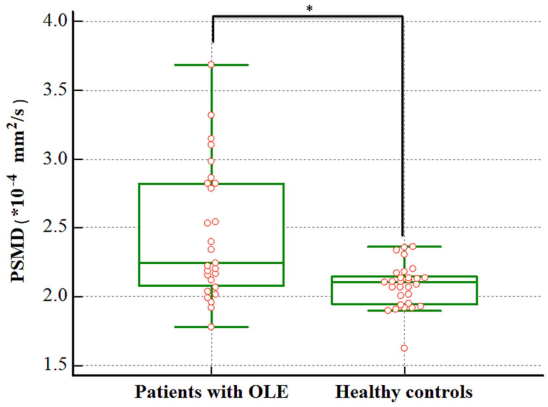

FIGURE 2
Difference in the PSMD between patients with OLE and healthy controls. The PSMD was higher in the OLE group than in the healthy control group (2.459 vs. 2.079 × 10^{-4} mm^2/s, $p < 0.001$). PSMD, peak width of skeletonized mean diffusivity; OLE, occipital lobe epilepsy. *$p < 0.05$.

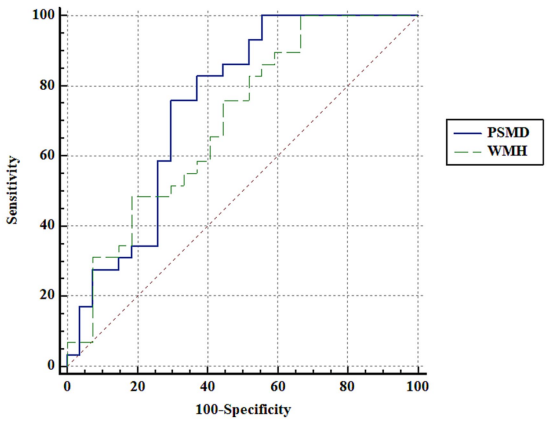

FIGURE 3
ROC curve analysis. ROC curve analysis using PSMD and the volumes of white matter hypointensities shows an area under curve (AUC) of 0.747 and 0.699, respectively, in distinguishing the patients with OLE and healthy controls. Although the AUC using PSMD is higher than that of the volumes of white matter hypointensities, there are no significant difference in the comparison of AUC between PSMD and the volumes of white matter hypointensities in distinguishing the groups ($p = 0.602$). PSMD, peak width of skeletonized mean diffusivity; WMH, the volumes of white matter hypointensities.

($r = 0.082$, $p = 0.695$), duration of epilepsy ($r = -0.127$, $p = 0.545$), and number of seizures prior to treatment ($r = 0.058$, $p = 0.770$).

4 Discussion

This study is the first to demonstrate that PSMD is higher in patients with OLE than in healthy controls, indicating the presence of white matter damage due to small vessel disease in these patients. In addition, in patients with OLE, PSMD increases proportionally with age, confirming that small vessel disease progresses further with aging.

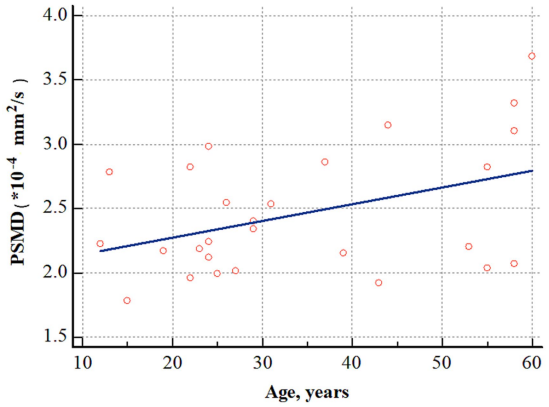

FIGURE 4
Correlation analysis between age and PSMD in patients with OLE. PSMD positively correlated with age ($r = 0.412$, $p = 0.032$). PSMD, peak width of skeletonized mean diffusivity; OLE, occipital lobe epilepsy.

This study demonstrates the presence of white matter damage due to small vessel disease in patients with OLE, which aligns with previous studies. Maxwell et al. (19) investigated the presence of small vessel disease in 105 patients with epilepsy, particularly late-onset epilepsy, and 105 healthy controls. They used periventricular and subcortical white matter lesions as indicators of small vessel disease. They found that small vessel disease was present in 49.5% of patients with epilepsy, compared to 32.3% of the healthy controls, concluding that small vessel disease is more prevalent in individuals with epilepsy. Hanby et al. (19) analyzed white matter hyperintensities with automatic quantitation in patients with focal epilepsy and healthy controls, revealing higher white matter hyperintensities volume in patients with epilepsy (1,340 mm^3) compared to controls (514 mm^3) (20). Another study examined the correlation between the location of white matter lesions and the frequency of clinical symptoms such as stroke, seizure, vertigo, and gait apraxia. They reported that seizures were more frequent when lesions were located in the parieto-occipital lobe (21). This finding suggests an association between OLE and small vessel disease, similar to the present study. However, a previous study reported that epilepsy associated with leukoaraiosis was most closely related to the temporal lobe; therefore, further research is needed (22).

The cross-sectional design of this study makes it challenging to establish a cause-and-effect relationship between small vessel disease and OLE. Thus, two primary hypotheses were considered. The first hypothesis for the small vessel disease-OLE relationship is that small vessel disease may cause OLE. Previous animal experiments demonstrated in hypertensive rats that small vessel disease induced focal epilepsy more often than generalized epilepsy (23). It was observed that early treatment with enalapril could reduce the incidence of epilepsy in these animals, suggesting a role for small vessel disease in epileptogenesis (23). Additionally, studies on humans have demonstrated that hypertension is an independent risk factor for epilepsy (24, 25). Patients with hypertension are approximately twice as likely to develop epilepsy compared to those without, with those having uncontrolled hypertension being up to 10 times more likely to develop epilepsy (24, 25). Small vessel disease can cause endothelial dysfunction and blood-brain barrier leakage, leading to extravasation of serum proteins and inflammation, which may contribute to epileptogenesis.

Diffuse cerebral microangiopathy can impair cerebral perfusion, leading to epileptogenesis via neurovascular uncoupling (26, 27).

Another hypothesis is that small vessel disease is caused by seizures that occur in patients with OLE. Recurrent seizures have shown to cause depolarization of pericytic mitochondria and subsequent vasoconstriction, resulting in small vessel disease, which is associated with impaired neurovascular coupling and increased blood-brain barrier permeability (28). Arteriole vasoconstriction, mediated by cyclooxygenase-2 and L-type calcium channels, plays an important role in hypoperfusion/hypoxia resulting from recurrent seizures (29). Furthermore, while the cerebral cortex is primarily involved in epileptic seizures, secondary changes in the cerebral white matter, including major association, commissural, and projection fibers, are well-documented. These changes are correlated with age of seizure onset and duration of epilepsy (30–32) and maybe induced by multiple mechanisms, including excitotoxicity with excessive glutamate release, inflammation response by microglia and astrocytes, oxidative stress by reactive oxygen species, and blood-brain barrier disruption (30–32).

We also confirmed that white matter damage due to small vessel disease worsened with age in patients with OLE. Several factors contribute to this worsening with age: endothelial dysfunction, atherosclerosis, increased reactive oxygen species, and chronic low-grade inflammation. The endothelium is located inside the blood vessels, and with aging, its function declines, making it difficult to maintain the integrity of the blood vessels and reducing its ability to regulate blood flow (33). Atherosclerosis is caused by the development of plaques in both large and small blood vessels. This plaque buildup impedes blood flow, increases vessel rigidity, and reduces perfusion (34). The increase in reactive oxygen species with age causes injury to the blood vessel walls (35). Finally, as we age, chronic low-grade inflammation occurs, which increases vessel stiffness and plaque formation, resulting in the destruction of the vascular endothelium (36). Through this study, we confirmed that small vessel disease worsens with age in patients with OLE, even in the absence of vascular risk factors, such as hypertension, diabetes, or dyslipidemia.

This study is the first to demonstrate white matter damage due to small vessel disease in patients with OLE. However, it has some limitations. The sample size, i.e., the number of patients enrolled in this study, was relatively small due to the rarity of OLE and the exclusion of patients with structural lesions that could affect DTI analysis. Additionally, to exclude the influence of anti-seizure medications on DTI measurements, only patients with their first diagnosis of epilepsy at the time of DTI imaging were enrolled. Another limitation of this study is the cross-sectional design, which did not allow us to establish a cause-and-effect relationship between small vessel disease and OLE. The study was conducted at a center specializing in epilepsy disorders; hence, the results cannot be generalized to all patients with epilepsy. In addition, the results were limited to OLE; therefore, further research with a larger sample size is needed for other focal epilepsy or generalized epilepsy. Lastly, we could not analyze the volumes of white matter hyperintensities, since some datasets lacked fluid attenuated inversion recovery images. Instead of the volumes of white matter hyperintensities, we analyzed the volumes of white matter hypointensites, which is another MRI marker for white matter damage based on T1-weighted imaging. Although the volumes of white matter hyperintensities are more accurate and widely used to assess white matter damage, they have strong correlation with the volumes of white matter hypointensites.

5 Conclusion

We demonstrated that patients with OLE had a higher PSMD than healthy controls, indicating the presence of small vessel disease in patients with OLE. This finding also highlights the potential of PSMD as a marker for detecting small vessel disease in epilepsy.

Data availability statement

The raw data supporting the conclusions of this article will be made available by the authors, without undue reservation.

Ethics statement

The studies involving humans were approved by Haeundai Paik Institutional Review Board. The studies were conducted in accordance with the local legislation and institutional requirements. The ethics committee/institutional review board waived the requirement of written informed consent for participation because the study is based solely on existing data.

Author contributions

JK: Data curation, Validation, Writing – original draft, Writing – review & editing. DL: Data curation, Formal analysis, Writing – original draft, Writing – review & editing. H-JL: Data curation, Formal analysis, Methodology, Visualization, Writing – original draft, Writing – review & editing. KP: Conceptualization, Formal analysis, Methodology, Project administration, Supervision, Writing – original draft, Writing – review & editing.

Funding

The author(s) declare that financial support was received for the research, authorship, and/or publication of this article. This research was supported by a grant of the Korea Health Technology R&D Project through the Korea Health Industry Development Institute (KHIDI), funded by the Ministry of Health & Welfare, Republic of Korea (Grant No. HR21C1003).

Conflict of interest

The authors declare that the research was conducted in the absence of any commercial or financial relationships that could be construed as a potential conflict of interest.

Generative AI statement

The authors declare that no Gen AI was used in the creation of this manuscript.

Publisher's note

References

1. Blume WT, Whiting SE, Girvin JP. Epilepsy surgery in the posterior cortex. *Ann Neurol*. (1991) 29:638–45. doi: 10.1002/ana.410290611

2. Specchio N, Wirrell EC, Scheffer IE, Nabbout R, Riney K, Samia P, et al. International League Against Epilepsy classification and definition of epilepsy syndromes with onset in childhood: position paper by the ILAE Task Force on Nosology and Definitions. *Epilepsia*. (2022) 63:1398–442. doi: 10.1111/epi.17241

3. Lilja Y, Nilsson DT. Strengths and limitations of tractography methods to identify the optic radiation for epilepsy surgery. *Quant Imaging Med Surg*. (2015) 5:288–99. doi: 10.3978/j.issn.2223-4292.2015.01.08

4. Szmuda M, Szmuda T, Springer J, Rogowska M, Sabisz A, Dubaniewicz M, et al. Diffusion tensor tractography imaging in pediatric epilepsy—a systematic review. *Neurol Neurochir Pol*. (2016) 50:1–6. doi: 10.1016/j.pjnns.2015.10.003

5. Leon-Rojas J, Cornell I, Rojas-Garcia A, D'Arco F, Panovska-Griffiths J, Cross H, et al. The role of preoperative diffusion tensor imaging in predicting and improving functional outcome in pediatric patients undergoing epilepsy surgery: a systematic review. *BJR Open*. (2021) 3:20200002. doi: 10.1259/bjro.20200002

6. Hatton SN, Huynh KH, Bonilha L, Abela E, Alhusaini S, Altmann A, et al. White matter abnormalities across different epilepsy syndromes in adults: an ENIGMA-epilepsy study. *Brain*. (2020) 143:2454–73. doi: 10.1093/brain/awaa200

7. Lee DA, Lee HJ, Park KM. Structural brain network analysis in occipital lobe epilepsy. *BMC Neurol*. (2023) 23:268. doi: 10.1186/s12883-023-03326-z

8. Kim J, Lee DA, Lee HJ, Park KM. Glymphatic system dysfunction in patients with occipital lobe epilepsy. *J Neuroimaging*. (2023) 33:455–61. doi: 10.1111/jon.13083

9. Zanon Zotin MC, Yilmaz P, Sveikata L, Schoemaker D, van Veluw SJ, Etherton MR, et al. Peak width of skeletonized mean diffusivity: a neuroimaging marker for white matter injury. *Radiology*. (2023) 306:e212780. doi: 10.1148/radiol.212780

10. Baykara E, Gesierich B, Adam R, Tuladhar AM, Biesbroek JM, Koek HL, et al. A novel imaging marker for small vessel disease based on skeletonization of white matter tracts and diffusion histograms. *Ann Neurol*. (2016) 80:581–92. doi: 10.1002/ana.24758

11. Vinciguerra C, Giorgio A, Zhang J, Di Donato I, Stromillo ML, Tappa Brocci R, et al. Peak width of skeletonized mean diffusivity (PSMD) as marker of widespread white matter tissue damage in multiple sclerosis. *Mult Scler Relat Disord*. (2019) 27:294–7. doi: 10.1016/j.msard.2018.11.011

12. Jochems ACC, Muñoz Maniega S, Clancy U, Jaime Garcia D, Arteaga C, Hewins W, et al. Associations of peak-width skeletonized mean diffusivity and post-stroke. *Cognition* Life. (2022) 12:1362. doi: 10.3390/life12091362

13. Zanon Zotin MC, Schoemaker D, Raposo N, Perosa V, Bretzner M, Sveikata L, et al. Peak width of skeletonized mean diffusivity in cerebral amyloid angiopathy: spatial signature, cognitive, and neuroimaging associations. *Front Neurosci*. (2022) 16:1051038. doi: 10.3389/fnins.2022.1051038

14. Low A, Mak E, Stefaniak JD, Malpetti M, Nicastro N, Savulich G, et al. Peak width of skeletonized mean diffusivity as a marker of diffuse cerebrovascular damage. *Front Neurosci*. (2020) 14:238. doi: 10.3389/fnins.2020.00238

15. Lam BYK, Leung KT, Yiu B, Zhao L, Biesbroek JM, Au L, et al. Peak width of skeletonized mean diffusivity and its association with age-related cognitive alterations and vascular risk factors. *Alzheimers Dement*. (2019) 11:721–9. doi: 10.1016/j.dadm.2019.09.003

16. Sveinbjornsdottir S, Duncan JS. Parietal and occipital lobe epilepsy: a review. *Epilepsia*. (1993) 34:493–521. doi: 10.1111/j.1528-1157.1993.tb02590.x

17. Angus-Leppan H, Clay TA. Adult occipital lobe epilepsy: 12-years on. *J Neurol*. (2021) 268:3926–34. doi: 10.1007/s00415-021-10557-y

18. Laso P, Cerri S, Sorby-Adams A, Guo J, Mateen F, Goebl Pet al. (2024). Quantifying white matter hyperintensity and brain volumes in heterogeneous clinical and low-field portable MRI. 2024 IEEE International Symposium on Biomedical Imaging (ISBI): IEEE.

19. Maxwell H, Hanby M, Parkes LM, Gibson LM, Coutinho C, Emsley HC. Prevalence and subtypes of radiological cerebrovascular disease in late-onset isolated seizures and epilepsy. *Clin Neurol Neurosurg*. (2013) 115:591–6. doi: 10.1016/j.clineuro.2012.07.009

20. Hanby MF, Al-Bachari S, Makin F, Vidyasagar R, Parkes LM, Emsley HC. Structural and physiological MRI correlates of occult cerebrovascular disease in late-onset epilepsy. *NeuroImage Clin*. (2015) 9:128–33. doi: 10.1016/j.nicl.2015.07.016

21. Okroglic S, Widmann CN, Urbach H, Scheltens P, Heneka MT. Clinical symptoms and risk factors in cerebral microangiopathy patients. *PLoS One*. (2013) 8:e53455. doi: 10.1371/journal.pone.0053455

22. Gasparini S, Ferlazzo E, Beghi E, Sofia V, Mumoli L, Labate A, et al. Epilepsy associated with leukoaraiosis mainly affects temporal lobe: a casual or causal relationship? *Epilepsy Res*. (2015) 109:1–8. doi: 10.1016/j.eplepsyres.2014.10.012

23. Russo E, Leo A, Scicchitano F, Donato A, Ferlazzo E, Gasparini S, et al. Cerebral small vessel disease predisposes to temporal lobe epilepsy in spontaneously hypertensive rats. *Brain Res Bull*. (2017) 130:245–50. doi: 10.1016/j.brainresbull.2017.02.003

24. Ng SK, Hauser WA, Brust JC, Susser M. Hypertension and the risk of new-onset unprovoked seizures. *Neurology*. (1993) 43:425–8. doi: 10.1212/wnl.43.2.425

25. Li X, Breteler MM, de Bruyne MC, Meinardi H, Hauser WA, Hofman A. Vascular determinants of epilepsy: the Rotterdam Study. *Epilepsia*. (1997) 38:1216–20. doi: 10.1111/j.1528-1157.1997.tb01219.x

26. Gibson LM, Allan SM, Parkes LM, Emsley HC. Occult cerebrovascular disease and late-onset epilepsy: could loss of neurovascular unit integrity be a viable model? *Cardiovasc Psychiatry Neurol*. (2011) 2011:130406:1–7. doi: 10.1155/2011/130406

27. de Souza A, Tasker K. Inflammatory cerebral amyloid angiopathy: a broad clinical spectrum. *J Clin Neurol*. (2023) 19:230–41. doi: 10.3988/jcn.2022.0493

28. Prager O, Kamintsky L, Hasam-Henderson LA, Schoknecht K, Wuntke V, Papageorgiou I, et al. Seizure-induced microvascular injury is associated with impaired neurovascular coupling and blood-brain barrier dysfunction. *Epilepsia*. (2019) 60:322–36. doi: 10.1111/epi.14631

29. Farrell JS, Colangeli R, Wolff MD, Wall AK, Phillips TJ, George A, et al. Postictal hypoperfusion/hypoxia provides the foundation for a unified theory of seizure-induced brain abnormalities and behavioral dysfunction. *Epilepsia*. (2017) 58:1493–501. doi: 10.1111/epi.13827

30. Hogan RE. Epilepsy as a disease of white matter. *Epilepsy Curr*. (2021) 21:27–9. doi: 10.1177/1535759720975744

31. Ran H, Chen G, Ran C, He Y, Xie Y, Yu Q, et al. Altered white-matter functional network in children with idiopathic generalized epilepsy. *Acad Radiol*. (2024) 31:2930–41. doi: 10.1016/j.acra.2023.12.043

32. Hou XX, Feng HX, Xu B, Li ZS, Lu YL, Zhao HM, et al. A tract-based spatial statistics study of white matter integrity in epilepsy. *Am J Transl Res*. (2022) 14:8980–90.

33. Cheng X, Potenza DM, Brenna A, Ajalbert G, Yang Z, Ming XF. Aging increases hypoxia-induced endothelial permeability and blood-brain barrier dysfunction by upregulating arginase-II. *Aging Dis*. (2024) 15:2710. doi: 10.14336/AD.2023.1225

34. Ma S, Xie X, Yuan R, Xin Q, Miao Y, Leng SX, et al. Vascular aging and atherosclerosis: a perspective on aging. *Aging Dis*. (2024) 16:33–48. doi: 10.14336/AD.2024.0201-1

35. MohanKumar SMJ, Murugan A, Palaniyappan A, MohanKumar PS. Role of cytokines and reactive oxygen species in brain aging. *Mech Ageing Dev*. (2023) 214:111855. doi: 10.1016/j.mad.2023.111855

36. Kong L, Li S, Fu Y, Cai Q, Du X, Liang J, et al. Mitophagy in relation to chronic inflammation/ROS in aging. *Mol Cell Biochem*. (2024). doi: 10.1007/s11010-024-05042-9

frontiers | Frontiers in Neurology

TYPE Systematic Review
PUBLISHED 14 March 2025
DOI 10.3389/fneur.2025.1505533

OPEN ACCESS

EDITED BY
Mingming Lu,
Characteristic Medical Center of Chinese People's Armed Police Force, China

REVIEWED BY
Han Cong,
Fifth Medical Center of the PLA General Hospital, China
Francesca Galassi,
University of Rennes 1, France
Baobao Li,
Fifth Medical Center of the PLA General Hospital, China

*CORRESPONDENCE
Wen-hua Xiong
✉ xiongwenhua3@163.com

RECEIVED 03 October 2024
ACCEPTED 24 February 2025
PUBLISHED 14 March 2025

CITATION
Lou J-c, Yu X-f, Ying J-j, Song D-q and Xiong W-h (2025) Exploring the potential of machine learning and magnetic resonance imaging in early stroke diagnosis: a bibliometric analysis (2004–2023). *Front. Neurol.* 16:1505533. doi: 10.3389/fneur.2025.1505533

Exploring the potential of machine learning and magnetic resonance imaging in early stroke diagnosis: a bibliometric analysis (2004–2023)

Jian-cheng Lou, Xiao-fen Yu, Jian-jun Ying, Da-qiao Song and Wen-hua Xiong*

Yiwu Hospital of Traditional Chinese Medicine, Yiwu, China

Objective: To examine the focal areas of research in the early diagnosis of stroke through machine learning identification of magnetic resonance imaging characteristics from 2004 to 2023.

Methods: Data were gathered from the Science Citation Index-Expanded (SCI-E) within the Web of Science Core Collection (WoSCC). Utilizing CiteSpace 6.2.R6, a thorough analysis was conducted, encompassing publications, authors, cited authors, countries, institutions, cited journals, references, and keywords. This investigation covered the period from 2004 to 2023, with the data retrieval completed on December 1, 2023, in a single day.

Results: In total, 395 articles were incorporated into the analysis. Prior to 2015, the annual publication count was under 10, but a significant surge in publications was observed post-2015. Institutions and authors from the USA and China have established themselves as mature academic entities on a global scale, forging extensive collaborative networks with other institutions. High-impact journals in this field predominantly feature in top-tier publications, indicating a consensus in the medical community on the application of machine learning for early stroke diagnosis. "deep learning," "magnetic resonance imaging," and "stroke" emerged as the most attention-gathering keywords among researchers. The development in this field is marked by a coexisting pattern of interdisciplinary integration and refinement within major disciplinary branches.

Conclusion: The application of machine learning in the early prediction and personalized medical plans for stroke patients using neuroimaging characteristics offers significant value. The most notable research hotspots currently are the optimal selection of neural imaging markers and the most suitable machine learning algorithm models.

KEYWORDS

stroke, machine learning, magnetic resonance imaging, bibliometric analysis, WoSCC

Introduction

Stroke is an acute cerebrovascular disorder, precipitates enduring cerebral damage, disability, and even mortality upon its onset (1–3). Studies have identified it as the second leading cause of death worldwide (4). Notably, 11% of stroke survivors experience a recurrence within a year, and 39% within a decade (5). Generally, strokes arise either from blood flow

obstruction (ischemic strokes, constituting 87%) or intracerebral hemorrhage (hemorrhagic strokes, accounting for 10%) (6, 7). Regardless of the type, prompt medical intervention is crucial, as early diagnosis and treatment significantly influence the outcome.

Magnetic resonance imaging (MRI) stands as the gold index in stroke diagnosis (8–10), boasting high temporal and spatial resolution capabilities that enable meticulous observation of subtle cerebral vascular changes (11, 12). Moreover, the analytical methods derived from multimodal MRI data facilitate a nuanced identification of cerebral structural and functional network regulations (13, 14). Hence, the objective visualization tools provided by MRI technology are instrumental in the early diagnosis of stroke. However, many patients fail to adhere to medical advice for regular MRI follow-ups, leading to acute stroke episodes (15, 16). Consequently, there's an urgent need in the medical field for a sophisticated neuroimaging algorithm capable of early stroke prediction, mitigating the issue of clinical data scarcity due to patient non-compliance.

Machine learning (ML) algorithms can automate the interpretation of abnormal imaging patterns, accelerating the diagnostic process in urgent scenarios (17–19). They integrate data from diverse sources, including MRI, clinical records, and vital signs, to assess an individual's future stroke risk. Additionally, ML enhances the precision and sensitivity of stroke diagnosis, particularly in early stages, by learning from extensive datasets (20). Deep learning, a subset of ML, represents one of the most advanced and specialized approaches within the broader ML framework. While ML encompasses a wide range of algorithms, deep learning focuses on neural network architectures capable of automatically extracting high-level features from complex data. In stroke diagnosis, deep learning has garnered significant attention due to its exceptional performance in processing MRI data, particularly for identifying subtle imaging markers of early stroke. Consequently, the bibliometric analysis in this study focuses on ML as the overarching framework, while acknowledging deep learning as a key contributor to advancements in this field. In recent years, ML has been increasingly applied to early stroke detection, with its reliability validated by authoritative multicentric randomized controlled trials (RCTs) (21) and meta-analysis (22) of high evidentiary value. However, the field of academic collaboration networks, developmental trends, and research frontiers in using ML for early stroke diagnosis through MRI feature recognition still lacks extensive bibliometric research.

CiteSpace software, a visualization tool, qualitatively and quantitatively elucidates the interconnected contributions of authors, regions, institutions, and their collaboration networks (23). Its most notable attribute is the insight into research hotspots and frontier areas, along with predictions on specific field's future development trajectories. Compared to traditional literature reviews and meta-analyses, the bibliometric analysis facilitated by CiteSpace offers a more profound and insightful perspective (24–26). This study aims to utilize CiteSpace to comprehensively search the WoSCC for relevant literature from the past two decades, conducting a bibliometric analysis on core authors, their collaboration networks, journals, countries, and affiliated academic institutions. This will deepen our understanding of the frontiers and developmental trends in the early diagnosis of stroke using ML to identify MRI characteristics.

Abbreviations: MRI, Magnetic resonance imaging; ML, Machine learning; RCTs, Randomized controlled trials; WOSCC, Web of Science Core Collection; SCI-E, Science Citation Index-Expanded; ASL, Arterial spin labeling; DWI, Diffusion weighted imaging; FC, Functional connectivity; CNNs, Convolutional neural networks; SVMs, Support vector machines; RFs, Random forests.

Materials and methods

Data sources and search strategy

Data sources

The data for this study were sourced from the Science Citation Index-Expanded (SCI-E) within the Web of Science Core Collection (WoSCC), a citation-based database that provides detailed citation information and abstracts. This allows for the calculation of bibliometric indicators such as cited authors, journals, impact factors, *h*-indexes, and citation reports. WoSCC encompasses over 12,000 high-quality academic journals spanning more than 250 disciplines, offering a comprehensive collection of interdisciplinary publications.

Compared to databases like PubMed, which focus primarily on biomedical literature and lack citation metrics, WoSCC offers superior bibliometric capabilities, including citation networks, co-authorship relationships, and keyword co-occurrence trends. Current bibliometric tools also do not support multi-database integration due to challenges such as inconsistent data formats and record duplication, complicating the research process and compromising data consistency.

While relying solely on WoSCC may exclude articles indexed in databases like PubMed or Scopus, which could contain relevant studies on machine learning and MRI in stroke diagnosis, WoSCC's interdisciplinary coverage and citation-based metrics make it suitable for this study. A broad search strategy was applied to minimize dataset bias. Future research could explore multi-database integration as methodologies evolve to address associated challenges.

Search strategy

The data retrieval strategy encompassed key topics such as "stroke," "magnetic resonance imaging," and "machine learning" (Figure 1). This encompassed a nearly two-decade span of publications, from December 1, 2004, to December 1, 2023, with the retrieval completed within a single day, December 10, 2023. We imposed no geographical restrictions on the publishing countries, but required the language to be English and the research type to be "article" (27–29). Details of the retrieval strategy and results are provided in Table 1. A total of 395 articles were identified, which, after importing into CiteSpace and eliminating duplicates, confirmed the absence of redundancies.

Analysis tool

The visualizations generated by CiteSpace 6.2.R6 typically include nodes, links, colors, clusters, and timelines. Nodes usually represent various research papers, authors, journals, or keywords, with the size of a node often indicating its significance or impact, such as citation frequency. Links denote the relationships between nodes, like citation or collaboration connections, with the thickness of a line possibly indicating the strength or frequency of the relationship. Different colors may represent different time periods or various research fields or categories. Clusters, composed of closely connected nodes, signify

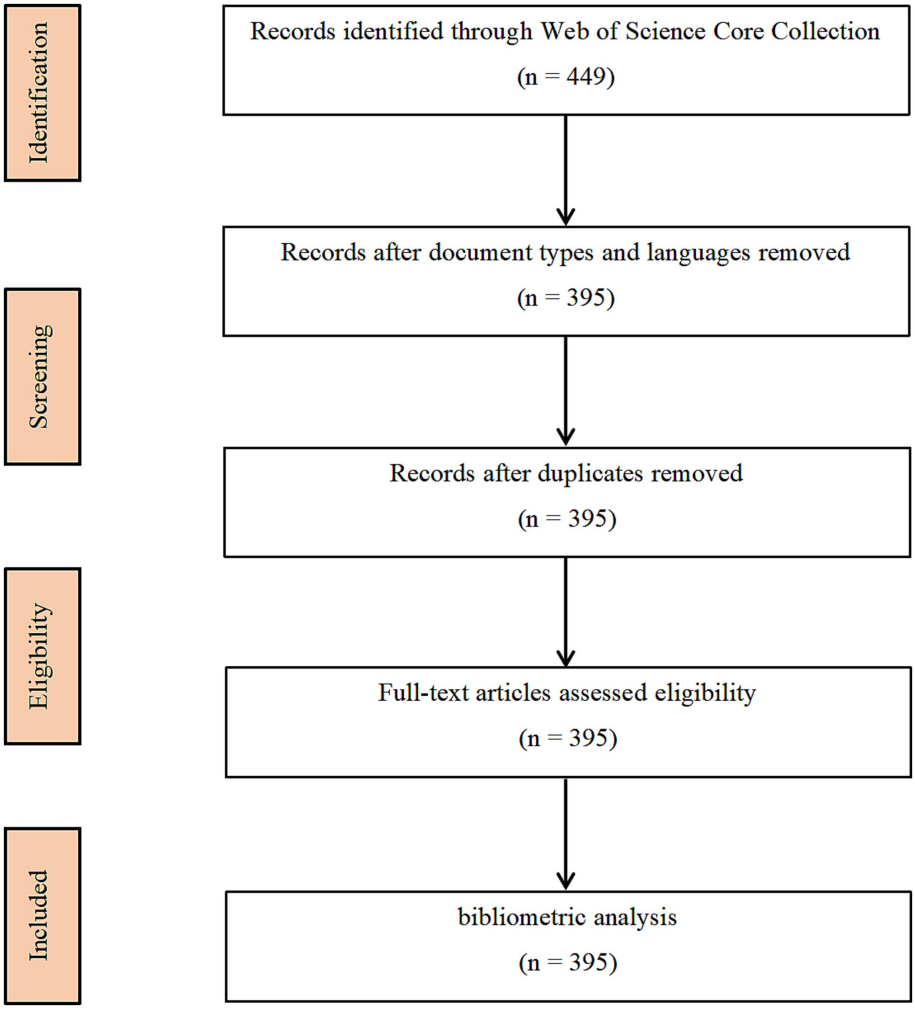

FIGURE 1
Map of literature screening process related to machine learning and MRI in early stroke diagnosis.

specific research themes or areas, aiding in understanding the primary branches and trends within a research field. The timeline exhibits the evolution of keywords or themes over time. Interpreting these visualizations aids in uncovering hot topics, developmental trends, and relationships in research concerning the application of ML in the field of stroke.

The parameters used in CiteSpace 6.2.R6 were as follows: time slices covered the period from 2004 to 2023, with each slice representing 1 year. All terms were included, such as "title," "abstract," "author keywords," and "keywords plus." To enhance the clarity of the final visualizations and facilitate the observation of relationships between publications, we set the *g*-index's *k*-value to 50 and employed the Pathfinder algorithm (30, 31).

Results

Annual publications

Figure 2 illustrates the annual publication trend in using ML to analyze MRI characteristics for the early diagnosis of stroke. It was observed that prior to 2015, the quantity of publications remained at a relatively low level, correlating significantly with the nascent phase of ML as an emerging discipline. From 2015 onwards, there has been a substantial increase in publications, attributed to advancements in the computational capabilities of ML and the refinement of algorithmic architectures. These developments have shown promise in enhancing the accuracy of diagnosing stroke, its subtyping, and prognostic predictions (32). Our investigation revealed that in 2015, the U.S. Food and Drug Administration (FDA) approved several ML-based medical devices, such as RapidAI® and Viz.ai®, which have played a pivotal role in the early diagnosis and treatment decision-making of strokes. The trajectory of the trend line leads us to infer that in the next 5–10 years, a new peak in the volume of publications is likely to emerge.

In addition to describing publication trends, the correlation analysis highlights a moderate positive relationship between the emergence of machine learning and its application in stroke research. This result indicates that advancements in ML directly influenced its adoption in stroke diagnosis and treatment. For example, the spike in publications after 2015 aligns with the FDA approval of ML-based

medical tools, such as RapidAI® and Viz.ai®, which are designed to enhance diagnostic workflows.

Analysis of authors

Figures 3 and Table 2 display the authorship information behind the 395 published articles. Each node represents an author, with the connecting lines indicating collaborative relationships between them. The top 10 authors, in descending order, are: Castillo, Jose (9 publications); Wang, Yongjun (9 publications); Jing, Jing (8 publications); Campos, Francisco (8 publications); Meng, Xia (7 publications); Iglesias-rey, Ramon (7 publications); Sobrino, Tomas (6 publications); Li, Zixiao (6 publications); Chen, Cheng (5 publications); Zhao, Xingquan (5 publications). It was observed that all of the top 10 authors hail from Spain and China. This pattern reflects the strong research infrastructure and significant investments in ML and medical research within these countries. For instance, Spain has long been recognized for its clinical stroke research expertise, while China has emerged as a leader in applying ML technologies to medical diagnostics due to its large patient datasets and growing interdisciplinary collaborations.

The collaboration network reveals that higher node degree correlates strongly with author centrality, suggesting that prominent authors often serve as key hubs in multi-center studies. For instance, Jose Castillo and Yongjun Wang exhibit significant influence in coordinating international collaborations, reflecting their pivotal roles in advancing research in this domain.

TABLE 1 The topic search query.

Set	Results	Search query
#1	205,292	TS = ((stoke) OR (brain infarction) OR (cerebrovascular) OR (cerebral infarction))
#2	909,543	TS = ((machine learning) OR (deep learning) OR (artificial intelligence) OR (machine intelligence) OR (neural network) OR (natural language processing) OR (hybrid intelligent system) OR (CNN) OR (LSTM) OR (RNN))
#3	588,300	((Magnetic Resonance Imaging) OR (Neuroimaging) OR (MRI))
#4	449	#1 AND #2 AND #3
#5	395	#4 AND Article (Document Types) AND English (Languages)

Web of Science Core Collection (December 1 2004 to December 1, 2023).

Analysis of countries

Figures 4 and Table 3 present the collaborative network among countries in this field of research, revealing a network comprising 54 nodes and 267 edges. The top contributors by publication volume are the People's Republic of China (136); USA (135); England (54); Germany (51); and Canada (34). However, a closer analysis reveals an interesting distinction between publication volume and centrality, which measures the influence of a country within the collaboration network. For example, while China leads in publication volume, its centrality is relatively low, indicating fewer collaborative connections with other nations compared to Germany (centrality: 0.24) and the USA (centrality: 0.14). This discrepancy suggests that while China and the USA dominate in output, Germany plays a more integrative role in fostering international collaborations. Such insights underline the importance of not only the quantity but also the quality and connectivity of research contributions in advancing the field.

In the country network, there is a strong positive correlation between publication volume and collaboration frequency, highlighting the synergy between research activity and international partnerships.

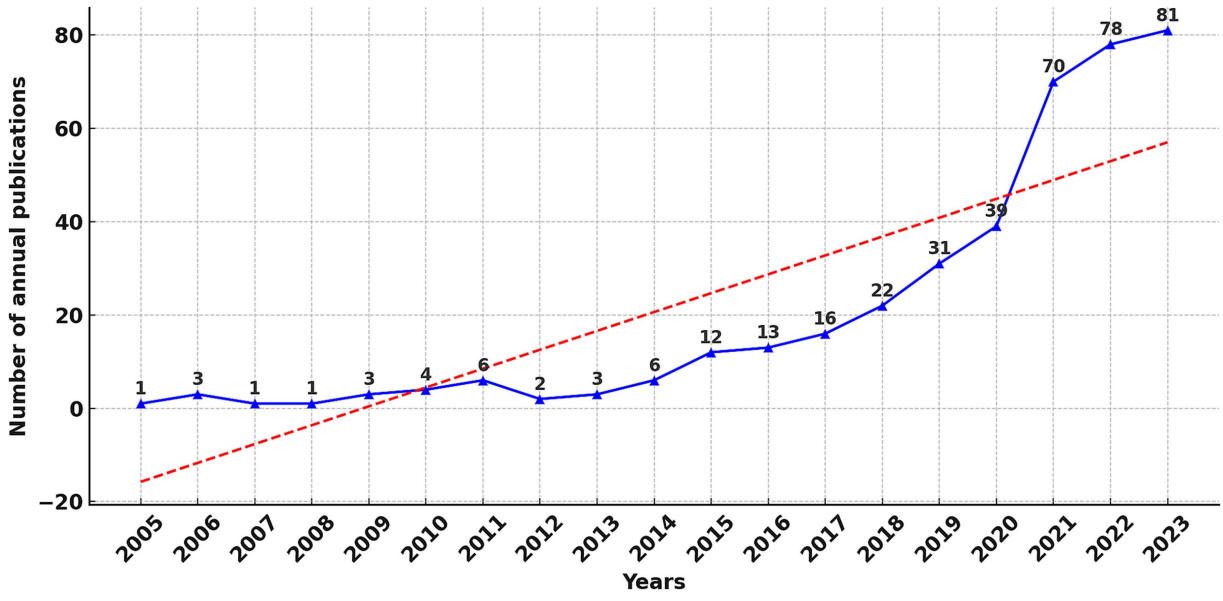

FIGURE 2
Map of annual publications related to machine learning and MRI in early stroke diagnosis.

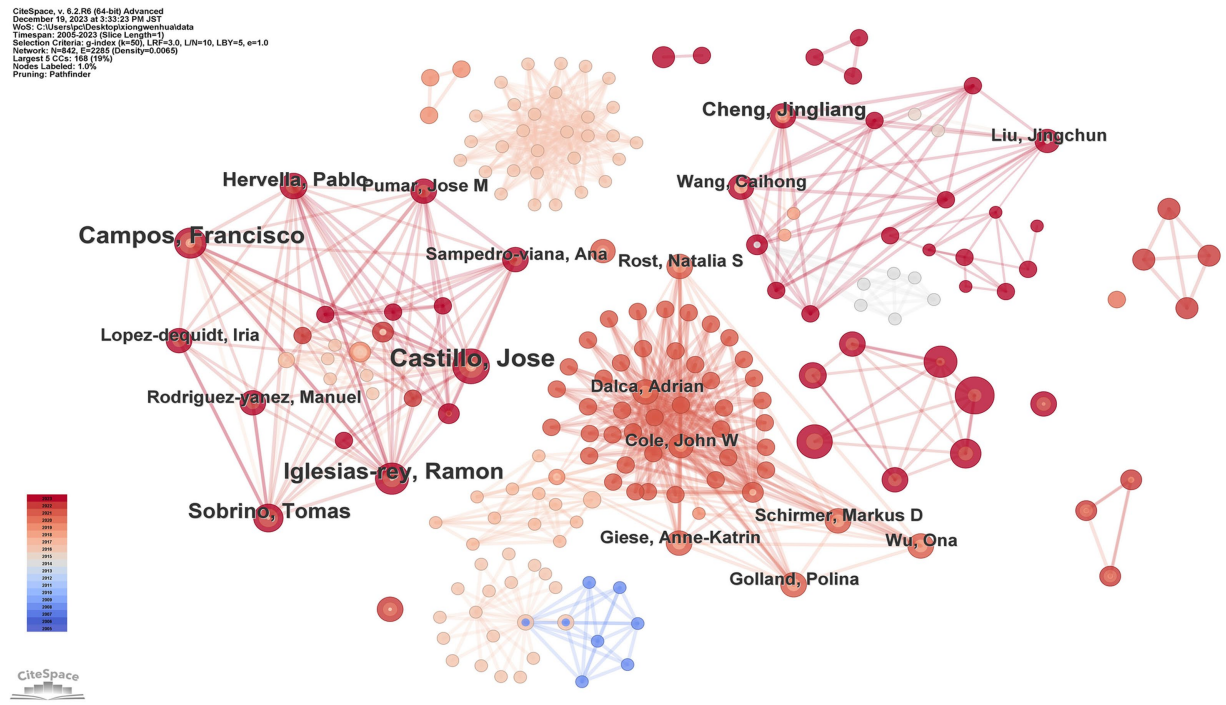

FIGURE 3
Map of authors related to machine learning and MRI in early stroke diagnosis.

TABLE 2 Top 10 authors related to machine learning and magnetic resonance imaging in early stroke diagnosis.

Rank	Author	Frequency	Year	Country
1	Castillo, Jose	9	2016	Spain
2	Wang, Yongjun	9	2022	People's Republic of China
3	Jing, Jing	8	2022	People's Republic of China
4	Campos, Francisco	8	2016	Spain
5	Meng, Xia	7	2022	People's Republic of China
6	Iglesias-rey, Ramon	7	2016	Spain
7	Sobrino, Tomas	6	2016	Spain
8	Li, Zixiao	6	2022	People's Republic of China
9	Chen, Cheng	5	2020	People's Republic of China
10	Zhao, Xingquan	5	2022	People's Republic of China

Interestingly, the correlation is weaker for centrality, indicating that publication volume does not always reflect the strategic importance of a country within the network. For instance, Germany, with a centrality of 0.24, leads in bridging interdisciplinary collaborations despite ranking fourth in publication volume.

Analysis of institutions

Figure 5 and Table 4 display the collaborative network of institutions, comprising 431 nodes and 1,709 edges. The top 10 institutions in terms of publication volume are as follows: University of California System (33 publications); Harvard University (33 publications); Massachusetts General Hospital (23 publications); Harvard Medical School (21 publications); Capital Medical University (20 publications); Chinese Academy of Sciences (18 publications); Chinese Academy of Medical Sciences—Peking Union Medical College (14 publications); Helmholtz Association (14 publications); Mayo Clinic (14 publications); University of California Los Angeles (13 publications). It was observed that academic institutions affiliated with the USA dominate the top 10 rankings. The interconnections between institutions across various countries highlight a significant network of collaborations, which is poised to further advance the discipline in this field.

Institutional collaboration analysis shows a moderate positive correlation between node degree and publication output. Institutions such as the University of California System and Harvard University,

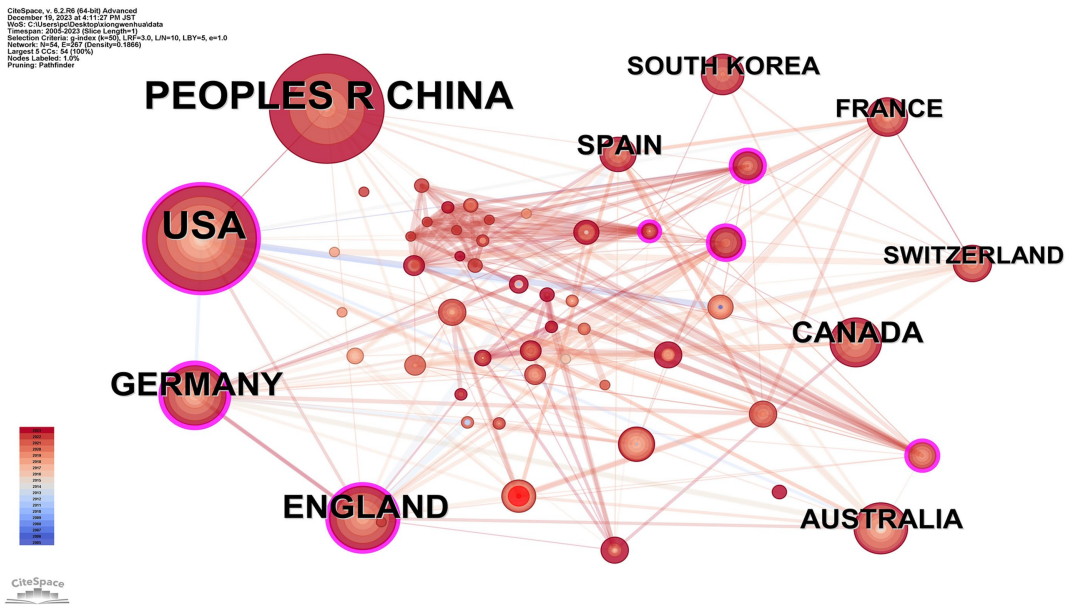

FIGURE 4
Map of countries related to machine learning and MRI in early stroke diagnosis.

TABLE 3 Top 10 frequency and centrality of countries related to machine learning and magnetic resonance imaging in early stroke diagnosis.

Rank	Frequency	Countries	Rank	Centrality	Countries
1	136	People's Republic of China	1	0.24	Germany
2	135	USA	2	0.19	India
3	54	England	3	0.15	England
4	51	Germany	4	0.15	Netherlands
5	34	Canada	5	0.15	Austria
6	27	Spain	6	0.14	USA
7	25	Australia	7	0.12	Czech Republic
8	20	South Korea	8	0.10	Switzerland
9	19	France	9	0.10	Saudi Arabia
10	18	Switzerland	10	0.07	Canada

which exhibit high node degrees, also demonstrate strong interconnectivity, fostering impactful collaborations that push the boundaries of ML applications in stroke research.

Analysis of cited journals

Figure 6 and Table 5 showcase the cited journal network, consisting of 838 nodes and 4,674 edges. The top 10 journals by citation frequency are: *Stroke* (248 citations); *NeuroImage* (215 citations); *Neurology* (183 citations); *PLoS One* (145 citations); *Brain* (127 citations); *Lancet Neurol* (125 citations); *J Cereb Blood Flow Metab* (125 citations); *Am J Neuroradiol* (119 citations); *Ann Neurol* (117 citations); *Hum Brain Mapp* (109 citations). Additionally, journals with notable centrality (indicated by purple rings) include *Ann NY Acad Sci* (0.12); *Am J Neuroradiol* (0.11); *Acta Neuropathol* (0.11). These journals primarily cover neurology, neuroimaging, and computer science. For instance, *Stroke* has an impact factor of 8.3, with *NeuroImage* and *Neurology* also being top-tier journals in this field.

The journals Stroke and NeuroImage exhibit the highest normalized citation impact, indicating their influence in bridging neurology and imaging studies. Additionally, metrics such as *h*-index and Eigenfactor score were analyzed for the top-cited journals to further evaluate their academic impact. For instance, Stroke has an impact factor of 8.3 and an *h*-index of 150, showcasing its long-standing relevance in stroke research. Similarly, NeuroImage demonstrates a significant *h*-index of 230, reflecting its importance in neuroimaging and machine learning studies. The cited journal analysis, complemented by impact metrics, highlights the interplay between foundational stroke research and emerging machine learning methodologies. This integrative approach provides robust evidence of the academic networks and key journals shaping this interdisciplinary field.

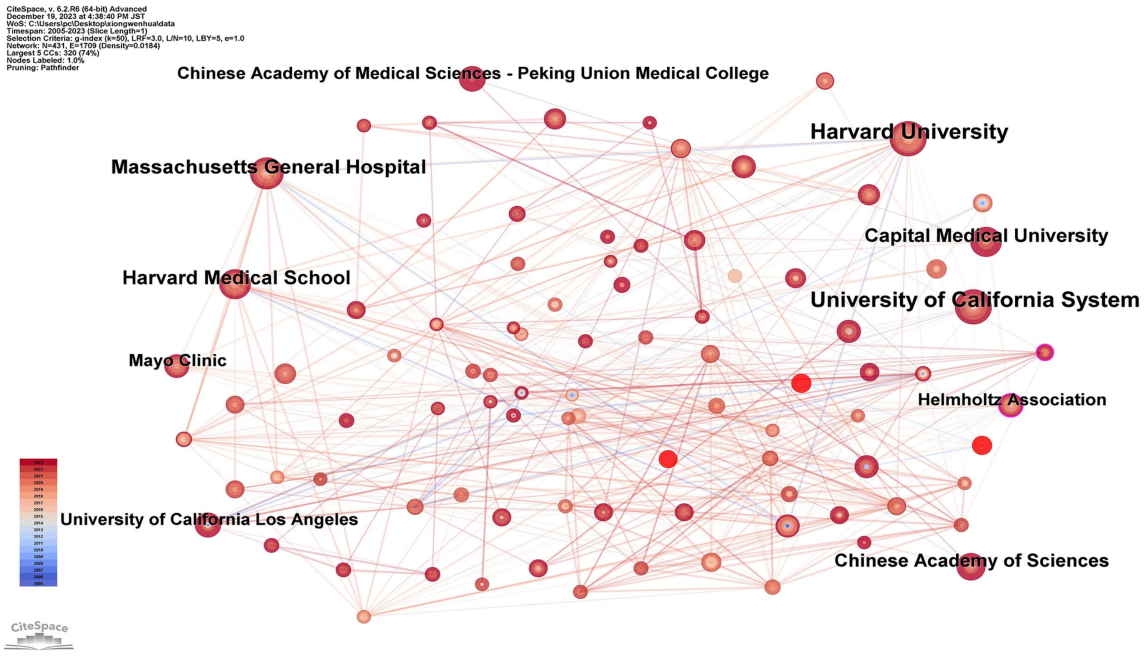

FIGURE 5
Map of institutions related to machine learning and MRI in early stroke diagnosis.

TABLE 4 Top 10 publications of institutions related to machine learning and magnetic resonance imaging in early stroke diagnosis.

Rank	Frequency	Year	Institutions
1	33	2006	University of California System
2	33	2005	Harvard University
3	23	2005	Massachusetts General Hospital
4	21	2006	Harvard Medical School
5	20	2019	Capital Medical University
6	18	2011	Chinese Academy of Sciences
7	14	2022	Chinese Academy of Medical Sciences—Peking Union Medical College
8	14	2012	Helmholtz Association
9	14	2017	Mayo Clinic
10	13	2006	University of California Los Angeles

Keywords co-occurrence and citation burst analysis

Figure 7 and Table 6 depict the network graph of keywords, encompassing 690 nodes and 2,513 edges. The top 10 keywords are: deep learning (46 occurrences); machine learning (45 occurrences); brain (39 occurrences); magnetic resonance imaging (36 occurrences); stroke (31 occurrences); MRI (25 occurrences); functional connectivity (25 occurrences); risk (24 occurrences); ischemic stroke (24 occurrences); Alzheimer's disease (23 occurrences). Analyzing the frequency and centrality of these keywords reveals that "deep learning," "magnetic resonance imaging," and "stroke" have emerged as prominent themes in this research area.

Figure 8 illustrates the top 20 keywords with the most robust citation bursts. The beginning and end of each burst are, respectively, marked as "Start" and "End," with the increase in influence correlating with the rise in the "Strength" value. The pale blue region delineates the study period, while the red portion signifies the start and peak of the bursts. It was observed that "machine learning" exhibited the highest burst strength, reaching 6.57. Furthermore, early attention to "functional MRI" and "diffusion tensor imaging" indicates that changes in brain structure and function had been applied in this field from an early stage. Mid-period keywords like "executive function" and "default mode network" experienced high burst rates, signifying researchers' growing focus on the interconnections between deep brain networks. In later periods, the frequent emergence of terms such as "prediction," "classification," and "machine learning" underscores the extensive application of ML in recent years for the early diagnosis of stroke and the development of individualized treatment plans to prevent the high mortality associated with acute stroke incidents.

The co-occurrence network reveals a strong positive correlation between keyword centrality and burst strength. Keywords such as "deep learning" and "machine learning" not only occur frequently but also drive significant citation bursts, underscoring their pivotal roles in shaping the field. Additionally, the temporal analysis suggests that early bursts in keywords like "functional MRI" paved the way for mid-period focuses on "executive function" and later trends emphasizing "classification" and "prediction."

Keywords timeline

Figure 9 presents the evolution and interconnections of keywords, arranged chronologically. The timeline extends from

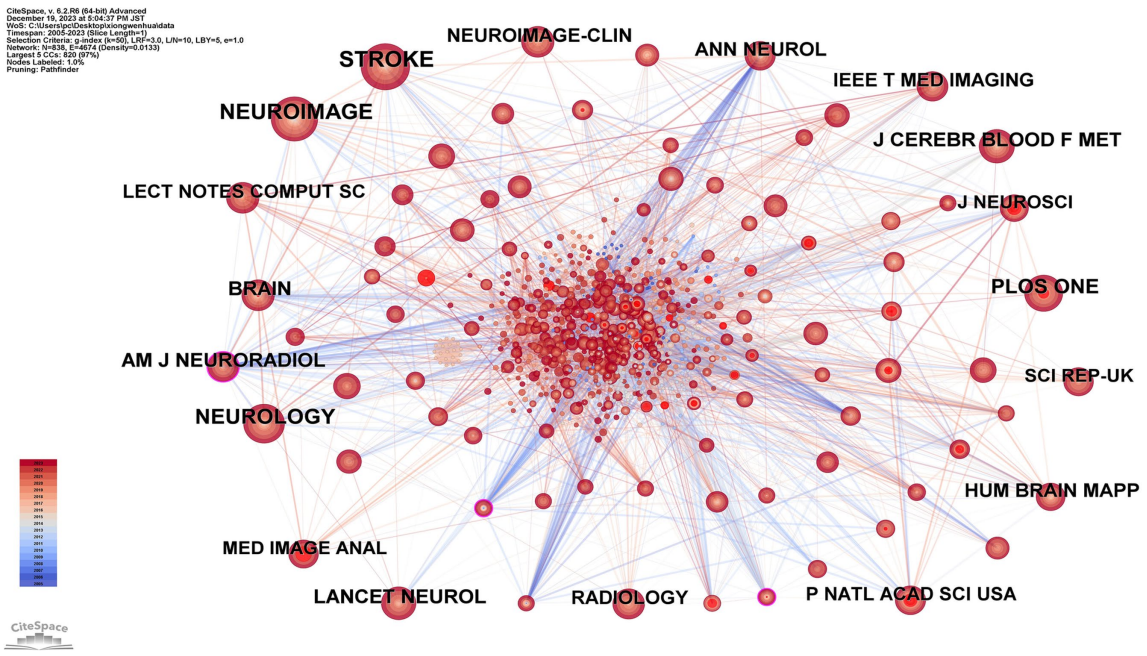

FIGURE 6
Map of cited journals related to machine learning and MRI in early stroke diagnosis.

TABLE 5 Top 10 frequency and centrality of cited journals related to machine learning and magnetic resonance imaging in early stroke diagnosis.

Rank	Frequency	Cited journals	Rank	Centrality	Cited journals
1	248	Stroke	1	0.12	Ann NY Acad Sci
2	215	NeuroImage	2	0.11	Am J Neuroradiol
3	183	Neurology	3	0.11	Acta Neuropathol
4	145	PLoS One	4	0.09	Ann Neurol
5	127	Brain	5	0.09	Acad Radiol
6	125	Lancet Neurol	6	0.09	IEEE Int Conf Neural Netw Proc
7	125	J Cereb Blood Flow Metab	7	0.08	Am J Cardiol
8	119	Am J Neuroradiol	8	0.07	IEEE Trans Med Imaging
9	117	Ann Neurol	9	0.07	Annu Rev Neurosci
10	109	Hum Brain Mapp	10	0.06	Arch Neurol

left to right, delineating the emergence and disappearance of research keywords from 2004 to 2023. Additionally, the diagram clusters various themes. A total of nine clusters (#0 to #8) are depicted. The first cluster (#0), labeled "temporal consistency," focuses on topics like deep learning, automated WMH detection, and amorphous object segmentation. The second cluster (#1), identified as "classification method," concentrates on magnetic resonance imaging, cerebral blood flow, and related themes. The third cluster is marked as "functional connectivity strength," highlighting areas such as intrinsic functional connectivity and graph theory analysis. The fourth cluster, labeled "final infarct volume," focuses on chronic venous disease, peripheral artery disease, and similar subjects. The fifth cluster, named "rural-urban disparities," is centered around risk factors and minority health.

Cluster dependencies of reference

Figure 10 showcases the dependency relationships among clusters based on referenced literature. Areas coded in different colors represent distinct clusters of references, while arrows indicate the developmental relationships between these clusters. The convergence of arrows signifies the emergence of new disciplinary branches, while the merging of arrowheads indicates the integration of different disciplines. This is because the tail of an arrow represents the cutting edge of current knowledge, while the head points to the sources of foundational literature.

The developmental pattern in this field primarily exists in a dual form: the coexistence of interdisciplinary integration and the refinement of major disciplinary branches. A detailed analysis reveals several cutting-edge directions of interdisciplinary integration:

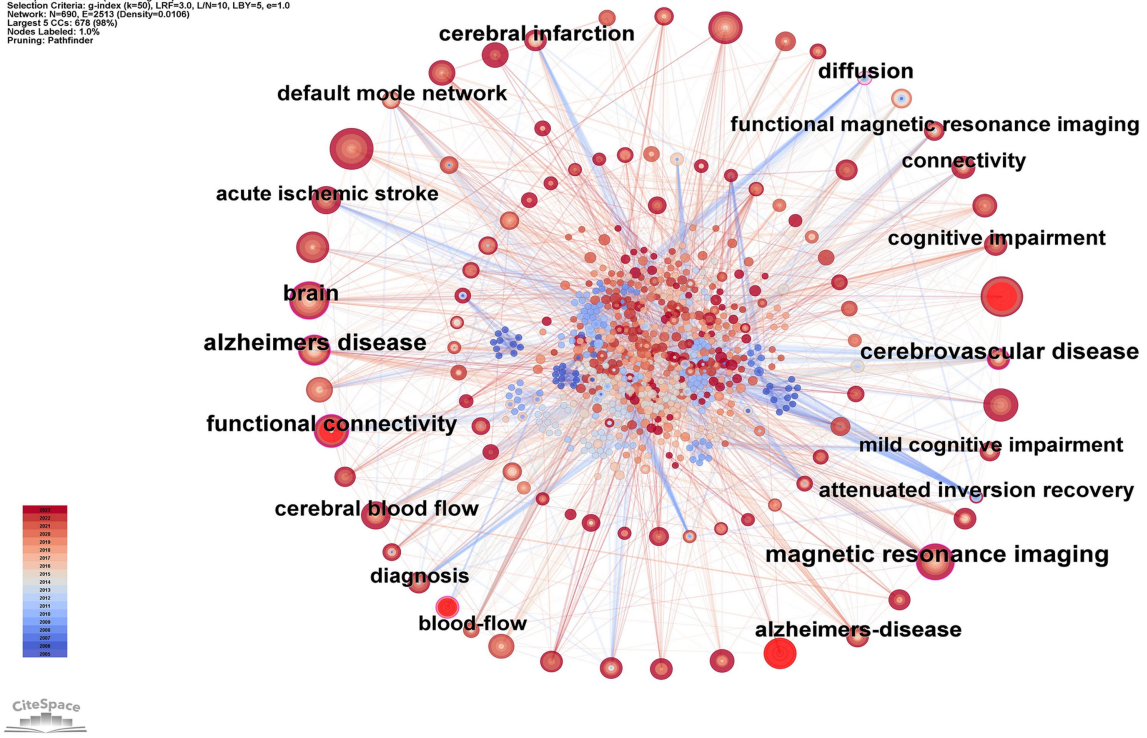

FIGURE 7
Map of keywords related to machine learning and MRI in early stroke diagnosis.

TABLE 6 Top 10 frequency and centrality of keywords related to machine learning and magnetic resonance imaging in early stroke diagnosis.

Rank	Frequency	Keywords	Rank	Centrality	Keywords
1	46	deep learning	1	0.19	Alzheimer's disease
2	45	machine learning	2	0.18	magnetic resonance imaging
3	39	brain	3	0.16	cerebrovascular disease
4	36	magnetic resonance imaging	4	0.15	brain
5	31	stroke	5	0.13	functional connectivity
6	25	MRI	6	0.11	functional MRI
7	25	functional connectivity	7	0.11	diffusion
8	24	risk	8	0.09	cerebral blood flow
9	24	ischemic stroke	9	0.09	Alzheimer's disease
10	23	Alzheimer's disease	10	0.09	functional magnetic resonance imaging

Neuroimaging and machine learning: The integration of advanced imaging modalities such as diffusion tensor imaging and convolutional neural networks has enabled the development of automated lesion segmentation and early diagnostic models for ischemic stroke. This integration bridges computational algorithms and clinical radiology, advancing both fields. Neurology and bioinformatics: The use of bioinformatics tools in analyzing imaging markers has enhanced the understanding of the molecular underpinnings of stroke. For example, integrating genetic data with MRI-based phenotypes offers new insights into personalized therapeutic strategies. Clinical decision support systems and artificial intelligence: AI-driven CDSS, leveraging ML-based prognostic models, has facilitated real-time decision-making in stroke management, particularly in identifying optimal therapeutic windows. This interdisciplinary collaboration integrates medical informatics, neurology, and computer science. For instance, cluster #17 represents the fusion of neuroimaging and ML (clusters #0 and #10), while cluster #5 reflects the branching of ML applications into

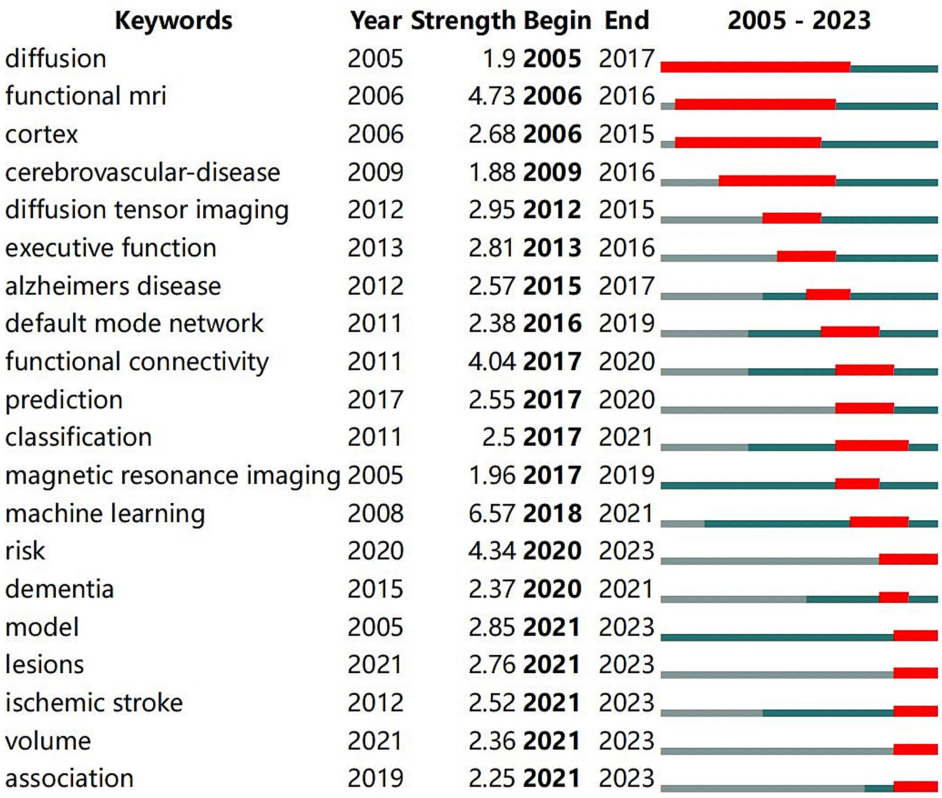

FIGURE 8
Top 20 keywords with the strongest citation bursts.

specific subdomains of neurology (clusters #1 and #3). These trends underscore the pivotal role of interdisciplinary integration in advancing the field of early stroke diagnosis.

Correlation analysis of the reference dependency network indicates a significant relationship between cluster size and the number of interdisciplinary connections. Larger clusters, such as #0 and #10, exhibit higher connectivity, reflecting their central roles in integrating neuroimaging and ML methodologies. This interdependency highlights the importance of large clusters in driving knowledge transfer and innovation across disciplinary boundaries.

Discussion

A bibliometric analysis was conducted using CiteSpace, focusing on the early diagnosis of stroke through ML identification of MRI characteristics from 2004 to 2023. This analysis encompassed the collaborative networks of core authors, affiliated institutions, countries, and journals. Comprehensive data were provided, highlighting the focal points and trends in the early diagnosis of stroke using ML to identify MRI characteristics.

General information

This study illustrates that over the past two decades, a total of 395 publications have been released in the field of early stroke diagnosis using ML to identify characteristics in MRI. The findings show that prior to 2015, the annual number of publications was consistently below 10, reflecting the nascent stage of ML as an academic discipline. Since 2015, there has been a marked increase in publications, a development attributed to the enhanced computational capabilities of ML and the refinement of its algorithmic structures, demonstrating potential in improving the accuracy of stroke diagnosis, subtype classification, and prognostic prediction. The trend line suggests an anticipation of a new peak in publication volume within the next 5–10 years.

An analysis of authors, countries, and their affiliated institutions with higher publication numbers reveals that institutions and authors from the USA and China have established mature academic communities on a global scale, forming extensive collaborative networks with other institutions. This indicates the reliance of ML on the technological level and talent reserves of a country. Notably, despite the lower volume of publications from less developed

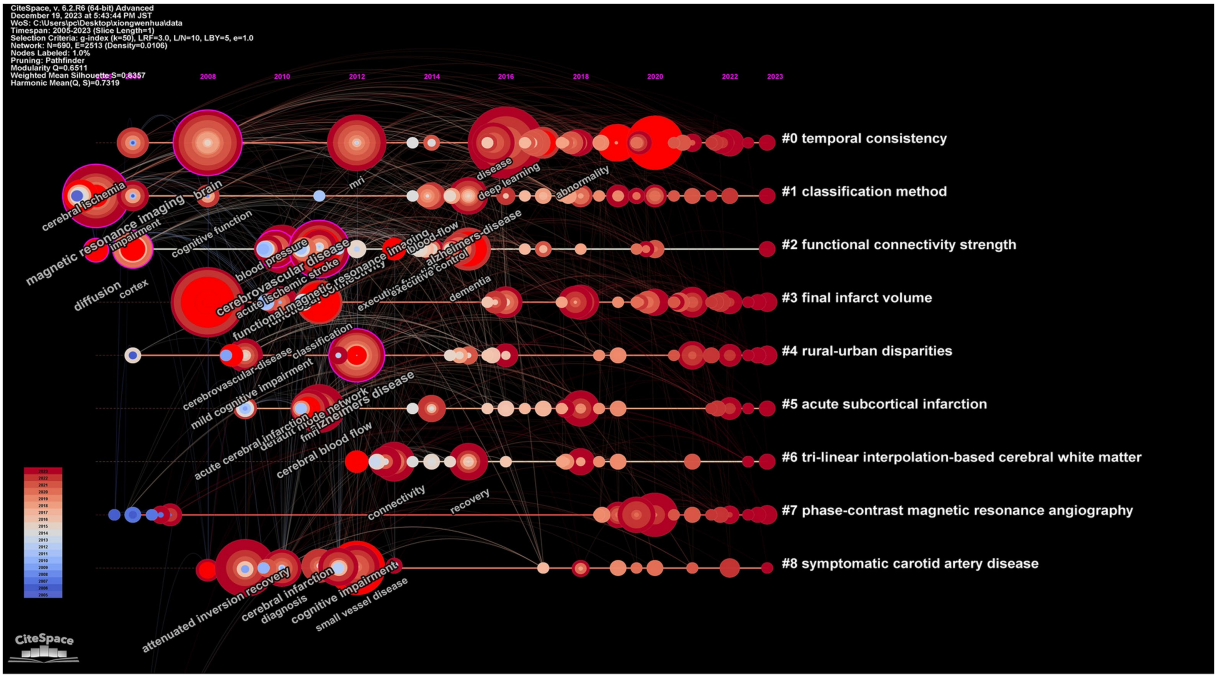

FIGURE 9
Map of keywords timeline related to machine learning and MRI in early stroke diagnosis.

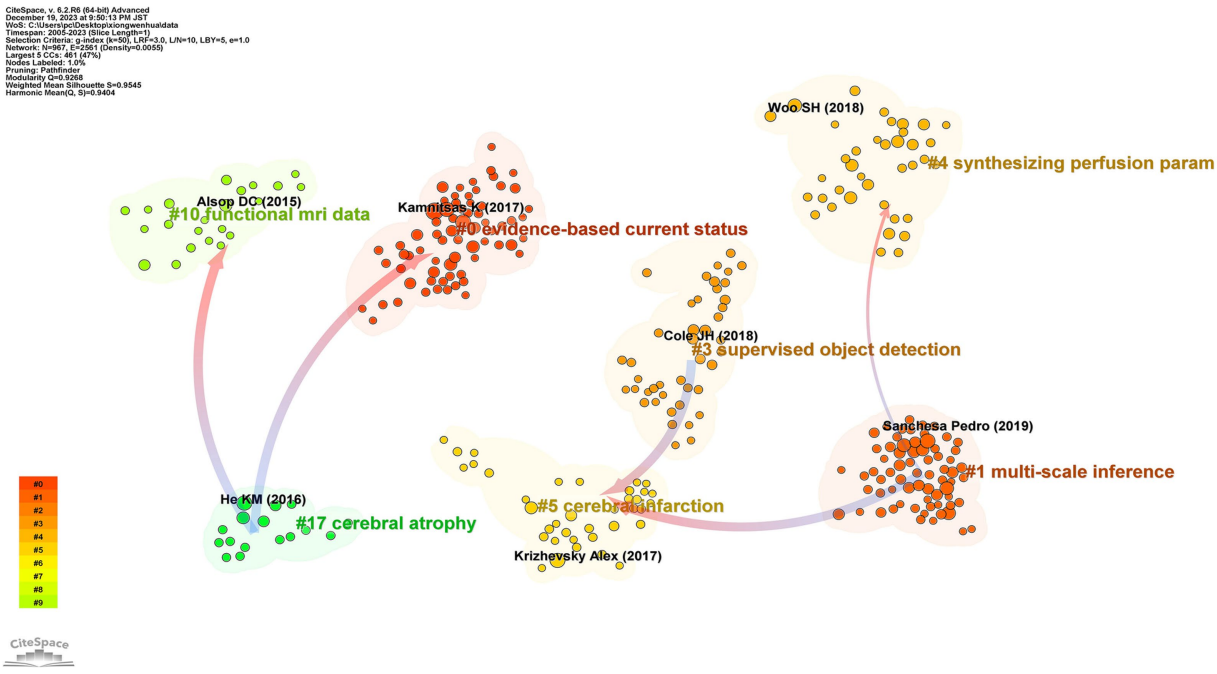

FIGURE 10
Map of reference of cluster dependencies related to machine learning and MRI in early stroke diagnosis.

countries, these nations may still experience high stroke incidence rates.

Through the analysis of interdependencies among clusters in references, it was found that the development pattern in the field of early stroke diagnosis using ML for MRI primarily exists in a form of coexistence between interdisciplinary integration and the refinement of major disciplinary branches. This unique characteristic is likely to promote resource integration, cross-disciplinary idea exchange, and academic innovation within the field.

In summary, ML as an emerging discipline, has shown immense value in early diagnosis of stroke through neuroimaging, medical efficiency, and personalized treatment, with a significant rise in publication volume in recent years. Based on the trends in annual publication volume and innovation in ML algorithms, significant advancements are expected in the next 5–10 years, ultimately aiming to provide precise medical services for stroke patients.

Research hotspots

Research hotspots in a field are encapsulated by keywords that represent the core content and central themes of studies within that domain. Techniques such as keyword co-occurrence analysis, keyword clustering, and keyword citation bursts enable the monitoring of various emerging trends in a given field. In the realm of using ML for early stroke diagnosis through the identification of MRI features, two primary research hotspots have emerged: the optimal selection of neural imaging markers and the most appropriate ML algorithm models.

Optimal selection of neural imaging markers

In the pursuit of the most effective neural imaging markers for stroke patients using MRI, researchers primarily focus on cerebral blood flow, brain structure, or brain function. From the perspective of cerebral blood flow, arterial spin labeling (ASL) is a predominant research method. For instance, Liu's et al. (33) study indicates that the combination of ML and ASL can predict the outcomes of acute ischemic strokes by examining collateral circulation. Regarding brain structure, diffusion weighted imaging (DWI) often serves as the main analytical approach. Yu et al. (34) and Zhu et al. (35), for example, discovered that deep learning using DWI and clinical data is highly sensitive in predicting patients with low-perfusion strokes. From the aspect of brain function, the most valued approach is brain network analysis using functional connectivity (FC) from functional MRI. Li's et al. (36) findings suggest that multispectral FC variations in brain regions are potential targets for differentiating stroke patients' recovery and treatment processes. Lu et al. (37) demonstrated that acupuncture could modulate bilateral cerebral hemispheres through distinct targets, restoring abnormal FC and thus facilitating post-stroke motor recovery. Moreover, many studies advocate the integration of multimodal MRI datasets as neural imaging markers, surpassing the predictive accuracy of early stroke onset compared to single-modality data (38–40).

Optimal machine learning algorithm models

ML algorithms are diverse and continually evolving, with researchers exploring various models for neuroimaging data from MRIs. Pérez Malla et al. (41) and Nishi et al. (42), for instance, regard convolutional neural networks (CNNs) as the most advanced method for early stroke prediction. Billot et al. (43) found that a combination of support vector machines (SVMs) and random forests (RFs) also exhibits commendable performance. Pinto et al. (44) proposed a fully automated deep learning approach encompassing both unsupervised and supervised learning, achieving satisfactory accuracy. Emerging deep learning techniques, such as deep neural networks (DNNs) and reinforcement learning (RL), are gaining traction due to their ability to automatically extract features from raw data and further improve model accuracy. These methods show substantial promise in enhancing early stroke detection by providing deeper, more nuanced insights into complex MRI data patterns. The introduction of these advanced techniques could lead to significant improvements in diagnostic accuracy, particularly in early-stage stroke diagnosis, where subtle changes in brain tissue are often challenging to detect.

Recent advancements in explainable AI (XAI) have also contributed to the interpretability of machine learning models, which is crucial in clinical settings. XAI approaches aim to provide transparent reasoning behind model predictions, enabling healthcare professionals to better understand and trust the automated results. Furthermore, multimodal approaches combining MRI with other data sources, such as genetic or clinical data, are gaining momentum. These methods harness the complementary strengths of different types of data to create more robust models that enhance diagnostic accuracy and prognostic prediction. By integrating various data types, multimodal systems can capture a more comprehensive view of the patient's condition, improving decision-making in early stroke diagnosis.

The integration of ML with neuroimaging offers significant potential for bridging current gaps in early stroke diagnosis. While traditional methods rely on visual interpretation of MRI scans, ML techniques allow for the automated detection and quantification of subtle patterns that may be overlooked by human evaluators. The ability of ML algorithms to process large volumes of complex MRI data and generate predictive models can improve diagnostic accuracy, particularly in the early stages of stroke, when clinical symptoms may not yet be fully manifest. Furthermore, ML can help to identify imaging markers that correlate with stroke outcomes, offering personalized treatment options for patients. This integration is particularly promising in addressing the challenge of time-sensitive diagnoses, where rapid and accurate assessments can directly impact patient prognosis and recovery. As ML algorithms, including deep learning and multimodal approaches, continue to evolve, their capacity to enhance diagnostic workflows, reduce human error, and accelerate decision-making processes in clinical settings will be invaluable in overcoming the challenges of early stroke diagnosis.

Conclusion

The application of ML in the early diagnosis, prediction, and individualized medical plans for stroke patients using neuroimaging features offers immense value. This study specifically focused on the role of ML in early stroke detection and prediction by analyzing its capacity to identify subtle imaging markers and enhance diagnostic precision in the critical early stages. The most compelling current research hotspots are the optimal selection of neural imaging markers and the most suitable ML algorithm models for these purposes. In the future, researchers can continue to develop high-performance algorithms, further advancing early diagnosis and personalized treatment strategies in this scientific domain.

Limitations

This study is subject to several limitations. Firstly, it primarily relies on data accessible within the WOSCC database. CiteSpace is incapable of integrating data from varied databases or performing citation analysis on sources outside of WOSCC. Secondly, while CiteSpace proves invaluable in detecting and visualizing emerging trends, it does not delve into the underlying mechanisms of machine algorithm models in the application of identifying MRI features for early stroke diagnosis. Despite these constraints, we have successfully employed CiteSpace to illustrate the latest research trends in the application of machine algorithm models in the early diagnosis of stroke through the recognition of MRI characteristics.

Data availability statement

The original contributions presented in the study are included in the article/supplementary material, further inquiries can be directed to the corresponding author.

Author contributions

J-cL: Conceptualization, Data curation, Formal analysis, Investigation, Methodology, Software, Validation, Writing – original draft, Writing – review & editing. X-fY: Conceptualization, Data curation, Investigation, Resources, Writing – original draft, Writing – review & editing. J-jY: Data curation, Investigation, Methodology, Software, Writing – original draft, Writing – review & editing. D-qS: Data curation, Investigation, Software, Visualization, Writing – original draft, Writing – review & editing. W-hX: Conceptualization, Data curation, Formal analysis, Investigation, Methodology, Project administration, Resources, Software, Supervision, Writing – original draft, Writing – review & editing.

Funding

The author(s) declare that no financial support was received for the research and/or publication of this article.

Acknowledgments

We extend our gratitude to Chaomei Chen of Drexel University for his contributions in developing CiteSpace. Additionally, we would like to express our appreciation to the reviewers for their valuable insights, which have enabled us to enhance this manuscript.

Conflict of interest

The authors declare that the research was conducted in the absence of any commercial or financial relationships that could be construed as a potential conflict of interest.

Generative AI statement

The authors declare that no Gen AI was used in the creation of this manuscript.

Publisher's note

All claims expressed in this article are solely those of the authors and do not necessarily represent those of their affiliated organizations, or those of the publisher, the editors and the reviewers. Any product that may be evaluated in this article, or claim that may be made by its manufacturer, is not guaranteed or endorsed by the publisher.

References

1. Tu WJ, Wang LDSpecial Writing Group of China Stroke Surveillance Report. China stroke surveillance report 2021. *Mil Med Res*. (2023) 10:33. doi: 10.1186/s40779-023-00463-x

2. Eskioglou E, Huchmandzadeh Millotte M, Amiguet M, Michel P. National institutes of health stroke scale zero strokes. *Stroke*. (2018) 49:3057–9. doi: 10.1161/STROKEAHA.118.022517

3. Papanagiotou P, White CJ. Endovascular reperfusion strategies for acute stroke. *JACC Cardiovasc Interv*. (2016) 9:307–17. doi: 10.1016/j.jcin.2015.11.014

4. Owolabi MO, Thrift AG, Mahal A, Ishida M, Martins S, Johnson WD, et al. Primary stroke prevention worldwide: translating evidence into action. *Lancet Public Health*. (2022) 7:e74–85. doi: 10.1016/S2468-2667(21)00230-9

5. Mohan KM, Wolfe CD, Rudd AG, Heuschmann PU, Kolominsky-Rabas PL, Grieve AP. Risk and cumulative risk of stroke recurrence: a systematic review and meta-analysis. *Stroke*. (2011) 42:1489–94. doi: 10.1161/STROKEAHA.110.602615

6. Hwang J, Kalra A, Shou BL, Whitman G, Wilcox C, Brodie D, et al. Epidemiology of ischemic stroke and hemorrhagic stroke in venoarterial extracorporeal membrane oxygenation. *Crit Care*. (2023) 27:433. doi: 10.1186/s13054-023-04707-z

7. Roger VL, Go AS, Lloyd-Jones DM, Benjamin EJ, Berry JD, Borden WB, et al. Heart disease and stroke statistics—2012 update: a report from the American Heart Association. *Circulation*. (2012) 125:e2–e220. doi: 10.1161/CIR.0b013e31823ac046

8. Shah S, Luby M, Poole K, Morella T, Keller E, Benson RT, et al. Screening with MRI for accurate and rapid stroke treatment: SMART. *Neurology*. (2015) 84:2438–44. doi: 10.1212/WNL.0000000000001678

9. Fiebach JB, Schellinger PD, Gass A, Kucinski T, Siebler M, Villringer A, et al. Stroke magnetic resonance imaging is accurate in hyperacute intracerebral hemorrhage: a multicenter study on the validity of stroke imaging. *Stroke*. (2004) 35:502–6. doi: 10.1161/01.STR.0000114203.75678.88

10. Liu L, Chang J, Liu Z, Zhang P, Xu X, Shang H. Hybrid contextual semantic network for accurate segmentation and detection of small-size stroke lesions from MRI. *IEEE J Biomed Health Inform*. (2023) 27:4062–73. doi: 10.1109/JBHI.2023.3273771

11. Raimondo L, Oliveira ĹAF, Heij J, Priovoulos N, Kundu P, Leoni RF, et al. Advances in resting state fMRI acquisitions for functional connectomics. *NeuroImage*. (2021) 243:118503. doi: 10.1016/j.neuroimage.2021.118503

12. Zhou XC, Huang YB, Wu S, Hong SW, Tian Y, Hu HJ, et al. Lever positioning manipulation alters real-time brain activity in patients with lumbar disc herniation: an amplitude of low-frequency fluctuation and regional homogeneity study. *Psychiatry Res Neuroimaging*. (2023) 334:111674. doi: 10.1016/j.pscychresns.2023.111674

13. Xuan K, Xiang L, Huang X, Zhang L, Liao S, Shen D, et al. Multimodal MRI reconstruction assisted with spatial alignment network. *IEEE Trans Med Imaging*. (2022) 41:2499–509. doi: 10.1109/TMI.2022.3164050

14. Choksi B, Mozafari M, VanRullen R, Reddy L. Multimodal neural networks better explain multivoxel patterns in the hippocampus. *Neural Netw*. (2022) 154:538–42. doi: 10.1016/j.neunet.2022.07.033

15. Schwarzbach CJ, Eichner FA, Rücker V, Hofmann AL, Keller M, Audebert HJ, et al. The structured ambulatory post-stroke care program for outpatient aftercare in patients with ischaemic stroke in Germany (SANO): an open-label, cluster-randomised controlled trial. *Lancet Neurol*. (2023) 22:787–99. doi: 10.1016/S1474-4422(23)00216-8

16. Olasoji EB, Uhm DK, Awosika OO, Doré S, Geis C, Simpkins AN. Trends in outpatient rehabilitation use for stroke survivors. *J Neurol Sci*. (2022) 442:120383. doi: 10.1016/j.jns.2022.120383

17. Qiu W, Kuang H, Teleg E, Ospel JM, Sohn SI, Almekhlafi M, et al. Machine learning for detecting early infarction in acute stroke with non-contrast-enhanced CT. *Radiology*. (2020) 294:638–44. doi: 10.1148/radiol.2020191193

18. Bonkhoff AK, Grefkes C. Precision medicine in stroke: towards personalized outcome predictions using artificial intelligence. *Brain*. (2022) 145:457–75. doi: 10.1093/brain/awab439

19. Castaneda-Vega S, Katiyar P, Russo F, Patzwaldt K, Schnabel L, Mathes S, et al. Machine learning identifies stroke features between species. *Theranostics*. (2021) 11:3017–34. doi: 10.7150/thno.51887

20. Chavva IR, Crawford AL, Mazurek MH, Yuen MM, Prabhat AM, Payabvash S, et al. Deep learning applications for acute stroke management. *Ann Neurol*. (2022) 92:574–87. doi: 10.1002/ana.26435

21. Oikonomou EK, Spatz ES, Suchard MA, Khera R. Individualising intensive systolic blood pressure reduction in hypertension using computational trial phenomaps and machine learning: a post-hoc analysis of randomised clinical trials. *Lancet Digit Health*. (2022) 4:e796–805. doi: 10.1016/S2589-7500(22)00170-4

22. Feng J, Zhang Q, Wu F, Peng J, Li Z, Chen Z. The value of applying machine learning in predicting the time of symptom onset in stroke patients: systematic review and meta-analysis. *J Med Internet Res*. (2023) 25:e44895. doi: 10.2196/44895

23. Zhou XC, Huang YB, Liu Z, Wu HJ, Huang HZ, Tian Y, et al. Bibliometric analysis of functional magnetic resonance imaging studies on manual therapy analgesia from 2002–2022. *J Pain Res*. (2023) 16:2115–29. doi: 10.2147/JPR.S412658

24. Li X, Wei W, Wang Y, Wang Q, Liu Z. Global trend in the research and development of acupuncture treatment on Parkinson's disease from 2000 to 2021: a bibliometric analysis. *Front Neurol*. (2022) 13:906317. doi: 10.3389/fneur.2022.906317

25. Liang YD, Li Y, Zhao J, Wang XY, Zhu HZ, Chen XH. Study of acupuncture for low back pain in recent 20 years: a bibliometric analysis via CiteSpace. *J Pain Res*. (2017) 10:951–64. doi: 10.2147/JPR.S132808

26. Chen YM, Wang XQ. Bibliometric analysis of exercise and neuropathic pain research. *J Pain Res*. (2020) 13:1533–45. doi: 10.2147/JPR.S258696

27. Xi M, Gao X. Bibliometric analysis of research relating to IgA nephropathy from 2010 to 2021. *Med Sci Monit*. (2022) 28:e937976. doi: 10.12659/MSM.937976

28. He Z, Dai L, Zuo Y, Chen Y, Wang H, Zeng H. Hotspots and frontiers in pulmonary arterial hypertension research: a bibliometric and visualization analysis from 2011 to 2020. *Bioengineered*. (2022) 13:14667–80. doi: 10.1080/21655979.2022.2100064

29. Wu F, Gao J, Kang J, Wang X, Niu Q, Liu J, et al. Knowledge mapping of exosomes in autoimmune diseases: a bibliometric analysis (2002–2021). *Front Immunol*. (2022) 13:939433. doi: 10.3389/fimmu.2022.939433

30. Chen C, Hu Z, Liu S, Tseng H. Emerging trends in regenerative medicine: a scientometric analysis in CiteSpace. *Expert Opin Biol Ther*. (2012) 12:593–608. doi: 10.1517/14712598.2012.674507

31. Chen C, Dubin R, Kim MC. Emerging trends and new developments in regenerative medicine: a scientometric update (2000–2014). *Expert Opin Biol Ther*. (2014) 14:1295–317. doi: 10.1517/14712598.2014.920813

32. Mainali S, Darsie ME, Smetana KS. Machine learning in action: stroke diagnosis and outcome prediction. *Front Neurol*. (2021) 12:734345. doi: 10.3389/fneur.2021.734345

33. Liu S, Fan D, Zang F, Gu N, Yin Y, Ge X, et al. Collateral circulation detected by arterial spin labeling predicts outcome in acute ischemic stroke. *Acta Neurol Scand*. (2022) 146:635–42. doi: 10.1111/ane.13694

34. Yu Y, Christensen S, Ouyang J, Scalzo F, Liebeskind DS, Lansberg MG, et al. Predicting hypoperfusion lesion and target mismatch in stroke from diffusion-weighted MRI using deep learning. *Radiology*. (2023) 307:e220882. doi: 10.1148/radiol.220882

35. Zhu H, Jiang L, Zhang H, Luo L, Chen Y, Chen Y. An automatic machine learning approach for ischemic stroke onset time identification based on DWI and FLAIR imaging. *NeuroImage Clin*. (2021) 31:102744. doi: 10.1016/j.nicl.2021.102744

36. Li J, Cheng L, Chen S, Zhang J, Liu D, Liang Z, et al. Functional connectivity changes in multiple-frequency bands in acute basal ganglia ischemic stroke patients: a machine learning approach. *Neural Plast*. (2022) 2022:1560748. doi: 10.1155/2022/1560748

37. Lu M, Du Z, Zhao J, Jiang L, Liu R, Zhang M, et al. Neuroimaging mechanisms of acupuncture on functional reorganization for post-stroke motor improvement: a machine learning-based functional magnetic resonance imaging study. *Front Neurosci*. (2023) 17:1143239. doi: 10.3389/fnins.2023.1143239

38. Yu H, Wang Z, Sun Y, Bo W, Duan K, Song C, et al. Prognosis of ischemic stroke predicted by machine learning based on multi-modal MRI radiomics. *Front Psychiatry*. (2023) 13:1105496. doi: 10.3389/fpsyt.2022.1105496

39. Carlson HL, Craig BT, Hilderley AJ, Hodge J, Rajashekar D, Mouches P, et al. Structural and functional connectivity of motor circuits after perinatal stroke: a machine learning study. *NeuroImage Clin*. (2020) 28:102508. doi: 10.1016/j.nicl.2020.102508

40. Chong B, Wang A, Borges V, Byblow WD, Alan Barber P, Stinear C. Investigating the structure-function relationship of the corticomotor system early after stroke using machine learning. *NeuroImage Clin*. (2022) 33:102935. doi: 10.1016/j.nicl.2021.102935

41. Pérez Malla CU, Valdés Hernández MDC, Rachmadi MF, Komura T. Evaluation of enhanced learning techniques for segmenting ischaemic stroke lesions in brain magnetic resonance perfusion images using a convolutional neural network scheme. *Front Neuroinform*. (2019) 13:33. doi: 10.3389/fninf.2019.00033

42. Nishi H, Oishi N, Ishii A, Ono I, Ogura T, Sunohara T, et al. Deep learning-derived high-level neuroimaging features predict clinical outcomes for large vessel occlusion. *Stroke*. (2020) 51:1484–92. doi: 10.1161/STROKEAHA.119.028101

43. Billot A, Lai S, Varkanitsa M, Braun EJ, Rapp B, Parrish TB, et al. Multimodal neural and behavioral data predict response to rehabilitation in chronic poststroke aphasia. *Stroke*. (2022) 53:1606–14. doi: 10.1161/STROKEAHA.121.036749

44. Pinto A, Pereira S, Meier R, Wiest R, Alves V, Reyes M, et al. Combining unsupervised and supervised learning for predicting the final stroke lesion. *Med Image Anal*. (2021) 69:101888. doi: 10.1016/j.media.2020.101888

frontiers | Frontiers in Neurology

TYPE Systematic Review
PUBLISHED 28 April 2025
DOI 10.3389/fneur.2025.1539736

OPEN ACCESS

EDITED BY
Mingming Lu,
Characteristic Medical Center of Chinese People's Armed Police Force, China

REVIEWED BY
Zhen Yuan,
University of Macau, China
Borhan Asadi,
University of Zaragoza, Spain

*CORRESPONDENCE
Yi Che
✉ 5813574@qq.com

†These authors share first authorship

RECEIVED 04 December 2024
ACCEPTED 11 April 2025
PUBLISHED 28 April 2025

CITATION
Liao X-Y, Jiang Y-E, Xu R-J, Qian T-T, Liu S-L and Che Y (2025) A bibliometric analysis of electroencephalogram research in stroke: current trends and future directions. *Front. Neurol.* 16:1539736. doi: 10.3389/fneur.2025.1539736

A bibliometric analysis of electroencephalogram research in stroke: current trends and future directions

Xiao-Yu Liao[1†], Yu-Er Jiang[2†], Ren-Jie Xu[3†], Ting-Ting Qian[1†], Shi-Lu Liu[4] and Yi Che[1*]

[1]Department of Rehabilitation Medicine, The Affiliated Suzhou Hospital of Nanjing Medical University, Suzhou, China, [2]Center for Excellence in Brain Science and Intelligence Technology, Institute of Neuroscience, Chinese Academy of Sciences, Shanghai, China, [3]Department of Rehabilitation Medicine, Kunshan Rehabilitation Hospital, Suzhou, China, [4]College School of Acupuncture-Moxibustion and Tuina, School of Health Preservation and Rehabilitation, Nanjing University of Chinese Medicine, Nanjing, China

Background: Electroencephalography (EEG) has become an indispensable tool in stroke research for real-time monitoring of neural activity, prognosis prediction, and rehabilitation support. In recent decades, EEG applications in stroke research have expanded, particularly in areas like brain-computer interfaces (BCI) and neurofeedback for motor recovery. However, a comprehensive analysis of research trends in this domain is currently unavailable.

Methods: The study collected data from the Web of Science Core Collection database, selecting publications related to stroke and EEG from 2005 to 2024. Visual analysis tools such as VOSviewer and CiteSpace were utilized to build knowledge maps of the research field, analyzing the distribution of publications, authors, institutions, journals, and collaboration networks. Additionally, co-occurrence, clustering, and burst detection of keywords were analyzed in detail.

Results: A total of 2,931 publications were identified, indicating a consistent increase in EEG research in stroke, with significant growth post-2017. The United States, China, and Germany emerged as the leading contributors, with high collaboration networks among Western institutions. Key research areas included signal processing advancements, EEG applications in seizure risk and consciousness disorder assessment, and EEG-driven rehabilitation techniques. Notably, recent studies have focused on integrating EEG with machine learning and multimodal data for more precise functional evaluations.

Conclusion: The findings reveal that EEG has evolved from a diagnostic tool to a therapeutic support platform in the context of stroke care. The advent of deep learning and multimodal integration has positioned EEG for expanded applications in personalized rehabilitation. It is recommended that future studies prioritize interdisciplinary collaboration and standardized EEG methodologies in order to facilitate clinical adoption and enhance translational potential in stroke management.

KEYWORDS

stroke, electroencephalogram, bibliometrix, CiteSpace, VOSviewer, visualization analysis

1 Introduction

Stroke is a leading cause of disability and mortality worldwide, classified mainly into ischemic stroke and hemorrhagic stroke (1). Stroke results in localized or widespread neurological impairment, frequently accompanied by motor, cognitive (e.g., aphasia, executive dysfunction, and memory deficits), and swallowing dysfunctions (2, 3). Specifically, cognitive impairments vary depending on the lesion location and severity, with common manifestations including visuospatial neglect (4) and attention disorder (5). These deficits not only undermine patients' functional independence but also impose long-term challenges for rehabilitation and quality of life. With the ongoing trend of population aging, the incidence of stroke is expected to continue rising, placing an even heavier burden on healthcare systems globally (6, 7). Traditional stroke diagnosis and evaluation rely heavily on imaging techniques such as magnetic resonance imaging (MRI) and computed tomography (CT), which are highly sensitive and specific in displaying structural brain abnormalities, particularly in the acute phase (8, 9). Furthermore, functional scales such as the NIH Stroke Scale and the Fugl-Meyer Assessment are employed to quantify functional deficits (10, 11). However, these methods are primarily oriented toward the detection of structural changes and may prove inadequate for the real-time monitoring of functional dynamics in stroke patients. Functional MRI (fMRI) and positron emission tomography (PET) can be used to assess changes in brain function but are often limited by high costs, restricting broader application (12, 13). In contrast, EEG is a non-invasive tool for monitoring brain function. It provides high temporal resolution data on neural activity by recording the electrophysiological activity of the brain (14). Furthermore, EEG is a straightforward and cost-effective method of data collection. EEG is particularly advantageous in the diagnosis and evaluation of stroke, offering the dual benefit of real-time monitoring of neurological changes in stroke patients and the identification of specific patterns of brain electrical activity through quantitative EEG (qEEG). This allows for the assessment of potential functional recovery and seizure risk (15). Post-stroke patients undergoing resting-state EEG often exhibit increased delta/theta power and decreased alpha/beta power, which correlate with motor and cognitive deficits. Functional connectivity analysis further reveals disrupted network topology in the affected hemisphere, reflecting impaired inter-regional communication (4, 16, 17). Post-stroke sleep architecture often shows reduced rapid-eye-movement sleep and increased sleep fragmentation, which correlates with poor recovery. Sleep spindles and slow-wave activity may serve as biomarkers for neuroplasticity (18, 19). In recent years, the application of EEG in stroke research has extended into advanced fields such as brain-computer interfaces (BCI) and neurofeedback (20, 21). BCI technology is capable of decoding EEG signals, thereby enabling stroke patients to control external devices through brain activity (20, 22). Neurofeedback training employs real-time EEG feedback to assist patients in self-regulating brain states, thereby promoting neuroplasticity and functional restoration (23). The combination of BCI and neurofeedback has demonstrated potential as a means of providing personalized training solutions for stroke rehabilitation. In light of these substantial applications, EEG research in the context of stroke has become of considerable value. This study employs bibliometric methods to conduct a systematic analysis of EEG research in stroke over the past 20 years. The analysis utilizes VOSviewer and CiteSpace to create a comprehensive knowledge map of the field, thereby uncovering the current state, key hotspots, and future trends. This knowledge map serves to inform and guide subsequent research.

Abbreviations: ACPP, average citation per publication; TC, total citations; TLS, total link strength.

2 Materials and methods

2.1 Data source and collection

The primary data for the bibliometric analysis were obtained from the Science Citation Index Expanded (SCI-Expanded) and Social Sciences Citation Index databases (SSCI) within the Web of Science Core Collection database (WoSCC). The data retrieval strategy was summarized as follows: # 1: TS = stroke; #2: TS = (Electroencephalography OR EEG OR Electroencephalogram*); the ultimate dataset: #1 AND #2. The utilization of a truncation symbol, "*," proved an effective means of preventing missed detections and enhancing retrieval efficacy. The study included only English-language studies. The time of search period was between January 1, 2005 and December 31, 2024. The search strategy is depicted in Figure 1. To minimize the potential bias from routine database updates, the literature search was conducted on a fixed date. A total of 2,931 productions were retrieved, including both reviews and research articles. To ensure the clarity and accuracy of the results and conclusions, we manually screened the 2,931 publications and categorized them into two groups: (A) "EEG in acute stroke and its early complications" and (B) "EEG in neurological rehabilitation." Category A contained 1,207 articles, while category B included 1724 articles. The data will be stored in three separate folders: "Dataset 1" (which contains all literature), "Dataset 2" (containing only category A literature), and "Dataset 3" (containing only category B literature). Upon completion of the retrieval process, the data were saved as complete records and cited references. The articles were then extracted and exported in "Plain text file" formats.

2.2 Bibliometric analysis

The articles meeting the inclusion criteria were exported as a plain text file named "download_xxx.txt," containing complete records and cited references. These files were imported into VOSviewer 1.6.19 and CiteSpace 6.2.R2 to construct visual knowledge maps. Additionally, Excel was used for chart creation and descriptive statistical analyses. The VOSviewer parameters were configured as follows: the normalization method was set to "association strength," with minimum thresholds for countries/regions, institutions, authors and journals set at 5, 10, 7 and 10 publications, respectively. Keyword occurrence frequency was also considered, with a minimum threshold of 20. In CiteSpace, the analysis covered the period from January 2005 to December 2024, with a one-year time slice. Node types included keywords, and the g-index selection criteria were set to k = 25 per slice. The pruning options used were pathfinder, sliced networks, and merged networks, with all other settings left at their default values. In this study, we first analyzed the number of papers from countries, institutions, authors and journals based on Dataset 1 to summarize

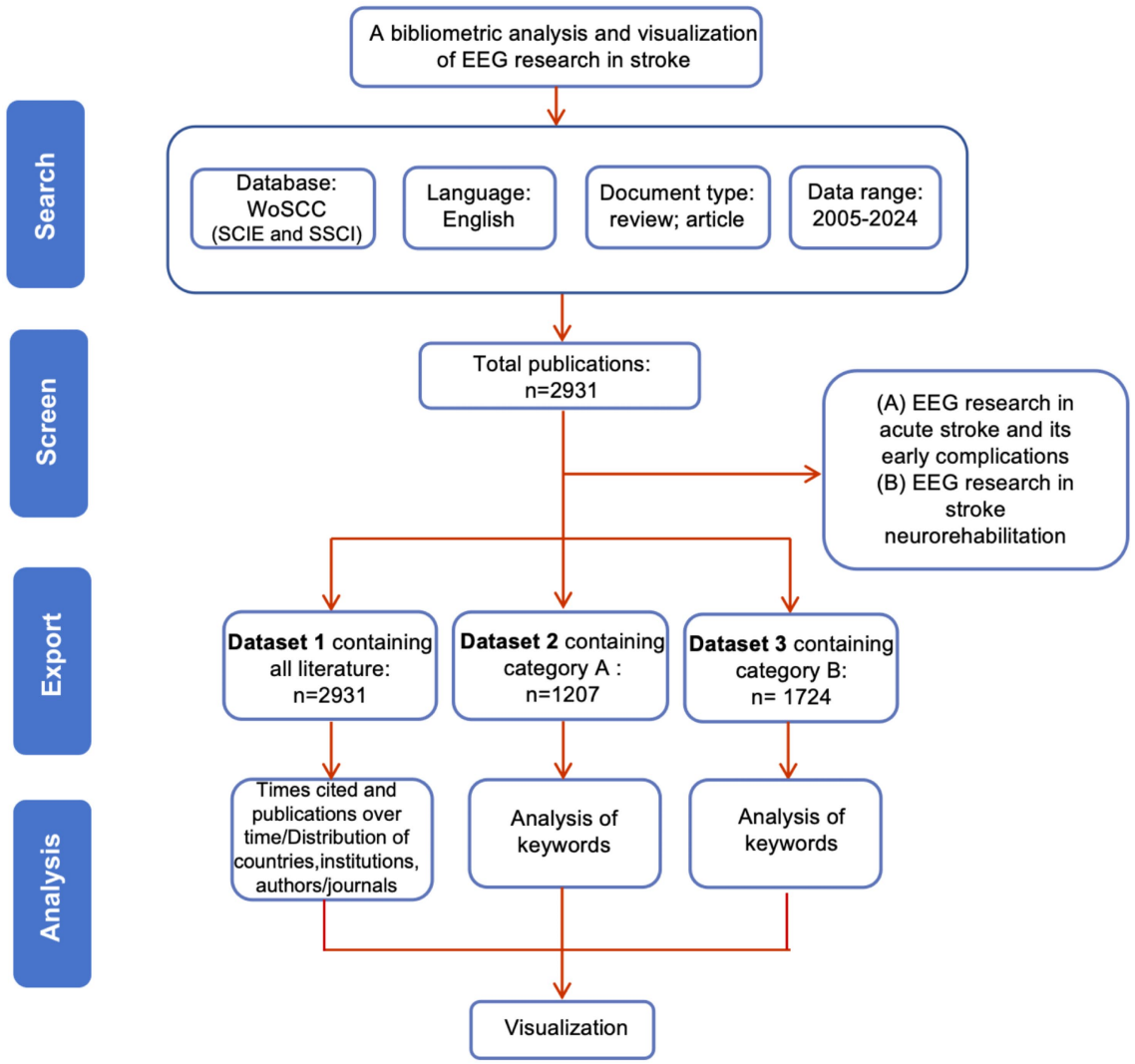

FIGURE 1
Flow chart of literature screening.

the current status of EEG research in stroke. We then used Dataset 2 and Dataset 3 to analyze keyword co-occurrence, keyword clustering, and emergent keywords, in order to identify current research hotspots and explore the frontiers and emerging trends in this field.

2.3 Annual publications and citations

The annual publication volume is a principal indicator for gauging research interest and predicting future dynamics in a field (24). The study encompassed 2,931 publications, comprising 2,610 original research articles (89%) and 321 review articles (11%). The total citations (TC) were 75,437. The average citation per publication (ACPP) was 25.73, and the h-index was 109. Figure 2A depicts the trajectory of annual publication volume (depicted on the left vertical axis in terms of the number of articles) and citation frequency (depicted on the right vertical axis) in the field of EEG research in stroke from 2005 to 2024. The figure illustrates an overall upward trend. The research trajectory can be delineated into two distinct phases. From 2005 to 2016, both the publication volume and the citation frequency exhibited a gradual increase. This early phase reflects the foundational work being done in the field. The moderate rise indicates a steady expansion in research and a corresponding increase in academic attention. During this period, EEG research in stroke likely laid the groundwork for more targeted clinical and experimental investigations. From 2017 onward, the field entered a phase of rapid growth, with both publication volume and citation frequency rising sharply, reaching a peak in 2024. The substantial increase in publications indicates that EEG research in stroke has gained significant traction, attracting an increasing number of researchers and funding. The rise in citations signifies a more extensive and profound integration of these studies within the broader stroke research and neurorehabilitation communities.

2.4 Distribution of countries/regions and institutions

A total of 2,931 publications were published by 92 countries and 3,539 institutions. A total of 57 countries and 139 institutions published at least five and ten articles, respectively, in this field. In

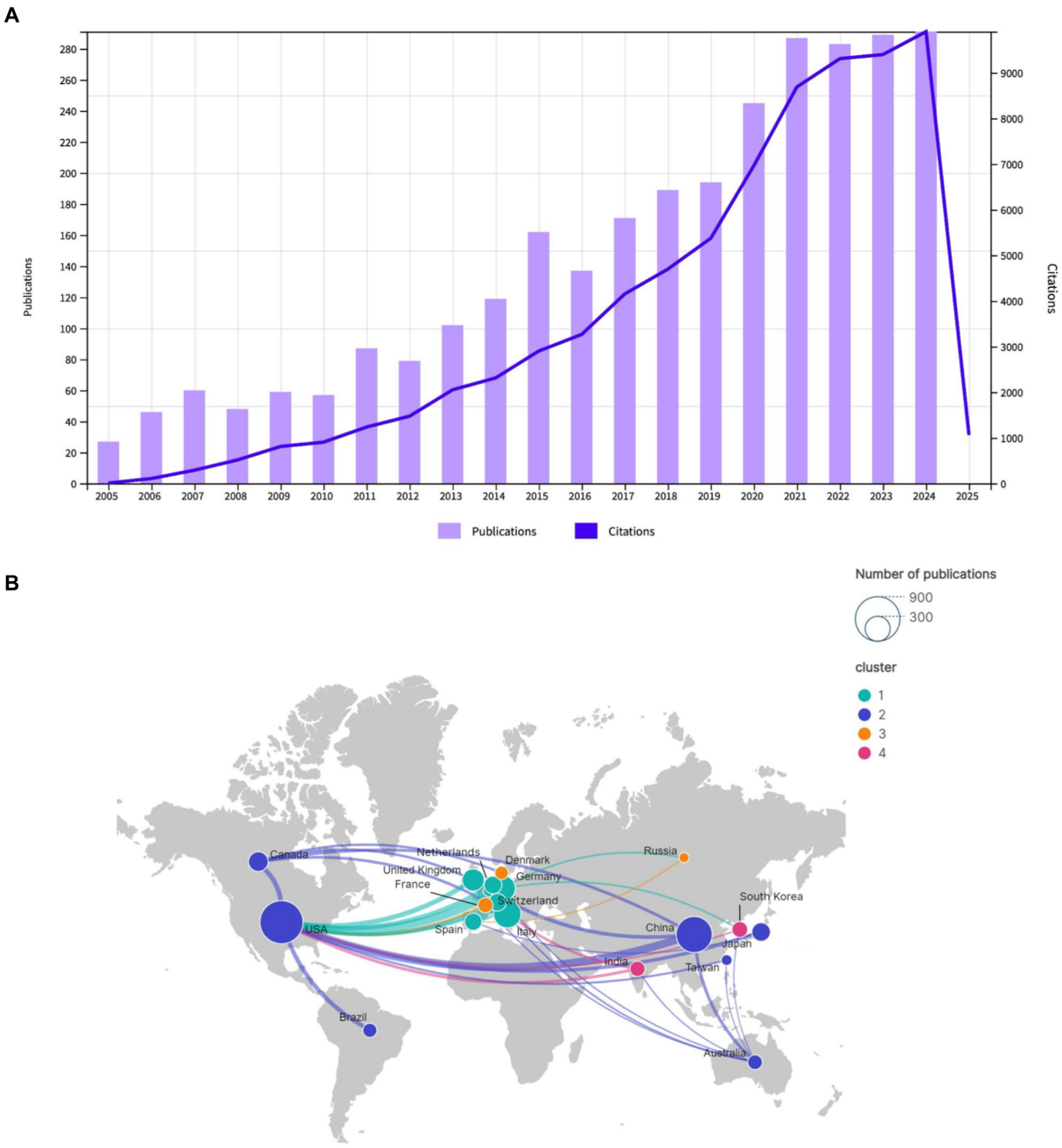

FIGURE 2
(A) Annual publications and citations trend chart for Dataset 1. **(B)** Geographical distribution and cooperation of publications Dataset 1.

terms of publication volume, the top five countries were the United States (778 publications), China (545 publications), Italy (316 publications), Germany (273 publications), and England (184 publications), as illustrated in Table 1. As illustrated in Figure 2B, the geographical distribution of cooperative endeavors among nations is depicted. The nodes, which represent countries, are sized according to the number of publications they have received. The upper right corner of the figure demonstrates the node sizes for publication counts of 300 and 900. The presence of lines connecting the nodes signifies cooperative interactions between countries, with the thickness of the lines denoting the frequency of collaboration. The map is color-coded into clusters and includes both the number of publications from each country as well as the strength of their collaborations. The map divides countries into four different clusters based on their collaborative relationships. Cluster 1: This cluster primarily includes countries/regions from Europe, such as Germany, England, Spain, Switzerland, Italy, and Netherlands. Cluster 2: This cluster includes countries/regions such as the United States, China, Canada, Japan, Australia, Brazil, and Taiwan. Cluster 3: This cluster includes countries/regions like France, Denmark, and Russia. Cluster 4: This cluster includes countries/regions like South Korea and India.

TABLE 1 Top 10 countries/regions ranked by number of publications.

Rank	Countries/ regions	Publications	TC	ACPP	TLS	Population (million)	Publications per million people
1	United States	778	24,966	32.02	526	333	2.33
2	China	545	5,401	10.61	211	1,426	0.38
3	Italy	316	10,861	33.20	343	60.4	5.23
4	Germany	273	13,641	47.17	426	84	3.25
5	England	184	5,530	28.94	326	56	3.29
6	Canada	162	3,398	22.90	167	39	4.15
7	Japan	144	4,094	26.70	103	123	1.15
8	Netherlands	131	3,730	27.75	132	17	7.71
9	Switzerland	130	5,720	42.11	180	9	14.44
10	Spain	125	6,509	49.10	185	47	2.66

Figure 3A depicts the institutional collaboration map. Table 2 provides a detailed overview of the top institutions involved in EEG research in stroke, showing their total number of publications, TC, TLS, ACPP, and country of origin. The top 10 institutions by publication volume in EEG research in stroke show a mix of global leaders from the United States, China, and Europe, reflecting the international prominence of these universities in advancing research in this field. As illustrated in Table 2, the University of Tübingen in Germany occupies the preeminent position with 64 publications, closely followed by institutions from China, including Capital Medical University (52 publications), Fudan University (42 publications), and Shanghai Jiao Tong University (41 publications). This observation highlights the substantial contributions of Chinese institutions to the scholarly landscape. Other prominent players include Northwestern University, University of Pittsburgh, and Harvard Medical School, all from the United States, with 42, 40, and 35 publications, respectively. These institutions from the United States are widely recognized for their impactful research and often lead the field in terms of citation frequency. Notably, Aalborg University demonstrates a particularly high citation impact, with 1,205 citations, indicating that their research has gained significant academic recognition.

2.5 Analysis of authors

A total of 13,234 authors contributed to this field between 2005 and 2024. Of these, 112 authors published at least seven articles with over 100 citations. The three most prolific authors in terms of publication volume were Birbaumer, N (29 publications), Jia, J (27 publications), and Ming, D (25 publications), as illustrated in Table 3. Professor Birbaumer, N from Germany is the most prolific researcher in the field, with the highest number of publications, TC, ACPP, and H-index. His research output is concentrated in the early period of his career, making him the founder and most influential scholar in the field. Among the top 10 high-impact authors, three are from China. Their publications are concentrated in recent years, and their collaborations are limited, with close collaboration within their teams but relatively few collaborations with teams outside their institutions, particularly across borders, as shown in Figure 3B. Notably, Van Putten, MJAM, a researcher from the Netherlands, has attained a commendable ACPP score of 49.85, underscoring the substantial academic recognition of his contributions to the field of EEG research in stroke.

2.6 Analysis of journals

A total of 2,931 publications were retrieved and published across 641 journals. Among the retrieved publications, 60 journals had at least 10 publications and over 100 citations, as illustrated in Figure 4. Table 4 presents the 10 journals with the highest TC. The top five journals in terms of citation frequency are *Clinical Neurophysiology* (3,191 citations), *Journal of Neural Engineering* (3,033 citations), *Neuroimage* (2,676 citations), *Frontiers in Neuroscience* (2,325 citations), and *Sensors* (2,251 citations). These journals are all ranked in the first and second quartiles by the Journal Citation Reports (JCR), which indicates that they are of high research quality and influence. Among the top 10 journals, *Brain* has the highest impact factor (IF), and despite a relatively lower publication count, it has the highest ACPP, which serves to underscore its academic prestige and broad influence in neuroscience.

2.7 Analysis of keywords

2.7.1 Analysis of keyword co-occurrence

Keywords are a high-level summary of the topic and content of the article. An analysis of keyword co-occurrence can reflect the hotspot and trend of research in the field (25). This study analyzes the keyword co-occurrence patterns across two distinct categories of EEG research in stroke. Table 5 shows the top 20 keywords from both Dataset 2 and Dataset 3 ranked by TLS. In Dataset 2 which includes 1,207 articles focused on "EEG in acute stroke and its early complications," the keyword co-occurrence network (Figure 5A) highlights terms like "stroke," "EEG," and "epilepsy" as central nodes emphasizing the focus on EEG applications for managing acute stroke complications such as seizures and non-convulsive status epilepticus. Figure 1 showcases a total of 83 keywords with a minimum co-occurrence frequency of seven. Other significant terms such as "ischemic stroke," "MRI," and "intracerebral hemorrhage" reflect the intersection of EEG studies with imaging and other neurological complications. This network illustrates how EEG is used to monitor

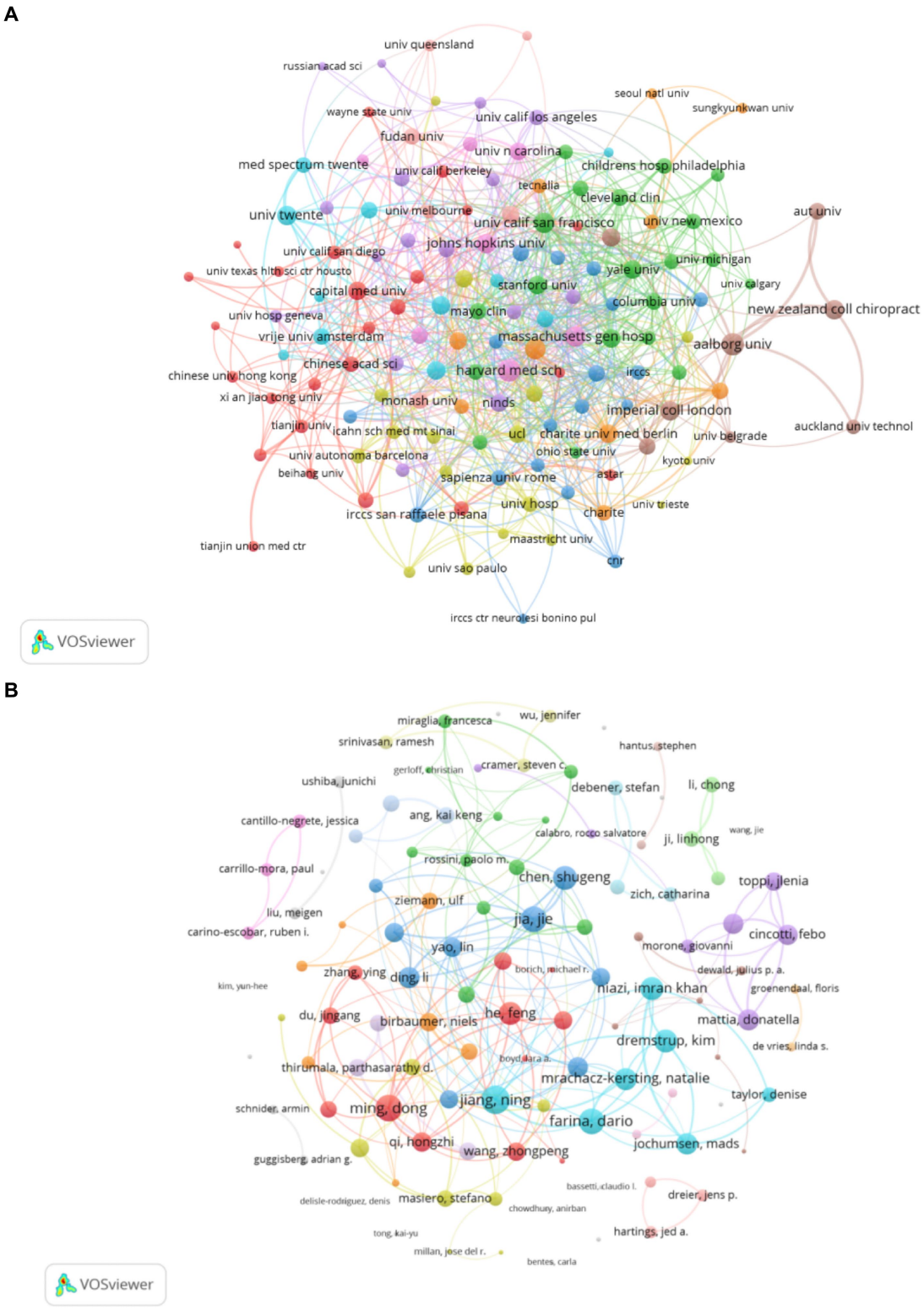

FIGURE 3
(A) Collaborative network knowledge map of institution Dataset 1. **(B)** Collaborative network knowledge map of author Dataset 1.

and manage the early consequences of stroke indicating the importance of EEG in understanding and addressing stroke-induced brain changes during the acute phase. Dataset 3 which includes 1,724 articles focusing on "EEG in neurological rehabilitation," shows a different pattern in its keyword co-occurrence network (Figure 5B). This figure displays a network of 137 keywords all of which appear with a minimum frequency of seven. These central terms like "brain-computer interface (BCI)," "motor imagery (MI)," and

TABLE 2 Top 10 institutions ranked by number of publications.

Rank	Institutions	Publications	TC	ACPP	TLS	Location
1	University of Tübingen	64	4,977	77.87	51	Germany
2	Capital Medical University	52	600	11.54	37	China
3	Northwestern University	42	611	14.54	36	USA
4	Fudan University	42	656	15.62	24	China
5	Aalborg University	41	1,205	29.39	69	Denmark
6	Shanghai Jiao Tong University	41	706	19.69	31	China
7	University of Pittsburgh	40	677	16.93	27	USA
8	Tianjin University	39	510	13.08	12	China
9	Harvard Medical School	35	539	15.37	63	USA
10	University of Twente	34	1,489	36.97	49	Netherlands

TABLE 3 Top 10 authors ranked by number of publications.

Rank	Author	Publications	TC	ACPP	H-index	TLS	Location
1	Birbaumer, N	29	3,268	112.34	117	27	Germany
2	Jia, J	27	480	17.78	39	52	China
3	Ming, D	25	374	14.96	20	57	China
4	Jochumsen, MR	22	555	25.23	21	38	Denmark
5	Ushiba, J	22	802	36.46	30	13	Japan
6	Jiang, N	22	1,002	21.50	37	66	China
7	Niazi, IK	21	839	39.95	29	44	New Zeeland
8	Van Putten, MJAM	20	997	49.85	47	2	Netherlands
9	Thirumala, PD	19	245	12.89	21	26	USA
10	Ziemann, U	19	631	33.21	102	22	Germany

"neurorehabilitation" are prominent reflecting the shift in focus toward using EEG in stroke recovery particularly in enhancing rehabilitation strategies through BCI systems. Keywords such as "functional connectivity," "training," and "rehabilitation" are tightly linked indicating the growing interest in leveraging EEG to promote motor recovery and brain plasticity in the chronic phase of stroke. Moreover terms like "virtual reality (VR)" suggest an expanding interest in integrating advanced technologies with EEG-based rehabilitation. Comparing the keyword co-occurrence networks of the two categories reveals clear differences: acute stroke research is primarily concerned with monitoring and managing immediate stroke-related complications while the rehabilitation category emphasizes long-term recovery and functional improvement through EEG-based interventions.

2.7.2 Analysis of keyword clustering

Analysis of keywords clustering is to categorize closely related keywords, which can reveal the hotspot of research in the field (26). The collected data were imported into CiteSpace for keyword clustering analysis, the smaller the cluster number, the more keywords the cluster contains. Modularity Q is a measure of the efficacy of clustering, with a range from 0 to 1. A value approaching 1 indicates a high degree of connectivity within clusters (14). For Dataset 2, which focuses on acute stroke and its early complications, the analysis revealed a Modularity Q of 0.7094, indicating substantial network modularity and high clustering quality, as shown in Figure 6A. The LLR clustering method identified 19 distinct clusters, each representing a distinct area of research, which were subsequently labeled with descriptive terms, including #0 carotid endarterectomy, #1 animal models, #2 cardiac surgery, #3 antiepileptic drug, #4 cerebrovascular disease, #5 stroke, #6 functional connectivity, #7 status epilepticus, #8 delayed cerebral ischemia, #9 spreading depression, #10 cognition, #11 biomedical signal processing, #12 stroke-related seizures, #13 temporal lobe epilepsy, #14 cerebral blood flow, #15 cortical excitability, #16 medulla-oblongata, #17 stroke-like episodes, #18 cortical infarction. Figure 6B presents the clustering results for Dataset 3, which is centered around EEG research in neurorehabilitation of stroke, also exhibited strong clustering results with a Modularity Q of 0.7791. The LLR clustering method was employed to identify distinct 19 clusters, including #0 quantitative electroencephalography, #1 stroke, #2 transcranial magnetic stimulation, #3 brain-computer interface, #4 functional connectivity, #5 ischemic stroke, #6 motor imagery, #7 carotid endarterectomy, #8 upper extremity, #9 feature extraction, #10 traumatic brain injury, #11 case report, #12 sensorimotor integration, #13 brain activity, #14 transcranial direct current stimulation, #15 cerebrovascular accident, #16 corticomuscular coherence, #17 brain plasticity, #18 seizures.

2.7.3 Analysis of keyword burst

Keyword burst analysis has been demonstrated to reveal the areas that have received the most attention within a specific timeframe thereby identifying the emerging research frontiers (26). Figure 7 illustrates the top 25 burst keywords. The "Begin" and "End" columns indicate the

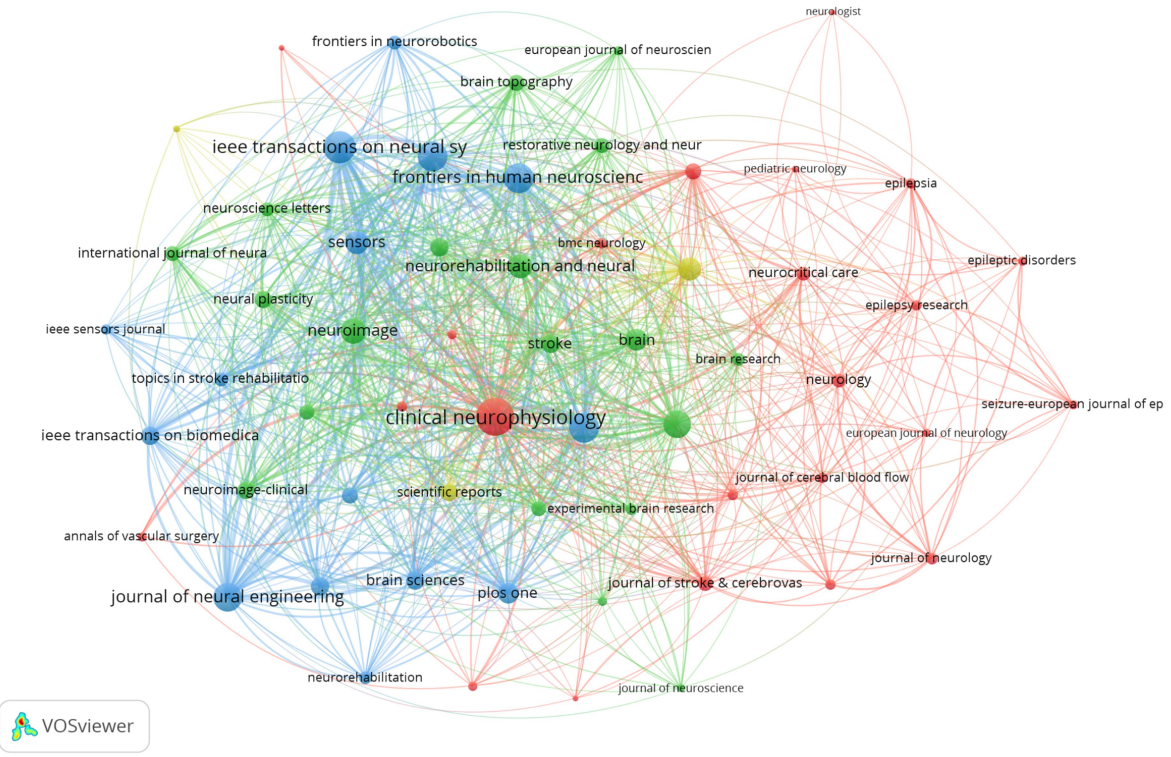

FIGURE 4
Journal co-citation network knowledge map Dataset 1.

TABLE 4 Top 10 journals ranked by citation frequency.

Rank	Journal	TC	Publications	ACPP	TLS	IF (2023)	JCR
1	Clinical Neurophysiology	3,191	85	35.81	963	3.7	Q1
2	Journal of Neural Engineering	3,033	74	40.75	522	3.7	Q2
3	Neuroimage	2,676	47	55.42	382	4.7	Q1
4	Frontiers in Neuroscience	2,325	78	119.94	565	3.2	Q2
5	Sensors	2,251	50	25.91	291	3.4	Q2
6	IEEE Transactions on Neural Systems and rehabilitation engineering	2,119	114	18.59	661	4.8	Q1
7	Journal of Neuroengineering and Rehabilitation	2,118	57	37.16	581	5.2	Q1
8	Brain	1945	15	129.67	261	10.6	Q1
9	Frontiers in Human Neuroscience	1828	81	22.57	563	2.4	Q2
10	Neurology	1,479	21	70.43	82	7.7	Q1

timeframe of the keyword burst while "strength" denotes the intensity of the burst. For Dataset 2 (analyzed with a 1-year duration parameter) Figure 7 displays the top 25 burst keywords. The earliest detected burst corresponds to "blood-flow," which also exhibits the longest sustained burst period. Notably "therapeutic hypothermia" demonstrates the highest burst strength. The keywords "functional connectivity," "guidelines," "acute symptomatic seizures," "patterns," "score," "connectivity," "acute ischemic stroke," and "outcm" are still experiencing bursts. For Dataset 3 Figure 8 reveals distinct patterns: "activation" emerges as the earliest burst keyword while "cortex" maintains the most prolonged burst duration and the keyword "task analysis" registers the strongest burst intensity. The following keywords are still experiencing bursts: "upper limb," "feature extraction," "stroke," "task analysis," "machine learning," "deep learning," "network," and "stimulation."

3 Discussion

3.1 Analysis of current research status

This study is the first to conduct a comprehensive bibliometric and visual analysis of EEG research in the field of stroke from 2005 to

TABLE 5 Top 20 keywords ranked by TLS.

Rank	Keyword was analyzed by Dataset 2	Frequency	TLS	Keyword was analyzed by Dataset 3	Frequency	TLS
1	Stroke	226	352	Stroke	443	1,108
2	EEG	146	227	EEG	333	772
3	Epilepsy	112	202	Electroencephalography	261	760
4	Electroencephalography	100	187	Brain-computer interface	164	444
5	Seizures	67	152	Motor imagery	133	394
6	Status epilepticus	53	94	Rehabilitation	123	375
7	Seizure	49	84	Stroke (medical condition)	45	288
8	Electroencephalogram	38	65	Neurorehabilitation	75	247
9	Outcome	25	49	Task analysis	33	202
10	Ischemic stroke	38	47	Training	30	180
11	Traumatic brain injury	21	46	Functional connectivity	59	150
12	MRI	22	41	Neurofeedback	46	136
13	Intracerebral hemorrhage	15	40	Electroencephalogram	67	135
14	Stroke (medical condition)	11	39	Stroke rehabilitation	57	127
15	Carotid endarterectomy	40	38	Virtual reality	37	127
16	Neurocritical care	17	36	BCI	46	120
17	Magnetic resonance imaging	19	34	brain-computer interface (BCI)	57	118
18	Neuroimaging	13	33	Neuroplasticity	32	108
19	Subarachnoid hemorrhage	14	33	Transcranial magnetic stimulation	36	105
20	Prognosis	17	32	Event-related desynchronization	42	100

2024, revealing key trends and developments. Over the past two decades, the number of publications and the frequency of citations in this area have exhibited a gradual increase. It is noteworthy that from 2000 to 2024, the annual publication volume remained above 200 publications, indicating a sustained growth trajectory in the field. This surge is indicative of the growing recognition of EEG as an essential tool in both the acute management of stroke and neurorehabilitation. The rising number of publications and the increased citation impact serve as evidence of this growing recognition.

At the national level, the analysis of publication volume and collaboration strength highlights the leading role of the United States in EEG research in stroke. Its high number of publications, citations, and collaborations with a range of countries position it as a central hub in this field. This global leadership reflects the United States' substantial investment in neuroscience and neurotechnology, fostering an environment that supports innovation and widespread dissemination of research findings. The robust international collaboration network, particularly with countries like Germany, Italy, and England, strengthens the global impact of the United States research, accelerating scientific progress in EEG applications for stroke. China's large volume of publications indicates a growing presence in the filed, but its relatively lower citation count and international collaboration strength suggest that its research may be more domestically focused. Countries such as Germany, Italy, and England also play pivotal roles in advancing EEG research. Germany's high ACPP indicates that its research is impactful, shaping key innovations in the field. Meanwhile, Switzerland and Canada, though publishing fewer papers, have demonstrated strong citation impacts, reinforcing the idea that quality research can have a disproportionate effect on the global scientific community. Switzerland's high publication count per million people further emphasizes the significant contributions of smaller nations in advancing specialized fields. As the field of EEG research in stroke continues to evolve, fostering deeper international collaboration, especially between countries with differing research capacities, will be essential for accelerating advancements.

At the institutional level, the majority of research institutions are situated in developed Western countries, with universities representing the primary contributors. This reflects the field's reliance on economic support and experimental facilities. The University of Tübingen in Germany is the leading institution in terms of publication volume and citation frequency, exerting considerable influence, particularly in the field of BCI research. One of their most highly cited studies provides a comprehensive overview of the clinical applications of invasive and non-invasive EEG-based BCI technologies in direct brain communication and post-stroke motor recovery for paralyzed patients, demonstrating significant potential in both animal and human models (27, 28). The University of Twente in the Netherlands, despite publishing fewer papers, has a high citation frequency, indicating that their research is widely recognized for its quality. Their research has focused on qEEG technology, which has advanced the monitoring of prognosis and therapeutic responses in patients who have suffered a stroke or anoxic coma. This has established a robust foundation for the application of EEG in neuroscience (29–31). While the international collaboration network is robust (as shown in Figure 2B), our analysis shows that many research institutions collaborate predominantly with national partners (as shown in

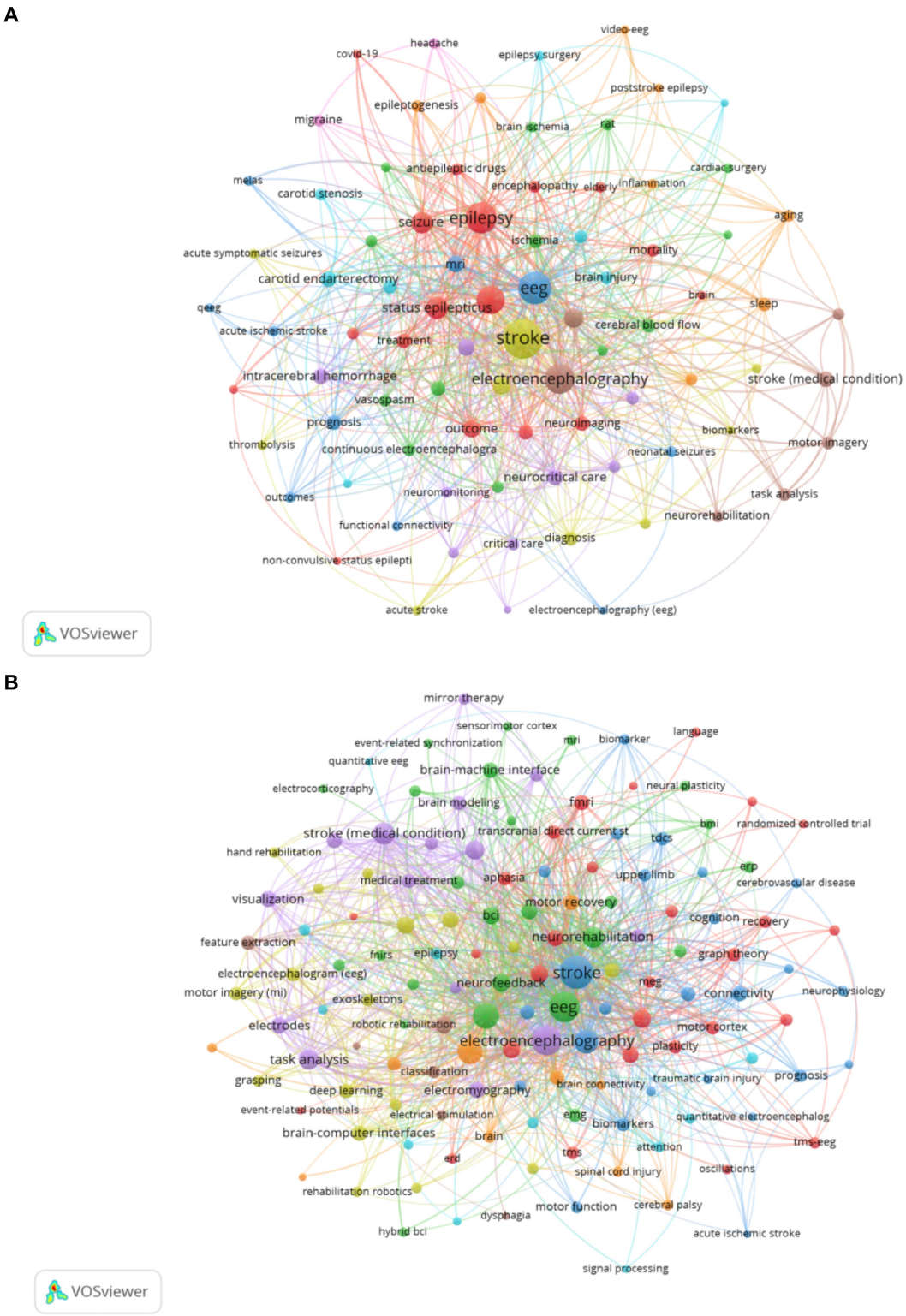

FIGURE 5
(A) Keyword co-occurrence network knowledge map for Dataset 2. **(B)** Keyword co-occurrence network knowledge map for Dataset 3.

Figure 3A), with fewer instances of extensive cross-border collaboration. This suggests that geographical proximity remains an important factor influencing patterns of collaboration EEG research in stroke.

At the level of the author, Professor Birbaumer, N from Germany is one of the most prominent scholars in the field of BCI. His team has developed techniques for direct communication between the brain and external devices via EEG and other neural signals, with the objective of

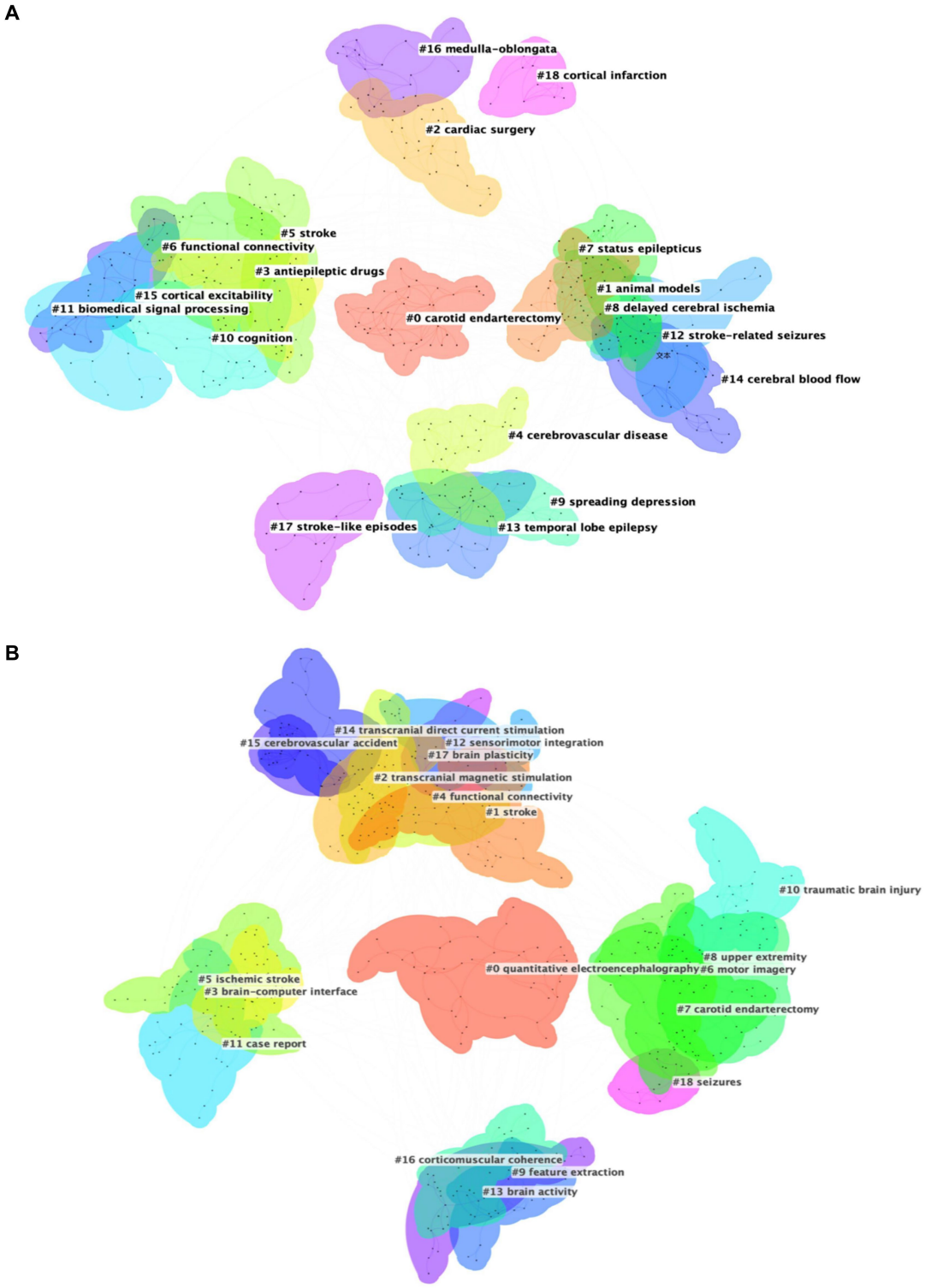

FIGURE 6
(A) Cluster map of keywords for Dataset 2. **(B)** Cluster map of keywords for Dataset 3.

assisting individuals with severe paralysis and atresia syndrome to communicate with the outside world. Patients are able to control computer cursors, letter boards, or robotic arms through brain signals, thereby significantly advancing the field of BCI technology (32–34). In recent years, Professor Jia, J has been at the forefront of research utilizing BCI technology to enhance stroke rehabilitation. By integrating connectivity network patterns with spatiotemporal analysis, she has optimized EEG feature selection, thereby enhancing the efficacy of BCI applications in rehabilitation training (35, 36). Moreover, she has utilized a combination of BCI and functional electrical stimulation to

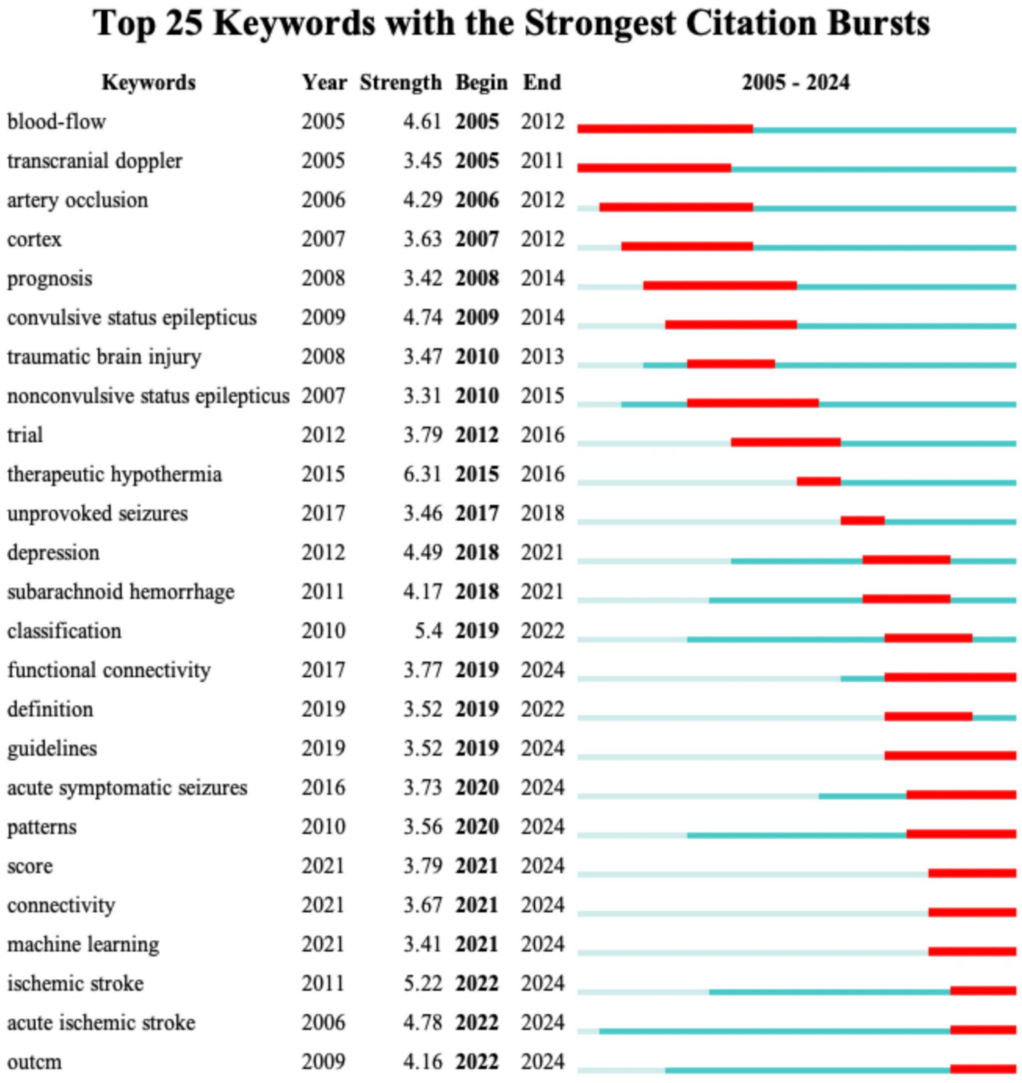

FIGURE 7
The top 25 keywords with the highest burst strength for Dataset 2.

markedly enhance motor function in individuals who have experienced a chronic stroke (37). Her research also encompasses traditional Chinese medicine techniques, such as electroacupuncture, and their regulatory effects on resting-state networks in stroke patients, as well as the potential clinical benefits of such techniques in rehabilitation (38). Professor Jiang N, another Chinese scholar, has also made significant contributions to the development of a single-trial detection system based on movement-related cortical potentials for BCI applications in gait initiation through extensive international collaboration (39). By interpreting patients' motor intentions in real time through EEG signals, his work provides a basis for rehabilitative interventions for gait-impaired patients.

In terms of journal distribution, most of the journals with high publication volume and citation frequency are high-quality journals, such as *Clinical Neurophysiology*, *Neurology* and *Brain*. These journals not only provide theoretical and experimental support for EEG research in the field of stroke, but also demonstrate the academic maturity of research results in this field. As research continues to progress, future publications may increasingly be concentrated in these high-impact journals, thus creating a virtuous cycle. The platform role of these journals not only facilitates the dissemination of research findings, but also encourages further innovation within the field.

3.2 Analysis of research hotspots and trends

This study provides a comprehensive analysis of the keyword trends in EEG research in stroke, revealing critical insights into the evolving landscape of this field. Through the analysis of keyword co-occurrence, clustering, and burst patterns, we have identified key research hotspots, emerging trends, and shifts in the focus of EEG applications for acute stroke management and neurological rehabilitation. These findings not only highlight the current state of research but also offer directions for future investigation.

FIGURE 8
The top 25 keywords with the highest burst strength for Dataset 3.

3.2.1 EEG research in acute stroke and early complications

EEG research in acute stroke primarily focuses on the early identification and management of complications such as epilepsy and disorders of consciousness. The keyword co-occurrence analysis for Dataset 2 reveals a dominant emphasis on using EEG for monitoring post-stroke complications, especially seizures and non-convulsive status epilepticus, which are crucial for early intervention. Terms such as "stroke," "EEG," and "epilepsy" prominently feature in the research landscape, reflecting the clinical focus on utilizing EEG to understand and manage stroke-induced brain changes.

The analysis of keywords highlights epilepsy and seizures as central themes in acute stroke research. Post-stroke epilepsy is significantly associated with adverse outcomes and elevated mortality rates (40). QEEG can assist in identifying the typical EEG patterns associated with stroke (41). Non-convulsive seizures are frequently unrecognized clinically, as standard observations may prove inadequate for detecting these anomalies. Nevertheless, EEG monitoring is capable of capturing essential electrophysiological changes. Non-convulsive seizures are frequently unrecognized clinically, as standard observations may prove inadequate for detecting these anomalies (42). However, EEG monitoring can effectively capture essential electrophysiological changes. Post-stroke epilepsy in EEG typically manifests as focal or generalized slowing, with some cases also showing lateralized periodic discharges. Bentes et al. (43) conducted a study of long-term follow-up of patients who had experienced an anterior ischemic circulation stroke, finding that 25.2% experienced seizures within the first year, with 22.7%

of these acute symptomatic seizures detected only by EEG. For instance, Bentes et al. (43) demonstrated that 64-channel EEG with synchronized video-polysomnography during the first post-stroke week captured electrographic seizures in over 20% of anterior ischemic stroke patients, with 62% of these events occurring during sleep. These findings emphasize the necessity of prolonged monitoring, as 22.7% of acute symptomatic seizures are identifiable only through EEG. Beyond seizure detection, EEG's predictive capacity extends to acute neurological deficits. Vanderschelden et al. (44) conducted a prospective study of 50 acute stroke patients evaluated by recording of EEG at rest state. The delta-theta/alpha-beta ratio (DTABR) was calculated. Multivariable modeling revealed that while age, diabetes status, and infarct volume explained 47% of NIHSS score variance, adding contralesional DTABR enhanced prediction, achieving 60% explanatory power. These seizures can contribute to worsened neurological outcomes, increased risk of mortality, and prolonged recovery time, highlighting the importance of EEG in reducing these adverse effects by enabling timely treatment (45).

Expanding beyond epilepsy, EEG provides objective biomarkers for post-stroke consciousness disorders. Reduced prefrontal-to-motor cortical information flow, measurable via transcranial magnetic stimulation coupled with high-density EEG (TMS-EEG), correlates with impaired arousal states. Bai et al. (46) reported that patients with unresponsive wakefulness syndrome exhibit ≥40% reductions in gamma band connectivity between prefrontal and motor regions, while minimally conscious patients show disrupted prefrontal-parietal alpha coherence predictive of 6-month recovery. Such electrophysiological signatures align with spectral shifts observed in consciousness research: elevated low-frequency oscillations (delta/theta) and attenuated cross-frequency coupling reflect diminished cortical integration, whereas preserved theta-gamma phase-amplitude interactions may signify recovery potential (47, 48). While EEG excels in detecting electrophysiological anomalies, its integration with advanced neuroimaging techniques enables deeper insights into structure–function relationships In a targeted investigation of thalamic stroke, researchers employed DTI-derived fractional anisotropy (FA) maps alongside qEEG to probe microstructural and functional connectivity disruptions. Correlational analyses linked theta-band EEG power reductions to FA decreases in the cingulum bundle and corpus callosum-key components of the default mode network known to modulate resting-state theta activity. Alpha-band power further correlated with FA in cortico-thalamic circuits, supporting the "thalamocortical dysrhythmia" model of stroke-induced network dysfunction. This multimodal approach also bridged behavioral deficits with neural markers: FA reductions in the right cingulum predicted impaired spatial memory, while splenium of the corpus callosum correlated with facial recognition deficits (49). Thus, EEG in acute stroke research is not only focused on identifying early stroke-related complications but also on understanding the underlying neurological processes that influence stroke recovery, especially in critical conditions like seizures and consciousness disorders. While the current study primarily focuses on EEG applications in neural monitoring and rehabilitation, we acknowledge the importance of exploring broader physiological mechanisms, including inflammation and oxidative stress (ROS), in stroke pathology (50–53). Although EEG itself does not directly measure inflammatory markers or ROS levels, emerging research highlights indirect correlations between EEG patterns and these mechanisms. For example, post-stroke neuroinflammation can disrupt cortical excitability and functional connectivity, which may manifest as altered EEG spectral power or coherence (54–57). Additionally, oxidative stress has been linked to impaired neurovascular coupling (58–60), potentially affecting EEG-derived metrics. Future studies could integrate EEG with biomarkers (e.g., serum cytokines, ROS assays) to investigate these relationships. The increasing emphasis on real-time monitoring and the integration of EEG with other diagnostic tools, such as MRI or PET scans, has great potential in enhancing the clinical management of acute stroke patients, reducing mortality and improving recovery rates.

3.2.2 Neurological rehabilitation in stroke

EEG research in neurological rehabilitation (Dataset 3) shifts its focus from immediate stroke complications to the long-term recovery process. The analysis of keywords for this dataset highlights the growing prominence of BCI technology, MI, and neurorehabilitation, reflecting the increased integration of EEG into rehabilitation efforts aimed at improving motor function and cognitive recovery. Terms such as functional connectivity, training, and rehabilitation emphasize the growing recognition of EEG's potential in promoting neural plasticity during stroke recovery, particularly in enhancing motor recovery through non-invasive brain-computer technologies. One of the most profound advancements in neurological rehabilitation is the use of BCI systems. MI enables patients to engage motor-related brain regions by imagining limb movements without actual physical execution, thereby promoting neural plasticity, particularly in the recovery of upper limb and hand function. BCI technology further enhances the effectiveness of MI by decoding patients' motor intentions and translating them into commands for external devices, thereby enabling hemiplegic patients to achieve indirect motor control (61). This not only improves motor function but also helps patients maintain active engagement during rehabilitation training. Benzy et al. (62) analyzed cortical activity during MI and successfully decoded the imagined hand movement direction (left/right) in stroke patients. The patients used the phase-locking value of EEG signals to decode the direction of imagined hand movement, which then controlled a motorized arm assistive device, allowing patients to move their impaired arms in the intended direction. The combination of EEG with EMG (electromyography) has also gained attention in recent years, particularly in enhancing the precision of motor control during rehabilitation. Li et al. (63) introduced EEG–EMG hybrid systems, which combine the advantages of both EEG for motor intention detection and EMG for muscle activity detection. This dual approach improves the accuracy of rehabilitation training, providing more personalized feedback to patients and potentially accelerating recovery. The hybrid system allows for more accurate decoding of patients' movements and enhances their ability to perform motor tasks during rehabilitation. Another notable advancement in EEG-based rehabilitation is the application of VR in conjunction

with EEG, offering patients immersive and interactive environments that stimulate motor recovery. As research progresses, the integration of EEG with VR systems is showing promise in fostering neuroplasticity by creating engaging and tailored rehabilitation experiences (64, 65). The development of signal processing technologies has greatly optimized EEG preprocessing, feature extraction, and classification methods. Traditional feature extraction frequently employs time-domain, frequency-domain, and time-frequency analyses, such as the utilization of power spectral density to examine patterns of brain activity across diverse frequency bands in patients (16, 66). The damaged regions of the brain in patients with stoke frequently exhibit augmented low-frequency bands and diminished high-frequency bands. The advent of deep learning, encompassing convolutional neural networks and generative adversarial networks, has facilitated the automated extraction of features. These neural network models allow for complex pattern recognition directly from raw EEG signals, facilitating a deeper understanding of post-stroke brain functions (67, 68). Tong et al. (69) constructed a deep learning model based on EEG signals for rapid detection of ischemic stroke. They gathered EEG data from 20 acute ischemic stroke patients and 19 healthy controls and introduced a fusion feature combining correlation-weighted phase lag index and sample entropy to explore inter-channel synchronization and functional connectivity. Recent studies have demonstrated that complex network analysis of EEG data can provide insights into the reorganization of brain networks after stroke. For example, one study (70) analyzing resting-state and task-state functional connectivity identified a "cognitive network" comprising nodes in the subcortical, frontoparietal, visual, and cerebellar networks. This network shows differential effective connectivity patterns that are sensitive to post-stroke cognitive impairment and improvement. Moreover, another study (71) focused on mild stroke patients compared EEG-based functional connectivity during cognitive tasks across groups with cortical infarctions, subcortical infarctions, and healthy controls. Their graph theory analysis revealed significantly reduced global and local efficiencies in patient groups, along with distinct nodal strength distributions that differed by lesion location. A systematic review (72) compared EEG-derived complex network parameters between stroke patients and healthy subjects. Although the effect sizes for parameters such as path length, clustering coefficient, and cohesion were modest, the review highlighted both structural differences and certain overlapping features between the groups. Additionally, multimodal data fusion techniques are increasingly applied to stroke EEG studies. By combining EEG with fMRI or near-infrared spectroscopy, researchers can obtain more comprehensive brain activity data, valuable for early prognosis prediction and evaluating the effectiveness of different rehabilitation interventions (73, 74). Stroke may not only damage local neural structures but also disrupt large-scale brain networks, affecting both structural and functional connectivity. Stroke-induced lesions may impair the integrity of the default mode network and the cortico-thalamic circuits, leading to reduced global efficiency and altered modular organization. Such disruptions may contribute to deficits in cognitive and motor function by impairing inter-hemispheric communication and reducing the integration of distributed neural systems (71, 75–77).

4 Limitation

Firstly, this bibliometric analysis is was confined to data drawn exclusively from the WoSCC, with the exclusion of data from other databases. This limited scope might result in the omission of some critical studies, potentially affecting the comprehensiveness of the analysis. Furthermore, the study was restricted to English-language publications, which excludes relevant research in other languages, particularly domestic studies from non-English speaking regions. This limitation could affect the representation of global research progress in the field of stroke-related EEG research. Secondly, the visual mapping generated using VOSviewer and CiteSpace required specific parameter settings, including node selection, threshold settings, and clustering methods based on data availability and study requirements. These settings may introduce some level of statistical bias, which could influence the results.

5 Conclusion

This study is among the first to employ bibliometric and visual analysis techniques to examine the evolution of EEG research in the field of stroke over the past two decades. The analysis was conducted using the VOSviewer and CiteSpace software tools. The results provide a systematic illustration of the current research landscape, identifying key areas of interest and future trends in this domain. The findings demonstrate that EEG is a widely utilized tool in the monitoring of neural functions associated with stroke, the assessment of epilepsy risk, and the facilitation of rehabilitation. These observations reflect a substantial academic interest and clinical relevance. The integration of deep learning and multimodal data fusion has enabled researchers to perform more complex analyses of post-stroke electrophysiological activity, laying a solid foundation for personalized rehabilitation plans. Furthermore, the use of EEG in the assessment of epilepsy and consciousness disorders improves the accuracy of post-stroke complication detection, particularly in the early identification of non-convulsive seizures and the assessment of consciousness recovery potential. In the future, as EEG technology continues to be integrated with other imaging modalities and high-efficiency algorithms, its application in stroke rehabilitation appears to be highly promising. In this context, EEG -driven BCI technologies have evolved from basic monitoring to more advanced intervention strategies. It is recommended that future research concentrate on the promotion of interdisciplinary applications of EEG and the establishment of standardized signal processing procedures. This will ensure the consistency of study outcomes and facilitate the adoption of EEG in a broader clinical context, as well as its use in translational applications.

Data availability statement

The original contributions presented in the study are included in the article/supplementary material, further inquiries can be directed to the corresponding author/s.

Author contributions

X-YL: Writing – review & editing, Writing – original draft, Methodology. Y-EJ: Data curation, Formal analysis, Visualization, Writing – original draft, Writing – review & editing. R-JX: Validation, Writing – review & editing. T-TQ: Conceptualization, Visualization, Data curation, Writing – review & editing, Formal analysis, Writing – original draft. S-LL: Data curation, Writing – review & editing. YC: Conceptualization, Writing – original draft, Writing – review & editing.

Funding

The author(s) declare that no financial support was received for the research and/or publication of this article.

Acknowledgments

The authors thank everyone who contributed to the writing and all the publications, and their authors involved in this study.

Conflict of interest

The authors declare that the research was conducted in the absence of any commercial or financial relationships that could be construed as a potential conflict of interest.

Generative AI statement

The authors declare that no Gen AI was used in the creation of this manuscript.

Publisher's note

References

1. Ma Q, Li R, Wang L, Yin P, Wang Y, Yan C, et al. Temporal trend and attributable risk factors of stroke burden in China, 1990-2019: an analysis for the global burden of disease study 2019. *Lancet Public Health*. (2021) 6:e897–906. doi: 10.1016/s2468-2667(21)00228-0

2. Jiang Z, Kuhnke P, Stockert A, Wawrzyniak M, Halai A, Saur D, et al. Dynamic reorganization of task-related network interactions in post-stroke aphasia recovery. *Brain*. (2025). doi: 10.1093/brain/awaf036

3. Mao L, Che X, Wang J, Jiang X, Zhao Y, Zou L, et al. Sub-acute stroke demonstrates altered beta oscillation and connectivity pattern in working memory. *J Neuroeng Rehabil*. (2024) 21:212. doi: 10.1186/s12984-024-01516-5

4. Ros T, Michela A, Mayer A, Bellmann A, Vuadens P, Zermatten V, et al. Disruption of large-scale electrophysiological networks in stroke patients with visuospatial neglect. *Netw Neurosci*. (2022) 6:69–89. doi: 10.1162/netn_a_00210

5. Vidal JPC, Danet L, Arribarat G, Pariente J, Péran P, Albucher JF, et al. Factors behind poor cognitive outcome following a thalamic stroke. *J Neurol*. (2025) 272:98. doi: 10.1007/s00415-024-12777-4

6. Krishnamurthi RV, Ikeda T, Feigin VL. Global, regional and country-specific burden of Ischaemic stroke, intracerebral Haemorrhage and subarachnoid Haemorrhage: a systematic analysis of the global burden of disease study 2017. *Neuroepidemiology*. (2020) 54:171–9. doi: 10.1159/000506396

7. Shih PC, Steele CJ, Hoepfel D, Muffel T, Villringer A, Sehm B. The impact of lesion side on bilateral upper limb coordination after stroke. *J Neuroeng Rehabil*. (2023) 20:166. doi: 10.1186/s12984-023-01288-4

8. Buck BH, Akhtar N, Alrohimi A, Khan K, Shuaib A. Stroke mimics: incidence, aetiology, clinical features and treatment. *Ann Med*. (2021) 53:420–36. doi: 10.1080/07853890.2021.1890205

9. Hilkens NA, Casolla B, Leung TW, de Leeuw FE. Stroke. *Lancet*. (2024) 403:2820–36. doi: 10.1016/s0140-6736(24)00642-1

10. Kwah LK, Diong J. National Institutes of Health stroke scale (NIHSS). *J Physiother*. (2014) 60:61. doi: 10.1016/j.jphys.2013.12.012

11. Shin S, Lee Y, Chang WH, Sohn MK, Lee J, Kim DY, et al. Multifaceted assessment of functional outcomes in survivors of first-time stroke. *JAMA Netw Open*. (2022) 5:e2233094. doi: 10.1001/jamanetworkopen.2022.33094

12. Czap AL, Sheth SA. Overview of imaging modalities in stroke. *Neurology*. (2021) 97:S42–s51. doi: 10.1212/wnl.0000000000012794

13. Wang H, Xiong X, Zhang K, Wang X, Sun C, Zhu B, et al. Motor network reorganization after motor imagery training in stroke patients with moderate to severe upper limb impairment. *CNS Neurosci Ther*. (2023) 29:619–32. doi: 10.1111/cns.14065

14. Liao XY, Gao YX, Qian TT, Zhou LH, Li LQ, Gong Y, et al. Bibliometric analysis of electroencephalogram research in Parkinson's disease from 2004 to 2023. *Front Neurosci*. (2024) 18:1433583. doi: 10.3389/fnins.2024.1433583

15. Sanossian N, Fink E. What will the Mobile stroke unit of the future look like, and will EEG have a role? *Neurology*. (2023) 101:1085–6. doi: 10.1212/wnl.0000000000208047

16. Saes M, Meskers CGM, Daffertshofer A, de Munck JC, Kwakkel G, van Wegen EEH. How does upper extremity Fugl-Meyer motor score relate to resting-state EEG in chronic stroke? A power spectral density analysis. *Clin Neurophysiol*. (2019) 130:856–62. doi: 10.1016/j.clinph.2019.01.007

17. Zhang JJ, Bai Z, Fong KNK. Resting-state cortical electroencephalogram rhythms and network in patients after chronic stroke. *J Neuroeng Rehabil*. (2024) 21:32. doi: 10.1186/s12984-024-01328-7

18. Pace M, Camilo MR, Seiler A, Duss SB, Mathis J, Manconi M, et al. Rapid eye movements sleep as a predictor of functional outcome after stroke: a translational study. *Sleep*. (2018) 41:zsy138. doi: 10.1093/sleep/zsy138

19. Tscherpel C, Mustin M, Massimini M, Paul T, Ziemann U, Fink GR, et al. Local neuronal sleep after stroke: the role of cortical bistability in brain reorganization. *Brain Stimul*. (2024) 17:836–46. doi: 10.1016/j.brs.2024.07.008

20. Miladinović A, Accardo A, Jarmolowska J, Marusic U, Ajčević M. Optimizing real-time MI-BCI performance in post-stroke patients: impact of time window duration on classification accuracy and responsiveness. *Sensors*. (2024) 24:6125. doi: 10.3390/s24186125

21. Rustamov N, Souders L, Sheehan L, Carter A, Leuthardt EC. IpsiHand brain-computer Interface therapy induces broad upper extremity motor rehabilitation in chronic stroke. *Neurorehabil Neural Repair*. (2024) 39:74–86. doi: 10.1177/15459683241287731

22. Su J, Wang J, Wang W, Wang Y, Bunterngchit C, Zhang P, et al. An adaptive hybrid brain-computer Interface for hand function rehabilitation of stroke patients. *IEEE Trans Neural Syst Rehabil Eng*. (2024) 32:2950–60. doi: 10.1109/tnsre.2024.3431025

23. Cioffi E, Hutber A, Molloy R, Murden S, Yurkewich A, Kirton A, et al. EEG-based sensorimotor neurofeedback for motor neurorehabilitation in children and adults: a scoping review. *Clin Neurophysiol*. (2024) 167:143–66. doi: 10.1016/j.clinph.2024.08.009

24. Ba H, Zhang L, He X, Li S. Knowledge mapping and global trends in the field of the objective structured clinical examination: bibliometric and visual analysis (2004-2023). *JMIR Med Educ*. (2024) 10:e57772. doi: 10.2196/57772

25. Wang J, Cao K, Chen Z, Lyu T, Xia Q, Liu L, et al. Research trends and hotspots of acupuncture therapy for obesity from 2004 to 2023: a bibliometric analysis. *Complement Ther Med*. (2024) 86:103092. doi: 10.1016/j.ctim.2024.103092

26. Xu Y, Huang H, Wu M, Zhuang Z, Liu H, Hou M, et al. Transcranial direct current stimulation for cognitive impairment rehabilitation: a bibliometric analysis. *Arch Med Res*. (2024) 56:103086. doi: 10.1016/j.arcmed.2024.103086

27. Birbaumer N, Cohen LG. Brain-computer interfaces: communication and restoration of movement in paralysis. *J Physiol*. (2007) 579:621–36. doi: 10.1113/jphysiol.2006.125633

28. Sitaram R, Zhang H, Guan C, Thulasidas M, Hoshi Y, Ishikawa A, et al. Temporal classification of multichannel near-infrared spectroscopy signals of motor imagery for

developing a brain-computer interface. *Neuroimage*. (2007) 34:1416–27. doi: 10.1016/j.neuroimage.2006.11.005

29. Hofmeijer J, Tjepkema-Cloostermans MC, van Putten MJ. Burst-suppression with identical bursts: a distinct EEG pattern with poor outcome in postanoxic coma. *Clin Neurophysiol*. (2014) 125:947–54. doi: 10.1016/j.clinph.2013.10.017

30. Sheorajpanday RV, Nagels G, Weeren AJ, van Putten MJ, De Deyn PP. Reproducibility and clinical relevance of quantitative EEG parameters in cerebral ischemia: a basic approach. *Clin Neurophysiol*. (2009) 120:845–55. doi: 10.1016/j.clinph.2009.02.171

31. Sheorajpanday RV, Nagels G, Weeren AJ, van Putten MJ, De Deyn PP. Quantitative EEG in ischemic stroke: correlation with functional status after 6 months. *Clin Neurophysiol*. (2011) 122:874–83. doi: 10.1016/j.clinph.2010.07.028

32. Birbaumer N. Breaking the silence: brain-computer interfaces (BCI) for communication and motor control. *Psychophysiology*. (2006) 43:517–32. doi: 10.1111/j.1469-8986.2006.00456.x

33. Birbaumer N, Weber C, Neuper C, Buch E, Haapen K, Cohen L. Physiological regulation of thinking: brain-computer interface (BCI) research. *Prog Brain Res*. (2006) 159:369–91. doi: 10.1016/s0079-6123(06)59024-7

34. Chaudhary U, Birbaumer N, Curado MR. Brain-machine interface (BMI) in paralysis. *Ann Phys Rehabil Med*. (2015) 58:9–13. doi: 10.1016/j.rehab.2014.11.002

35. Lin Y, Jiang Z, Zhan G, Su H, Kang X, Jia J. Brain network characteristics between subacute and chronic stroke survivors in active, imagery, passive movement task: a pilot study. *Front Neurol*. (2023) 14:1143955. doi: 10.3389/fneur.2023.1143955

36. Shu X, Chen S, Yao L, Sheng X, Zhang D, Jiang N, et al. Fast recognition of BCI-inefficient users using physiological features from EEG signals: a screening study of stroke patients. *Front Neurosci*. (2018) 12:93. doi: 10.3389/fnins.2018.00093

37. Shaheiwola N, Zhang B, Jia J, Zhang D. Using tDCS as an add-on treatment prior to FES therapy in improving upper limb function in severe chronic stroke patients: a randomized controlled study. *Front Hum Neurosci*. (2018) 12:233. doi: 10.3389/fnhum.2018.00233

38. Lin YF, Liu XH, Cui ZY, Song ZT, Zou F, Chen SG, et al. Weakened effective connectivity related to Electroacupuncture in stroke patients with prolonged flaccid paralysis: an EEG pilot study. *Neural Plast*. (2021) 2021:1–10. doi: 10.1155/2021/6641506

39. Jiang N, Gizzi L, Mrachacz-Kersting N, Dremstrup K, Farina D. A brain-computer interface for single-trial detection of gait initiation from movement related cortical potentials. *Clin Neurophysiol*. (2015) 126:154–9. doi: 10.1016/j.clinph.2014.05.003

40. Galovic M, Ferreira-Atuesta C, Abraira L, Döhler N, Sinka L, Brigo F, et al. Seizures and epilepsy after stroke: epidemiology, biomarkers and management. *Drugs Aging*. (2021) 38:285–99. doi: 10.1007/s40266-021-00837-7

41. Sinka L, Abraira L, Imbach LL, Zieglgänsberger D, Santamarina E, Álvarez-Sabín J, et al. Association of Mortality and Risk of epilepsy with type of acute symptomatic seizure after ischemic stroke and an updated prognostic model. *JAMA Neurol*. (2023) 80:605–13. doi: 10.1001/jamaneurol.2023.0611

42. Sutcliffe L, Lumley H, Shaw L, Francis R, Price CI. Surface electroencephalography (EEG) during the acute phase of stroke to assist with diagnosis and prediction of prognosis: a scoping review. *BMC Emerg Med*. (2022) 22:29. doi: 10.1186/s12873-022-00585-w

43. Bentes C, Martins H, Peralta AR, Morgado C, Casimiro C, Franco AC, et al. Epileptic manifestations in stroke patients treated with intravenous alteplase. *Eur J Neurol*. (2017) 24:755–61. doi: 10.1111/ene.13292

44. Vanderschelden B, Erani F, Wu J, de Havenon A, Srinivasan R, Cramer SC. A measure of neural function provides unique insights into behavioral deficits in acute stroke. *Stroke*. (2023) 54:e25–9. doi: 10.1161/strokeaha.122.040841

45. Gettings JV, Mohammad Alizadeh Chafjiri F, Patel AA, Shorvon S, Goodkin HP, Loddenkemper T. Diagnosis and management of status epilepticus: improving the status quo. *Lancet Neurol*. (2025) 24:65–76. doi: 10.1016/s1474-4422(24)00430-7

46. Bai Y, Yang L, Meng X, Huang Y, Wang Q, Gong A, et al. Breakdown of effective information flow in disorders of consciousness: insights from TMS-EEG. *Brain Stimul*. (2024) 17:533–42. doi: 10.1016/j.brs.2024.04.011

47. Lee M, Baird B, Gosseries O, Nieminen JO, Boly M, Postle BR, et al. Connectivity differences between consciousness and unconsciousness in non-rapid eye movement sleep: a TMS-EEG study. *Sci Rep*. (2019) 9:5175. doi: 10.1038/s41598-019-41274-2

48. Purdon PL, Pierce ET, Mukamel EA, Prerau MJ, Walsh JL, Wong KF, et al. Electroencephalogram signatures of loss and recovery of consciousness from propofol. *Proc Natl Acad Sci USA*. (2013) 110:E1142–51. doi: 10.1073/pnas.1221180110

49. Duru AD, Duru DG, Yumerhodzha S, Bebek N. Analysis of correlation between white matter changes and functional responses in thalamic stroke: a DTI & EEG study. *Brain Imaging Behav*. (2016) 10:424–36. doi: 10.1007/s11682-015-9397-1

50. Gutiérrez M, Merino JJ, Alonso de Leciñana M, Díez-Tejedor E. Cerebral protection, brain repair, plasticity and cell therapy in ischemic stroke. *Cerebrovasc Dis*. (2009) 27:177–86. doi: 10.1159/000200457

51. Maida CD, Norrito RL, Rizzica S, Mazzola M, Scarantino ER, Tuttolomondo A. Molecular pathogenesis of ischemic and hemorrhagic strokes: background and therapeutic approaches. *Int J Mol Sci*. (2024) 25:6297. doi: 10.3390/ijms25126297

52. Qin C, Yang S, Chu YH, Zhang H, Pang XW, Chen L, et al. Signaling pathways involved in ischemic stroke: molecular mechanisms and therapeutic interventions. *Signal Transduct Target Ther*. (2022) 7:215. doi: 10.1038/s41392-022-01064-1

53. Regenhardt RW, Das AS, Lo EH, Caplan LR. Advances in understanding the pathophysiology of lacunar stroke: a review. *JAMA Neurol*. (2018) 75:1273–81. doi: 10.1001/jamaneurol.2018.1073

54. Chaturvedi S, De Marchis GM. Inflammatory biomarkers and stroke subtype: an important new frontier. *Neurology*. (2024) 102:e208098. doi: 10.1212/wnl.0000000000208098

55. Hankey GJ. Stroke. *Lancet*. (2017) 389:641–54. doi: 10.1016/s0140-6736(16)30962-x

56. Shi K, Tian DC, Li ZG, Ducruet AF, Lawton MT, Shi FD. Global brain inflammation in stroke. *Lancet Neurol*. (2019) 18:1058–66. doi: 10.1016/s1474-4422(19)30078-x

57. Zhao Y, Li Q, Niu J, Guo E, Zhao C, Zhang J, et al. Neutrophil membrane-camouflaged Polyprodrug Nanomedicine for inflammation suppression in ischemic stroke therapy. *Adv Mater*. (2024) 36:e2311803. doi: 10.1002/adma.202311803

58. Cai W, Zhang K, Li P, Zhu L, Xu J, Yang B, et al. Dysfunction of the neurovascular unit in ischemic stroke and neurodegenerative diseases: an aging effect. *Ageing Res Rev*. (2017) 34:77–87. doi: 10.1016/j.arr.2016.09.006

59. Fang J, Wang Z, Miao CY. Angiogenesis after ischemic stroke. *Acta Pharmacol Sin*. (2023) 44:1305–21. doi: 10.1038/s41401-023-01061-2

60. Foreman B, Claassen J. Quantitative EEG for the detection of brain ischemia. *Crit Care*. (2012) 16:216. doi: 10.1186/cc11230

61. Liu H, Wei P, Wang H, Lv X, Duan W, Li M, et al. An EEG motor imagery dataset for brain computer interface in acute stroke patients. *Sci Data*. (2024) 11:131. doi: 10.1038/s41597-023-02787-8

62. Benzy VK, Vinod AP, Subasree R, Alladi S, Raghavendra K. Motor imagery hand movement direction decoding using brain computer Interface to aid stroke recovery and rehabilitation. *IEEE Trans Neural Syst Rehabil Eng*. (2020) 28:3051–62. doi: 10.1109/tnsre.2020.3039331

63. Li H, Ji H, Yu J, Li J, Jin L, Liu L, et al. A sequential learning model with GNN for EEG-EMG-based stroke rehabilitation BCI. *Front Neurosci*. (2023) 17:1125230. doi: 10.3389/fnins.2023.1125230

64. Shen J, Gu X, Fu J, Yao Y, Li Y, Zeng M, et al. Virtual reality-induced motor function of the upper extremity and brain activation in stroke: study protocol for a randomized controlled trial. *Front Neurol*. (2023) 14:1094617. doi: 10.3389/fneur.2023.1094617

65. Tang Z, Wang H, Cui Z, Jin X, Zhang L, Peng Y, et al. An upper-limb rehabilitation exoskeleton system controlled by MI recognition model with deep emphasized informative features in a VR scene. *IEEE Trans Neural Syst Rehabil Eng*. (2023) 31:4390–401. doi: 10.1109/tnsre.2023.3329059

66. Delcamp C, Srinivasan R, Cramer SC. EEG provides insights into motor control and neuroplasticity during stroke recovery. *Stroke*. (2024) 55:2579–83. doi: 10.1161/strokeaha.124.048458

67. Choi YA, Park SJ, Jun JA, Pyo CS, Cho KH, Lee HS, et al. Deep learning-based stroke disease prediction system using real-time bio signals. *Sensors*. (2021) 21:4269. doi: 10.3390/s21134269

68. Vecchio F, Caliandro P, Reale G, Miraglia F, Piludu F, Masi G, et al. Acute cerebellar stroke and middle cerebral artery stroke exert distinctive modifications on functional cortical connectivity: a comparative study via EEG graph theory. *Clin Neurophysiol*. (2019) 130:997–1007. doi: 10.1016/j.clinph.2019.03.017

69. Tong W, Yue W, Chen F, Shi W, Zhang L, Wan J. MSE-VGG: a novel deep learning approach based on EEG for rapid ischemic stroke detection. *Sensors*. (2024) 24:4234. doi: 10.3390/s24134234

70. Zhang J, Tang H, Zuo L, Liu H, Liu C, Li Z, et al. Identification of a cognitive network with effective connectivity to post-stroke cognitive impairment. *Cogn Neurodyn*. (2024) 18:3741–56. doi: 10.1007/s11571-024-10139-4

71. Xu M, Qian L, Wang S, Cai H, Sun Y, Thakor N, et al. Brain network analysis reveals convergent and divergent aberrations between mild stroke patients with cortical and subcortical infarcts during cognitive task performing. *Front Aging Neurosci*. (2023) 15:1193292. doi: 10.3389/fnagi.2023.1193292

72. Asadi B, Cuenca-Zaldivar JN, Nakhostin AN, Ibáñez J, Herrero P, Calvo S. Brain analysis with a complex network approach in stroke patients based on electroencephalography: a systematic review and Meta-analysis. *Healthcare*. (2023) 11:666. doi: 10.3390/healthcare11050666

73. Liang J, Song Y, Belkacem AN, Li F, Liu S, Chen X, et al. Prediction of balance function for stroke based on EEG and fNIRS features during ankle dorsiflexion. *Front Neurosci*. (2022) 16:968928. doi: 10.3389/fnins.2022.968928

74. Saj A, Pierce JE, Ronchi R, Ros T, Thomasson M, Bernati T, et al. Real-time fMRI and EEG neurofeedback: a perspective on applications for the rehabilitation of spatial neglect. *Ann Phys Rehabil Med*. (2021) 64:101561. doi: 10.1016/j.rehab.2021.101561

75. Grefkes C, Fink GR. Connectivity-based approaches in stroke and recovery of function. *Lancet Neurol*. (2014) 13:206–16. doi: 10.1016/s1474-4422(13)70264-3

76. Siegel JS, Ramsey LE, Snyder AZ, Metcalf NV, Chacko RV, Weinberger K, et al. Disruptions of network connectivity predict impairment in multiple behavioral domains after stroke. *Proc Natl Acad Sci USA*. (2016) 113:E4367–76. doi: 10.1073/pnas.1521083113

77. Yu X, Mei D, Wu K, Li Y, Chen C, Chen T, et al. High modularity, more flexible of brain networks in patients with mild to moderate motor impairments after stroke. *Exp Gerontol*. (2024) 195:112527. doi: 10.1016/j.exger.2024.112527

frontiers | Frontiers in Neurology

TYPE Original Research
PUBLISHED 30 April 2025
DOI 10.3389/fneur.2025.1587347

OPEN ACCESS

EDITED BY
Mingming Lu,
Characteristic Medical Center of Chinese People's Armed Police Force, China

REVIEWED BY
Yuto Uchida,
Johns Hopkins University, United States
Yuqi Luo,
Capital Medical University, China

*CORRESPONDENCE
Junli Ke
✉ 15157005017@163.com

RECEIVED 04 March 2025
ACCEPTED 17 April 2025
PUBLISHED 30 April 2025

CITATION
Pei L, Han X, Ni C and Ke J (2025) Prediction of prognosis in acute ischemic stroke after mechanical thrombectomy based on multimodal MRI radiomics and deep learning. *Front. Neurol.* 16:1587347.
doi: 10.3389/fneur.2025.1587347

Prediction of prognosis in acute ischemic stroke after mechanical thrombectomy based on multimodal MRI radiomics and deep learning

Lei Pei, Xiaowei Han, Chenfeng Ni and Junli Ke*

Department of Radiology, The Quzhou Affiliated Hospital of Wenzhou Medical University, Quzhou People's Hospital, Quzhou, China

Background: Acute ischemic stroke (AIS) is a major global health threat associated with high rates of disability and mortality, highlighting the need for early prognostic assessment to guide treatment. Currently, there are no reliable methods for the early prediction of poor prognosis in AIS, especially after mechanical thrombectomy. This study aimed to explore the value of radiomics and deep learning based on multimodal magnetic resonance imaging (MRI) in predicting poor prognosis in patients with AIS who underwent mechanical thrombectomy. This study aimed to provide a more accurate and comprehensive tool for stroke prognosis.

Methods: This study retrospectively analyzed the clinical data and multimodal MRI images of patients with stroke at admission. Logistic regression was employed to identify the risk factors associated with poor prognosis and to construct a clinical model. Radiomics features of the stroke-affected regions were extracted from the patients' baseline multimodal MRI images, and the optimal radiomics features were selected using a least absolute shrinkage and selection operator regression model combined with five-fold cross-validation. The radiomics score was calculated based on the feature weights, and machine learning techniques were applied using a logistic regression classifier to develop the radiomics model. In addition, a deep learning model was devised using ResNet101 and transfer learning. The clinical, radiomics, and deep learning models were integrated to establish a comprehensive multifactorial logistic regression model, termed the CRD (Clinic-Radiomics-Deep Learning) model. The performance of each model in predicting poor prognosis was assessed using receiver operating characteristic (ROC) curve analysis, with the optimal model visualized as a nomogram. A calibration curve was plotted to evaluate the accuracy of nomogram predictions.

Results: A total of 222 patients with AIS were enrolled in this study in a 7:3 ratio, with 155 patients in the training cohort and 67 in the validation cohort. Statistical analysis of clinical data from the training and validation cohorts identified two independent risk factors for poor prognosis: the National Institutes of Health Stroke Scale score at admission and the occurrence of intracerebral hemorrhage. Of the 1,197 radiomic features, 16 were selected to develop the radiomics model. Area under the ROC curve (AUC) analysis of specific indicators demonstrated varying performances across methods and cohorts. In the training cohort, the clinical, radiomics, deep learning, and integrated CRD models achieved AUC values of 0.762, 0.755, 0.689, and 0.834, respectively. In the validation cohort,

the clinical model exhibited an AUC of 0.874, the radiomics model achieved an AUC of 0.805, the deep learning model attained an AUC of 0.757, and the CRD model outperformed all models, with an AUC of 0.908. Calibration curves indicated that the CRD model showed exceptional consistency and accuracy in predicting poor prognosis in patients with AIS. Decision curve analysis revealed that the CRD model offered the highest net benefit compared with the clinical, radiomics, and deep learning models.

Conclusion: The CRD model based on multimodal MRI demonstrated high diagnostic efficacy and reliability in predicting poor prognosis in patients with AIS who underwent mechanical thrombectomy. This model holds considerable potential for assisting clinicians with risk assessment and decision-making for patients experiencing ischemic stroke.

KEYWORDS

multimodal MRI, radiomics, deep learning, acute ischemic stroke, prognosis

1 Introduction

Stroke, particularly acute ischemic stroke (AIS), is a major global health concern. It is not only one of the leading causes of death worldwide, responsible for approximately six million fatalities annually, but also the primary cause of mortality among residents of China (1). AIS accounts for 70% of all cerebrovascular diseases, primarily resulting from prolonged or permanent occlusion of cerebral vessels, which leads to ischemia and hypoxia in the brain tissue, causing localized neurological deficits or permanent loss of function (2). This condition is characterized by high rates of morbidity, disability, and mortality, with significant implications for patient prognosis, which is closely linked to the timeliness and efficacy of treatment. Despite substantial efforts by researchers worldwide to improve treatment approaches for AIS, including surgical and pharmacological interventions, the short-term prognosis remains unsatisfactory (3). The epidemiological features of AIS not only pose a severe threat to individual health and quality of life but also impose a substantial medical and economic burden on both society and families, emerging as one of the most pressing challenges in global public health.

The treatment of acute cerebral infarction is a complex multidisciplinary task that demands close collaboration across various departments and stages, with the ultimate goal of delivering timely and effective care to patients. Among therapeutic modalities, intravenous thrombolysis is widely employed, primarily through the administration of agents such as recombinant tissue plasminogen activator, urokinase, and tenecteplase, to restore blood flow (4). However, despite the ability of intravenous recombinant tissue plasminogen activator thrombolysis to alleviate symptoms in the short term in most patients, a subset of patients still face the risk of functional impairment and hemorrhagic transformation. In recent years, endovascular mechanical thrombectomy has emerged as a significant advancement in the treatment of AIS, particularly in patients with ischemic stroke due to large arterial occlusions, and it has been shown to substantially improve prognosis. However, some patients have a poor prognosis even after mechanical thrombectomy. Regardless of the treatment modality employed, early prognosis prediction for patients is of paramount importance, as it not only aids in the formulation of more precise pretreatment strategies but also facilitates the provision of more personalized care (5). Therefore, predicting the occurrence and progression of poor prognosis in AIS at an early stage and implementing proactive clinical interventions remain the central focus of current studies.

Previous studies have confirmed that factors such as the Alberta Stroke Program Early Computed Tomography (CT) Score (ASPECTS), patient age, presence of atrial fibrillation, and National Institutes of Health Stroke Scale (NIHSS) score are closely associated with the prognosis of recovery in patients with stroke (6). Smaller infarct volumes, well-developed collateral circulation, and lower NIHSS scores typically suggest a better prognosis for patients following endovascular treatment. Radiomics has recently emerged as a focal point of medical research and clinical practice. Advancements in neuroimaging have transcended its traditional role as a diagnostic tool and assumed an increasingly critical role in clinical decision-making (7). The integration of machine learning with radiomics has ushered in a revolutionary transformation in medical diagnostics, with successful applications in stroke research, such as the identification of acute cerebral infarction lesions based on CT- or magnetic resonance imaging (MRI)-derived radiomic features. Deep learning, a subset of machine learning techniques, constructs multilayered neural networks that can learn complex feature representations from vast datasets (8). Traditional stroke diagnostic methods have predominantly relied on physicians' visual interpretation of brain images, whereas deep learning enables the automatic extraction of features from brain images, thereby assisting clinicians in making more accurate and timely diagnoses.

The field of medical diagnosis and treatment is currently faced with new opportunities and challenges arising from the integration of machine learning and radiomics. Currently, the application of MRI-based radiomics in predicting the prognosis of patients with stroke remains insufficient, with most studies relying solely on diffusion-weighted imaging (DWI) sequences, and the use of deep learning models is relatively limited. Considering this, the present study aimed to leverage multimodal MRI sequence data from patients with AIS, in conjunction with various machine learning algorithms and deep learning models, to construct a comprehensive predictive model for AIS prognosis after mechanical thrombectomy and assess its predictive performance. Through this study, we sought to provide a more accurate and holistic tool for the prognostic evaluation of patients with stroke.

2 Methods

2.1 Patients

This retrospective study was approved by the Medical Ethics Committee of Quzhou People's Hospital, which waived the requirement for informed consent from the participants. We included patients with AIS who underwent brain MRI at the hospital's radiology department between January 2021 and May 2024. The diagnosis of AIS in this study strictly followed the current clinical guidelines, and all patients met the following criteria: (1) presence of symptoms of acute neurological deficit with an NIHSS score ≥2; (2) brain MRI-DWI sequence showing acute infarction in the responsible vascular blood supply area; and (3) exclusion of other non-vascular causes (such as epilepsy and metabolic encephalopathy). The inclusion criteria were as follows: (1) patients aged ≥18 years; (2) patients who met the diagnostic criteria for AIS; (3) patients who underwent high-quality MRI scans upon admission with complete clinical data; (4) patients who received mechanical thrombectomy treatment; and (5) patients who underwent MRI examinations before mechanical thrombectomy. The exclusion criteria were as follows: (1) severe liver or kidney dysfunction, hematological disorders, or malignant tumors; (2) intracranial lesions affecting prognosis, such as trauma or tumors; and (3) MRI images with artifacts or other factors that compromised image quality. We conducted a retrospective analysis of clinical data and biochemical results, including age, sex, smoking history, alcohol consumption, and history of hypertension, diabetes mellitus, and cardiovascular diseases. Prognostic evaluation at discharge was performed using the modified Rankin Scale (mRS), with a score of 3–6 indicating poor prognosis, and a score of 0–2 indicating good prognosis. All enrolled patients underwent ICH imaging evaluation prior to mechanical thrombectomy, and the diagnostic criteria were based on the following features: abnormal isohyperintense lesions on T1WI (excluding vascular artifacts) and hypointensity with peripheral hyperintense rings on FLAIR; chronic microbleeds are characterized by hypointense lesions. In this study, the clinical guidelines for mechanical thrombectomy were strictly followed, and patients with ICH (24 h < onset) or a significant mass effect (blood loss > 30 mL) in the acute phase were excluded as absolute contraindications. For patients with chronic phase microhemorrhage (cerebral microhemorrhage < 5 mm) or old hemorrhage, we have established a multidisciplinary decision-making process in which at least two neurointerventional physicians and one neuroimaging expert jointly evaluate the patient's bleeding stability, lesion location, and vascular pathway relationship, and make a comprehensive judgment based on the patient's NIHSS score and clinical indications to decide whether they should be included. A total of 222 patients were randomly divided into training and validation cohorts at a ratio of 7:3. In the training cohort, clinical features with statistically significant differences were selected using logistic regression, and a clinical model was developed. The workflow of this study is illustrated in Figure 1.

2.2 Image acquisition

Magnetic resonance imaging was performed using two distinct MRI machines (Siemens Skyra 3.0 T MRI from Germany and GE Signa Voyager 1.5 T MRI from the United States). The patient was placed in a supine position and continuous scanning was performed from the feet to the head, covering the range from the posterior fossa to the cranial vertex. Standard cranial MRI protocols encompassing axial T1WI, fluid-attenuated inversion recovery (FLAIR), and DWI sequences were employed. The repetition times for the 3.0 T MR were 2719/8600/2000 ms, with echo times of 9/106/57 ms. For the 1.5T MR, the repetition times were 488/8000/3543 ms and the echo times were 15/100/133 ms. For both MR scanners, the slice thickness was 5 mm, the field of view was 24 × 24 mm, and the matrix size was 512 × 512 pixels.

The MRI images were initially subjected to standardization procedures, including voxel resampling to 1 × 1 × 1 mm, adjustment of window width and level, N4 bias field correction, and normalization using *Z*-scores. Two radiologists, who were blinded to all patient information, assessed the MRI images. The axial MRI images of the enrolled patients were imported in DICOM format into the ITK-SNAP 3.8.0 software[1]. First, T1WI, FLAIR, and DWI sequences of the patients' images were recorded. Given the challenges in delineating stroke lesion boundaries using T1WI and FLAIR images, stroke lesions were manually outlined on DWI images while considering the reference T1WI and FLAIR images (Figure 2). Disagreements were discussed until a consensus was reached. The software subsequently fused the region of interest for each image slice, yielding three-dimensional structural data of the lesions (volume of interest). To ensure the consistency and stability of lesion segmentation, 40 randomly selected MRI images from other patients were independently assessed by a second radiologist who applied the same methodology to outline the lesions and extract radiomics features. The intraclass correlation coefficient (ICC) was used to evaluate the consistency of the extracted features, with values exceeding 0.75 indicating good reproducibility.

2.3 Radiomics procedure

Radiomic features were extracted using the Pyradiomics package of Python 4.8.1, yielding 1,197 features for each region of interest. Feature type: the extracted image group features include multi-scale features after the original image features (Original), wavelet filtering (Wavelet) and LoG (Laplacian of Gaussian) filtering (σ = 2.0/3.0/4.0/5.0 mm), covering three categories of features: shape, first-order statistics, and texture (GLCM/GLRLM/GLSZM/NGTDM). The original image features were extracted directly after preprocessing (N4 bias correction and normalization), and the unfiltered feature set has been explicitly labeled as the "Original" group. To mitigate multicollinearity and achieve dimensionality reduction, the least absolute shrinkage and selection operator (LASSO) regression model was employed to select significant features. The optimal λ value corresponding to the minimum binomial deviance was determined using five-fold cross-validation, and features with non-zero coefficients were retained to form the final feature subset. The radiomics score was calculated based on the weighted summation of these features. A logistic regression classifier was employed for machine learning to construct the radiomic model, which was subsequently validated

1 http://www.itksnap.org/

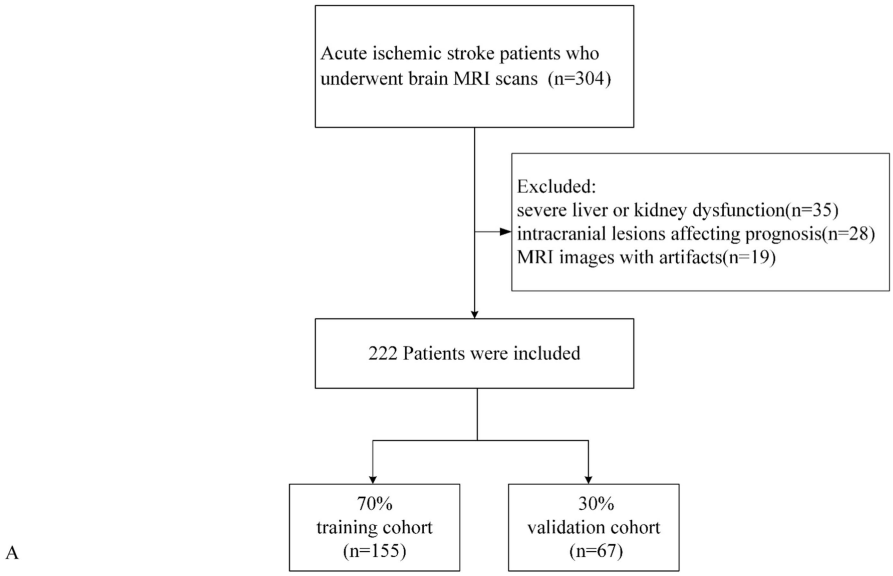

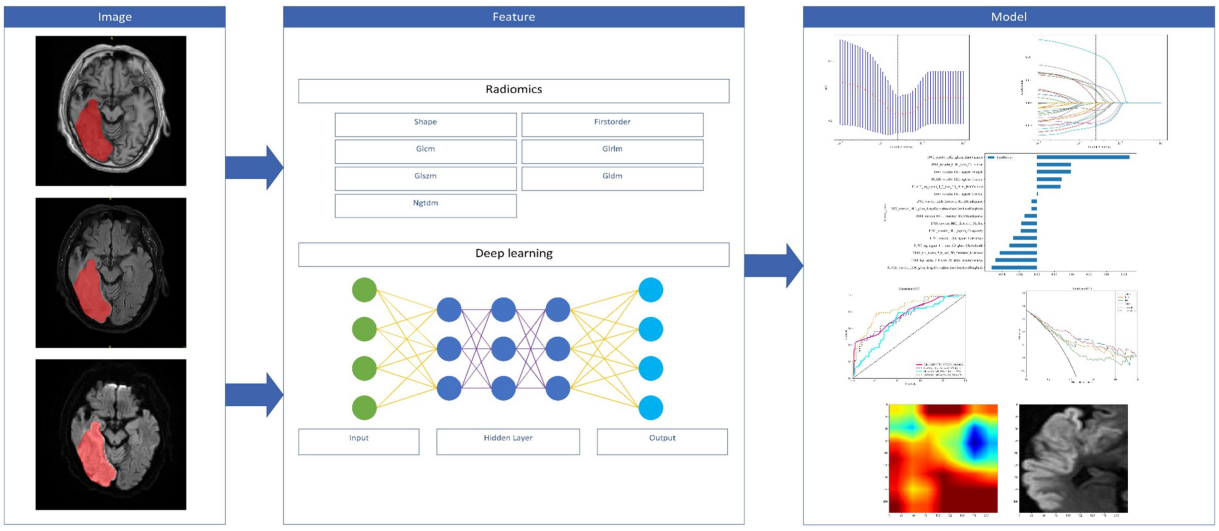

FIGURE 1
Workflow of the study. **(A)** Study flowchart of participant selection. **(B)** Workflow of the radiomics and deep learning analysis of AIS.

using an independent dataset. The radiomics score was computed using the following equation:

$$\text{Radiomics score} = \sum \beta i \cdot Xi + \text{Intercept}\left(i = 0,1,2,3\right)$$

Where *Xi* represents the radiomic feature values selected by LASSO, and βi is the coefficient corresponding to each selected feature *Xi*.

2.4 Deep learning procedure

In this study, we implemented a deep-learning network using the "PyTorch" framework in Python 4.8.1. By constructing a deep, non-linear convolutional neural network with multiple hidden layers, we progressively extracted and combined low-level features to form high-level abstract features, thereby simplifying the complex feature extraction process that is typical of traditional machine learning methods. We selected ResNet, a classical classification network known for its core residual structure, as the backbone model. By establishing shortcut connections between the earlier and later layers, ResNet effectively facilitates gradient backpropagation during training, thereby addressing the degradation problem that is inherent in traditional deep networks. ResNet101, consisting of 101 layers, is considered to have a relatively shallow structure. Building on ResNet101, we developed a 2.5D convolutional neural network (CNN) model using a residual structure to extract features. Using transfer learning, we converted the dataset features into vectors, which were then fused through fully connected layers to classify stroke prognosis.

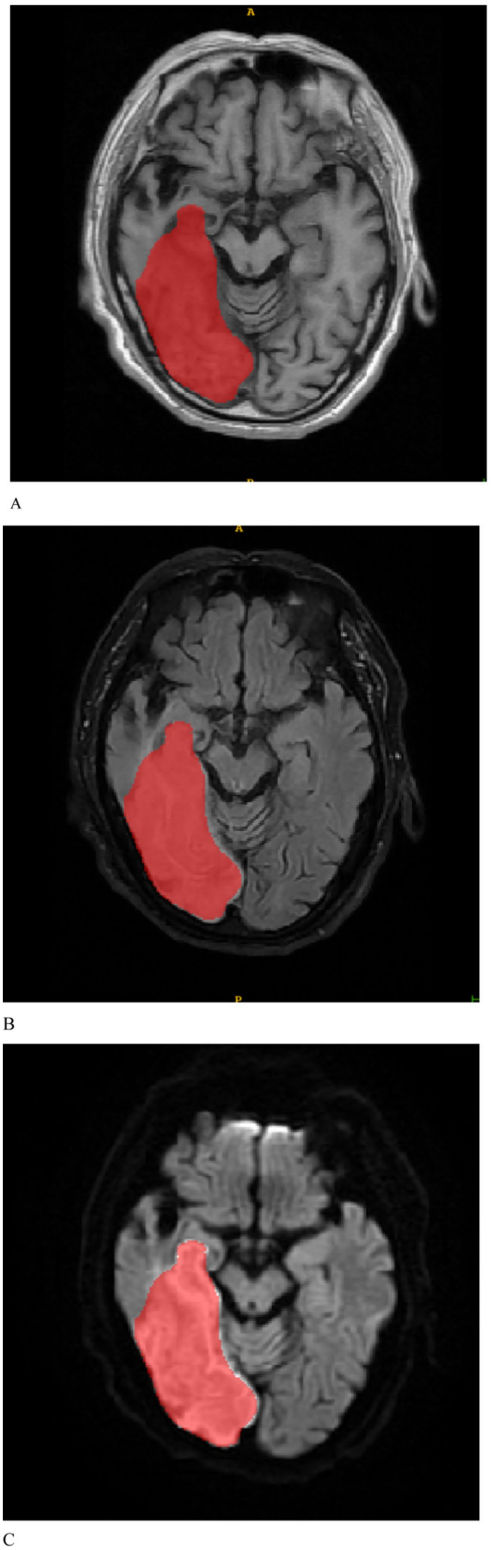

FIGURE 2
Based on the manually delineated regions of interest for patients with stroke, **(A–C)** represent the T1WI, FLAIR, and DWI sequences, respectively.

In practice, we first identified the slice with the largest stroke area, assuming it to be the nth slice of the input volume. Subsequently, we extracted the (n−2), n, and (n + 2) slices for fusion, which were then input into the 2.5D CNN model. To enhance the generalizability of the model and mitigate overfitting, various data augmentation strategies were employed during training, including random translation, scaling, rotation, and shearing, as well as the addition of Gaussian noise, blurring, and Laplacian transformations. We applied L2 regularization to further optimize the model. The model parameters were optimized using the Adam algorithm, and all pretrained layers were fine-tuned to adapt to the current task. The initial learning rate was set to 0.0005, weight decay to 0.0001, and the L2 penalty coefficient to 0.01. Once the model achieved optimal accuracy on the test set, we saved all the model weights and validated the model using an independent test set.

2.5 CRD model establishment and statistical analysis

This study integrated clinical, radiomics, and deep learning models to construct a comprehensive multivariate logistic regression model, designated the CRD (Clinic-Radiomics-Deep Learning) model. A personalized nomogram was then generated to visualize the model, and decision curve analysis (DCA) was applied to quantify the net benefit across varying thresholds, thereby assessing the practical applicability of the CRD model. Clinical data were analyzed using Python 4.8.1 and SPSS version 26.0. For normally distributed data, the results are presented as mean ± standard deviation ($x \pm s$) and were analyzed using independent t-tests. For non-normally distributed data, the median and interquartile range are reported, and comparisons were made using the Mann–Whitney U test. Categorical data are presented as frequencies (percentages) (n [%]), and comparisons were performed using chi-square tests. Logistic regression analysis was used to develop the predictive model, and the area under the receiver operating characteristic curve (AUC) was used to evaluate the predictive capability of the model. The DeLong test was employed to compare the AUCs of multiple models, DCA was used to evaluate the clinical utility of the model, and the optimal model was visualized as a nomogram. Calibration curves were used to assess the accuracy of the nomogram predictions, with statistical significance set at $p < 0.05$.

3 Results

3.1 Baseline characteristics

A total of 222 patients diagnosed with AIS were included in this study in a 7:3 ratio, with 155 patients in the training cohort and 67 in the validation cohort. Table 1 shows that there were no significant differences between the training and validation cohorts in terms of age, sex, NIHSS score at admission, hypertension, diabetes, cardiogenic diseases, smoking, drinking, or intracerebral hemorrhage (ICH) ($p > 0.05$). Table 2 indicates that the clinical data comparisons between the two cohorts were analyzed using independent t-tests or chi-square tests, with $p < 0.05$ considered statistically significant. Two independent risk factors for poor prognosis were identified: NIHSS score at admission and ICH.

TABLE 1 Patients' baseline characters of our cohorts.

Characteristics	ALL	Validation cohort	Training cohort	*p*-value
Age	68.99 ± 12.05	70.39 ± 11.81	68.39 ± 12.14	0.324621
NIHSS at admission	7.41 ± 4.69	7.82 ± 5.49	7.23 ± 4.30	0.491425
Gender				1
0	98(44.14)	30(44.78)	68(43.87)	
1	124(55.86)	37(55.22)	87(56.13)	
Hypertension				0.448426
0	103(46.40)	28(41.79)	75(48.39)	
1	119(53.60)	39(58.21)	80(51.61)	
Diabetes				0.944928
0	168(75.68)	50(74.63)	118(76.13)	
1	54(24.32)	17(25.37)	37(23.87)	
Cardiogenic diseases				0.554017
0	198(89.19)	58(86.57)	140(90.32)	
1	24(10.81)	9(13.43)	15(9.68)	
Smoking				0.966679
0	147(66.22)	45(67.16)	102(65.81)	
1	75(33.78)	22(32.84)	53(34.19)	
Drinking				1
0	165(74.32)	50(74.63)	115(74.19)	
1	57(25.68)	17(25.37)	40(25.81)	
ICH				0.561503
0	201(90.54)	59(88.06)	142(91.61)	
1	21(9.46)	8(11.94)	13(8.39)	

3.2 Radiomics and deep learning models

Using univariate logistic regression analysis and LASSO regression for dimensionality reduction, 16 of the 1,197 radiomic features were selected to construct the radiomics model. These features included 14 shapes, 234 first-order features, 286 features from the gray-level co-occurrence matrix (GLCM), 208 from the gray-level run length matrix (GLRLM), 208 from the gray-level size zone matrix, 182 from the gray-level dependence matrix, and 65 from the neighborhood gray tone difference matrix. The ICC was >0.75. Based on the LASSO regression model, the optimal λ obtained from five-fold cross-validation was used to select the best radiomic features with non-zero coefficients. The distribution of the LASSO coefficients for these features is shown in Figure 3.

3.3 CRD model

The AUC analysis of the specific indicators revealed varying degrees of performance across the different methods and cohorts (Figure 4). In the training cohort, the clinical, radiomics, deep learning, and CRD models achieved AUC values of 0.762, 0.755, 0.689, and 0.834, respectively (Table 3). In the validation cohort, the clinical model exhibited an AUC of 0.874, the radiomics model achieved an AUC of 0.805, the deep learning model attained an AUC of 0.757, and the CRD model again outperformed all other methods with an AUC of 0.908. These findings suggest that the CRD model exhibited the most consistent and robust performance in distinguishing between classes, with significantly superior AUC values compared to the other methods in both the training and validation cohorts.

The calibration curve revealed that the CRD model demonstrated exceptional consistency and calibration in predicting poor stroke prognosis and actual results (Figure 4). The Hosmer–Lemeshow test showed that P was > 0.05, indicating that there was no significant difference between the predicted and true values. DeLong's test indicated that in the training cohort, the CRD model outperformed both the clinical and deep learning models ($p = 0.01$ and $p = 0.001$, respectively). In the validation cohort, the CRD model surpassed the radiomics and deep learning models in terms of predictive performance ($p = 0.01$ and $p = 0.008$, respectively; Figure 5). Figure 5 also shows the DCA for the four models, with the CRD model achieving the highest net benefit compared with the radiomics, deep learning, and clinical models. Using the CRD model, a visual nomogram (Figure 5) was constructed to estimate the risk of a poor prognosis. As illustrated in the nomogram, the NIHSS score at admission was the most influential factor in the scoring system.

4 Discussion

AIS is a non-communicable disease that severely threatens public health and is characterized by high incidence, disability,

TABLE 2 Comparison of patients' baseline characters for poor prognosis in the training cohort and validation cohort.

Characteristics	Training cohort			Validation cohort		
	Good prognosis	Poor prognosis	*P*-value	Good prognosis	Poor prognosis	*p*-value
Age	67.29 ± 12.09	70.28 ± 12.10	0.139155	67.43 ± 11.63	76.86 ± 9.57	0.001881
NIHSS at admission	5.84 ± 3.08	9.63 ± 5.03	<0.001	5.52 ± 3.88	12.86 ± 5.19	<0.001
Gender			0.868411			0.266734
0	42(42.86)	26(45.61)		18(39.13)	12(57.14)	
1	56(57.14)	31(54.39)		28(60.87)	9(42.86)	
Hypertension			0.173769			0.224226
0	52(53.06)	23(40.35)		22(47.83)	6(28.57)	
1	46(46.94)	34(59.65)		24(52.17)	15(71.43)	
Diabetes			0.258194			0.478261
0	78(79.59)	40(70.18)		36(78.26)	14(66.67)	
1	20(20.41)	17(29.82)		10(21.74)	7(33.33)	
Cardiogenic diseases			1			0.804267
0	89(90.82)	51(89.47)		39(84.78)	19(90.48)	
1	9(9.18)	6(10.53)		7(15.22)	2(9.52)	
Smoking			0.484597			0.824463
0	62(63.27)	40(70.18)		30(65.22)	15(71.43)	
1	36(36.73)	17(29.82)		16(34.78)	6(28.57)	
Drinking			1			0.616132
0	73(74.49)	42(73.68)		33(71.74)	17(80.95)	
1	25(25.51)	15(26.32)		13(28.26)	4(19.05)	
ICH			0.004568			0.105598
0	95(96.94)	47(82.46)		43(93.48)	16(76.19)	
1	3(3.06)	10(17.54)		3(6.52)	5(23.81)	

recurrence, and economic burden. The lifetime risk of stroke is notably elevated among individuals aged ≥25 years in China, with the recurrence rate in the first year after the initial stroke ranging between 9.8 and 23.0% (9, 10). Recurrent strokes are associated with high rates of disability and mortality. Although mechanical thrombectomy in patients with acute stroke achieves a high recanalization rate, a significant proportion of patients still experience poor outcomes. Early prediction of the functional prognosis allows for timely intervention and rehabilitation, such as blood pressure and glucose control, individualized early anticoagulation and antiplatelet therapies, and neurocognitive rehabilitation, thereby enhancing the patient's quality of life (11). Therefore, early prognostic evaluation is of great significance in guiding personalized clinical treatment strategies. Previous studies have shown that factors such as age, atrial fibrillation, and NIHSS scores are closely associated with stroke prognosis. However, the mechanisms underlying functional outcomes after mechanical thrombectomy for acute stroke are complex, and the prediction of stroke prognosis remains controversial (12).

In recent years, neuroimaging technologies have evolved from basic diagnostic tools to play more critical roles, particularly in guiding reperfusion therapy and predicting prognosis. Currently, AIS is primarily diagnosed using CT and MRI, with DWI and FLAIR sequences being particularly sensitive to ischemic stroke (13). The DWI sequence, as part of the first-line diagnostic approach for acute stroke, is considered the most accurate method for assessing infarct volume, and MRI may play a crucial role in predicting AIS recurrence. High-signal areas on DWI are typically indicative of the core infarct regions (14). Previous studies have suggested that the infarct volume in patients with acute stroke correlates closely with prognosis, with smaller infarct volumes before treatment often being associated with better outcomes. However, the manual evaluation of MRI images is inherently subjective, and the predictive capacity of traditional imaging parameters for stroke prognosis remains limited (15).

In recent years, radiomics has emerged as a prominent research area that provides multiparametric, morphological, and functional data. Radiomics transcends traditional medical imaging models based on morphology and semi-quantitative analysis by utilizing high-throughput feature extraction algorithms to quantitatively analyze imaging data (16). This approach allows for comprehensive exploration and analysis of the hidden information embedded within images, thereby optimizing the utility of imaging results and supporting personalized treatment strategies in clinical practice. Radiomics has demonstrated immense potential as an advanced technological tool in the field of oncology. This success can

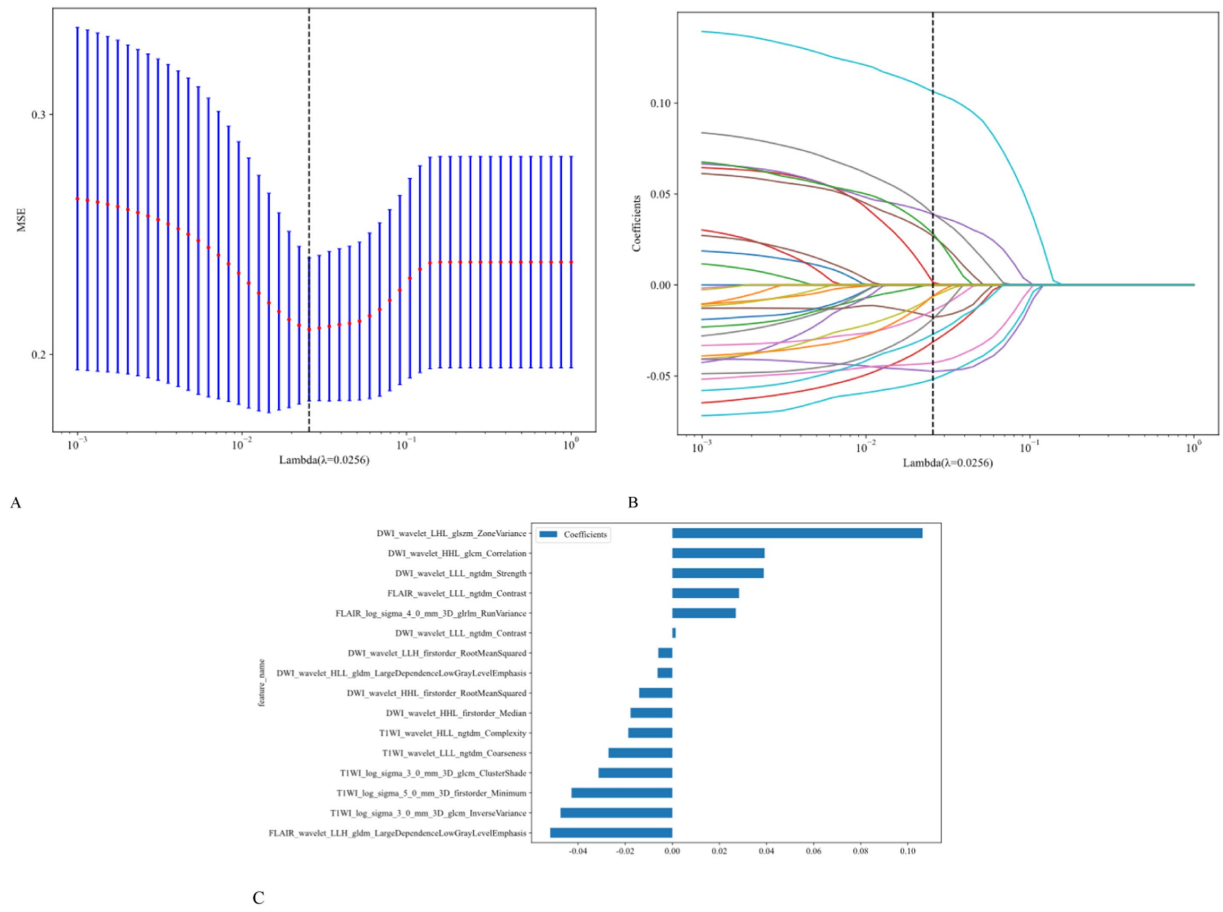

FIGURE 3
Utilization of the LASSO algorithm for feature selection. **(A)** The LASSO model employs five-fold cross-validation to select and fine-tune the parameters (λ). **(B)** Each colored line represents the coefficient of a specific feature, resulting in the final selection of 16 radiomic features **(C)**.

be attributed to the support provided by genomic projects and biomolecular research data, which have enabled researchers to apply radiomics to tumor imaging and extract valuable insights from it. In tumor imaging, the application of radiomics has expanded to include the prediction of tissue pathology, tumor grading, genetic mutations, patient survival rates, and therapeutic outcomes (17).

However, the application of radiomics is not limited to tumor imaging; any digital medical image can benefit from radiomic analysis. Inspired by the successful experiences in tumor imaging, researchers have begun applying these techniques to non-oncological diseases, including cerebral aneurysms, ischemic stroke, hemorrhagic stroke, cerebral arteriovenous malformations, and demyelinating diseases. MRI radiomics holds significant value in predicting the prognosis of patients with AIS who have undergone mechanical thrombectomy (18). Studies have shown that effective prognostic models can be developed by extracting features from DWI sequences and employing support vector machine classifiers (19). Additionally, radiomics can be used to analyze the source of AIS thrombosis, thereby guiding clinical decisions regarding thrombolytic or thrombectomy approaches. In one study focusing on the prognosis of patients with stroke undergoing mechanical thrombectomy, those with higher NIHSS scores at admission typically had a poorer prognosis. Using radiomics models, multiple features that were significantly correlated with AIS prognosis were identified, including first-order, shape, and texture features (20). Among these, the GLCM reflects the homogeneity and heterogeneity of lesions, indirectly revealing the potential impact of stroke-related changes in heterogeneity on patient prognosis. GLRLM, on the other hand, captures the directional and roughness aspects of the image texture, where directional textures may exhibit longer runs at specific angles. These features capture local heterogeneity and gray-level variations in images, providing a more accurate and comprehensive radiomic basis for patient prognostic evaluation (21).

Wang et al. (22) extracted 402 radiomics features from DWI sequences. Significant differences in age, infarct volume, baseline and 24-h NIHSS scores, and hemorrhagic status were observed between the groups with favorable and unfavorable functional outcomes. Eleven radiomic parameters were identified, showing strong predictive performance in both the training and validation cohorts, with AUCs of 0.69 (0.59–0.78) and 0.73 (0.63–0.82), respectively. A radiomic nomogram combining clinical features (age, hemorrhage, and 24-h NIHSS score) and radiomic features showed strong discriminatory power in the training cohort (AUC = 0.80; 95% confidence interval [CI] 0.75–0.86) and was validated in the validation cohort (AUC = 0.73; 95% CI 0.63–0.82). This study did not consider the

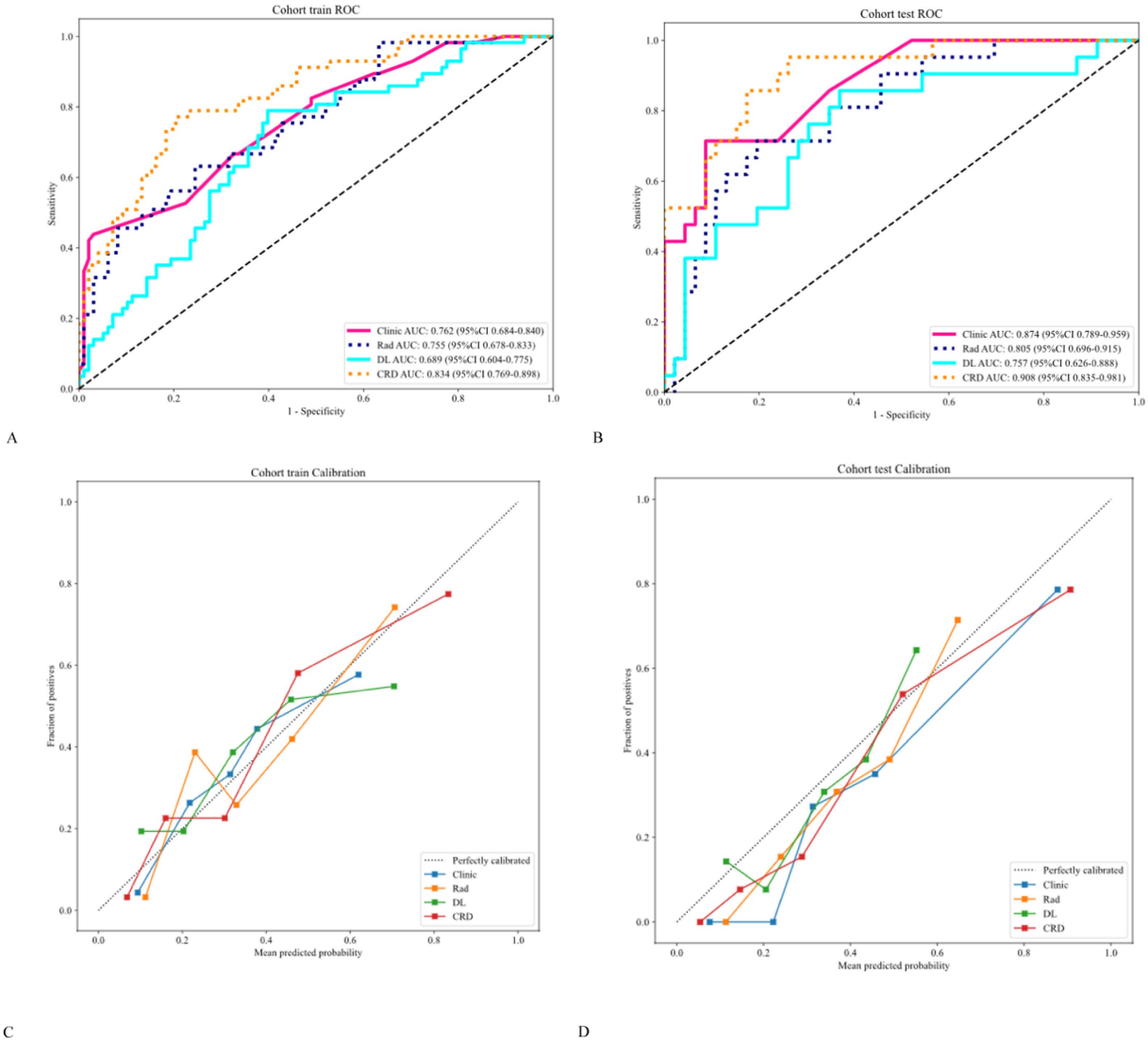

FIGURE 4
(A,B) Receiver operating characteristic curves showing that the CRD model exhibited significantly higher AUC values than the other methods in both cohorts. **(C,D)** Calibration curves showing that the CRD model exhibited exceptional consistency and calibration in predicting a poor prognosis for patients with AIS.

TABLE 3 **Predictive performance of different models to estimate the risk of poor prognosis.**

Model	Accuracy	AUC	95% CI	Sensitivity	Specificity	PPV	NPV	Cohort
Clinic	0.774194	0.762084	0.6842–0.8399	0.421053	0.979592	0.923077	0.744186	Training
Radiomics	0.703226	0.75546	0.6776–0.8333	0.614035	0.755102	0.59322	0.770833	Training
Deep learning	0.664516	0.689402	0.6040–0.7748	0.77193	0.602041	0.53012	0.819444	Training
CRD	0.780645	0.833691	0.7691–0.8983	0.754386	0.795918	0.68254	0.847826	Training
Clinic	0.791045	0.874224	0.7894–0.9591	0.523809	0.913043	0.733333	0.807692	Validation
Radiomics	0.761194	0.805383	0.6956–0.9152	0.666667	0.804348	0.608696	0.840909	Validation
Deep learning	0.686567	0.756729	0.6258–0.8876	0.809524	0.630435	0.5	0.878788	Validation
CRD	0.791045	0.907867	0.8352–0.9805	0.904762	0.73913	0.612903	0.944444	Validation

location and size of the ischemic injury, which may have affected the results. Although radiomic features and clinical variables showed high specificity, their sensitivity was lower, likely because of the generally favorable outcomes in most patients.

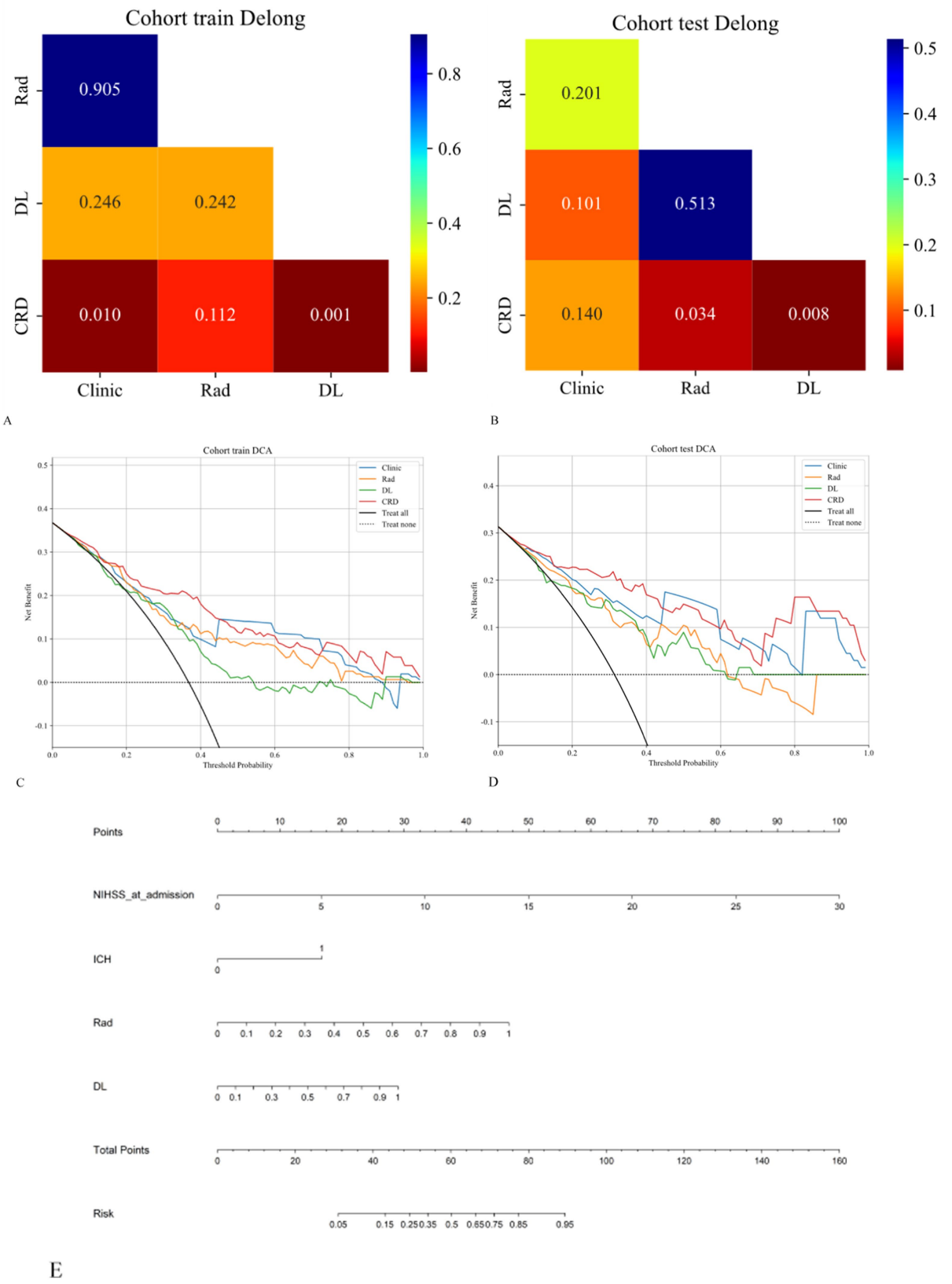

FIGURE 5
(A,B) The DeLong test was applied to both the training and validation cohorts to evaluate the statistical significance of the differences between the models. **(C,D)** DCA curves demonstrating that the CRD model offers the greatest net benefit compared to the clinical, radiomics, and deep learning models. **(E)** A nomogram was constructed for the CRD model based on the NIHSS score at admission, ICH, radiomics score, and deep learning score.

Liu et al. (21) divided patients with AIS into recurrent and non-recurrent groups based on stroke recurrence within 1 year. From the 1,037 radiomic features extracted from the DWI images, 20 were selected for machine learning models. In the validation cohort, LightGBM exhibited the highest level of accuracy. The radiomic data yielded a sensitivity of 0.65, specificity of 0.671, and AUC of 0.647. The clinical data achieved a sensitivity of 0.7, specificity of 0.799, and AUC of 0.735. When combined, the data resulted in a sensitivity of 0.85, specificity of 0.805, and AUC of 0.789. The top factors of the LightGBM model included clinical indicators, such as hemoglobin, platelet-to-large platelet ratio, and age, along with radiomic features. However, the study used only 2D images, limiting the potential of 3D imaging, and may have overlooked certain clinical factors. Future research should expand the dimensionality of the clinical data.

Compared with traditional methods that solely analyze imaging data, radiomics enables a deeper exploration of image information, facilitating the transformation of images into higher-dimensional data (23). This not only enhances the accuracy of prognostic assessments but also provides stronger support for clinical treatment decisions. Radiomic features can reflect the gray-level distribution within images and the interrelationships between voxels, and quantify the heterogeneity within lesions that are invisible to the naked eye, thus aiding in the recognition and classification of diseases (24). Radiomics has already been employed in stroke-related research, such as identifying acute cerebral infarction lesions based on CT- or MRI-derived radiomic features, with MRI-based radiomic features being particularly useful for assisting with the early diagnosis of post-stroke cognitive impairment. Previous studies have predominantly utilized DWI sequences for image processing and data extraction (25). MRI offers superior tissue resolution, demonstrates exceptional sensitivity and specificity for diagnosing AIS, and has gained widespread clinical recognition. Multimodal MRI, which combines conventional and specialized sequences, reflects the pathophysiological changes in ischemic brain tissue. Its utility extends beyond diagnosis, offering insights into collateral circulation, hemodynamics, and molecular metabolism (26). This comprehensive approach allows for an integrated evaluation of the cerebral parenchyma, cerebrovascular conditions, and cerebral hemodynamics, thereby providing a precise reflection of the pathological and physiological state of patients with AIS, ultimately guiding the development of more personalized and accurate treatment strategies.

Deep learning is a pivotal branch within the broader field of machine learning. It emulates the learning process of the human brain through the construction of multilayered neural networks, thereby enabling comprehension and analysis of intricate data (27). Compared with traditional machine learning algorithms, deep learning models exhibit a superior capacity for representation learning and generalization, autonomous extraction of features from data, and the generation of higher-level abstract representations (28). The fundamental concept of deep learning is the iterative transformation of data features through successive layers of neural networks, effectively mapping data from a raw, low-level feature space to a more advanced, abstract feature space (29). In this process, each layer applies a non-linear transformation to the output of the preceding layer, thereby extracting increasingly abstract and meaningful features. This layered transformation enables deep-learning models to address increasingly complex and abstract tasks. The success of deep learning can be attributed to the availability of vast datasets, formidable computational power, and advanced algorithmic models. With the widespread proliferation of the Internet and the acceleration of the digitalization process, the volume of data available has increased exponentially. Such data provide rich training and testing samples, facilitating outstanding performances using deep learning models across diverse and complex scenarios. As computer hardware continues to evolve and parallel computing technologies advance, the training time of deep learning models will be significantly reduced, making deep learning more practical for real-world applications.

Deep learning is progressively transforming our understanding and practice of medicine. Owing to its robust capabilities in feature extraction and pattern recognition, deep learning technology has instigated revolutionary changes in various facets of medical practice, including diagnosis, treatment, and prognostic evaluation. For example, CNNs have been extensively applied for the automatic analysis of pulmonary CT images, aiding in the detection and diagnosis of diseases such as lung cancer. Moreover, deep learning models can segment and annotate medical images, facilitating more precise localization and measurement of pathological areas (1). In addition, deep learning has demonstrated immense potential for disease prediction and prevention. By analyzing and learning from large-scale medical datasets, deep learning models can identify the risk factors and early warning signals associated with specific diseases.

As medical technology continues to advance and digitalization accelerates, the volume of medical data is growing exponentially. In this context, deep learning, a powerful machine learning technique, has demonstrated enormous potential for processing and analyzing large-scale medical datasets (30). In particular, the application of deep learning in stroke diagnosis and treatment has attracted increasing attention. Traditional stroke diagnostic methods often rely heavily on the clinical experience and subjective judgment of healthcare providers. In contrast, deep learning can automatically extract and recognize complex features and patterns associated with stroke by learning from vast amounts of medical data, thereby enhancing the diagnostic accuracy and efficiency. An accurate assessment of the infarct core plays a pivotal role in predicting patient outcomes (31). Although CT is more convenient, it is not particularly sensitive to early infarction changes. To address this issue, Lu et al. (32) developed a deep learning model to identify early subtle AISs in non-contrast CT scans. Their CNN model effectively captured the deep image feature differences between the region of interest and normal tissue and successfully identified and localized lesions. Evaluation using the AUC, sensitivity, specificity, and accuracy metrics (with 95% CIs) showed that the diagnostic performance of the model significantly outperformed that of two experienced radiologists. After referencing the model, the diagnostic accuracy of the radiologists also showed marked improvement, with results highly consistent with the infarct lesion volumes obtained from DWI.

In this study, we developed a 2.5D CNN model based on ResNet101, utilizing residual structures to perform feature extraction from brain MRI images. Through transfer learning, the dataset features were converted into vectors, which were then fused through fully connected layers, to ultimately classify stroke prognosis. The model weights were saved when the highest accuracy was achieved in

the validation cohort, and a deep learning model was subsequently constructed based on these parameters. This study introduces a 2.5D CNN model designed to extract brain MRI features and fuse multimodal information for the precise identification of stroke prognosis-related factors. While reducing the scale and parameter count of 3D convolution models, multimodal imaging is leveraged to ensure comprehensive feature extraction and accurate classification outcomes. This model does not require complex preprocessing of raw images, and the regions of interest in the images were validated using visualization techniques. The 2.5D CNN combines 2D and 3D convolutions, offering two distinct approaches for three-dimensional image segmentation: one based on 2D networks and the other on 3D networks. However, 2D network-based segmentation utilizes only in-slice information, whereas the 3D network approach may risk overfitting when computational resources are limited. The 2.5D method introduces interlayer information to enhance segmentation accuracy, considering the spatial information from adjacent layers. The fusion of multi-view perspectives and integration of adjacent layers as inputs, along with the incorporation of 3D features, significantly improved the model's prediction results.

Magnetic resonance imaging, particularly quantitative susceptibility mapping and R2* relaxometry, plays a vital role in diagnosing AIS and elucidating its pathophysiology. These techniques can quantify iron concentration and myelin volume fraction, providing insights into the evolution of iron and myelination status in ischemic lesions. One study explored the relationship between iron deposition and myelination changes and neurological outcomes in patients with AIS. The results showed that patients with branch atheromatous disease (BAD) exhibited a higher susceptibility to changes, indicating increased iron deposition (33). Changes in NIHSS scores were significantly associated with changes in magnetic susceptibility values, but not with R2* values. Patients with increased iron and demyelination levels showed less improvement in neurological outcomes than those with decreased iron and remyelination levels. The BAD subtype, characterized by increased iron content and demyelination, was associated with worse neurological outcomes.

The ischemic penumbra, a region between irreversibly infarcted and normal brain tissue, is crucial in acute stroke treatment. Existing detection methods, such as ^{15}O-positron emission tomography, are considered the gold standard, but are impractical in emergency settings. One study investigated the feasibility of using quantitative susceptibility mapping to estimate the oxygen extraction fraction for detecting the ischemic penumbra in patients with AIS (34). In 11 patients with a perfusion-core mismatch ratio $\geq$1.8, the volumes of increased oxygen extraction fraction (>51.5%) correlated positively with the ischemic penumbra volumes ($r = 0.636$, $p = 0.035$) and negatively with the 30-day change in NIHSS scores ($r = -0.624$, $p = 0.041$). The Dice similarity coefficient between the penumbra volumes analyzed using both the Dice similarity coefficient and oxygen extraction fraction methods was 0.724, indicating high consistency.

This study has several limitations that need to be addressed. First, it was a retrospective analysis with an insufficient sample size. Our analysis was based on a single-center study and lacked independent external validation, which restricted its generalizability. Second, the imaging data utilized in the study were obtained at the time of discharge, and the duration of clinical trial participation varied across cases, potentially limiting the predictive capability of the model in the early stages. Third, we did not perform a subgroup analysis of anterior and posterior circulation strokes. Given the substantial differences in infarction mechanisms and prognostic factors between these regions, such an analysis is crucial for uncovering the specific biological associations of a model.

5 Conclusion

The CRD model based on multimodal MRI demonstrated high diagnostic efficacy and reliability in predicting poor prognoses in patients with ischemic stroke. This approach holds considerable potential to assist clinicians in the risk assessment and decision-making processes for patients with AIS.

Data availability statement

The original contributions presented in the study are included in the article/Supplementary material, further inquiries can be directed to the corresponding author.

Ethics statement

The studies involving humans were approved by Medical Ethics Committee of Quzhou People's Hospital. The studies were conducted in accordance with the local legislation and institutional requirements. The ethics committee/institutional review board waived the requirement of written informed consent for participation from the participants or the participants' legal guardians/next of kin because this study is a retrospective investigation, approved by the Medical Ethics Committee of Quzhou People's Hospital, which exempted the requirement for informed consent from participants.

Author contributions

LP: Writing – original draft, Writing – review & editing. XH: Writing – original draft. CN: Writing – review & editing. JK: Writing – original draft, Writing – review & editing.

Funding

The author(s) declare that no financial support was received for the research and/or publication of this article.

Conflict of interest

The authors declare that the research was conducted in the absence of any commercial or financial relationships that could be construed as a potential conflict of interest.

Generative AI statement

The authors declare that no Gen AI was used in the creation of this manuscript.

Publisher's note

All claims expressed in this article are solely those of the authors and do not necessarily represent those of their affiliated organizations, or those of the publisher, the editors and the reviewers. Any product that may be evaluated in this article, or claim that may be made by its manufacturer, is not guaranteed or endorsed by the publisher.

Supplementary material

The Supplementary material for this article can be found online at: https://www.frontiersin.org/articles/10.3389/fneur.2025.1587347/full#supplementary-material

References

1. Lee T-Y. Deep learning to predict functional outcome in acute ischemic stroke. *Radiology*. (2024) 313:e242705. doi: 10.1148/radiol.242705

2. Han N, Hu W, Ma Y, Zheng Y, Yue S, Ma L, et al. A clinical-radiomics combined model based on carotid atherosclerotic plaque for prediction of ischemic stroke. *Front Neurol.* (2024) 15:1343423. doi: 10.3389/fneur.2024.1343423

3. Zhang H, Polson JS, Wang Z, Nael K, Rao NM, Speier WF, et al. A deep learning approach to predict recanalization first-pass effect following mechanical Thrombectomy in patients with acute ischemic stroke. *AJNR Am J Neuroradiol.* (2024) 45:1044–52. doi: 10.3174/ajnr.A8272

4. Guo Y, Yang Y, Cao F, Wang M, Luo Y, Guo J, et al. A focus on the role of DSC-PWI dynamic Radiomics features in diagnosis and outcome prediction of ischemic stroke. *J Clin Med.* (2022) 11:5364. doi: 10.3390/jcm11185364

5. Kim J, Oh SW, Lee HY, Choi MH, Meyer H, Huwer S, et al. Assessment of deep learning-based triage application for acute ischemic stroke on brain MRI in the ER. *Acad Radiol.* (2024) 31:4621–8. doi: 10.1016/j.acra.2024.04.046

6. Fang T, Jiang Z, Zhou Y, Jia S, Zhao J, Nie S. Automatic assessment of DWI-ASPECTS for acute ischemic stroke based on deep learning. *Med Phys.* (2024) 51:4351–64. doi: 10.1002/mp.17101

7. Nishio M, Koyasu S, Noguchi S, Kiguchi T, Nakatsu K, Akasaka T, et al. Automatic detection of acute ischemic stroke using non-contrast computed tomography and two-stage deep learning model. *Comput Methods Prog Biomed.* (2020) 196:105711. doi: 10.1016/j.cmpb.2020.105711

8. Gheibi Y, Shirini K, Razavi SN, Farhoudi M, Samad-Soltani T. CNN-res: deep learning framework for segmentation of acute ischemic stroke lesions on multimodal MRI images. *BMC Med Inform Decis Mak.* (2023) 23:192. doi: 10.1186/s12911-023-02289-y

9. Li Y, Liu Y, Hong Z, Wang Y, Lu X. Combining machine learning with radiomics features in predicting outcomes after mechanical thrombectomy in patients with acute ischemic stroke. *Comput Methods Prog Biomed.* (2022) 225:107093. doi: 10.1016/j.cmpb.2022.107093

10. Altmann S, Grauhan NF, Brockstedt L, Kondova M, Schmidtmann I, Paul R, et al. Ultrafast brain MRI with deep learning reconstruction for suspected acute ischemic stroke. *Radiology*. (2024) 310:e231938. doi: 10.1148/radiol.231938

11. Cui L, Fan Z, Yang Y, Liu R, Wang D, Feng Y, et al. Deep learning in ischemic stroke imaging analysis: a comprehensive review. *Biomed Res Int*. (2022) 2022:2456550. doi: 10.1155/2022/2456550

12. Luo J, Dai P, He Z, Huang Z, Liao S, Liu K. Deep learning models for ischemic stroke lesion segmentation in medical images: a survey. *Comput Biol Med.* (2024) 175:108509. doi: 10.1016/j.compbiomed.2024.108509

13. Peng Y, Liu J, Yao R, Wu J, Li J, Dai L, et al. Deep learning-assisted diagnosis of large vessel occlusion in acute ischemic stroke based on four-dimensional computed tomography angiography. *Front Neurosci.* (2024) 18:1329718. doi: 10.3389/fnins.2024.1329718

14. Nageler G, Gergel I, Fangerau M, Breckwoldt M, Seker F, Bendszus M, et al. Deep learning-based assessment of internal carotid artery anatomy to predict difficult intracranial access in endovascular recanalization of acute ischemic stroke. *Clin Neuroradiol.* (2023) 33:783–92. doi: 10.1007/s00062-023-01276-0

15. Ryu W-S, Schellingerhout D, Lee H, Lee K-J, Kim CK, Kim BJ, et al. Deep learning-based automatic classification of ischemic stroke subtype using diffusion-weighted images. *J Stroke*. (2024) 26:300–11. doi: 10.5853/jos.2024.00535

16. Mittmann BJ, Braun M, Runck F, Schmitz B, Tran TN, Yamlahi A, et al. Deep learning-based classification of DSA image sequences of patients with acute ischemic stroke. *Int J Comput Assist Radiol Surg.* (2022) 17:1633–41. doi: 10.1007/s11548-022-02654-8

17. Bretzner M, Bonkhoff AK, Schirmer MD, Hong S, Dalca A, Donahue K, et al. Radiomics-derived brain age predicts functional outcome after acute ischemic stroke. *Neurology*. (2023) 100:e822–33. doi: 10.1212/WNL.0000000000201596

18. Beaudoin A-M, Ho JK, Lam A, Thijs V. Radiomics studies on ischemic stroke and carotid atherosclerotic disease: a reporting quality assessment. *Can Assoc Radiol J.* (2024) 75:549–57. doi: 10.1177/08465371241234545

19. Guo Y, Yang Y, Cao F, Liu Y, Li W, Yang C, et al. Radiomics features of DSC-PWI in time dimension may provide a new chance to identify ischemic stroke. *Front Neurol.* (2022) 13:889090. doi: 10.3389/fneur.2022.889090

20. Li L, Li M, Chen Z, Lu F, Zhao M, Zhang H, et al. Prognostic value of radiomics-based hyperdense middle cerebral artery sign for patients with acute ischemic stroke after thrombectomy strategy. *Front Neurol.* (2022) 13:1037204. doi: 10.3389/fneur.2022.1037204

21. Liu J, Wu Y, Jia W, Han M, Chen Y, Li J, et al. Prediction of recurrence of ischemic stroke within 1 year of discharge based on machine learning MRI radiomics. *Front Neurosci.* (2023) 17:1110579. doi: 10.3389/fnins.2023.1110579

22. Wang H, Sun Y, Ge Y, Wu P-Y, Lin J, Zhao J, et al. A clinical-Radiomics nomogram for functional outcome predictions in ischemic stroke. *Neurol Ther.* (2021) 10:819–32. doi: 10.1007/s40120-021-00263-2

23. Meng Y, Wang H, Wu C, Liu X, Qu L, Shi Y. Prediction model of hemorrhage transformation in patient with acute ischemic stroke based on multiparametric MRI Radiomics and machine learning. *Brain Sci.* (2022) 12:858. doi: 10.3390/brainsci12070858

24. Zeng Y, Long C, Zhao W, Liu J. Predicting the severity of neurological impairment caused by ischemic stroke using deep learning based on diffusion-weighted images. *J Clin Med.* (2022) 11:4008. doi: 10.3390/jcm11144008

25. Wei L, Pan X, Deng W, Chen L, Xi Q, Liu M, et al. Predicting long-term outcomes for acute ischemic stroke using multi-model MRI radiomics and clinical variables. *Front Med.* (2024) 11:1328073. doi: 10.3389/fmed.2024.1328073

26. Zhang Y, Zheng T, Wang H, Zhu J, Duan S, Song B. Predicting functional outcomes of endovascular Thrombectomy in acute ischemic stroke using a clinical-Radiomics nomogram. *World Neurosurg.* (2024) 193:911–9. doi: 10.1016/j.wneu.2024.10.073

27. Koska IO, Selver A, Gelal F, Uluc ME, Çetinoğlu YK, Yurttutan N, et al. Deep learning classification of ischemic stroke territory on diffusion-weighted MRI: added value of augmenting the input with image transformations. *J Imaging Inform Med.* (2024). doi: 10.1007/s10278-024-01277-6

28. Cao Z, Xu J, Song B, Chen L, Sun T, He Y, et al. Deep learning derived automated ASPECTS on non-contrast CT scans of acute ischemic stroke patients. *Hum Brain Mapp.* (2022) 43:3023–36. doi: 10.1002/hbm.25845

29. Aktar M, Reyes J, Tampieri D, Rivaz H, Xiao Y, Kersten-Oertel M. Deep learning for collateral evaluation in ischemic stroke with imbalanced data. *Int J Comput Assist Radiol Surg.* (2023) 18:733–40. doi: 10.1007/s11548-022-02826-6

30. Wei J, Shang K, Wei X, Zhu Y, Yuan Y, Wang M, et al. Deep learning-based automatic ASPECTS calculation can improve diagnosis efficiency in patients with acute ischemic stroke: a multicenter study. *Eur Radiol.* (2024) 35:627–39. doi: 10.1007/s00330-024-10960-9

31. Chiang P-L, Lin S-Y, Chen M-H, Chen Y-S, Wang C-K, Wu M-C, et al. Deep learning-based automatic detection of ASPECTS in acute ischemic stroke: improving stroke assessment on CT scans. *J Clin Med.* (2022) 11:5159. doi: 10.3390/jcm11175159

32. Lu J, Zhou Y, Lv W, Zhu H, Tian T, Yan S, et al. Identification of early invisible acute ischemic stroke in non-contrast computed tomography using two-stage deep-learning model. *Theranostics*. (2022) 12:5564–73. doi: 10.7150/thno.74125

33. Uchida Y, Kan H, Kano Y, Onda K, Sakurai K, Takada K, et al. Longitudinal changes in Iron and myelination within ischemic lesions associate with neurological outcomes: a pilot study. *Stroke.* (2024) 55:1041–50. doi: 10.1161/STROKEAHA.123.044606

34. Uchida Y, Kan H, Inoue H, Oomura M, Shibata H, Kano Y, et al. Penumbra detection with oxygen extraction fraction using magnetic susceptibility in patients with acute ischemic stroke. *Front Neurol.* (2022) 13:752450. doi: 10.3389/fneur.2022.752450

frontiers | Frontiers in Neurology

TYPE Original Research
PUBLISHED 13 May 2025
DOI 10.3389/fneur.2025.1556822

OPEN ACCESS

EDITED BY
Jieqiong Wang,
Chinese Academy of Sciences, China

REVIEWED BY
Xiang Li,
Washington University in St. Louis, United States
Yiyuan Yao,
Exosome Diagnostics, Inc., United States

*CORRESPONDENCE
Fating Zhou
✉ zhoufating@163.com
Haizhen Duan
✉ dhzh1027@163.com

†These authors have contributed equally to this work

RECEIVED 07 January 2025
ACCEPTED 18 April 2025
PUBLISHED 13 May 2025

CITATION
Wei H, Zhu H, Liu M, Zhu X, Yu A, Luo C, Zeng Q, Zhou F and Duan H (2025) Grey-to-white matter ratio on computed tomography for predicting neurological outcome in patients with heat stroke: a retrospective cohort study. *Front. Neurol.* 16:1556822. doi: 10.3389/fneur.2025.1556822

Grey-to-white matter ratio on computed tomography for predicting neurological outcome in patients with heat stroke: a retrospective cohort study

Hua Wei[1†], Hongling Zhu[2,3†], Menglong Liu[1,2†], Xiaodan Zhu[2,4], Anyong Yu[1], Can Luo[1,2], Qingbo Zeng[1,2], Fating Zhou[2,4*] and Haizhen Duan[1*]

[1]Department of Emergency Medicine, Affiliated Hospital of Zunyi Medical University, Zunyi, Guizhou, China, [2]Chongqing Key Laboratory of Emergency Medicine, Chongqing, China, [3]Department of Interventional Radiology, Yichang Central People's Hospital, Yichang, China, [4]Bioengineering College, Chongqing University, Emergency department, Chongqing University Central Hospital (Chongqing Emergency Medical Center), Chongqing, China

Objective: Grey-to-white matter ratio (GWR) is an early and sensitive indicator of cerebral oedema in patients with hypoxic-ischaemic brain injury, we aimed to evaluate the prognostic value of GWR for predicting neurological outcome in heat stroke patients.

Methods: This multicentre retrospective analysis included 86 patients with heat stroke patients who underwent cranial computed tomography (CT). Patients were stratified by Cerebral Performance Category (CPC) scores at discharge: good outcome (CPC 1–2, n = 65) versus poor outcome (CPC 3–5, n = 21) in the derivation cohort. Seven GWR parameters were calculated from Hounsfield unit measurements at three different regions (basal ganglia, centrum semiovale, high convexity): putamen/corpus callosum (PU/CC), caudate nucleus/posterior limb of internal capsule (CN/PLIC), CN/CC, PU/PLIC, $GWR_{basal\ ganglia}$, $GWR_{cerebrum}$, and $GWR_{average}$. Prognostic performance of GWR was compared with qSOFA using receiver operating characteristic (ROC) analysis. And a validation cohort was used to verify the reliability.

Results: All GWRs were significantly lower in the poor outcome group than in the good outcome group. ROC analysis showed the following areas under the curve: PU/CC, 0.836; CN/PLIC, 0.815; CN/CC, 0.858; PU/PLIC, 0.814; $GWR_{basal\ ganglia}$, 0.855; $GWR_{cerebrum}$, 0.803; $GWR_{average}$, 0.837. The cutoff values with 90.77% specificity in predicting poor outcome were as follows: PU/CC, 1.20 (sensitivity, 76.19%); CN/PLIC, 1.17 (sensitivity, 52.38%); CN/CC, 1.20 (sensitivity, 76.19%); PU/PLIC, 1.20 (sensitivity, 61.90%); $GWR_{basal\ ganglia}$, 1.23 (sensitivity, 80.95%); $GWR_{cerebrum}$, 1.19 (sensitivity, 57.14%); $GWR_{average}$, 1.23 (sensitivity, 71.43%). The sensitivity of $GWR_{basal\ ganglia}$ significantly increased when combined with qSOFA in the derivation and validation cohorts.

Discussion: A low GWR was strongly associated with poor outcome in the heat stroke patients. The GWR may be useful as an objective early predictor of poor neurological outcome in the heat stroke patients. Incorporating the GWR with qSOFA significantly enhanced the prediction performance.

KEYWORDS

heat stroke, grey-to-white matter ratio, basal ganglia, neurological outcome, computed tomography (CT)

1 Introduction

Heat stroke, which is caused by global warming and the increasing intensity of global heatwaves, is a common and life-threatening disorder with a high mortality rate (1). Approximately 1.2 billion people would be at risk of a heat stroke worldwide annually by the year 2,100, and the case fatality rate of heat stroke is 10–20% (2, 3). For patients with severe heat stroke, the 28-day mortality rate is nearly 60% (4, 5). Furthermore, numerous survivors have long-term neurological sequelae, such as dysarthria, cognitive impairment, personality change, and limb paresis (3, 6). Brain imaging of survivors with neurological dysfunction identified damage to the prefrontal cortex, cerebellum, and/or hippocampus several months later (7). Thus, early and accurate assessment of neurological outcome is vital in making appropriate therapeutic decisions in patients with heat stroke.

Currently, several classic indicators for evaluating prognosis of heat stroke have been identified: temperature, heart rate, systolic blood pressure, creatinine, aspartate aminotransferase, activated partial thromboplastin time, international normalised ratio, and cooling time (8–10). Based on these indicators, predictive prognosis systems for heat stroke have been developed, including the Sequential Organ Failure Assessment (SOFA) score, Acute Physiology and Chronic Health II score, and Exertional Heat Stroke Score (11, 12). However, all above scoring systems cannot be rapidly obtained due to the requirement for several tests. Thus, a novel, easy-to-access and reproducible tool is needed for predicting neurological outcome of heat stroke patients.

During diagnostic procedures, cranial computed tomography (CT) scans are performed to rule out stroke and brain haemorrhage in patients with heat stroke. Simultaneously, brain oedema can be assessed by differences in the grey and white matter in cranial CT (13, 14). Grey matter (GM) is composed of neuronal bodies and synapses; white matter (WM) mainly consists of myelinated axons. The differences between GM and WM on cranial CT images arise because of the low lipid content and high-water content of GM resulting in a lower carbon concentration as well as a higher oxygen concentration, increasing the level of photoelectric uptake (15). The selective susceptibility of GM to ischemia is due to its higher metabolic rate, greater blood flow, and susceptibility to excitotoxicity (15). A previous retrospective study revealed that severe loss of grey–white matter discrimination is an early and sensitive radiographic indicator of severe brain damage in patients with heat stroke (13). The loss of grey-white matter discrimination can be measured and quantified by the ratio of the grey matter to the white matter (GWR), which is a recommended and effective tool for predicting neurological outcome in comatose cardiac arrest survivors by guidelines for cardiopulmonary resuscitation (14, 16). Based on current evidence, we aimed to evaluate the reliability of GWR in predicting neurological prognostication for patients with heat stroke.

2 Materials and methods

2.1 Ethics approval

The study was approved by the Human Ethical Committee of Chongqing Emergency Medical Center and was in accordance with the Declaration of Helsinki. The Ethics Committee/Institutional Review Board waived the requirement for written informed consent to participate owing to the retrospective nature of the study, but the patients provided informed consent for the publication of the cranial CT images. All clinical information about the patients was maintained in confidence, and the data were analysed in an anonymous manner.

2.2 Study population

This multicentre retrospective study enrolled heat stroke patients from the Affiliated Hospital of Zunyi Medical University, Chongqing Emergency Medicine Hospital, Fifth People's Hospital of Chongqing, Dianjun District People's Hospital of Yichang and Yichang Central People's Hospital between January 2020 and November 2023 (ChiCTR2400079671). Cases of heat stroke were screened using the International Classification of Diseases, Tenth Revision code from the electronic database. Heat stroke was defined as a core body temperature >40°C, accompanied by central nervous system abnormalities, including coma, delirium, and convulsion (17). Clinical data, including age, sex, comorbidity, temperature, presentation, laboratory tests, cranial CT, and outcome, were collected from medical records. The qSOFA score of enrolled patients on admission were obtained.

The inclusion criteria were patients who met the heat stroke diagnostic criteria, who were older than 18 years, and who underwent cranial CT. Those with incomplete medical records and data, with traumatic brain injury and acute stroke, and who underwent cranial CT after resuscitation were excluded. The reasons for performing cranial CT scans were not relevant to this study. Most of the patients with heat stroke underwent cranial CT to rule out primary intracranial events. Heat stroke patients were divided into derivation and validation groups according to the city. These patients were included in the derivation group from the Zunyi and Chongqing. The remaining heat stroke patients from Yichang were included in the validation group. Of the 108 patients with heat stroke who were enrolled into derivation cohort, 22 were excluded; finally, 86 patients with heat stroke were included in the derivation group (Figure 1). In addition, 42 heat stroke patients from Yichang were used to verify the reliability of GWR.

2.3 GWR determination

Participants were scanned by a SOMATOM Sensation 64 CT scanner (Siemens Healthiness, Erlangen, Germany) with 5-mm slices. Regions of interest (ROI) were detected independently by three

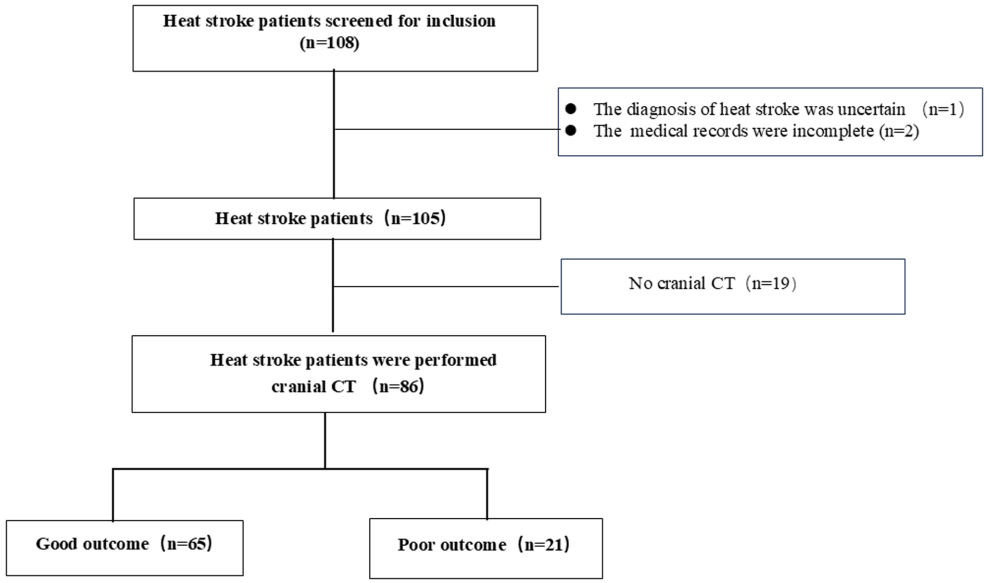

FIGURE 1
Flow diagram illustrating heat stroke patients' selection process.

investigators. They were blinded to the outcome and clinical information of patients during GWR determination (17). After adjustment of the window to the brain, investigators reviewed CT scans using a commercial image-viewing software and identified comparable brain slices. Circular regions of measurement (10 mm^2) were placed over the ROI bilaterally (Figure 2), and the average attenuation was recorded with Hounsfield units (HU). The basal ganglia level was determined from the putamen (PU), caudate nucleus (CN), corpus callosum (CC), and posterior limb of internal capsule (PLIC). The centrum semiovale and high convexity levels were determined from the medial cortex (MC1 and MC2) and medial white matter (MW1 and MW2), respectively. The GWRs were calculated by seven methods according to previous reports (18, 19): PU/CC, CN/PLIC, CN/CC, PU/PLIC, $GWR_{basal\ ganglia}$ = (PU + CN)/(CC + PLIC), $GWR_{cerebrum}$ = (MC1 + MC2)/(WM1 + WM2), and $GWR_{average}$ = (PU + CN + MC1 + MC2)/(CC + PLIC+WM1 + WM2).

2.4 Outcome measure

The primary outcome of patients with heat stroke was clinical outcome at hospital discharge, which was assessed using the Cerebral Performance Category (CPC) score (Supplementary Table S1), and patients were divided into good outcome group (CPC 1–2) and poor outcome group (CPC 3–5).

2.5 Statistical analyses

Continuous variables are expressed as mean±standard deviation or median with interquartile ranges. Categorical data are expressed as number and frequency. Differences between two groups were tested with the independent two-sample *t* test or Mann–Whitney U test. Comparisons of categorical variables were tested using the chi-square test or Fisher's exact test, as appropriate. Obtaining the optimal threshold for predicting prognosis with GWRs was determined through receiver operating characteristic (ROC) curve analysis. The statistical performance of the outcome predictive models was estimated by the area under the curve (AUC), with 95% confidence interval (CI). These AUC values were compared with the Delong test. All statistical analyses were performed in SPSS version 19.0 (IBM Corp., Armonk, NY, United States). A two-tailed p value <0.05 was considered statistically significant.

3 Results

3.1 Clinical characteristics

The average age of the patients was >65 years, most were male, and most presented with underlying diseases, including hypertension, diabetes, and coronary artery disease. Of the 86 patients, 65 had good neurological outcome, and 21 had poor neurological outcome. The baseline characteristics are presented in Table 1. Except for faecal or urinary incontinence, there was no significant difference between the groups in terms of age, sex, comorbidities, symptoms, and duration from onset of symptoms to cranial CT scans. However, patients in the poor outcome group had higher rectal temperature (41.8°C versus 40.5°C), heart rate (123.0 versus 97.0 bpm), respiratory rate (28.0 versus 20.0 bpm), qSOFA (3.0 versus 1.0), and length of stay of hospital (12.0 versus 5.0 days) than those in good outcome group. Furthermore, the patients in the poor outcome group were more likely to experience multiorgan dysfunction (95.2% versus 36.9%) and to be admitted to the intensive care unit (95.2% versus 38.5%) than those in the good outcome group.

3.2 Cranial CT finding

Cranial CT indicated cerebral sulci and effacement of brainstem cisterns, decreased cortical density, and loss of the normal differentiation

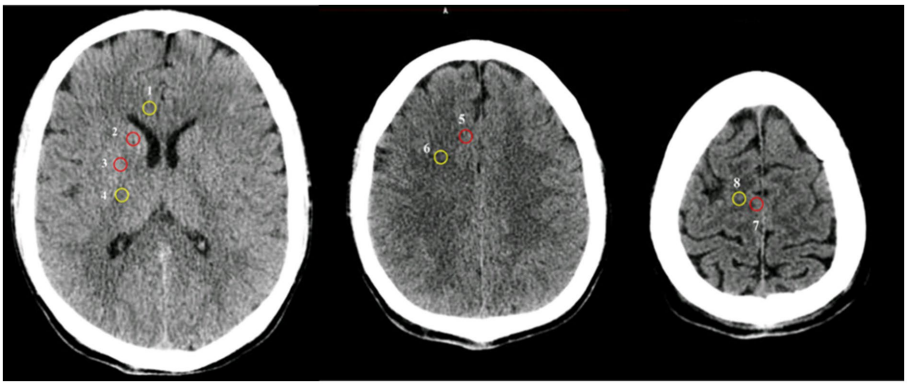

FIGURE 2
Circular regions of interest were placed bilaterally in the Cranial CT. 1 corpus callosum (CC), 2 caudate nucleus (CN), 3 putamen (PU), 4 posterior limb of internal capsule (PLIC), 5 cortex matter at the centrum semiovale level (MC1), 6 white matters at the centrum semiovale level (WM1), 7 cortexes at the high convexity level (MC2), 8 white matters at the high convexity level (WM2). Red circle: grey matter, yellow circle: white matter.

TABLE 1 Characteristics of the study population (*n* = 86).

	Good outcome (*n* = 65)	Poor outcome (*n* = 21)	*p*-value
Age (years)	70.0 (56.5–77.5)	77.8 (55.5–85.5)	0.231
Male gender, *n* (%)	36 (55.4)	15 (71.4)	0.193
Comorbidities			
Hypertension, *n* (%)	23 (35.4)	5 (23.8)	0.325
Diabetes, *n* (%)	11 (16.9)	4 (19.0)	0.527
Coronary artery disease, *n* (%)	3 (4.6)	2 (9.5)	0.592
Stroke, *n* (%)	3 (4.6)	3 (14.3)	0.153
Symptoms and signs			
Fecal or urinary incontinence, *n* (%)	4 (6.1)	6 (28.6)	0.012
Cramp, *n* (%)	13 (20)	3 (14.3)	0.751
Weakness, *n* (%)	13 (20)	3 (14.3)	0.751
Vomiting, *n* (%)	5 (7.7)	2 (9.5)	1.000
From onset of symptoms to admission (h)	2.0 (1.00–5.00)	3.0 (1.50–6.50)	0.430
From onset of symptoms to cranial CT	2.8 (1.65–5.45)	6 (1.95–23.00)	0.094
Rectal temperature (°C)	40.5 (40.1–40.4)	41.8 (40.4–42.2)	0.022
Heart rate (bpm)	97.0 (82.5–115.5)	123.0 (98.5–142.0)	0.002
Respiratory rate (bpm)	20.0 (19.0–24.0)	28.0 (23.5–36.0)	<0.0001
Shock, *n* (%)	4 (6.2%)	10 (47.6%)	<0.0001
MODS, *n* (%)	24 (36.9%)	20 (95.2%)	<0.0001
qSOFA scores	1.0 (0.0–2.0)	3.0 (2.0–3.0)	<0.0001
Staying intensive unit, *n* (%)	25 (38.5%)	20 (95.2%)	<0.0001
Length of stay (days)	5.0 (2.0–9.0)	12.0 (2.0–24.5)	0.034

CT, computed tomography; MODS, multiple organ dysfunction syndrome; qSOFA, quick sepsis related organ failure assessment.

of the white and the grey matter. The imaging signs were clearly observed in the basal ganglia, centrum semioval, and high convexity levels. For patients with poor outcome, diffuse cerebral oedema was clearly visible, and the values of the white matter were nearly similar to those of the grey matter (Figure 3). There were no cases of central nervous system haemorrhage or displaced anatomical structures.

3.3 GWR on cranial CT

The attenuation values and GWRs are presented in Table 2. The attenuation values of the grey matter at high convexity were significantly lower in the poor outcome group than in the good outcome group, and the attenuation values of the white matter at the

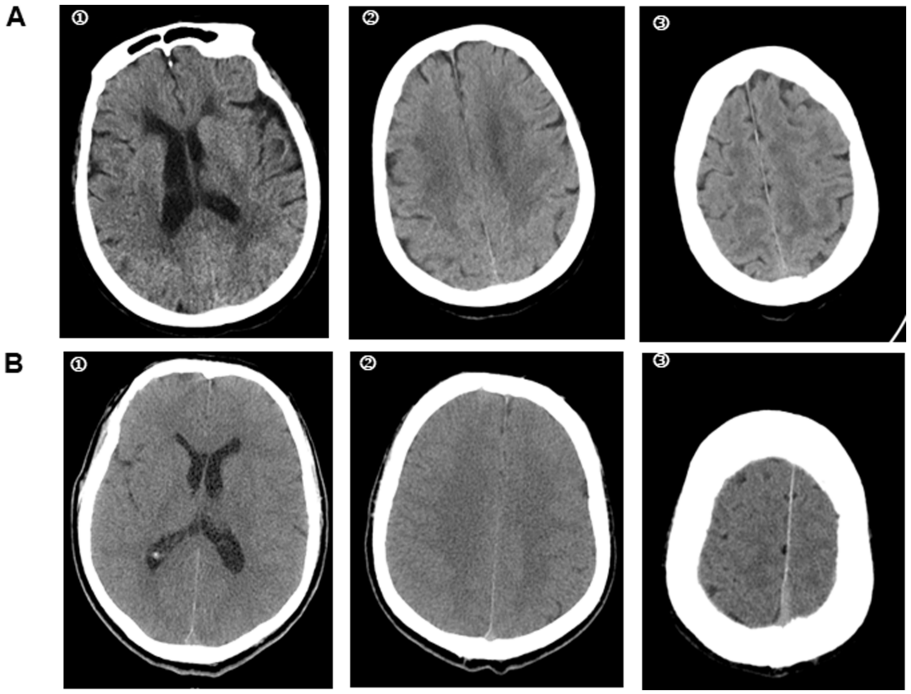

FIGURE 3
Cranial CT in heat stroke patients with different neurological outcome. A heat stroke patient was admitted to the hospital. Cranial CT in the emergency department showed a well-defined grey-white matter difference in the brain. He was discharged from the hospital with CPC 1 **(A)**. While, the cranial CT in another heat stroke patient suggested cerebral oedema with loss of grey-white matter discrepancy. The CPC was 5 at discharge from hospital **(B)**. ① basal ganglia level; ② centrum semiovale level; ③ high convexity level.

TABLE 2 Attenuation values and grey to white matter ratios.

	Good outcome (*n* = 65)	Poor outcome (*n* = 21)	*p*-value
Basal ganglia			
Caudate nucleus (CN)	31.0 (28.0–33.0)	30.0 (27.5–32.0)	0.269
Putamen (PU)	31.0 (28.0–33.0)	30.0 (28.0–33.0)	0.793
Corpus callosum (CC)	23.0 (20.0–25.0)	27.0 (24.0–28.5)	<0.0001
Posterior limb of internal capsule (PLIC)	22.0 (20.0–24.0)	26.0 (23.5–26.5)	0.001
Centrum semiovale			
Medial cortex (MC1)	29.0 (26.0–32.5)	27.0 (24.0–31.5)	0.117
Medial white matter (MW1)	21.0 (19.0–24.1)	23.0 (22.5–24.0)	0.103
High convexity			
Medial cortex (MC2)	29 (26.0–32.0)	27.0 (27.0–29.5)	0.043
Medial white matter (MW2)	21.0 (19.0–25.0)	22.0 (21.0–26.0)	0.111
Grey matter to white matter ratio (GWR)			
PU/CC	1.350 (1.280–1.450)	1.097 (1.037–1.242)	<0.0001
CN/PLIC	1.391 (1.293–1.523)	1.154 (1.113–1.275)	<0.0001
CN/CC	1.364 (1.250–1.461)	1.100 (1.052–1.244)	<0.0001
PU/PLIC	1.391 (1.275–1.477)	1.154 (1.108–1.307)	<0.0001
$GWR_{basal\ ganglia}$	1.372 (1.307–1.452)	1.136 (1.094–1.221)	<0.0001
$GWR_{cerebrum}$	1.353 (1.292–1.418)	1.163 (1.077–1.272)	0.001
$GWR_{average}$	1.2321 (1.262–1.405)	1.134 (1.115–1.305)	<0.0001

CC, corpus callosum; CN, caudate nucleus; PU, putamen; PLIC, posterior limb of internal capsule; MC1, cortex matter at the centrum semiovale level; WM1, white matter at the centrum semiovale level; MC2, cortexes at the high convexity level; WM2, white matter at the high convexity level; GWR, grey white matter ratio.

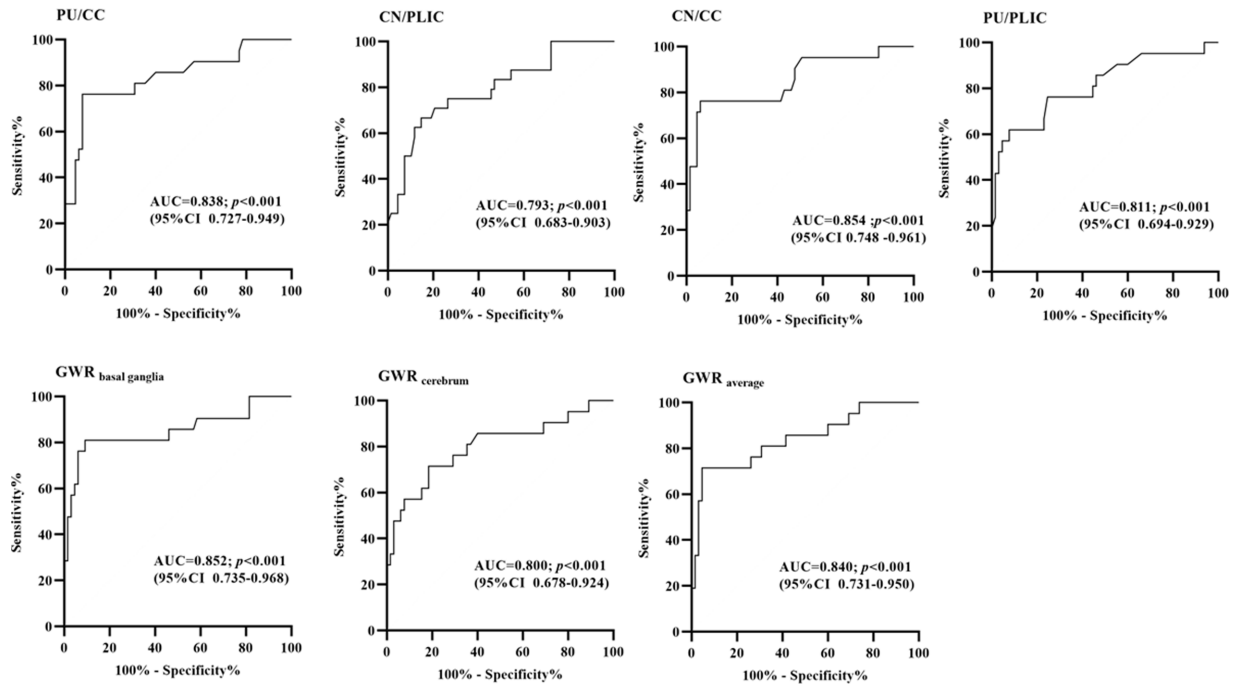

FIGURE 4
Receiver-operating characteristic curves for 7 different GWRs with multivariate logistic regression (AUC, area under curve; CI, confidence intervals).

TABLE 3 Sensitivity and specificity for poor outcome of attenuation measurements and GWR.

	Cut-off value	Sensitivity	Specificity	PPV	NPV	AUC (95% CI)
PU/CC	1.04	28.57%	100%	100%	58.33%	0.838
	1.18	76.19%	90.77%	89.19%	79.22%	(0.727–0.949)
CN/PLIC	1.10	20.83%	100%	100%	58.24%	0.793
	1.15	50.00%	90.77%	85.01%	64.58%	(0.683–0.903)
CN/CC	1.06	28.57%	100%	100%	58.33%	0.854
	1.18	76.19%	90.77%	90.83%	79.50%	(0.748–0.961)
PU/PLIC	1.08	19.05%	100%	100%	55.26%	0.811
	1.18	61.90%	90.77%	87.02%	70.43%	(0.694–0.929)
$GWR_{basal\ ganglia}$	1.08	28.57%	100%	100%	58.33%	0.852
	1.21	80.95%	90.77%	89.76%	81.91%	(0.735–0.968)
$GWR_{cerebrum}$	1.08	28.57%	100%	100%	58.33%	0.800
	1.17	57.14%	90.77%	86.09%	67.93%	(0.67–0.924)
$GWR_{average}$	1.10	19.05%	100%	100%	55.26%	0.840
	1.20	71.43%	90.77%	88.56%	76.06%	(0.731–0.950)

basal ganglia was higher in poor outcome group, whereas the grey matter attenuation values of basal ganglia and centrum semiovale showed no significant difference between the two groups. Interestingly, both white and grey matter attenuation values failed to show significant differences at the centrum semiovale level. All seven GWRs were significantly lower in the poor outcome group than in the good outcome group: median CN/CC: poor outcome group, 1.110; good outcome group, 1.364 ($p < 0.05$); median PU/CC, poor outcome group, 1.097; good outcome group, 1.350 ($p < 0.05$); $GWR_{basal\ ganglia}$: poor outcome group, 1.136; good outcome group, 1.372 ($p < 0.05$).

3.4 Prognostic performances of GWRs

For the ROC curve analysis for the prediction of poor outcome (Figure 4; Table 3), all seven GWRs predicted poor outcomes, with sensitivities ranging from 19.05 to 28.57% at cut-off values with 100%

specificity. The AUC values of the GWRs were between 0.793 and 0.854. The CN/CC had an AUC of 0.854 (95% CI, 0.748–0.961), and its cut-off value for 100% specificity of predicting the poor outcome was 1.06. $GWR_{basal\ ganglia}$ had an AUC of 0.852 (95% CI, 0.735–0.968), and its cut-off value for 100% specificity for poor outcome was 1.08. At 90.77% specificity, $GWR_{basal\ ganglia}$ had the highest sensitivity (80.95%; cut-off value, 1.21) among all methods.

3.5 qSOFA improves GWR for predicting poor outcome

As described before, qSOFA is a reliable predictor in assessing outcome of heat stroke. Compared to the SOFA score, it consists of three parameters and not requiring auxiliary examinations. Our previous results also revealed that patients with heat stroke of poor outcome presented with significantly higher qSOFA scores than those in the good outcome group. Further analysis indicated that qSOFA had an AUC of 0.931 (95% CI, 0.878–0.984), and its cutoff value for 67.69% specificity for poor outcome was 2, but the specificity increased to 70.77% when combined with $GWR_{basal\ ganglia}$ (Figure 5), and the sensitivity of $GWR_{basal\ ganglia}$ with qSOFA increased to 61.90%. Compared to the AUC predicting neurological prognosis with $GWR_{basal\ ganglia}$, the AUC was significantly greater after combination of qSOFA score ($p = 0.034 < 0.05$) with the Delong tests.

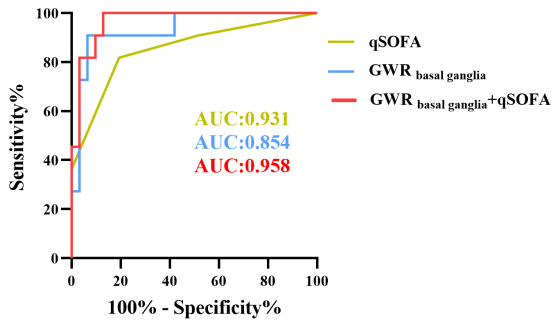

FIGURE 5
GWR improved qSOFA for predicting neurological outcome in heat stroke patients.

3.6 Validation of the GWR in predicting neurological outcome in heat stroke patients

To confirm the clinical usefulness of GWR, we collected an additional 42 heat stroke patients in the validation cohort. The median age was 69.0 years, and this group included 26 male patients (61.9%). Of 42 heat stroke patients, 11 patients (26.19%) presented with poor outcome at discharge. Furthermore, we detected the predict performance of $GWR_{basal\ ganglia}$ in predicting neurological outcome. The results indicated that $GWR_{basal\ ganglia}$ had AUC of 0.936 (95% CI, 0.851–1.000), and its cutoff value for 80.65% specificity for poor outcome was 1.224, but the specificity of $GWR_{basal\ ganglia}$ with qSOFA increased to 90.32% (Supplementary Table S2). Combination $GWR_{basal\ ganglia}$ with qSOFA was presented with greater net benefit than $GWR_{basal\ ganglia}$ over a wide range of threshold probabilities (Figure 6).

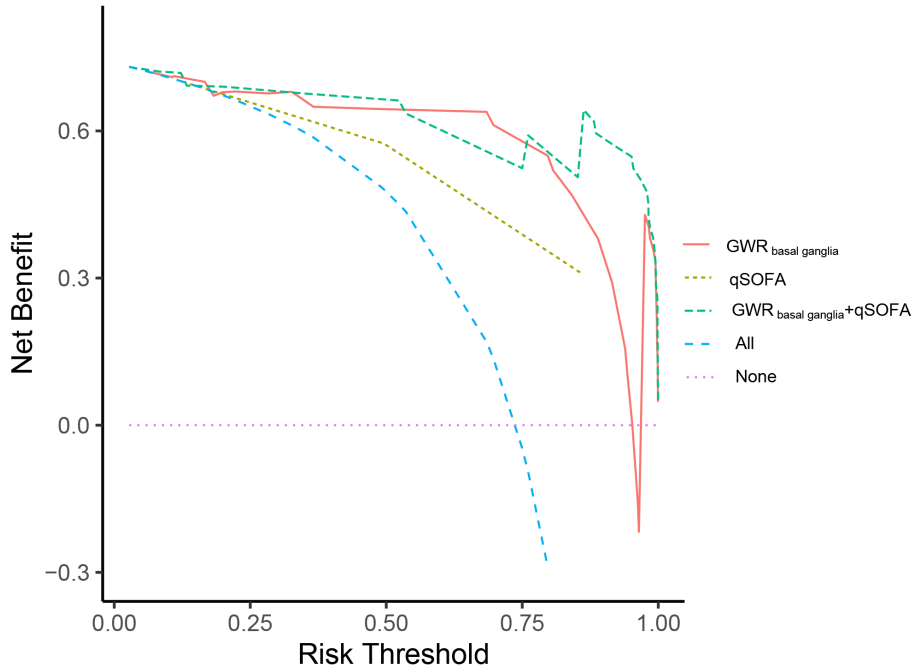

FIGURE 6
Decision-curve analysis (DCA) for predicting neurological outcome of heat stroke patients at discharge. Decision curve analysis for the qSOFA, $GWR_{basal\ ganglia}$ and $GWR_{basal\ ganglia}$ + qSOFA. The x-axis displayed the threshold probability, and y-axis detected the net benefit. Red line: $GWR_{basal\ ganglia}$; yellow line: qSOFA; green line: $GWR_{basal\ ganglia}$ +qSOFA.

4 Discussion

The brain is one of the organs most vulnerable to hyperthermia (20). Neurological impairments are the most characteristic clinical manifestations in patients with heat stroke (21), and these neurological symptoms may present in the early stage, may persist for a long time, and are closely related to long-term cognitive and motor disability in survivors of heat stroke. Therefore, developing a novel and effective biomarker that detects brain injury and predicts delayed central nervous system damage is important.

Currently, several neurobiomarkers, including neuron-specific enolase (NSE), S-100 calcium-binding protein B (S-100 B), glial fibrillary acidic protein, and tau protein, are known to significantly increase in patients with heat stroke (21, 22). Of these markers, NSE and S-100 B have been proposed for heat stroke encephalopathy (22, 23). Under physiological conditions, S-100 B and NSE are abundantly expressed in astrocytes and neurons, with low levels in serum and cerebrospinal fluid (24), but their concentrations increase considerably during acute brain injuries, such as traumatic brain injury, cardiac arrest, and stroke (25–27). Increasing evidence showed that the concentration of S-100 B was strongly correlated with neurological outcomes for up to 7 days post-heat stroke (9). Chun et al. (23) reported that the serum S-100 B concentration of patients with heat stroke was 5 times higher in the poor outcome group than in the good outcome group, and its sensitivity in predicting poor outcome was 86% at cutoff value of 0.61 μg/L, with 86% specificity (23). On the contrary, a study of moderate-intensity exercise with heat strain revealed no differences in serum S-100 B level during exercise (28). Limited by the scarcity of studies, the reliability of neurobiomarkers in predicting neurological prognosis remains to be further clarified.

Apart from neurobiomarkers, cranial CT is commonly used for early detection and differential diagnosis of patients with cerebrovascular accidents and those with heat stroke with impaired consciousness. Several case reports on heat stroke revealed that diffusive cerebral oedema appeared as a loss of grey–white matter discrimination, which predicts poor outcome (29, 30). In physiological state, the difference between grey and white matter is clearly visible in cranial CT (31), but this difference gradually disappears during cerebral oedema (32). This cranial CT finding is also known as "loss of boundary" or "reverse sign" and can be measured quantitatively using the GWR value (13, 19). Similarly, a lower GWR is associated with severe cerebral oedema and neurological impairments.

The present study found that the GWR of patients with heat stroke was lower in the poor outcome group than that in the good outcome group. In fact, GWR was a classic indicator of predicting neurological prognosis in patients post-cardiac arrest syndrome. The sensitivity of GWR can be affected by various factors, including ROI for determining GWR and cutoff values. A study of out-of-hospital cardiac arrest conducted by Lee et al. (33) revealed that the sensitivities of the GWR of PU/CC, PU/PLIC, CC/PLIC, and $GWR_{basal\ ganglia}$ were significantly different in predicting poor outcome. Similarly, Ali et al. (34) demonstrated that GWR had good correlation with cognitive function and quality of life in the aneurysmal subarachnoid hemorrhage patients, and a low GWR indicated cognitive dysfunction. Based on the above findings, we evaluated the neurological outcome of patients with heat stroke with seven different GWRs at the basal ganglia, centrum semiovale, and high convexity levels. The ROC curve analysis revealed that $GWR_{basal\ ganglia}$ presented with the highest sensitivity.

APACHE II and SOFA scores are the common tools used for predicting mortality in the emergency department. In comparison with this two scores, qSOFA can be obtained rapidly at the bedside from respiratory rate, systolic blood pressure and state of consciousness and is not reliant on arterial serum analysis, routine blood examination and coagulation tests. Although qSOFA includes consciousness, it mainly focuses on systemic dysfunction. The state of consciousness is susceptible to hypothermia treatment. Thus, the specificity for assessing the neurological outcome of heat stroke is limited. In contrast to qSOFA, GWR measures brain oedema and directly reflects brain dysfunction. Unlike qSOFA, GWR is used as an indicator of cerebral oedema. Therefore, when qSOFA is used in combination with $GWR_{basal\ ganglia}$, the reliability is significantly improved.

The study has some limitations. Firstly, this was a retrospective multicentre study with a limited number of patients and quality of data. Some patients with heat stroke underwent cranial magnetic resonance imaging without CT scans. Because of the small sample number, the study might not have enrolled rare cases with favourable neurological outcome despite the development of brain oedema in the early stage. We also cannot perform subgroup analyses of heat stroke patients according to CT scanners Secondly, our hospital is the largest emergency centre in Southwest China. Patients with heat stroke are usually treated with cooling therapy out of hospital. Some of the patients returned home without hospitalisation after their temperature quickly returned to normal and neurological function improved, but inpatients are likely to have a more severe condition than patients with heat stroke in other hospitals. Thirdly, this study did not use serial cranial CT or automated GWR determination. Further studies are needed to identify the optimal time to capture CT scans for GWR determination. Fourthly, grey and white matter detection is influenced by traumatic brain injury and acute cerebral infarction, and the GWR is also disturbed in patients following cardiopulmonary resuscitation for heat stroke; therefore, the above patients were excluded from the present study. Finally, we did not evaluate neurological prognosis together with other prognostic indicators such as S-100 B and NSE. These neurobiomarkers are seldom examined in patients with heat stroke, especially in primary hospitals.

In conclusion, among patients with heat stroke who underwent cranial CT, $GWR_{basal\ ganglia}$ <1.22 was a predictor of poor neurological outcome. Incorporating the GWR with qSOFA significantly improved the reliability of prediction.

Data availability statement

The original contributions presented in the study are included in the article/Supplementary material, further inquiries can be directed to the corresponding authors.

Ethics statement

The studies involving humans were approved by the Human Ethical Committee of Chongqing Emergency Medical Center. The studies were conducted in accordance with the local legislation and

institutional requirements. The ethics committee/institutional review board waived the requirement of written informed consent for participation from the participants or the participants' legal guardians/next of kin due to the retrospective nature of the study.

Author contributions

HW: Data curation, Formal analysis, Investigation, Methodology, Writing – original draft. HZ: Data curation, Formal analysis, Investigation, Software, Writing – original draft. ML: Data curation, Formal analysis, Investigation, Software, Writing – original draft. XZ: Data curation, Investigation, Software, Writing – original draft. AY: Formal analysis, Methodology, Software, Writing – review & editing. CL: Data curation, Investigation, Software, Writing – original draft. QZ: Data curation, Formal analysis, Investigation, Software, Writing – original draft. FZ: Conceptualization, Funding acquisition, Supervision, Validation, Writing – review & editing. HD: Funding acquisition, Resources, Supervision, Validation, Writing – review & editing.

Funding

The author(s) declare that financial support was received for the research and/or publication of this article. This work was supported by the National Natural Science Foundation of China (82260385), Science and Technology Project of Guizhou Province (2023580), Health Commission of Guizhou Province (gzwkj2022-103), Eagle Talent Project of Chongqing Emergency Medical Center, and a key project co-organised by the Health Commission and the Science & Technology Bureau of Chongqing Province (2024ZDXM024). The General Project of Chongqing Province Natural Science Foundation (CSTB2024NSCQ-MSX0873) and Chongqing Key Laboratory of Emergency Medicine (2023-KFKT-03) also supported this study. The funders did not participate in the study design, data collection, analysis, decision to submit the manuscript, or the submission process.

Acknowledgments

We would like to thank Tie Deng (Radiology Department, Chongqing Emergency Medical Center, Chongqing, China) for providing technical assistance for GWR determination and Editage for English language editing.

Conflict of interest

The authors declare that the research was conducted in the absence of any commercial or financial relationships that could be construed as a potential conflict of interest.

Generative AI statement

The authors declare that no Gen AI was used in the creation of this manuscript.

Publisher's note

Supplementary material

The Supplementary material for this article can be found online at: https://www.frontiersin.org/articles/10.3389/fneur.2025.1556822/full#supplementary-material

References

1. Patz JA, Campbell-Lendrum D, Holloway T, Foley JA. Impact of regional climate change on human health. *Nature*. (2005) 438:310–7. doi: 10.1038/nature04188

2. Glaser J, Lemery J, Rajagopalan B, Diaz HF, Garcia-Trabanino R, Taduri G, et al. Climate change and the emergent epidemic of CKD from heat stress in rural communities: the case for heat stress nephropathy. *Clin J Am Soc Nephrol*. (2016) 11:1472–83. doi: 10.2215/CJN.13841215

3. Zhong L, Wu M, Liu Z, Liu Y, Ren G, Su L, et al. Risk factors for the 90-day prognosis of severe heat stroke: a case-control study. *Shock*. (2021) 55:61–6. doi: 10.1097/SHK.0000000000001589

4. Argaud L, Ferry T, Le QH, Marfisi A, Ciorba D, Achache P, et al. Short- and long-term outcomes of heatstroke following the 2003 heat wave in Lyon, France. *Arch Intern Med*. (2007) 167:2177–83. doi: 10.1001/archinte.167.20.ioi70147

5. Hifumi T, Kondo Y, Shimizu K, Miyake Y. Heat stroke. *J Intensive Care*. (2018) 6:30. doi: 10.1186/s40560-018-0298-4

6. Garcia CK, Renteria LI, Leite-Santos G, Leon LR, Laitano O. Exertional heat stroke: pathophysiology and risk factors. *BMJ Med*. (2022) 1:e000239. doi: 10.1136/bmjmed-2022-000239

7. Leon LR, Bouchama A. Heat stroke. *Compr Physiol*. (2015) 5:611–47. doi: 10.1002/cphy.c140017

8. Xing L, Liu SY, Mao HD, Zhou KG, Song Q, Cao QM. The prognostic value of routine coagulation tests for patients with heat stroke. *Am J Emerg Med*. (2021) 44:366–72. doi: 10.1016/j.ajem.2020.04.062

9. Schlader ZJ, Davis MS, Bouchama A. Biomarkers of heatstroke-induced organ injury and repair. *Exp Physiol*. (2022) 107:1159–71. doi: 10.1113/EP090142

10. Liu S, Xing L, Wang J, Xin T, Mao H, Zhao J, et al. The relationship between 24-hour indicators and mortality in patients with exertional heat stroke. *Endocr Metab Immune Disord Drug Targets*. (2022) 22:241–6. doi: 10.2174/1871530321666210122153249

11. Zhong L, Wu M, Ji J, Liu Z. Usefulness of sequential organ failure assessment score on admission to predict the 90-day mortality in patients with exertional heatstroke: an over 10-year intensive care survey. *Am J Emerg Med*. (2022) 61:56–60. doi: 10.1016/j.ajem.2022.08.042

12. Li P, Yang L, Liu R, Chen RL. The value of the exertional heat stroke score for the prognosis of patients with exertional heat stroke. *Am J Emerg Med*. (2021) 50:352–5. doi: 10.1016/j.ajem.2021.08.036

13. Szold O, Reider G II, Ben Abraham R, Aviram G, Segev Y, Biderman P, et al. Gray-white matter discrimination--a possible marker for brain damage in heat stroke? *Eur J Radiol*. (2002) 43:1–5. doi: 10.1016/s0720-048x(01)00467-3

14. Panchal AR, Bartos JA, Cabanas JG, Donnino MW, Drennan IR, Hirsch KG, et al. Part 3: adult basic and advanced life support: 2020 American Heart Association guidelines for cardiopulmonary resuscitation and emergency cardiovascular care. *Circulation*. (2020) 142:S366–468. doi: 10.1161/CIR.0000000000000916

15. Gutierrez LG, Rovira A, Portela LA, Leite Cda C, Lucato LT. CT and MR in non-neonatal hypoxic-ischemic encephalopathy: radiological findings with pathophysiological correlations. *Neuroradiology*. (2010) 52:949–76. doi: 10.1007/s00234-010-0728-z

16. Nolan JP, Sandroni C, Bottiger BW, Cariou A, Cronberg T, Friberg H, et al. European resuscitation council and European Society of Intensive Care Medicine

Guidelines 2021: post-resuscitation care. *Resuscitation*. (2021) 161:220–69. doi: 10.1016/j.resuscitation.2021.02.012

17. Lipman GS, Gaudio FG, Eifling KP, Ellis MA, Otten EM, Grissom CK. Wilderness medical society clinical practice guidelines for the prevention and treatment of heat illness: 2019 update. *Wilderness Environ Med*. (2019) 30:S33–46. doi: 10.1016/j.wem.2018.10.004

18. Lee YH, Oh YT, Ahn HC, Kim HS, Han SJ, Lee JJ, et al. The prognostic value of the grey-to-white matter ratio in cardiac arrest patients treated with extracorporeal membrane oxygenation. *Resuscitation*. (2016) 99:50–5. doi: 10.1016/j.resuscitation.2015.11.009

19. Zhou F, Wang H, Jian M, Wang Z, He Y, Duan H, et al. Gray-white matter ratio at the level of the basal ganglia as a predictor of neurologic outcomes in cardiac arrest survivors: a literature review. *Front Med (Lausanne)*. (2022) 9:847089. doi: 10.3389/fmed.2022.847089

20. Bazille C, Megarbane B, Bensimhon D, Lavergne-Slove A, Baglin AC, Loirat P, et al. Brain damage after heat stroke. *J Neuropathol Exp Neurol*. (2005) 64:970–5. doi: 10.1097/01.jnen.0000186924.88333.0d

21. Yaqub B, Al DS. Heat strokes: aetiopathogenesis, neurological characteristics, treatment and outcome. *J Neurol Sci*. (1998) 156:144–51. doi: 10.1016/s0022-510x(98)00037-9

22. Stacey MJ, Leckie T, Fitzpatrick D, Hodgson L, Barden A, Jenkins R, et al. Neurobiomarker and body temperature responses to recreational marathon running. *J Sci Med Sport*. (2023) 26:566–73. doi: 10.1016/j.jsams.2023.09.011

23. Chun JK, Choi S, Kim HH, Yang HW, Kim CS. Predictors of poor prognosis in patients with heat stroke. *Clin Exp Emerg Med*. (2019) 6:345–50. doi: 10.15441/ceem.18.081

24. Wang CH, Chang WT, Su KI, Huang CH, Tsai MS, Chou E, et al. Neuroprognostic accuracy of blood biomarkers for post-cardiac arrest patients: a systematic review and meta-analysis. *Resuscitation*. (2020) 148:108–17. doi: 10.1016/j.resuscitation.2020.01.006

25. Olivecrona M, Rodling-Wahlstrom M, Naredi S, Koskinen LO. S-100B and neuron specific enolase are poor outcome predictors in severe traumatic brain injury treated by an intracranial pressure targeted therapy. *J Neurol Neurosurg Psychiatry*. (2009) 80:1241–8. doi: 10.1136/jnnp.2008.158196

26. Honegger T, Schweizer J, Bicvic A, Westphal LP, Schutz V, Inauen C, et al. Serum S-100B adds incremental value for the prediction of symptomatic intracranial hemorrhage and brain edema after acute ischemic stroke. *Eur Stroke J*. (2023) 8:309–19. doi: 10.1177/23969873221145391

27. Perkins GD, Callaway CW, Haywood K, Neumar RW, Lilja G, Rowland MJ, et al. Brain injury after cardiac arrest. *Lancet*. (2021) 398:1269–78. doi: 10.1016/S0140-6736(21)00953-3

28. Cheuvront SN, Chinevere TD, Ely BR, Kenefick RW, Goodman DA, McClung JP, et al. Serum S-100beta response to exercise-heat strain before and after acclimation. *Med Sci Sports Exerc*. (2008) 40:1477–82. doi: 10.1249/MSS.0b013e31816d65a5

29. Lee S, Lee SH. Exertional heat stroke with reversible severe cerebral edema. *Clin Exp Emerg Med*. (2021) 8:242–5. doi: 10.15441/ceem.19.085

30. Mozzini C, Xotta G, Garbin U, Fratta Pasini AM, Cominacini L. Non-exertional heatstroke: a case report and review of the literature. *Am J Case Rep*. (2017) 18:1058–65. doi: 10.12659/ajcr.905701

31. Brooks RA, Di Chiro G, Keller MR. Explanation of cerebral white--gray contrast in computed tomography. *J Comput Assist Tomogr*. (1980) 4:489–91. doi: 10.1097/00004728-198008000-00016

32. Esdaille CJ, Coppler PJ, Faro JW, Weisner ZM, Condle JP, Elmer J, et al. Duration and clinical features of cardiac arrest predict early severe cerebral edema. *Resuscitation*. (2020) 153:111–8. doi: 10.1016/j.resuscitation.2020.05.049

33. Lee BK, Kim WY, Shin J, Oh JS, Wee JH, Cha KC, et al. Prognostic value of gray matter to white matter ratio in hypoxic and non-hypoxic cardiac arrest with non-cardiac etiology. *Am J Emerg Med*. (2016) 34:1583–8. doi: 10.1016/j.ajem.2016.05.063

34. Ali A, Tanirgan G, Sabanci PA, Sivrikoz N, Abdullah T, Sencer A, et al. Relation of gray-white matter ratio with long-term cognitive functions and quality of life in patients with mild to moderate aneurysmal subarachnoid hemorrhage: a prospective observational study. *Acta Neurochir*. (2018) 160:181–9. doi: 10.1007/s00701-017-3374-y

frontiers | Frontiers in Neurology

TYPE Original Research
PUBLISHED 14 May 2025
DOI 10.3389/fneur.2025.1589198

OPEN ACCESS

EDITED BY
Jieqiong Wang,
Chinese Academy of Sciences, China

REVIEWED BY
Yuto Uchida,
Johns Hopkins University, United States
Minglu Yan,
University of Texas Southwestern Medical Center, United States

*CORRESPONDENCE
Wenbin Wu
✉ wwb1201@vip.sina.com
Huaqiang Liao
✉ 767030837@qq.com

†These authors have contributed equally to this work

RECEIVED 07 March 2025
ACCEPTED 23 April 2025
PUBLISHED 14 May 2025

CITATION
Zeng L, Wang J, Wang Q, Zhang Y, Liao H and Wu W (2025) Cerebral hemodynamics evaluation of FLAIR vascular hyperintensity in TIA patients with large artery severe stenosis or occlusion.
Front. Neurol. 16:1589198.
doi: 10.3389/fneur.2025.1589198

Cerebral hemodynamics evaluation of FLAIR vascular hyperintensity in TIA patients with large artery severe stenosis or occlusion

Lichuan Zeng[1,2†], Jiamei Wang[2†], Qu Wang[1], Yaodan Zhang[1], Huaqiang Liao[1*] and Wenbin Wu[1*]

[1]Hospital of Chengdu University of Traditional Chinese Medicine, Chengdu, China, [2]Deyang Hospital Affiliated Hospital of Chengdu University of Traditional Chinese Medicine, Deyang, China

Purpose: To assess the practicality and utility of employing dual post-label delay (PLD) arterial spin labeling (ASL) in transient ischemic attack (TIA) individuals exhibiting Fluid-attenuated inversion recovery (FLAIR) vascular hyperintensity (FVH).

Materials and methods: We conducted a retrospective review of clinical data from TIA patients presenting with unilateral severe atherosclerotic stenosis or obstruction of either the intracranial internal carotid artery or the middle cerebral artery. Participants were categorized into two groups based on the presence or absence of FVH: FVH positive and FVH negative. All individuals underwent pseudo-continuous ASL perfusion imaging, utilizing distinct PLD durations (1,525 and 2,525 ms) alongside qualitative visual assessments of ASL perfusion irregularities. Standardized TIA evaluations, which included medical history reviews, neuropsychological assessments, and ABCD2 scoring, were performed on all subjects. We explored the correlations between FVHs, clinical manifestations, vascular risk factors, and perfusion metrics.

Results: A total of 50 patients were included in this investigation, with FVH detected in 16 subjects (32.0%). The ABCD2 score was notably elevated within the FVH positive cohort compared to the FVH negative group. At a PLD of 1,525 ms, cerebral blood flow (CBF) values for the affected and healthy hemispheres in the FVH positive group were recorded at 19.55 ± 6.67 and 40.32 ± 6.83, respectively; corresponding values in the FVH negative group were 23.74 ± 5.03 and 46.43 ± 7.91. For a PLD of 2,525 ms, the CBF values for the affected and healthy sides in the FVH positive group were 34.11 ± 5.87 and 50.27 ± 8.57, while the FVH negative group recorded values of 42.79 ± 7.03 and 52.07 ± 7.29, respectively. The differential CBF (ΔCBF) for the affected side in the FVH positive and negative groups was 14.57 ± 4.34 and 19.05 ± 6.10, respectively. A significant negative correlation was established between ΔCBF and ABCD2 scores (Kendall's tau-b = -0.578, $p < 0.001$).

Conclusion: The findings of this study indicate a strong association between the presence of FVH signs and a marked reduction in cerebral blood flow, as well as diminished blood flow reserve. This underscores the potential role of FVH as a biomarker for hemodynamic impairment in TIA patients.

KEYWORDS

arterial spin labeling, post label delay, FLAIR vascular hyperintensity, hyperintense vessel, magnetic resonance imaging

1 Background

Cerebral stenotic or occlusive disorders are associated with a significant decrease in flow velocity attributable to vascular stenosis or occlusion, and the development of collateral blood flow (1). Patients suffering from atherosclerotic steno-occlusive cerebrovascular disease exhibit a considerable, albeit variable, risk of subsequent stroke. A transient ischemic attack (TIA) is typically defined by the rapid onset of a focal neurological deficit of vascular origin, which completely resolves within 24 h (2–4). TIA patients with steno-occlusive cerebrovascular conditions have long been acknowledged as being at heightened risk for subsequent stroke events.

Fluid-attenuated inversion recovery (FLAIR) vascular hyperintensities (FVHs) are described as focal, linear, or serpentine hyperintensities that correspond to arteries within the subarachnoid space and are frequently observed in patients with large artery severe stenosis or occlusion (LASO) (5, 6). FVHs are often detected in individuals with acute ischemic stroke, suggesting considerable hemodynamic impairment and sluggish retrograde flow in the ischemic region (7, 8). Possible explanations for their presence include stagnant blood flow and delayed antegrade or retrograde filling (9). The collateral circulation of the leptomeninges plays a critical role in certain clinical scenarios involving transient ischemic attack (TIA) patients, particularly those with LASO. Some individuals within this cohort exhibit FLAIR vascular hyperintensity, while others do not. However, investigations focusing on the correlation between focal vascular hyperintensities (FVHs) and cerebral perfusion remain sparse.

The use of dynamic magnetic resonance imaging with sensitivity to contrast agents may elevate the potential for complications related to the administration of exogenous contrast materials (10, 11). Arterial spin labeling (ASL) magnetic resonance perfusion imaging serves as a valuable technique for visualizing cerebral perfusion and assessing cerebral blood flow (CBF). This method employs magnetically tagged protons in arterial blood as an intrinsic tracer, thereby negating the necessity for external contrast agents or radioactive tracers (12–16). A strong correlation has been consistently identified in many studies when assessing cerebral perfusion using ASL and CT perfusion (17, 18). An essential parameter in ASL is the post-label delay (PLD) time, defined as the interval between the conclusion of the pulse sequence and the subsequent image acquisition. A brief PLD may not allow for adequate delivery of labeled blood to the target tissue, while an excessively long PLD can result in substantial T1 decay, ultimately diminishing the signal-to-noise ratio (19, 20). When utilizing a singular conventional PLD, the labeled bolus may not completely reach the parenchyma intended for examination, particularly in junctional zones, leading to significant local signal attenuation that could be misinterpreted as false hypoperfusion. Conversely, in patients with well-developed collateral circulation, a single conventional PLD may present apparent hyperperfusion in areas where collateral blood flow is stagnant, a phenomenon referred to as the arterial transit artifact (19). It is thus recommended to employ multiple PLD strategies to enhance the accuracy of CBF quantification (21, 22). The aim of this study was to assess the cerebral hemodynamic state in TIA patients experiencing severe stenosis or occlusion of large arteries, particularly those exhibiting FLAIR vascular hyperintensity.

2 Materials and methods

2.1 Subjects

We performed a retrospective analysis of TIA patients diagnosed with unilateral severe atherosclerotic stenosis (greater than 70%) or occlusion of the intracranial internal carotid artery (ICA, C6, or C7 segment) or middle cerebral artery (MCA, M1 segment) at our institution from January 2023 to December 2024. The inclusion criteria encompassed: (1) Transient neurological symptoms that a clinical neurologist assessed to potentially have a vascular origin; (2) Confirmation of unilateral stenosis or occlusion of the ICA or MCA via MRA or CTA; (3) Non-specific findings on general MRI and diffusion-weighted imaging (DWI); and (4) Completion of an MRI study incorporating ASL with PLD values of 1,525 and 2,525 ms. Exclusion criteria included: (1) Presence of intracranial hemorrhage, brain tumors, cranial trauma, psychiatric disorders, or other recognized brain abnormalities; (2) Poor quality of ASL imaging and failure to perform standard imaging; (3) Other cerebrovascular conditions such as Moyamoya disease or various cerebrovascular malformations; and (4) Incomplete or absent clinical data for patients. All subjects underwent routine screening for TIA, with ABCD2 scores evaluated by trained neurologists through the review of electronic medical records. The study received approval from the Ethics Committee of the Hospital of Chengdu University of Traditional Chinese Medicine, which waived the necessity for written informed consent due to the retrospective nature of the research.

2.2 MR imaging

All patients underwent MRI scans utilizing a Discovery MR750 3.0 T system (GE Healthcare, Milwaukee, WI, United States) outfitted with an 8-channel phased array head coil. The imaging protocol included T1-weighted imaging (T1WI), T2-weighted imaging (T2WI), T2 fluid-attenuated inversion recovery (T2-FLAIR), diffusion-weighted imaging (DWI), angiography (MRA) and pseudo-continuous arterial spin labeling (ASL) perfusion imaging were performed using two distinct post-labeling delays (PLDs) of 1,525 and 2,525 ms. The acquisition of the whole-brain three-dimensional pCASL perfusion sequence was executed utilizing a fast spin-echo methodology with background suppression, adhering to the specified parameters: labeling duration of 1,525 ms, repetition time (TR) of 4,632 ms, echo time (TE) of 10.5 ms, 36 slices, a slice thickness of 4.0 mm, a field of view of 24 cm × 24 cm, and an acquisition duration of 4 min and 29 s. Subsequently, the PLD was adjusted to 2,525 ms, while retaining all other parameters constant, resulting in an acquisition time of 5 min and 9 s.

2.3 Image evaluation

In terms of image evaluation, focal FVH was characterized as a serpentine or speckled hyperintensity located in the sulcus and subarachnoid space on T2-FLAIR imaging. Two independent neuroradiologists, each possessing a minimum of 5 years of MRI experience, scrutinized the images to identify the presence of FVH signs and ASL perfusion anomalies through qualitative visual assessment, deliberately excluding identifiable and clinical information. The ASL cerebral blood flow (CBF) maps for both patient groups underwent post-processing and were generated utilizing the Function Tool (Advanced Workstation 4.6; GE Healthcare). For each patient, a rounded region of interest (ROI) was meticulously delineated on the 3D PCASL images to symmetrically assess CBF values on both the affected and healthy hemispheres. Careful placement of the ROIs was ensured to circumvent blood vessels, cerebral sulci, or cerebral cisterns. Three ROIs were employed in each brain region to quantify CBF, and the average value was utilized for subsequent analysis. In patients experiencing hemispheric transient ischemic attacks, the assessment of perfusion disturbances was conducted to ascertain their correlation with the hemispheric localization of presenting symptoms.

2.4 Statistical analysis

Inter-observer agreement was assessed using kappa (κ) statistics. $\kappa > 0.6$ is considered to indicate good agreement, while $\kappa > 0.8$ is regarded as excellent. Continuous variables that follow a normal distribution are presented as mean ± standard deviation (SD), whereas categorical variables are reported in terms of frequency (%). The differences in each of the categorical variables between the two groups were analyzed using one-way ANOVA, the chi-square test, and Fisher's exact test (when the expected cell frequency was < 5). Statistical significance was set at $p < 0.05$. All statistical analyses were performed using SPSS software (version 20.0, SPSS Inc., Chicago, IL, United States).

3 Results

3.1 Demographic and clinical information

Fifty patients (mean age: 60.5 ± 9.0 years; 27 males) satisfied the inclusion criteria and were recruited for the study. The inter-reader agreement for FVH detection was determined to be good ($\kappa = 0.86$). Among the cohort, FVH was identified in 16 patients (32.0%). The ABCD2 scores for subjects in the study were 4 (3–5) in the FVH-positive group and 2 (1–3) in the FVH-negative group, showcasing a statistically significant difference ($p < 0.05$). Furthermore, significant disparities were noted between the FVH negative and FVH positive groups in terms of prior stroke history and symptom duration ($p < 0.05$). Notably, cardiovascular risk factors, including hypertension, hyperlipidemia, and smoking history, did not exhibit significant differences between patients with and without FVH. Detailed characteristics of TIA patients, both with and without FVH signs, are outlined in Table 1.

TABLE 1 Baseline characteristics of the TIA patients with and without FVH sign.

	FVH(+) (n = 16)	FVH(–) (n = 34)	p-value
Age (years), mean ± SD	64.0 ± 6.5	58.9 ± 9.6	0.061
Male gender	10(62.5%)	17(50.0%)	0.408
Previous stroke	5(31.3%)	2(2.9%)	0.016*
ABCD2 score (median, IQR)	4(3–5)	2(1–3)	<0.001*
Hypertension	11(68.8%)	19(55.9%)	0.386
Diabetes mellitus	4(25.0%)	8(23.5%)	0.910
Hyperlipidemia	7(43.8%)	8(23.5%)	0.146
Smoking history	7(43.8%)	12(35.3%)	0.472
Atrial fbrillation	4(25.0%)	8(23.5%)	0.910
Symptom duration (>1 h)	13(81.3%)	15(44.1%)	0.014*
Coronary heart disease	7(43.8%)	8(23.5%)	0.146
Occlusive site			
MCA	6(37.5%)	9(26.5%)	0.427
ICA	10(62.5%)	25(73.5%)	0.427

ABCD2, age, blood pressure, clinical symptoms, duration of TIA and diabetes; FVH, FLAIR vascular hyperintensity; MCA, middle cerebral artery; ICA, internal carotid artery. *There is significant difference between two groups.

3.2 Characteristics of cerebral perfusion parameters

The ASL markers in the current study demonstrated good reproducibility between raters ($\kappa = 0.82$). The detailed ASL perfusion data for patients from both groups is summarized in Table 2. For the PLD of 1,525 ms, the CBF values were recorded at 19.55 ± 6.67 and 40.32 ± 6.83 for the affected and healthy sides, respectively, within the FVH positive group, whereas the FVH negative group exhibited corresponding values of 23.74 ± 5.03 and 46.43 ± 7.91. In the scenario of a PLD of 2,525 ms, the CBF values were noted as 34.11 ± 5.87 and 50.27 ± 8.57 for the affected and healthy sides in the FVH positive group, whereas in the FVH negative group, the respective values were 42.79 ± 7.03 and 52.07 ± 7.29. The D-value (ΔCBF) for both groups was compared on the affected side across different PLDs, yielding values of 14.57 ± 4.34 and 19.05 ± 6.10, respectively. Representative cases of FVH positive and FVH negative patients with varying PLDs are depicted in Figures 1, 2. Notably, a significant negative correlation was identified between ΔCBF and ABCD2 scores (Kendall's tau-b = −0.578, $p < 0.001$).

4 Discussion

This investigation focused on the correlation between FVH and perfusion through ASL at varying PLDs in patients suffering from TIA and intracranial aortic stenosis or occlusion. The study presents three primary conclusions. Firstly, FVHs were identified in 32% of TIA patients who underwent LASO, aligning with findings from prior research (23). Secondly, our analysis indicated that TIA patients with LASO exhibiting positive FVH were substantially more likely to have reduced CBF and a more critically compromised blood flow reserve

TABLE 2 Results of ASL in different PLDs in patients with and without FVH sign.

CBF (mL·100 g^{-1}·min^{-1})	FVH(+) (n = 16)		FVH(–) (n = 34)		p-value
	Affected side	Healthy side	Affected side	Healthy side	
CBF1	19.55 ± 6.67	40.32 ± 6.83	23.74 ± 5.03	46.43 ± 7.91	0.017*
CBF2	34.11 ± 5.87	50.27 ± 8.57	42.79 ± 7.03	52.07 ± 7.29	<0.001*
△CBF	14.57 ± 4.34		19.05 ± 6.10		0.011*

CBF1, CBF in PLD 1,525 ms; CBF2, CBF in PLD 2,525 ms; △CBF, CBF2-CBF1. *There is significant difference in affected side between two groups.

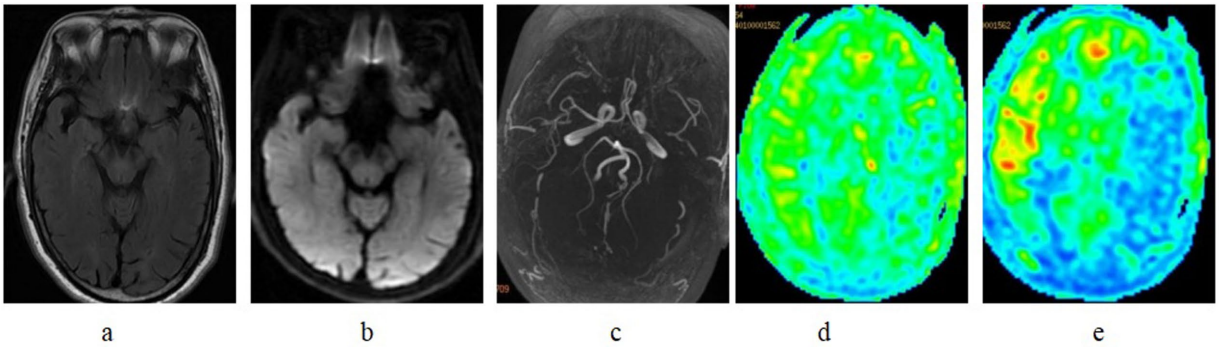

FIGURE 1
FLAIR vascular hyperintensity in a patient with left middle cerebral artery occlusion. **(a)** Serpentine hyperintense signal of the middle cerebral artery branches in the left sylvian fissure in T2 FLAIR. **(b)** DWI demonstrate negative finding. **(c)** MRA showed occlusion of the left MCA M1. **(d)** On ASL with a PLD of 1525 ms markedly decreased ASL signals are noted in the extended area of the left hemisphere. ASL with a PLD of 2525 ms, **(e)** the decreased area is somewhat improved, but there is still a slight laterality compared with the right side.

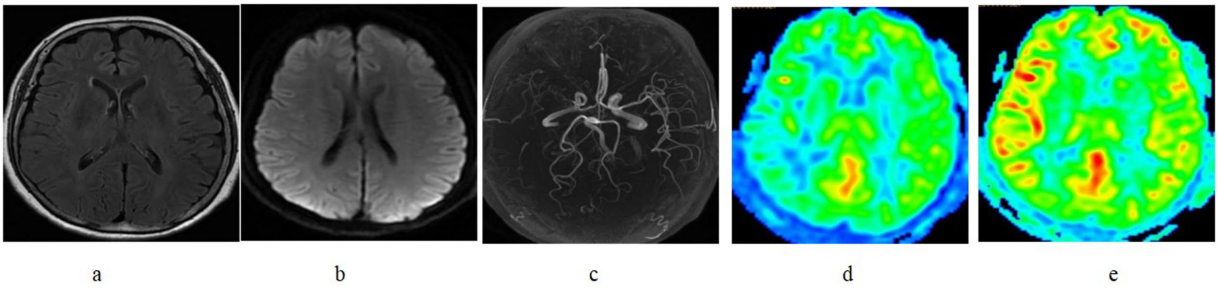

FIGURE 2
FLAIR vascular hyperintensity absent in a patient with right middle cerebral artery occlusion. **(a)** FLAIR vascular hyperintensity absent in T2 FLAIR and **(b)** DWI demonstrate negative finding. **(c)** MRA showed occlusion of the right MCA M1. The area of the right MCA demonstrated to be hypoperfused on ASLwith a PLD of 1525 ms **(d)** but improved on ASL with a PLD of 2525 ms **(e)**.

compared to those without FVH. Correlation assessments demonstrated significant negative relationships between ΔCBF and ABCD2 scores. Thirdly, patients with TIA and positive FVH encountered a notably elevated ABCD2 risk score, a frequently utilized metric for assessing stroke risk post-TIA. These results provide valuable insights for clinicians in understanding hemodynamic conditions and collateral compensation, which are essential for accurately identifying disease states and presenting reliable imaging evidence for both primary and secondary stroke prevention.

While much of the existing literature has concentrated on FVH manifestations in patients with acute cerebral infarctions, the prevalence of FVH is highly variable across different studies. The assessment of FVH in TIA patients remains less comprehensive compared to those with ischemic strokes. Maeda et al. (24) evaluated the progression of FVH in acute and subacute cerebral infarctions within the middle cerebral artery territory and observed that FVH appeared in 100% of evaluations conducted within 24 h of symptom onset, but only in 18% of assessments performed 5–9 days post-symptom onset. The occurrence of FVH correlates with the duration between stroke onset and MRI imaging, with its frequency diminishing over time. Ding et al. (25) noted that FVH was detected in as many as 81.6% (31/38) of hospitalized TIA patients exhibiting severe stenosis or occlusion, with MR scans executed within 48 h of symptom onset, a timeframe significantly shorter than that of our study.

Most research suggests a relationship between FVH and either large-vessel occlusion or severe stenosis, as well as hemodynamic impairment. Lyu et al. (5) examined whether FVH could serve as a prognostic indicator for ischemic events in patients with ICA or MCA occlusion. Their findings indicated that the FVH-ASPECTS was substantially lower in the asymptomatic occlusion cohort compared to the symptomatic

group, implying that FVH might be predictive of stroke occurrence. Bunker and Hillis (26) reported that the typical location of FVHs matched regions of hypoperfusion in corresponding vascular territories captured via perfusion-weighted imaging. Nam et al. (27) investigated the relationship between FVH and early ischemic lesion recurrence in patients with lesion-negative TIA. Their results demonstrated that FVH is significantly associated with early ischemic lesion recurrence in this patient population. Our study quantitatively illustrates that TIA patients with significant arterial vessel occlusion who also present with FVH exhibit markedly lower CBF values and more severely diminished blood flow reserves than those without FVH. In cases of unilateral LASO, it is essential to consider the effects of delayed anterograde flow along with both primary and secondary collateral circulations when evaluating hemodynamic status.

Disruption of the blood–brain barrier (BBB) represents a critical pathological feature of ischemic stroke. Preserving BBB integrity is vital for maintaining central nervous system homeostasis (28). Cerebrovascular stenosis triggers pathological cascades via hemodynamic alterations. Atherosclerotic narrowing not only decreases cerebral perfusion pressure but also elevates turbulent flow, thereby inducing endothelial shear stress. This stress activates matrix metalloproteinases (MMPs) and compromises tight junction proteins, leading to BBB dysfunction. The resultant BBB compromise facilitates erythrocyte extravasation and hemoglobin degradation, releasing ferrous iron that catalyzes Fenton reactions. The subsequent production of reactive oxygen species (ROS) perpetuates neuroinflammation and exacerbates BBB disruption through vascular endothelial growth factor (VEGF)-mediated vascular remodeling. Importantly, hemosiderin deposition in perivascular spaces generates paramagnetic susceptibility effects detectable on susceptibility-weighted imaging (SWI) MRI. Furthermore, chronic iron overload accelerates tau phosphorylation and amyloid-β aggregation via ferroptosis pathways, establishing a self-sustaining cycle of neurodegeneration (29). Uchida et al. (30) conducted a combined quantitative MRI analysis using QSM and R2* relaxometry, demonstrating that increased iron concentration in ischemic lesions is associated with reduced improvement in neurological outcomes following stroke rehabilitation.

Conventional magnetic resonance imaging has a satisfactory resolution ratio for components of brain tissue, but cannot provide blood flow perfusion information. ASL imaging enables detection of absolute perfusion values. PLD is the most important parameter contributing to the accurate assessment of CBF (31, 32). Cerebral blood flow imaging can sensitively and specifically detect abnormal perfusion changes (33). The present study targeted the noninvasive assessment of cerebral hemodynamics with a quantitative measure of CBF perfusion using the ASL technique. This technique has good reproducibility and does not require radiation or gadolinium-based tracers, thereby avoiding potential adverse effects. CBF readings obtained from a single PLD scan may not accurately reflect the true cerebral perfusion status, particularly in patients with extensive vascular lesions. A PLD of 2,525 ms may detect slower blood flow through secondary collateral circulation, while a PLD of 1,525 ms may not capture such dynamics. This study validated dual-PLD settings of 1,525 and 2,525 ms for assessing the hemodynamic condition of patients with transient ischemic attack (TIA) who underwent large artery stenosis occlusion. Moreover, we explored the clinical significance of supplementary ASL and FVH signs. Patients experiencing transient ischemic attacks frequently exhibit similar pathophysiological mechanisms to individuals suffering from other cerebrovascular stenotic or obstructive diseases, characterized by a pronounced reduction in blood flow velocity resulting from arterial stenosis or occlusion, alongside the establishment of collateral circulation. Intracranial atherosclerosis is a notable contributor to cerebral stenosis and insufficient cerebral perfusion, playing a crucial role in both the initial onset and the recurrence of ischemic strokes (5). Individuals exhibiting transient neurological symptoms alongside confirmed evidence of LASO are at an increased risk of subsequent strokes due to compromised CBF and disturbed cerebral perfusion. The ABCD2 scoring system, which is based on specific risk factors and clinical presentations of TIA, revealed that patients with TIA and FLAIR hyperintensities (FVH) had significantly elevated ABCD2 risk scores, potentially correlating with adverse outcomes. Collateral circulation can sustain brain tissue viability for extended periods following the occlusion of major cerebral arteries, thereby serving a vital function in TIA patients. Therefore, enhancing or preserving collateral circulation emerges as a promising therapeutic target. Given that chronic hemodynamic impairment often leads to progressive cortical neuronal degeneration, early intervention is advocated for TIA patients presenting with FVH to avert stroke occurrence.

The application of ASL magnetic resonance imaging with dual PLD holds significant potential for evaluating cerebral hemodynamics in TIA patients. This method addresses limitations of single-PLD ASL by capturing both early and delayed perfusion phases, which is critical for assessing collateral-dependent blood flow and cerebrovascular reserve (CVR) in regions with prolonged arterial transit times (ATT). For instance, studies in patients with internal carotid artery steno-occlusion demonstrated that hypoperfusion observed at PLD 1.5 s often improved at PLD 2.5 s due to delayed collateral flow, as validated by digital subtraction angiography (DSA) (19, 34). This dual-PLD approach also differentiates stagnant collateral pathways from functional hyperperfusion, which is essential for identifying tissue at risk of ischemic injury in TIA patients (19). Furthermore, dual-PLD ASL correlates with acetazolamide-challenged SPECT in assessing CVR, highlighting its utility for noninvasive evaluation of hemodynamic compromise (35). In periictal hyperperfusion studies, dual PLD revealed distinct hemodynamic patterns ("fast flow" vs. "gradual flow"), suggesting its adaptability to dynamic perfusion changes (36). For TIA patients, combining these capabilities could enable precise stratification of cerebral hemodynamic status, guiding interventions to prevent stroke progression. The method's repeatability and lack of contrast agents further support its practicality in serial monitoring of TIA-related perfusion alterations (34, 35).

Despite meticulous participant selection and data scrutiny, certain limitations must be acknowledged. Firstly, this investigation was a retrospective study conducted at a single center, which might introduce selection bias. Further prospective research is warranted to elucidate the underlying pathophysiological mechanisms. Secondly, while the study cohort was relatively small, it encompassed a homogenous group of TIA patients who underwent dual PLD assessments. Future research should aim to replicate this investigation with a larger sample size. Thirdly, longitudinal studies are essential to ascertain the prognostic significance of FVH.

5 Conclusion

In conclusion, this study establishes that FVH signs exhibit a strong correlation with diminished cerebral blood flow and a

significantly impaired blood flow reserve, potentially reflecting the underlying pathomechanisms associated with stroke. The dual-PLD approach is a noninvasive and straightforward method for evaluating cerebral hemodynamics in TIA patients. We are optimistic that this methodology will evolve into a valuable instrument for prevention and early intervention in the future.

Data availability statement

The raw data supporting the conclusions of this article will be made available by the authors, without undue reservation.

Ethics statement

The studies involving humans were approved by the Ethics Committee of the Hospital of Chengdu University of Traditional Chinese Medicine. The studies were conducted in accordance with the local legislation and institutional requirements. The ethics committee/institutional review board waived the requirement of written informed consent for participation from the participants or the participants' legal guardians/next of kin due to the retrospective nature of the study.

Author contributions

LZ: Conceptualization, Data curation, Writing – original draft, Writing – review & editing. JW: Data curation, Writing – original draft. QW: Data curation, Writing – original draft. ZY: Data curation, Writing – original draft. HL: Data curation, Investigation, Methodology, Supervision, Writing – review & editing. WW: Conceptualization, Data curation, Investigation, Supervision, Writing – original draft, Writing – review & editing.

Funding

The author(s) declare that financial support was received for the research and/or publication of this article. This research was funded by the National Natural Science Foundation of China (No. 82174358) and the "Xing-lin Scholars" Project of Chengdu University of Traditional Chinese Medicine (No. CCYB2022004).

Conflict of interest

The authors declare that the research was conducted in the absence of any commercial or financial relationships that could be construed as a potential conflict of interest.

Generative AI statement

The authors declare that no Gen AI was used in the creation of this manuscript.

Publisher's note

References

1. Li Z, Li N, Qu Y, Gai F, Zhang G, Zhang G. Application of 3.0T magnetic resonance arterial spin labeling (ASL) technology in mild and moderate intracranial atherosclerotic stenosis. *Exp Ther Med*. (2016) 12:297–301. doi: 10.3892/etm.2016.3318

2. Khan F, Yogendrakumar V, Lun R, Ganesh A, Barber PA, Lioutas VA, et al. Long-term risk of stroke after transient ischemic attack or minor stroke: A systematic review and meta-analysis[J]. *JAMA*. (2025). doi: 10.1001/jama.2025.2033

3. Wolf M-E, Held V-E, Hennerici M-G. Risk scores for transient ischemic attack[J]. *Front Neurol Neurosci*. (2014) 3341–68. doi: 10.1159/000351891

4. Okada Y. Transient ischemic attack as a medical emergency. *Front Neurol Neurosci*. (2014) 33:19–29. doi: 10.1159/000351889

5. Lyu J, Hu J, Wang X, Bian X, Wei M, Wang L, et al. Association of fluid-attenuated inversion recovery vascular hyperintensity with ischaemic events in internal carotid artery or middle cerebral artery occlusion. *Stroke Vasc Neurol*. (2023) 8:69–76. doi: 10.1136/svn-2022-001589

6. Zeng L, Wang Q, Liao H, Ren F, Zhang Y, du J, et al. FLAIR vascular Hyperintensity: an important MRI marker in patients with transient ischemic attack. *Int J Gen Med*. (2022) 15:6165–71. doi: 10.2147/IJGM.S371894

7. Lv B, Ran Y, Lv J, Lou X, Tian C. Individualized interpretation for the clinical significance of fluid-attenuated inversion recovery vessel hyperintensity in ischemic stroke and transient ischemic attack: a systematic narrative review. *Eur J Radiol*. (2023) 166:111010. doi: 10.1016/j.ejrad.2023.111010

8. Legrand L, Le Berre A, Seners P, Benzakoun J, Hassen WB, Lion S, et al. FLAIR vascular Hyperintensities as a surrogate of collaterals in acute stroke: DWI matters. *AJNR Am J Neuroradiol*. (2023) 44:26–32. doi: 10.3174/ajnr.A7733

9. Lee KY, Kim JW, Park M, Suh SH, Ahn SJ. Interpretation of fluid-attenuated inversion recovery vascular hyperintensity in stroke. *J Neuroradiol*. (2021) 49:258–66. doi: 10.1016/j.neurad.2021.01.009

10. Souillard-Scemama R, Tisserand M, Calvet D, Jumadilova D, Lion S, Turc G, et al. An update on brain imaging in transient ischemic attack. *J Neuroradiol*. (2015) 42:3–11. doi: 10.1016/j.neurad.2014.11.001

11. Tung CE, Olivot JM, Albers GW. Radiological examinations of transient ischemic attack. *Front Neurol Neurosci*. (2014) 33:115–22. doi: 10.1159/000351913

12. Lv Y, Wei W, Song Y, Han Y, Zhou C, Zhou D, et al. Non-invasive evaluation of cerebral perfusion in patients with transient ischemic attack: an fMRI study. *J Neurol*. (2019) 266:157–64. doi: 10.1007/s00415-018-9113-3

13. Havsteen I, Willer L, Ovesen C, Nybing JD, Ægidius K, Marstrand J, et al. Significance of arterial spin labeling perfusion and susceptibility weighted imaging changes in patients with transient ischemic attack: a prospective cohort study. *BMC Med Imaging*. (2018) 18:24. doi: 10.1186/s12880-018-0264-6

14. Grams RW, Kidwell CS, Doshi AH, Drake K, Becker J, Coull BM, et al. Tissue-negative transient ischemic attack: is there a role for perfusion MRI? *AJR Am J Roentgenol*. (2016) 207:157–62. doi: 10.2214/AJR.15.15447

15. Hartkamp NS, van Osch MJ, Kappelle J, Bokkers RPH. Arterial spin labeling magnetic resonance perfusion imaging in cerebral ischemia. *Curr Opin Neurol*. (2014) 27:42–53. doi: 10.1097/WCO.0000000000000051

16. Lyu J, Duan Q, Xiao S, Meng Z, Wu X, Chen W, et al. Arterial spin labeling-based MRI estimation of penumbral tissue in acute ischemic stroke. *J Magn Reson Imaging*. (2023) 57:1241–7. doi: 10.1002/jmri.28364

17. Xu X, Tan Z, Fan M, Ma M, Fang W, Liang J, et al. Comparative study of multi-delay Pseudo-continuous arterial spin labeling perfusion MRI and CT perfusion in ischemic stroke disease. *Front Neuroinform*. (2021) 15:719719. doi: 10.3389/fninf.2021.719719

18. Xu H, Han H, Liu Y, Huo R, Lang N, Yuan H, et al. Perioperative cerebral blood flow measured by arterial spin labeling with different postlabeling delay in patients undergoing carotid endarterectomy: a comparison study with CT perfusion. *Front Neurosci*. (2023) 17:1200273. doi: 10.3389/fnins.2023.1200273

19. Akiyama T, Morioka T, Shimogawa T, Haga S, Sayama T, Kanazawa Y, et al. Arterial spin-labeling magnetic resonance perfusion imaging with dual Postlabeling delay in internal carotid artery Steno-occlusion: validation with digital subtraction angiography. *J Stroke Cerebrovasc Dis*. (2016) 25:2099–108. doi: 10.1016/j.jstrokecerebrovasdis.2016.06.005

20. Golay X, Ho ML. Multidelay ASL of the pediatric brain. *Br J Radiol*. (2022) 95:20220034. doi: 10.1259/bjr.20220034

21. Woods JG, Achten E, Asllani I, Bolar DS, Dai W, Detre JA, et al. Recommendations for quantitative cerebral perfusion MRI using multi-timepoint arterial spin labeling: acquisition, quantification, and clinical applications. *Magn Reson Med*. (2024) 92:469–95. doi: 10.1002/mrm.30091

22. Jaafar N, Alsop DC. Arterial spin labeling: key concepts and Progress towards use as a clinical tool. *Magn Reson Med Sci*. (2024) 23:352–66. doi: 10.2463/mrms.rev.2024-0013

23. Yoshioka K, Ishibashi S, Shiraishi A, Yokota T, Mizusawa H. Distal hyperintense vessels on FLAIR images predict large-artery stenosis in patients with transient ischemic attack. *Neuroradiology*. (2013) 55:165–9. doi: 10.1007/s00234-012-1092-y

24. Maeda M, Koshimoto Y, Uematsu H, Yamada H, Kimura H, Kawamura Y, et al. Time course of arterial hyperintensity with fast fluid-attenuated inversion-recovery imaging in acute and subacute middle cerebral arterial infarction. *J Magn Reson Imaging*. (2001) 13:987–90. doi: 10.1002/jmri.1142

25. Ding B, Chen Y, Jiang H, Zhang H, Huang J, Ling HW. Fluid-attenuated inversion recovery vascular Hyperintensities in transient ischemic attack within the anterior circulation. *Biomed Res Int*. (2020) 2020:7056056. doi: 10.1155/2020/7056056

26. Bunker LD, Hillis AE. Location of Hyperintense vessels on FLAIR associated with the location of perfusion deficits in PWI. *J Clin Med*. (2023) 12:1554. doi: 10.3390/jcm12041554

27. Nam KW, Kim CK, Kim TJ, Oh K, Han MK, Ko SB, et al. FLAIR vascular hyperintensities predict early ischemic recurrence in TIA. *Neurology*. (2018) 90:e738–44. doi: 10.1212/WNL.0000000000005034

28. Liang Y, Jiang Y, Liu J, Li X, Cheng X, Bao L, et al. Blood-brain barrier disruption and imaging assessment in stroke. *Transl Stroke Res*. (2024). doi: 10.1007/s12975-024-01300-6

29. Montagne A, Barnes SR, Sweeney MD, Halliday MR, Sagare AP, Zhao Z, et al. Blood-brain barrier breakdown in the aging human hippocampus. *Neuron*. (2015) 85:296–302. doi: 10.1016/j.neuron.2014.12.032

30. Uchida Y, Kan H, Kano Y, Onda K, Sakurai K, Takada K, et al. Longitudinal changes in Iron and myelination within ischemic lesions associate with neurological outcomes: a pilot study. *Stroke*. (2024) 55:1041–50. doi: 10.1161/STROKEAHA.123.044606

31. Zaidat OO, Yoo AJ, Khatri P, Tomsick TA, von Kummer R, Saver JL, et al. Recommendations on angiographic revascularization grading standards for acute ischemic stroke: a consensus statement. *Stroke*. (2013) 44:2650–63. doi: 10.1161/STROKEAHA.113.001972

32. Bivard A, Stanwell P, Levi C, Parsons M. Arterial spin labeling identifies tissue salvage and good clinical recovery after acute ischemic stroke. *J Neuroimaging*. (2013) 23:391–6. doi: 10.1111/j.1552-6569.2012.00728.x

33. He Q, Li G, Jiang M, Zhou Q, Gao Y, Yan J. Predicting a favorable (mRS 0-2) or unfavorable (mRS 3-6) stroke outcome by arterial spin labeling and amide proton transfer imaging in post-thrombolysis stroke patients. *J Pers Med*. (2023) 13:248. doi: 10.3390/jpm13020248

34. Zhang GR, Zhang YY, Liang WB, Ding D. Cerebral perfusion in patients with unilateral internal carotid artery occlusion by dual post-labeling delays arterial spin labeling imaging. *World J Radiol*. (2024) 16:429–38. doi: 10.4329/wjr.v16.i9.429

35. Haga S, Morioka T, Shimogawa T, Akiyama T, Murao K, Kanazawa Y, et al. Arterial spin labeling perfusion magnetic resonance image with dual Postlabeling delay: a correlative study with acetazolamide loading (123)I-Iodoamphetamine single-photon emission computed tomography. *J Stroke Cerebrovasc Dis*. (2016) 25:1–6. doi: 10.1016/j.jstrokecerebrovasdis.2015.08.025

36. Takahara K, Morioka T, Shimogawa T, Haga S, Kameda K, Arihiro S, et al. Hemodynamic state of periictal hyperperfusion revealed by arterial spin-labeling perfusion MR images with dual postlabeling delay. *eNeurologicalSci*. (2018) 12:5–18. doi: 10.1016/j.ensci.2018.06.001

frontiers | Frontiers in Aging Neuroscience

TYPE Original Research
PUBLISHED 13 June 2025
DOI 10.3389/fnagi.2025.1486381

OPEN ACCESS

EDITED BY
Jianming Cai,
People's Liberation Army General Hospital, China

REVIEWED BY
Ruth Stephen,
University of Eastern Finland, Finland
Mingming Lu,
Characteristic Medical Center of Chinese People's Armed Police Force, China

*CORRESPONDENCE
Yuchun Yuan
✉ yycyhy1008@163.com

RECEIVED 11 September 2024
ACCEPTED 28 May 2025
PUBLISHED 13 June 2025

CITATION
Yu T, Bai Q, Guo Y and Yuan Y (2025) Investigation of gray matter volume in individuals with heart failure and preserved ejection fraction.
Front. Aging Neurosci. 17:1486381.
doi: 10.3389/fnagi.2025.1486381

Investigation of gray matter volume in individuals with heart failure and preserved ejection fraction

Tianyi Yu[1], Qiuyun Bai[2], Yiting Guo[2] and Yuchun Yuan[2]*

[1]Department of Radiology, Shandong Provincial Hospital Affiliated to Shandong First Medical University, Jinan, China, [2]Department of Radiology, The Second Affiliated Hospital of Shandong University of Traditional Chinese Medicine, Jinan, China

Object: This study employs voxel-based morphometry techniques to identify potential areas of brain injury in patients with heart failure with preserved ejection fraction (HFpEF). It further assesses the correlation between clinical indicators, cardiac function parameters, and gray matter volume (GMV). This provides an imaging-based anatomical biomarker for in-depth research into the brain structure in patients with HFpEF.

Materials and methods: This study recruited 51 patients with HFpEF (26 males and 25 females) and 40 healthy controls (27 males and 13 females). Data on NT-proBNP levels, echocardiographic parameters, and cognitive function scores were collected for both groups. High-resolution 3D T1-weighted imaging (3D-T1WI) structural MRI data were collected from all participants. The changes in GMV between the two groups were assessed using voxel-based morphometry (VBM).

Results: The study involved 40 patients with HFpEF and 28 healthy controls (HC). No significant differences were observed between the groups regarding age, gender, education, or BMI. The HFpEF group exhibited larger measurements for Left Ventricular Posterior Wall (LVPW), Interventricular Septal Thickness (IVST), Left Atrial Diameter (LAD), Right Atrial Diameter (RAD), and Right Ventricular Diameter (RVD). However, they maintained preserved systolic function and achieved lower scores on the MoCA, indicating deficits in visuospatial/executive functions, naming, attention, language, and memory. Compared to HC, HFpEF patients had reduced GMV in specific brain regions. NT-proBNP levels were negatively correlated with GM reduction in various cerebellar, frontal, temporal, and postcentral regions. Cognitive performance was inversely related to GM shrinkage, with different brain regions correlating with specific cognitive deficits.

Conclusion: Abnormalities in GMV in several brain areas have been identified in patients with HFpEF. Furthermore, these abnormal GMV are associated with NT-proBNP levels, echocardiographic indices, and neurocognitive scoring. These observations could provide fresh perspectives on the pathogenic mechanisms of HFpEF.

KEYWORDS

heart failure with preserved ejection fraction, gray matter volume, MRI, VBM, cognitive function

1 Introduction

Heart failure (HF) comprises a range of syndromes marked by various structural or functional cardiac disorders. These impairments lead to difficulties in ventricular filling and/or ejection, causing cardiac output to be inadequate for meeting the metabolic needs of body tissues. Consequently, this results in insufficient blood flow to the lungs and other organs and tissues (Hanon et al., 2014). The 2016 European Society of Cardiology guidelines for heart failure stratify the condition into three categories based on Left Ventricular Ejection Fraction (LVEF): HFrEF is defined as LVEF < 40%, while Heart Failure with Mid-Range Ejection Fraction (HFmrEF) applies to LVEF between 40 and 49%. Heart Failure with Preserved Ejection Fraction (HFpEF) is characterized by an LVEF of 50% or greater (Savarese et al., 2022). HFpEF, in particular, is a complex and phenotypically diverse syndrome featured by ventricular diastolic dysfunction coupled with high end-diastolic pressure, while maintaining a normal or near-normal LVEF, thus is also known as Diastolic Heart Failure (DHF) (Eltelbany et al., 2022). Previous studies have reported cognitive impairment (CI) in patients with HF, particularly affecting processing speed, verbal memory, and executive function (Cui et al., 2020). Brain injury may be the main contributor to these clinical symptoms, and changes in the brain's gray matter (GM) structure have been reported in HF patients (Steinberg et al., 2012). The centers for cognitive and executive functions are concentrated in the cortical structures of the brain (Zhou et al., 2021), which are highly sensitive to hypoxia, with irreversible damage occurring if oxygen deprivation exceeds 4–5 min. Therefore, recognizing the changes in the anatomical structure of the brain's GM is crucial for understanding the cognitive dysfunction associated with HFpEF.

Since 2000, voxel-based morphometry (VBM) has been increasingly applied in the study of neuropsychiatric disorders (Whitwell, 2009). VBM is an automated, voxel-wise method for analyzing neuroanatomy, utilizing statistical techniques to process high-resolution three-dimensional magnetic resonance imaging (MRI) data. This approach enables precise detection and quantification of local gray and white matter density and volume. A key advantage of VBM is its capacity to identify subtle structural changes in the brain without requiring predefined regions of interest, thus minimizing operator bias. This high sensitivity makes VBM particularly effective for detecting diseases associated with neuropsychological dysfunction before any macroscopic structural changes occur (Good et al., 2001; Ridgway et al., 2008).

This study employs voxel-based morphometry to identify potential brain injury regions in HFpEF and to assess the associations between clinical indicators, cardiac functional parameters, and gray matter volume (GMV), thereby providing an anatomical biomarker via imaging for further investigation into the cerebral function of HFpEF.

2 Method

The experimental subjects included a total of 51 subjects in the HFpEF group (26 males and 25 females), and 40 members in the HC group (27 males and 13 females). Patients enrolled in this study met the diagnostic criteria for HFpEF, exhibiting typical signs and symptoms of heart failure, with BNP ≥ 35 pg./mL or NT-proBNP > 125 ng/L. Echocardiographic examination demonstrated structural cardiac abnormalities and/or impaired diastolic or systolic function, with LVEF ≥ 50%. Eligible participants were right-handed individuals aged between 45 and 80 years who provided written informed consent and were willing to cooperate with the study procedures.

Exclusion criteria included acute exacerbation of heart failure within the past 2 months, unstable cardiovascular or cerebrovascular diseases, dementia, uncontrolled hypertension, psychiatric disorders, a history of traumatic brain injury or brain tumor, obstructive sleep apnea, severe metabolic diseases (such as hepatic or renal failure, or decompensated diabetes mellitus), alcohol or substance dependence, illiteracy, and epilepsy. These exclusion criteria were also applied to the healthy control (HC) group.

2.1 Clinical data

All patients fasted overnight for at least 8 h before venous blood samples were collected the following day for analysis. The tests included serum hypersensitive C-reactive protein (hs-CRP), fasting plasma glucose (FPG), triglycerides (TG), total cholesterol (TC), and N-terminal pro-brain natriuretic peptide (NT-proBNP). All aforementioned laboratory tests were carried out by the Department of Laboratory Medicine at the Affiliated Provincial Hospital of Shandong First Medical University.

All patients underwent echocardiographic examinations at the Echocardiography Laboratory of the Affiliated Provincial Hospital of Shandong First Medical University, where the following data were collected and recorded: LVEF, left ventricular end-diastolic diameter (LVDD), left atrial diameter (LAD), interventricular septal thickness (IVST), left ventricular posterior wall thickness (LVPWT), right atrial transverse diameter (RAD), and right ventricular anteroposterior diameter (RVD).

2.2 Neuropsychological examinations

The participants in the study were evaluated for their cognitive status using the Montreal Cognitive Assessment (MoCA) scales (Nasreddine et al., 2005). The MoCA scale evaluates a range of cognitive functions, including visuospatial and executive abilities, naming skills, attention, language proficiency, abstraction, memory recall, and orientation. These assessments were conducted following standardized procedures in a quiet environment. The maximum score for both scales is 30 points. Scores below 26 on the MoCA indicate poor cognitive function.

2.3 Magnetic resonance imaging protocol

Whole-brain images were obtained at the Shandong Provincial Hospital Affiliated to Shandong First Medical University using a Siemens 3.0 T Prisma MR system and a 64-channel head coil for brain scanning. Participants were carefully positioned inside the machine, and foam padding was used to minimize any movement during the scanning process.

T1-weighted whole-brain magnetization prepared rapid acquisition gradient echo imaging were collected to capture anatomical details using the following parameters: TR = 2,530 ms,

TE = 2.98 ms, TI = 1,100 ms, FOV = 256 × 256 mm^2, in-plane resolution = 256 × 256 mm^2, flip angle = 7°, and 192 axial slices.

All MRI images were reviewed by two senior neuroimaging diagnosticians.

2.4 Data preprocessing

The preprocessing of all 3D-T1WI structural image data was performed using the CAT12 software within the SPM12 (based on the Matlab 7.10 platform). The main process is as follows: First, MRI data were converted from DICOM format to NIFTI format using the MRIcron software. The 3D T1-weighted structural images of the entire brain were then bias-corrected and segmented in GM, white matter, and cerebrospinal fluid. Subsequently, the GM images were affine registered to the standard brain template of the Montreal Neurological Institute (MNI) and a study-specific template was created for this tissue utilizing the Diffeomorphic Anatomical Registration Through Exponentiated Lie (DARTEL) algorithm. The original GM images were then spatially registered to the newly generated template and further normalized to the MNI space (with isotropic voxels of 1.5 mm). The resulting GM images were modulated using the Jacobian determinants to account for volume changes. Finally, the modulated GM images were smoothed with an isotropic Gaussian kernel that had a full width at half maximum of 8 mm.

2.5 Statistical analysis

Data analysis was carried out using SPSS 22.0 statistical software. Quantitative data were expressed as mean ± standard deviation ($\bar{x} \pm s$). The two-sample t-test was used to evaluate differences between the two groups in terms of age, education level, BMI, MoCA scores, and clinical indicators. Gender differences were assessed using the chi-square test. GMV between the two groups was compared using two-sample t-tests with SPM8 statistical software, including each subject's gender, age, education level, and BMI as covariates. Clusters were set to a minimum size of 200 voxels, and statistical results were corrected using the Gaussian Random Field Theory (GRF), with a significance level of $p < 0.05$ indicating regions of GM with significant differences. The relationship between VBM values and MoCA scores, cardiac function, and laboratory tests were examined using Pearson correlation analysis, with $p < 0.05$ considered statistically significant.

3 Results

In this study, a total of 51 patients with HFpEF participated. However, 11 individuals were excluded for the following reasons: 3 voluntarily withdrew from the study, 2 were excluded due to severe image artifacts caused by head movement, 3 had multiple lacunar strokes, 2 suffered from claustrophobia, and 1 had an arachnoid cyst. Consequently, 40 patients were included in the data analysis. As for the HC, 40 individuals initially participated, but exclusions were made as follows: 3 voluntarily withdrew, 2 were found to have mild cognitive impairment (MCI), 4 were excluded due to head movement artifacts, and 3 had multiple lacunar strokes, leaving 28 participants included in the study.

3.1 Comparison of clinical data between HFpEF group and HC group

There were no statistically significant differences in age, gender, education level, and BMI between the HFpEF group and the HC group ($p > 0.05$). The HFpEF group exhibited significantly higher values of LVPW, IVST, LAD, and RAD compared to the HC group, with no notable impairment in systolic function observed. The MoCA scores of the HFpEF group were significantly lower than those of the HC group, revealing CI primarily in the areas of visuospatial and executive functions, naming, attention, language, and memory ($p < 0.05$). In contrast, no statistical significance was found in abstract thinking and orientation ($p > 0.05$) (Table 1).

3.2 Comparison of gray matter volume between HFpEF group and HC group

In the HFpEF group, regions of decreased GMV were observed in the bilateral cerebellar hemispheres, right posterior cingulate gyrus, right inferior frontal gyrus, right supplementary motor area, bilateral

TABLE 1 Comparison of demographic data between HFpEF group and HC group.

Variable	HF	HC	*P*
	40	28	
Age (years), mean (SD)	60.20 ± 7.91	60.42 ± 7.99	0.90
Male sex, No. (%)	24 (60%)	17 (61%)	0.95
Education, years	10.75 ± 4.36	9.85 ± 3.21	0.36
BMI (Kg/m^2)	25.93 ± 2.85	25.05 ± 1.22	0.13
Smokers (*n*%)	14 (35%)	11 (39%)	0.72
Drinkers (*n*%)	15 (38%)	12 (43%)	0.66
Hypertension (*n*%)	23 (58%)	15 (54%)	0.75
Dyslipidemia (*n*%)	11 (27.5%)	9 (32%)	0.68
Diabetes mellitus (*n*%)	6 (15%)	7 (25%)	0.30
MOCA Score	22.95 ± 3.54	27.32 ± 2.69	0
NT-proBNP (pg/mL)	283.33 ± 241.04	78.69 ± 130.84	0.0001
CRP	2.03 ± 2.31	3.42 ± 8.13	0.38
Glucose	5.09 ± 1.32	5.22 ± 0.83	0.61
Total cholesterol	4.34 ± 0.95	4.59 ± 0.92	0.28
Triglyceride	1.36 ± 0.44	1.74 ± 0.92	0.05
LVEF	59.9 ± 2.91	61.75 ± 1.81	0.0041
LVDD	4.90 ± 0.45	4.67 ± 0.43	0.03
LVPW	0.98 ± 0.10	0.86 ± 0.14	0.0002
IVST	0.99 ± 0.11	0.88 ± 0.15	0.0016
LAD	4.08 ± 0.54	3.24 ± 0.42	0
RAD	4.21 ± 0.57	3.49 ± 0.56	0
RVD	2.08 ± 0.23	2.27 ± 0.45	0.04

middle frontal gyri, right middle temporal gyrus, right superior frontal gyrus, left calcarine fissure and adjacent cortex, left inferior frontal gyrus, left superior frontal gyrus, and left postcentral gyrus (Figure 1, Table 2).

3.3 Correlation analysis

In this study, NT-proBNP levels were negatively correlated with decreased GMV in several brain regions, including the right and left cerebellar hemispheres, right posterior cingulate gyrus, right inferior frontal gyrus, right supplementary motor area, right and left middle frontal gyri, right superior frontal gyrus, left superior frontal gyrus, left postcentral gyrus, and right middle temporal gyrus. These findings suggest that reductions in GMV in these regions are associated with cognitive dysfunction in HFpEF patients.

The shrinkage of GM in the right cerebellar hemisphere was negatively correlated with performance in naming, attention, and language tasks. A similar reduction in the left cerebellar hemisphere was negatively associated with attention, language, and memory scores. Decreased GM in the right posterior cingulate gyrus was negatively correlated with naming and language scores, while the right inferior frontal gyrus showed a negative correlation with naming, language, and memory scores. The shrinkage of the right supplementary motor area was negatively related to language performance.

Additionally, reductions in GMV in the right superior frontal gyrus were negatively correlated with memory scores. The volume reduction in the left inferior frontal gyrus was associated with attention and language scores, and the reduction in the left middle frontal gyrus was negatively correlated with naming and language scores. The left superior frontal gyrus volume reduction was negatively associated with attention and language scores, while the left

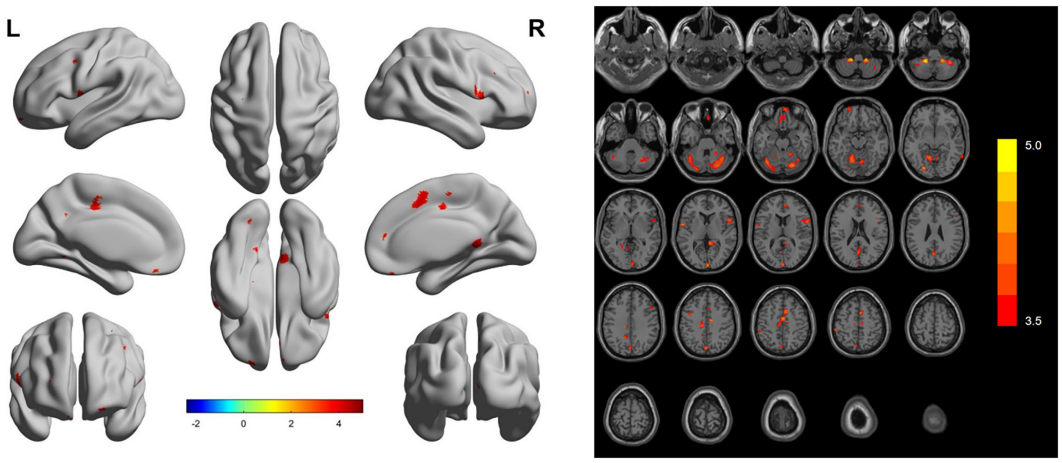

FIGURE 1
Differences in gray matter volume between the HFpEF group and the HC group. The two images represent the differences of gray matter volume between HFpEF group and HC group (The red area represents the area where the gray matter volume increases).

TABLE 2 Comparative analysis of gray matter volume between HFpEF group and HC group.

Regions	Hemi	AAL	MNI coordinates	Volume (mm^3)	*T*
Cerebellar hemisphere	R	100	18, −39, −49.5	10202.6	4.6576
Cerebellar hemisphere	L	91	−24, −81 −4.5	5666.62	4.6243
Posterior cingulate gyrus	R	36	7.5, −42, 7.5	4363.88	4.1102
Inferior frontal gyrus	R	12	55.5, 12, 3	2561.62	4.0094
Supplementary motor area	R	20	6, 7.5, 52.5	1778.62	4.3156
Calcarine fissure and surrounding cortex	L	43	1.5, −96, 9	1768.5	4.4721
Superior frontal gyrus, medial orbital	R	26	11, 61, −21	1549.12	3.6469
Inferior frontal gyrus, opercular part	L	11	−58.5, 1.5, 7.5	955.125	4.2078
Middle frontal gyrus	L	7	−22.5, 58.5, −13.5	590.625	3.5885
Superior frontal gyrus, medial	L	23	3, 46.5, 16.5	573.75	3.7497
Postcentral gyrus	L	57	−54, −33, 54	486	4.3503
Middle frontal gyrus	R	8	48, 22.5, 31.5	438.75	3.8014
Middle temporal gyrus	R	86	67.5, −55.5, −6	384.75	3.7726

postcentral gyrus showed a negative correlation with attention and language scores. Finally, the reduction in the right middle temporal gyrus was negatively correlated with naming scores.

Figures 2, 3 illustrate these significant negative correlations between GMV reductions and cognitive function scores across the different brain regions.

4 Discussion

This study utilized VBM technology to assess alterations in GM structure within HFpEF patients. Compared to the HC group, HFpEF individuals displayed reduced GMV in several areas, including the bilateral cerebellar hemispheres, right posterior cingulate gyrus, right inferior frontal gyrus, right supplementary motor area, bilateral middle frontal gyri, right middle temporal gyrus, right superior frontal gyrus, left calcarine fissure and adjacent cortex, left inferior frontal gyrus, left superior frontal gyrus, and left postcentral gyrus. The HFpEF group scored significantly lower on the MoCA, particularly in the domains of visuospatial and executive functions, naming, attention, language, and memory. Reductions in GMV in the right cerebellar hemisphere, right inferior frontal gyrus, right supplementary motor area, cortex surrounding the left calcarine fissure, right medial orbitofrontal gyrus, left superior frontal gyrus,

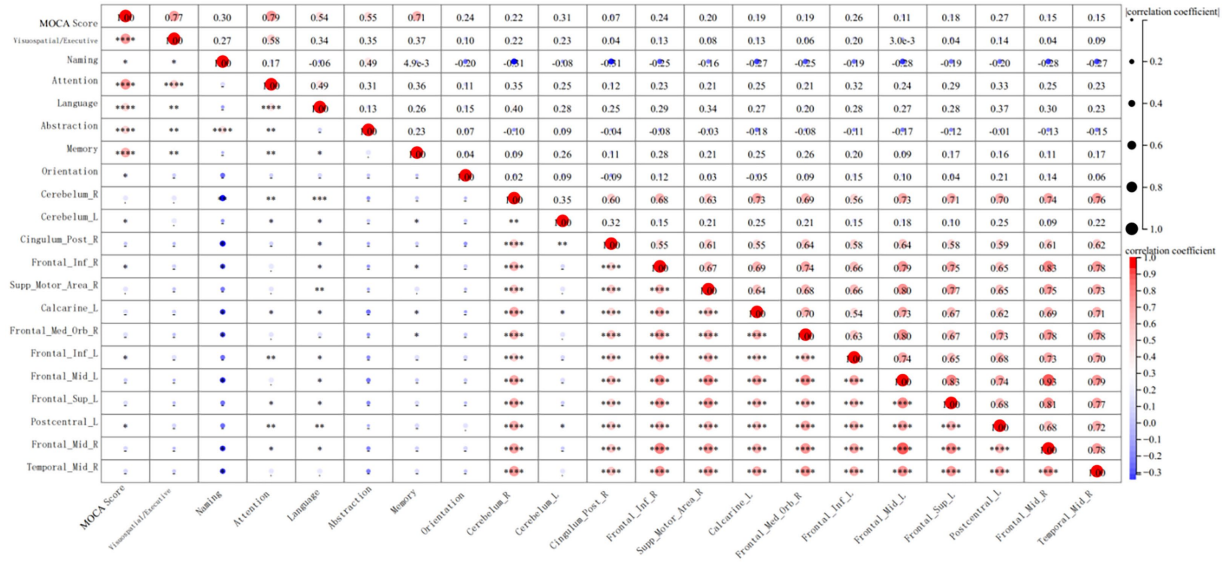

FIGURE 2
Correlation analysis between gray matter volume and cognitive function in HFpEF group.

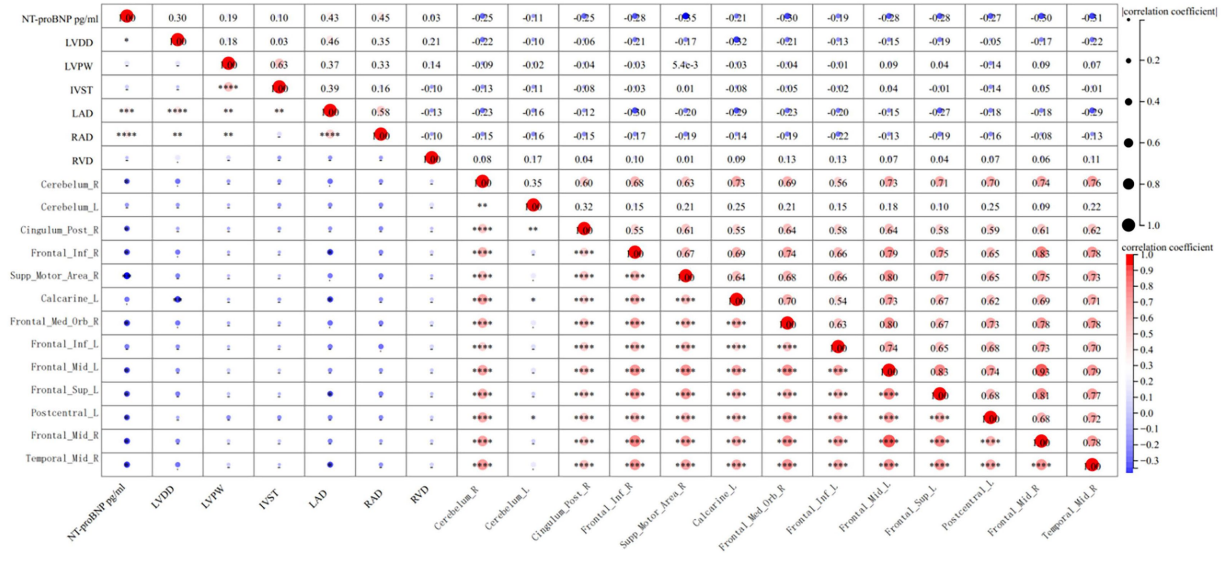

FIGURE 3
Correlation analysis between gray matter volume and clinical indexes in HFpEF group.

and right middle temporal gyrus were associated with abnormalities in cardiac and cognitive functions.

The findings of this study are not completely consistent with previous reports on changes in GMV in patients with heart failure. However, the study confirms the presence of neuronal damage in HFpEF patients and further reveals the brain regions affected by the impaired GM structures. These brain areas play an important role in key cognitive domains such as executive functions, memory, and naming. The decreased GMV in the right and left cerebellar hemispheres may affect motor control and balance regulation. The cerebellum is a key structure for coordinating movement and maintaining postural balance, and its dysfunction could lead to motor incoordination and balance disorders, which in turn affect the executive aspects of cognitive function (Houghton et al., 2021). The frontal lobe is a crucial brain area for central functions like movement, memory, language, impulse control, and social behavior (Arain et al., 2013). Damage to or functional abnormalities in the right supplementary motor area may affect patients' motor planning and execution abilities, leading to issues such as motor incoordination and difficulty with movement pre-setting (Ding et al., 2023). These motor-related problems may be closely related to common symptoms in heart failure patients, such as fatigue and decreased exercise endurance. Damage to or functional abnormalities in the cortex surrounding the left calcarine fissure may affect patients' language abilities and motor control (Chu et al., 2023). This could lead to issues such as impaired speech fluency, difficulty with speech comprehension, and inflexibility in hand movements, affecting patients' daily life and social interactions. The parietal and occipital cortices are also involved in cognitive and behavioral functions; the parietal cortex has the function of understanding, encoding, consolidating, and retrieving written language and manipulating working memory (Koenigs et al., 2009). The occipital lobe is involved in memory, visuo-constructional skills, calculation, and task execution (Brownsett and Wise, 2010). Meanwhile, hippocampal structures within the temporal lobe are involved in memory function (Csernansky et al., 2005). Therefore, cortical damage in these areas may result in functional changes, manifesting as abnormalities in cognitive behavior.

The decrease in brain GMV in HFpEF patients is generally caused by loss of neuronal cells or neuronal damage (Ahad et al., 2020). Reduced GMV in the brain indicates atrophy of brain tissue and damage at the vascular or cellular level, including neurodegenerative changes (Wang et al., 2017). Initially, HF patients' brain structures may show no global atrophy, with only the integrity of white matter fiber structures being impaired (Vogels et al., 2007). Current research on localized GMV reduction is not sufficiently in-depth, and many study results are inconsistent (Frey et al., 2021). Some scholars have found (Ogoh et al., 2022) structural abnormalities in areas such as the frontal lobe and cerebellum in heart failure patients, suggesting that atrophy in these brain regions may play an important role in the CI of chronic heart failure patients. International studies using conventional MRI techniques, such as those by Kumar et al. (2009), have quantitatively measured the brain regions' volumes, including the frontal lobe, hippocampus, and mammillary bodies, in heart failure patients, revealing significant brain atrophy in the mentioned areas. Although the results are not entirely consistent, they at least all suggest that chronic heart failure can lead to atrophy of the brain's GM structure in patients. In experimental work exploring the pathogenesis of cognitive dysfunction, it is widely considered that differences in brain areas such as the frontal lobe, temporal lobe, caudate nucleus, and cerebellum play an important role. These differences may be attributed to the heterogeneity of the study populations, MRI acquisition techniques, voxel-based morphological analysis methods, as well as differences in statistical analysis and processing procedures.

Increasing evidence suggests that brain atrophy is not solely attributable to neurodegenerative mechanisms but is also closely associated with cerebrovascular factors (Ye et al., 2022). Chronic cerebral hypoperfusion, impaired cerebral autoregulation, and endothelial dysfunction are commonly observed in HF patients, potentially leading to both gray and white matter damage, thus providing a vascular basis for neuronal injury (Ni et al., 2023). Notably, periventricular and deep white matter hyperintensities (WMHs) are imaging manifestations of small vessel disease and are often assessed using the Fazekas scale. These lesions have been consistently linked to cognitive decline in multiple studies (Prins and Scheltens, 2015; Zhang et al., 2023). WMHs represent chronic ischemic damage, which may disrupt cortical–subcortical circuits, consequently affecting executive functions and memory—domains frequently impaired in HFpEF-related cognitive dysfunction. Although this study focuses on GMV changes, future research incorporating WMHs assessment could offer a more comprehensive understanding of the brain structural changes associated with HFpEF.

The reduction in brain GMV may stem from hypoxia-induced neuroinflammation and neuroglial cell damage, indicating an immune response in the affected GM areas (Brooks and Mias, 2019). Imaging technologies are key tools in identifying brain injury related to HFpEF, including advanced functional MRI techniques such as diffusion tensor imaging and magnetic resonance spectroscopy, which provide important information about local anatomical structure and neurochemical environmental changes for clinical use (Spilling et al., 2017). Pathological examination is considered the gold standard for diagnosing abnormalities in brain GMV, but due to the invasiveness of brain tissue biopsy and the potential damage to local GM function, it is not suitable for use in clinical trials (Lancaster et al., 2013). Moreover, the reduction in brain GMV also reflects structural changes in the local GM due to the long-term impact of disease. Brain function abnormalities in patients with HFpEF may lead to MCI, a condition that may remain undetected for many years. Therefore, assessing the duration of cognitive dysfunction or the affected time span of neuropsychological performance in HFpEF patients is crucial for understanding their brain structural changes. For example, although numerous studies have indicated hippocampal atrophy in patients with heart failure, this study did not find significant abnormal changes in hippocampal volume. Whether these subtle changes in GM nuclei affect cortical brain function remains unclear, hence, it is necessary to combine structural and functional analysis to further investigate changes in these brain regions.

The reduction in GMV in HFpEF patients may also result from common systemic factors that contribute to the aging of both the heart and brain. These include hypertension, diabetes, atrial fibrillation, and endothelial dysfunction. These shared pathologies may impair the integrity of both myocardial and cerebral vasculature, leading to compromised perfusion and tissue damage (Ye et al., 2022). Preventive strategies targeting vascular health, such as strict blood pressure control, physical activity, blood glucose management, and anti-inflammatory

interventions, may help protect the structure and function of both the heart and brain (Liori et al., 2022; Mene-Afejuku et al., 2019). Therefore, cardiovascular-neurological integrated treatment could be crucial in delaying or preventing cognitive decline in HFpEF patients.

This study identified a negative correlation between NT-proBNP levels and volume reductions in various brain regions, such as the right cerebellar hemisphere, right posterior cingulate gyrus, right inferior frontal gyrus, right supplementary motor area, right superior frontal gyrus, left middle frontal gyrus, left superior frontal gyrus, left postcentral gyrus, right middle frontal gyrus, and right middle temporal gyrus. This negative correlation may reflect the impact of heart failure on these brain areas. Notably, these regions play an important role in functions such as movement and cognition; thus, NT-proBNP levels may serve as a biomarker for brain structural changes in patients with HFpEF. These findings further emphasize that heart failure not only affects cardiac function but may also have a negative impact on brain structure and function. Future research could further explore the mechanistic links between NT-proBNP and brain structural changes, as well as how this relationship affects the clinical presentations and prognosis of patients with heart failure.

4.1 Limitation

Our study does have certain limitations that should be acknowledged. The primary limitation lies in the small sample size, which could limit the generalizability of our findings and diminish the statistical power of our analysis. Additionally, the recruitment of study participants from a singular medical institution may introduce recruitment bias and may not accurately reflect the broader HF population. Therefore, further studies with larger and more diverse samples are needed to validate our results. Additionally, in terms of neuropsychological examination, we only utilized the MoCA scales to assess the cognitive function of the subjects. While these scales provide valuable insights, they may not comprehensively evaluate all aspects of cognitive decline. In future studies, it will be important to include a broader range of cognitive assessment tools to obtain a more precise understanding of the degree of decline in various cognitive functions. Furthermore, we did not compare brain MRI differences between HFpEF and HFrEF patients. Including such a comparison in future studies would help highlight the specific structural changes in HFpEF and enhance the novelty of the findings.

5 Conclusion

In conclusion, compared to the healthy control group, the HFpEF patient group showed cognitive decline and abnormal changes in gray matter volume in specific brain regions. These changes were closely linked to laboratory results, cardiac function, and cognitive dysfunction, indicating brain structure damage due to neuronal injury. Localized gray matter changes may result from hypoxia-related inflammation. Future research should explore the effects of interventions on these findings. Understanding these anatomical abnormalities is crucial for improving clinical interventions, prognosis, and therapeutic strategies.

Data availability statement

The raw data supporting the conclusions of this article will be made available by the authors, without undue reservation.

Ethics statement

The studies involving humans were approved by Ethics Committee of Provincial Hospital Affiliated to Shandong First Medical University. The studies were conducted in accordance with the local legislation and institutional requirements. The participants provided their written informed consent to participate in this study.

Author contributions

TY: Writing – original draft, Writing – review & editing. QB: Writing – original draft. YG: Conceptualization, Writing – original draft. YY: Writing – review & editing.

Funding

The author(s) declare that no financial support was received for the research and/or publication of this article.

Conflict of interest

The authors declare that the research was conducted in the absence of any commercial or financial relationships that could be construed as a potential conflict of interest.

Publisher's note

References

Ahad, M. A., Kumaran, K. R., Ning, T., Mansor, N. I., Effendy, M. A., Damodaran, T., et al. (2020). Insights into the neuropathology of cerebral ischemia and its mechanisms. *Rev. Neurosci.* 31, 521–538. doi: 10.1515/revneuro-2019-0099

Arain, M., Haque, M., Johal, L., Mathur, P., Nel, W., Rais, A., et al. (2013). Maturation of the adolescent brain. *Neuropsychiatr. Dis. Treat.* 9, 449–461. doi: 10.2147/NDT.S39776

Brooks, L. R. K., and Mias, G. I. (2019). Data-driven analysis of age, sex, and tissue effects on gene expression variability in Alzheimer's disease. *Front. Neurosci.* 13:392. doi: 10.3389/fnins.2019.00392

Brownsett, S. L. E., and Wise, R. J. S. (2010). The contribution of the parietal lobes to speaking and writing. *Cereb. Cortex* 20, 517–523. doi: 10.1093/cercor/bhp120

Chu, Q., Guo, X., Zhang, T., Huo, C., Zhang, X., Xu, G., et al. (2023). Stroke-related alterations in the brain's functional connectivity response associated with upper limb multi-joint linkage movement. *Brain Sci.* 13:338. doi: 10.3390/brainsci13020338

Csernansky, J. G., Wang, L., Swank, J., Miller, J. P., Gado, M., McKeel, D., et al. (2005). Preclinical detection of Alzheimer's disease: hippocampal shape and volume predict dementia onset in the elderly. *Neuroimage* 25, 783–792. doi: 10.1016/j.neuroimage.2004.12.036

Cui, X., Thunström, E., Dahlström, U., Zhou, J., Ge, J., and Fu, M. (2020). Trends in cause-specific readmissions in heart failure with preserved vs. reduced and mid-range ejection fraction. *ESC Heart Fail.* 7, 2894–2903. doi: 10.1002/ehf2.12899

Ding, H., Seusing, N., Nasseroleslami, B., Anwar, A. R., Strauss, S., Lotze, M., et al. (2023). The role of ipsilateral motor network in upper limb movement. *Front. Physiol.* 14:1199338. doi: 10.3389/fphys.2023.1199338

Eltelbany, M., Shah, P., and deFilippi, C. (2022). Biomarkers in HFpEF for diagnosis, prognosis, and biological phenotyping. *Curr. Heart Fail. Rep.* 19, 412–424. doi: 10.1007/s11897-022-00578-7

Frey, A., Homola, G. A., Henneges, C., Mühlbauer, L., Sell, R., Kraft, P., et al. (2021). Temporal changes in total and hippocampal brain volume and cognitive function in patients with chronic heart failure-the COGNITION.MATTERS-HF cohort study. *Eur. Heart J.* 42, 1569–1578. doi: 10.1093/eurheartj/ehab003

Good, C. D., Johnsrude, I. S., Ashburner, J., Henson, R. N., Friston, K. J., and Frackowiak, R. S. (2001). A voxel-based morphometric study of ageing in 465 normal adult human brains. *Neuroimage* 14, 21–36. doi: 10.1006/nimg.2001.0786

Hanon, O., Vidal, J.-S., de Groote, P., Galinier, M., Isnard, R., Logeart, D., et al. (2014). Prevalence of memory disorders in ambulatory patients aged ≥70 years with chronic heart failure (from the EFICARE study). *Am. J. Cardiol.* 113, 1205–1210. doi: 10.1016/j.amjcard.2013.12.032

Houghton, C., Isope, P., Apps, R., and Cerminara, N. L. (2021). Editorial: information processing in the cerebellum. *Front. Syst. Neurosci.* 15:752719. doi: 10.3389/fnsys.2021.752719

Koenigs, M., Barbey, A. K., Postle, B. R., and Grafman, J. (2009). Superior parietal cortex is critical for the manipulation of information in working memory. *J. Neurosci. Off. J. Soc. Neurosci.* 29, 14980–14986. doi: 10.1523/JNEUROSCI.3706-09.2009

Kumar, R., Woo, M. A., Birrer, B. V. X., Macey, P. M., Fonarow, G. C., Hamilton, M. A., et al. (2009). Mammillary bodies and fornix fibers are injured in heart failure. *Neurobiol. Dis.* 33, 236–242. doi: 10.1016/j.nbd.2008.10.004

Lancaster, M. A., Renner, M., Martin, C.-A., Wenzel, D., Bicknell, L. S., Hurles, M. E., et al. (2013). Cerebral organoids model human brain development and microcephaly. *Nature* 501, 373–379. doi: 10.1038/nature12517

Liori, S., Arfaras-Melainis, A., Bistola, V., Polyzogopoulou, E., and Parissis, J. (2022). Cognitive impairment in heart failure: clinical implications, tools of assessment, and therapeutic considerations. *Heart Fail. Rev.* 27, 993–999. doi: 10.1007/s10741-021-10118-5

Mene-Afejuku, T. O., Pernia, M., Ibebuogu, U. N., Chaudhari, S., Mushiyev, S., Visco, F., et al. (2019). Heart failure and cognitive impairment: clinical relevance and therapeutic considerations. *Curr. Cardiol. Rev.* 15, 291–303. doi: 10.2174/1573403X15666190313112841

Nasreddine, Z. S., Phillips, N. A., Bédirian, V., Charbonneau, S., Whitehead, V., Collin, I., et al. (2005). The Montreal Cognitive Assessment, MoCA: a brief screening tool for mild cognitive impairment. *J. Am. Geriatr. Soc.* 53, 695–699.

Ni, R. S. S., Mohamed Raffi, H. Q., and Dong, Y. (2023). The pathophysiology of cognitive impairment in individuals with heart failure: a systematic review. *Front. Cardiovasc. Med.* 10:1181979. doi: 10.3389/fcvm.2023.1181979

Ogoh, S., Sugawara, J., and Shibata, S. (2022). Does cardiac function affect cerebral blood flow regulation? *J. Clin. Med.* 11:6043. doi: 10.3390/jcm11206043

Prins, N. D., and Scheltens, P. (2015). White matter hyperintensities, cognitive impairment and dementia: an update. *Nat. Rev. Neurol.* 11, 157–165. doi: 10.1038/nrneurol.2015.10

Ridgway, G. R., Henley, S. M. D., Rohrer, J. D., Scahill, R. I., Warren, J. D., and Fox, N. C. (2008). Ten simple rules for reporting voxel-based morphometry studies. *Neuroimage* 40, 1429–1435. doi: 10.1016/j.neuroimage.2008.01.003

Savarese, G., Stolfo, D., Sinagra, G., and Lund, L. H. (2022). Heart failure with mid-range or mildly reduced ejection fraction. *Nat. Rev. Cardiol.* 19, 100–116. doi: 10.1038/s41569-021-00605-5

Spilling, C. A., Jones, P. W., Dodd, J. W., and Barrick, T. R. (2017). White matter lesions characterise brain involvement in moderate to severe chronic obstructive pulmonary disease, but cerebral atrophy does not. *BMC Pulm. Med.* 17:92. doi: 10.1186/s12890-017-0435-1

Steinberg, B. A., Zhao, X., Heidenreich, P. A., Peterson, E. D., Bhatt, D. L., Cannon, C. P., et al. (2012). Trends in patients hospitalized with heart failure and preserved left ventricular ejection fraction: prevalence, therapies, and outcomes. *Circulation* 126, 65–75. doi: 10.1161/CIRCULATIONAHA.111.080770

Vogels, R. L. C., van der Flier, W. M., van Harten, B., Gouw, A. A., Scheltens, P., Schroeder-Tanka, J. M., et al. (2007). Brain magnetic resonance imaging abnormalities in patients with heart failure. *Eur. J. Heart Fail.* 9, 1003–1009. doi: 10.1016/j.ejheart.2007.07.006

Wang, C., Ding, Y., Shen, B., Gao, D., An, J., Peng, K., et al. (2017). Altered gray matter volume in stable chronic obstructive pulmonary disease with subclinical cognitive impairment: an exploratory study. *Neurotox. Res.* 31, 453–463. doi: 10.1007/s12640-016-9690-9

Whitwell, J. L. (2009). Voxel-based morphometry: an automated technique for assessing structural changes in the brain. *J. Neurosci. Off. J. Soc. Neurosci.* 29, 9661–9664. doi: 10.1523/JNEUROSCI.2160-09.2009

Ye, S., Huynh, Q., and Potter, E. L. (2022). Cognitive dysfunction in heart failure: pathophysiology and implications for patient management. *Curr. Heart Fail. Rep.* 19, 303–315. doi: 10.1007/s11897-022-00564-z

Zhang, S., Hu, Y., Yang, H., Li, Q., Chen, J., and Bai, H. (2023). Value of white matter hyperintensity volume and total white matter volume for evaluating cognitive impairment in patients with cerebral small-vessel disease. *Front. Aging Neurosci.* 15:1096808. doi: 10.3389/fnagi.2023.1096808

Zhou, L., Guo, Z., Wang, B., Wu, Y., Li, Z., Yao, H., et al. (2021). Risk prediction in patients with heart failure with preserved ejection fraction using gene expression data and machine learning. *Front. Genet.* 12:652315. doi: 10.3389/fgene.2021.652315

frontiers | Frontiers in Neurology

TYPE Original Research
PUBLISHED 16 June 2025
DOI 10.3389/fneur.2025.1583857

OPEN ACCESS

EDITED BY
Mingming Lu,
Characteristic Medical Center of Chinese People's Armed Police Force, China

REVIEWED BY
Beibei Sun,
Shanghai Jiao Tong University, China
Weizhuang Yuan,
Chinese Academy of Medical Sciences and Peking Union Medical College, China

*CORRESPONDENCE
Beom Joon Kim
✉ Kim.BJ.Stroke@gmail.com

RECEIVED 26 February 2025
ACCEPTED 27 May 2025
PUBLISHED 16 June 2025

CITATION
Kang D-W, Kim J, Kim DY, Baik SH, Jung C, Menon BK, Song JW, Han M-K, Bae H-J and Kim BJ (2025) Temporal changes in symptomatic intracranial arterial disease: a longitudinal high-resolution vessel wall imaging study.
Front. Neurol. 16:1583857.
doi: 10.3389/fneur.2025.1583857

Temporal changes in symptomatic intracranial arterial disease: a longitudinal high-resolution vessel wall imaging study

Dong-Wan Kang[1,2], Jonguk Kim[1,3], Do Yeon Kim[1,4,5], Sung Hyun Baik[6], Cheolkyu Jung[6], Bijoy K. Menon[7], Jae W. Song[8], Moon-Ku Han[1], Hee-Joon Bae[1] and Beom Joon Kim[1]*

[1]Department of Neurology, Seoul National University College of Medicine, Seoul National University Bundang Hospital, Seongnam, Republic of Korea, [2]Department of Neurosurgery, Seoul National University Bundang Hospital, Seongnam, Republic of Korea, [3]Department of Neurology, Inha University Hospital, Incheon, Republic of Korea, [4]Department of Public Health, Seoul National University Bundang Hospital, Seongnam, Republic of Korea, [5]Department of Neurology, Gyeonggi Provincial Medical Center, Icheon Hospital, Icheon, Republic of Korea, [6]Department of Radiology, Seoul National University Bundang Hospital, Seongnam, Republic of Korea, [7]Department of Clinical Neurosciences, Cumming School of Medicine, University of Calgary, Calgary, AB, Canada, [8]Department of Radiology, Hospital of the University of Pennsylvania, Philadelphia, PA, United States

Introduction: The temporal dynamics of the vessel wall in intracranial arterial disease (ICAD) may differ depending on the etiology. We investigated temporal changes in narrowed intracranial arteries after ischemic stroke using serial high-resolution vessel wall imaging (HR-VWI).

Methods: We retrospectively recruited patients with ICAD-related ischemic stroke who underwent two or more HR-VWI scans. The lumen area (LA), total vessel area (TVA), and enhancing area (EA) of the narrowest part of the culprit lesion were manually segmented. Degree of stenosis was estimated as [1-LA/TVA] × 100(%), the enhancing proportion as EA/TVA × 100(%), and enhancement ratio as $(T1GD_{lesion}/T1GD_{ref})/(T1_{lesion}/T1_{ref})$. Linear mixed models were used to investigate temporal changes in these parameters and whether such changes differed by etiologies.

Results: Of a total of 208 patients, ICAD-related stroke was caused by atherosclerosis (69%), arterial dissection (24%), vasculitis (3%), moyamoya disease (1%), and other (2%). The median follow-up was 319 [IQR, 125–409] days. HR-VWI imaging parameters, namely, degree of stenosis, enhancing proportion, and enhancement ratio showed a trend to decrease over time. Patients with intracranial dissection as a cause of intracranial narrowing showed a faster reduction in degree of stenosis and enhancing proportion vs. when such narrowing was identified as due to atherosclerosis (β [95% CI], −0.59%[−0.80% ~ −0.38%] and −0.81%[−1.23% ~ −0.39%], respectively, both $p < 0.01$). The enhancement ratio did not change over time in dissection, while it decreased in atherosclerosis (−0.01 [−0.02 ~ 0], $p = 0.04$).

Conclusion: Intracranial vessel narrowing in patients with ischemic stroke changes over time with different stroke etiologies having their own unique temporal patterns.

KEYWORDS

intracranial arterial disease, ischemic stroke, magnetic resonance imaging, high-resolution vessel wall imaging, follow-up MRI

Introduction

Numerous patients experiencing ischemic stroke present with stenosis in the ipsilesional intracranial arteries. This imaging observation indicates intracranial arterial disease (ICAD), which is frequently implicated in the risk of recurrent strokes (1–3). ICAD may stem from atherosclerosis, while it may also manifest as non-atherosclerotic conditions including arterial dissections or vasculitis (4). Distinguishing between these diverse etiologies remains a formidable clinical challenge.

Conventional imaging modalities, such as time-of-flight (TOF) MR angiography or digital subtraction angiography (DSA), predominantly visualize the vascular lumen and are thus insufficient for conclusively identifying the underlying etiology of ICAD, which originates from the vascular walls. In contrast, high-resolution vessel wall imaging (HR-VWI) provides sub-millimeter spatial resolution capable of elucidating reveal vessel wall abnormalities (5). It enables the visualization of distinctive pathologic features associated with various conditions such as intracranial arterial dissection, moyamoya disease, vasculitis, and atherosclerotic plaque (6). Nevertheless, differentiation among these etiologies remain limited due to overlapping radiologic features observed even with HR-VWI (7, 8).

Understanding the unique interplay between pathological changes and natural healing processes in vascular injuries is crucial for interpreting temporal changes in ICAD. Given the paucity of targeted research in this area (9–11), we conducted a detailed analysis of serial HR-VWI data from over 200 patients with ischemic strokes attributable to ICAD. Our focus was on quantifying temporal changes in wall morphology, specifically evaluating the degree of stenosis and the extent of wall enhancement at the culprit segment. This research aims to deepen our understanding of the pathophysiological mechanisms governing ICAD and to discern whether distinct temporal changes might be indicative of specific etiologies.

Methods

Study population

Study subjects were retrospectively identified from a prospective registry of consecutive patients presenting with ICAD-related acute ischemic stroke at the Cerebrovascular Center of the Seoul National University Bundang Hospital, over a period from June 2016 to June 2019 (12). Eligibility for inclusion required patients to have undergone at least 2 HR-VWI scans during their admission and follow-up periods to assess disease progression and response to therapeutic interventions. Exclusion criteria included patients whose final diagnosis did not confirm stroke, those in whom the culprit vessel could not be definitively identified, and cases where the vessel was too diminutive for accurate quantitative analysis (Figure 1).

Stroke management adhered to prevailing clinical guidelines, with HR-VWI scans integrated into routine clinical assessments for ICAD patients. The local institutional review boards approved the study with a waiver of consent (No. B-2102-667-103). The data that support the findings of this study are available from the corresponding author upon reasonable request.

Clinical characteristics

Baseline demographic and clinical information was retrieved from the prospective stroke registry, encompassing sex, stroke history, and cardiovascular risk factors, such as hypertension, diabetes, dyslipidemia, smoking, and atrial fibrillation. Culprit lesions were defined as the most distal relevant intracranial artery that could account for all observed stroke lesions. These were identified using the initial CT or MR angiographies alongside the HR-VWI scan. The etiology of ICAD was established through a comprehensive clinical and imaging evaluation conducted during the index stroke admission. Clinical evaluation, performed by experienced stroke neurologists, included an assessment of age, associated vascular risks and laboratory tests. Imaging assessments were carried out by experienced neuroradiologists, who performed a detailed review of all available imaging data, including HR-VWI.

ICAD was classified as atherosclerotic when HR-VWI showed typical findings of iso- or hyperdense T1/proton density lesions indicative of a lipid core or high signal lesions on non-contrast T1-weighted imaging suggestive of intraplaque hemorrhage, paired with a corresponding clinical profile (13). Intracranial arterial dissections were diagnosed in the presence of intramural hematoma, double lumen or intimal flap were identified on the HR-VWI or DSA, often accompanied by a sudden severe headache at stroke onset (6). Moyamoya disease (MMD) was diagnosed according to the 2021 diagnostic criteria, which require imaging evidence of stenosis or occlusion at the terminal portion of the intracranial internal carotid artery (ICA) or the proximal portion of the anterior and/or middle cerebral artery (MCA), along with abnormal vascular networks near

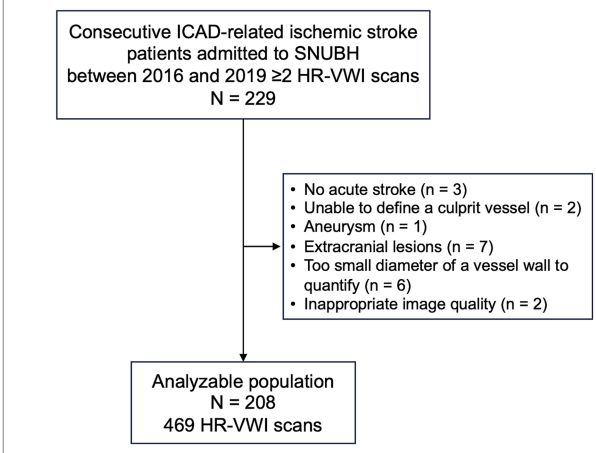

FIGURE 1
Study profile.

the lesion and bilateral reduction in the outer diameter of the lesions (14). To confirm the diagnosis, other etiologies such as autoimmune diseases and meningitis were excluded. Notably, HR-VWI revealed characteristic findings of concentric wall thickening with negative remodeling (7, 14, 15). Vasculitis was suspected when HR-VWI findings were suggestive of the inflammatory vasculopathy, characterized by smooth, homogeneous, strong concentric mural enhancement in the intracranial arteries (16–18). The diagnosis was established after confirming neuroinflammation at cerebrospinal fluid and excluding other vasculopathies, including fibromuscular dysplasia, moyamoya disease (MMD), and reversible cerebral vasoconstriction syndrome (RCVS). Vasculitis included both primary angiitis of the central nervous system and secondary vasculitis with identifiable causes such as infection, systemic vasculitis, or malignancy (19).

HR-VWI protocol

All patients underwent HR-VWI on a 3.0-T MRI scanner (Philips Achieva or Ingenia; Philips Healthcare, Best, The Netherlands) with 8-channel or 32-channel head coils. The imaging protocol was standardized across the cohort over the study period, incorporating T1-weighted image (T1-WI), proton density (PD) images, and gadolinium-enhanced T1 images (T1-Gd) with concurrent TOF MR angiography. Blood signal suppression was achieved using improved motion-sensitized driven-equilibrium (iMSDE) in T1-WI, PD, and T1-Gd sequences. Other common image parameters included a field of view of 180 × 180 mm, matrix of 300 × 300, flip angle of 90 degrees, and a spatial resolution of $0.6 \times 0.6 \times 0.6$ mm^3. Repetition time/echo time was 570/37 m/sec for T1-WI, 2000/32 m/sec for PD, and 570/37 for T1-Gd. The MR imaging protocol, including both stroke and HR-VWI sequences, took approximately 40 min. MR protocol details are further provided in Supplementary Table 1.

Image quantification

Image analysis on HR-VWI focused on the most stenotic segment of the culprit lesion and analyzed the vessel's perpendicular section (20). Manual segmentation and quantification of the lumen area (LA), total vessel area (TVA), and enhancing area (EA) were conducted using ITK-SNAP 4.1 (21). The LA was delineated from the T1-weighted image, while the TVA was measured using PD images at the corresponding plane. The EA was segmented and analyzed at the same most stenotic site on the T1GD image. The EA was quantified into the number of voxels, and its signal intensity was normalized against adjacent normal brain parenchyma by using a manual standard of 15 mm^2, as reported previously (20, 22).

The degree of stenosis was calculated as (1-LA/TVA) × 100(%), and the enhancing proportion was defined as EA/TVA × 100(%). The enhancement ratio of the enhancing lesion was quantified as $(T1GD_{lesion}/T1GD_{ref})/(T1_{lesion}/T1_{ref})$.

Blinded to clinical data, three board-certified vascular neurologists (DWK) and interventional neurologists (JK and DYK) with over 5 years of clinical practice independently evaluated HR-VWI scans. A consensus on the segmentation was reached after reviewing and annotating the first 50 cases. The analysis dataset was constructed through independent measurement by three raters, and acceptable inter-rater agreement was documented. Intraclass correlation coefficients for the degree of stenosis, enhancement ratio, and enhancing the proportion of DWK and JK were 0.89, 0.91, and 0.62, respectively. Those of DYK and JK were 0.87, 0.78, and 0.53, respectively. Discrepancies among the raters were resolved through discussions with the senior authors who had 15 years of clinical practice (BJK).

Statistical analysis

Descriptive statistics were used to summarize the demographic and clinical data. Baseline characteristics were summarized as means ± standard deviations, medians [interquartile ranges], and frequencies (percentages), as deemed appropriate. The quantified imaging parameters were analyzed based on linear mixed-effects regression models with random effects of intercept and slope models to accommodate the hierarchical structure of the data. These models were implemented using the *lme4* package in R. Three progressive models were constructed to explore the effect of various predictors on the imaging outcomes. Model 1 included the fixed effects of time, age, and sex. Model 2 extended model 1 by incorporating ICAD etiologies and their interaction with time. Model 3 further included variables for hypertension, diabetes, and dyslipidemia. All statistical tests were two-tailed, with significance levels at $p < 0.05$. Statistical computations were performed using R, version 4.3.2 (R Foundation for Statistical Computing).

Results

Patient characteristics

Of the initial cohort of 229 patients, 21 were excluded from the final analysis for the following reasons: presence of an aneurysm ($n = 1$), extracranial lesions ($n = 7$), absence of acute stroke ($n = 3$), indeterminate culprit vessel ($n = 2$), vessel wall diameter too small for quantitative analysis ($n = 6$), and suboptimal image quality ($n = 2$). Consequently, the study included 208 patients who had experienced acute ischemic stroke and underwent at least 2 HR-VWI scans post-index event. The demographic profile comprised 121 males (58%) with an average age of 57 ± 14 years.

Etiological classification based on clinical and imaging evaluations identified atherosclerosis in 144 cases (69%), followed by arterial dissection in 49 cases (24%). Other identified etiologies included Moyamoya disease in 3 cases (1%), vasculitis in 7 cases (3%), and various other vasculopathies in 5 cases (2.4%)—specifically, antiphospholipid antibody syndrome, cerebral autosomal dominant arteriopathy with subcortical infarcts and leukoencephalopathy (CADASIL), fibromuscular dysplasia, RCVS, and one undetermined case. Analysis of lesion distribution showed that anterior circulation was involved in 132 cases (63%), while posterior circulation was affected in 76 cases (37%) (Table 1 and Supplementary Figure 1). A more detailed description of baseline characteristics stratified by

TABLE 1 Baseline characteristics of the enrolled patients.

Patient characteristics	Total (*N* = 208)
Male sex	121 (58.2%)
Age	56.7 ± 14.3
Total MRI follow-up time (days)	319 [125, 409]
Onset-to-HR-VWI (days)	4 [2, 8]
Hypertension	113 (54.3%)
Diabetes	56 (26.9%)
Dyslipidemia	59 (28.4%)
Smoking	79 (38.0%)
Atrial fibrillation	6 (2.9%)
History of stroke	23 (11.1%)
Coronary heart disease	9 (4.3%)
Medication before stroke	
Antiplatelets	62 (29.8%)
Anticoagulants	1 (0.5%)
Etiology	
Atherosclerosis	144 (69.2%)
Dissection	49 (23.6%)
Moyamoya disease	3 (1.4%)
Vasculitis	7 (3.4%)
Others	5 (2.4%)
Culprit vessel	
dICA	12 (5.8%)
ACA	8 (3.8%)
MCA	112 (53.8%)
BA	17 (8.2%)
VA	41 (19.7%)
PCA	2 (1.0%)
PICA	15 (7.2%)
Posterior choroidal artery	1 (0.5%)

HR-VWI, high-resolution vessel wall imaging; dICA, distal internal carotid artery; ACA, anterior cerebral artery; MCA, middle cerebral artery; BA, basilar artery; VA, vertebral artery; PCA, posterior cerebral artery; PICA, posterior inferior cerebellar artery.

etiology is provided in Supplementary Table 2. The dataset encompassed 469 HR-VWI scans, averaging 2.3 scans per patient with a median inter-scan interval of 319 [IQR, 125–409] days (Supplementary Figure 2).

Distribution of quantified HR-VWI image parameters

In the patients included in this study, the baseline HR-VWI scans revealed a median degree of stenosis at 77.1% [IQR, 56.0–87.6%], a median enhancement ratio of 2.02 [IQR, 1.50–2.59], and a median enhancing proportion of 45.8% [IQR, 29.0–71.6%]. No significant correlations were observed among these image parameters (Supplementary Figure 3). Detailed distributions of these image parameters across different ICAD etiologies are presented in Supplementary Table 3.

Temporal change of MRI parameters over time

A longitudinal analysis of the imaging parameters derived from HR-VWI scans indicated a general decreasing trend throughout the follow-up period. Specifically, linear regression analyses demonstrated decreases of 0.17% ± 0.03% in the degree of stenosis, 0.008 ± 0.001 in the enhancement ratio, and 0.39% ± 0.06% in the enhancing proportion per 10-day interval. Notably, these trends varied significantly by ICAD etiology (Figure 2). In the arterial dissection group, the degree of stenosis and the enhancing proportion showed markedly steeper declines compared to those in the atherosclerotic group: 0.70% ± 0.09% versus 0.08% ± 0.02% for the degree of stenosis and 1.33% ± 0.20% versus 0.30% ± 0.04% for the enhancing proportion, respectively (both P-for-difference <0.01). Conversely, the decrease in the enhancing ratio was less pronounced in the arterial dissection group compared to the atherosclerotic group, 0.0005 ± 0.005 versus 0.01 ± 0.001 per 10 days (P-for-difference <0.01). Representative cases illustrating these findings are depicted in Figure 3.

Temporal dynamics of HR-VWI image parameters by ICAD etiology

In the context of differing ICAD etiologies, the arterial dissection group, when compared to the atherosclerosis group, exhibited a notable reduction in both the degree of stenosis and enhancing proportion over time, as evidenced by linear mixed effects regression models; β coefficients were −0.59% (95% confidence intervals [CI] −0.80% ~ −0.38%) and −0.81% (95% CI −1.23% ~ −0.39%), respectively, both achieving statistical significance (p-value <0.01, Table 2). In contrast, the enhancement ratio remained unchanged over time in dissection but decreased in atherosclerosis (−0.01 [95% CI −0.02 ~ 0], p-value = 0.04, Table 2 and Supplementary Table 6). Additionally, the moyamoya disease group demonstrated a significant increase in the enhancing proportion over time (2.8% [95% CI 1.343 ~ 4.258], p-value <0.01; Table 2).

Stroke recurrence

A summary of treatments is provided in Supplementary Table 8. Most patients were prescribed antiplatelet agents and statins, and other secondary prevention medications were administered appropriately based on individual comorbidities. Among the included 208 patients, 27 (13.0%) experienced recurrent strokes or transient ischemic attacks (TIA) over a median follow-up period of 335 days (IQR, 107–648). Among those with atherosclerotic stroke, 23 recurrent events (16.0%) were recorded, with 15 cases (65%) originating from the culprit vessel. Notably, no recurrent strokes/TIAs

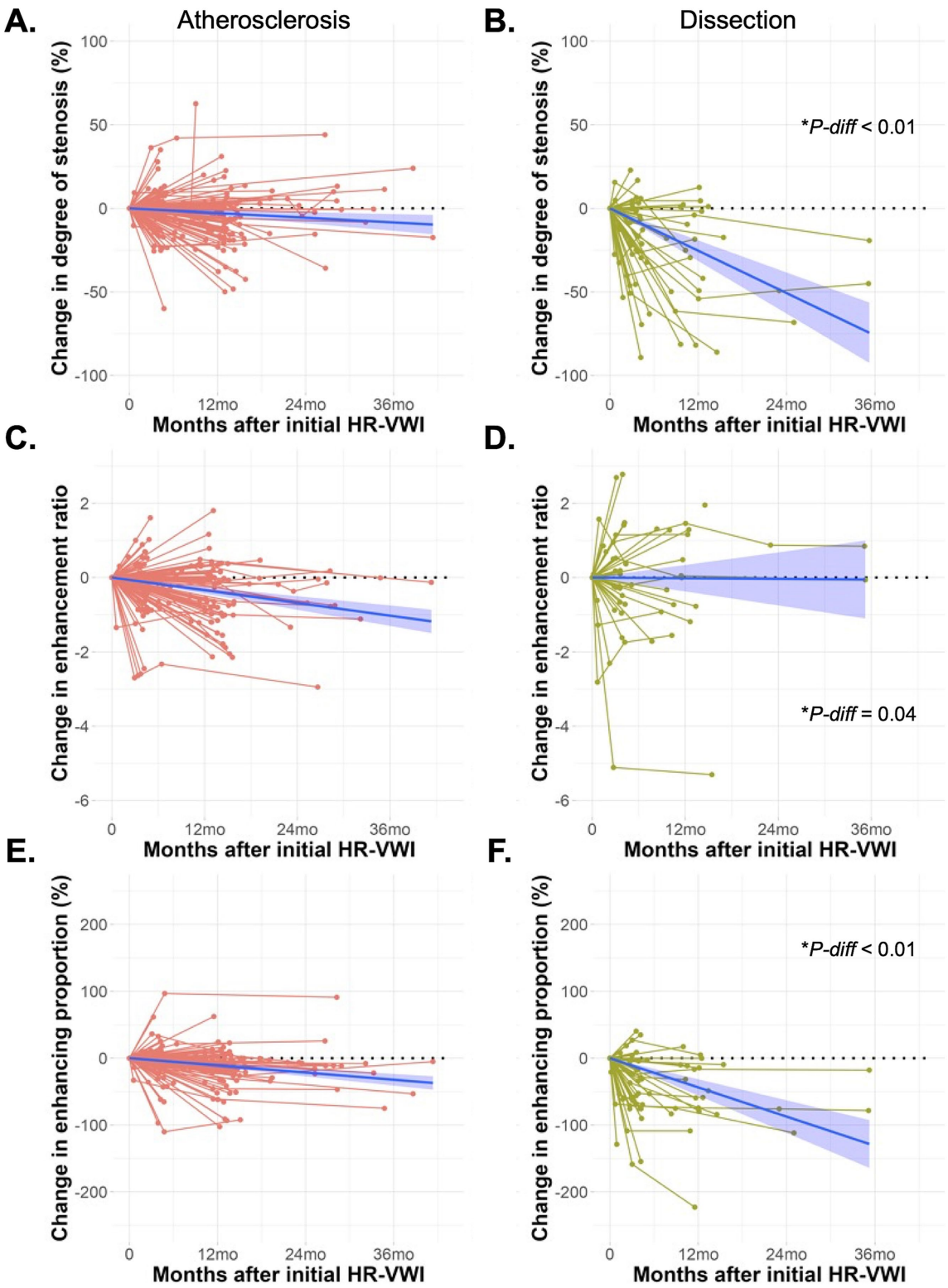

FIGURE 2
Graphs showing the change in degree of stenosis **(A,B)**, enhancement ratio **(C,D)**, and enhancing proportion **(E,F)** over time for patients with atherosclerosis and arterial dissection. Blue lines are linear regression lines with 95% confidence intervals. *P-diff* indicates *p* values for the difference in MRI parameters between the atherosclerosis and arterial dissection groups over time, derived from linear mixed effects models.

were observed within intracranial arterial dissection. Among the other groups, one of the three patients with MMD experience two recurrent strokes; one of the seven patients with vasculitis had a non-aneurysmal subarachnoid hemorrhage; and one patient with CADASIL experienced two recurrent events, one of which originated from the culprit vessel and another from a different artery.

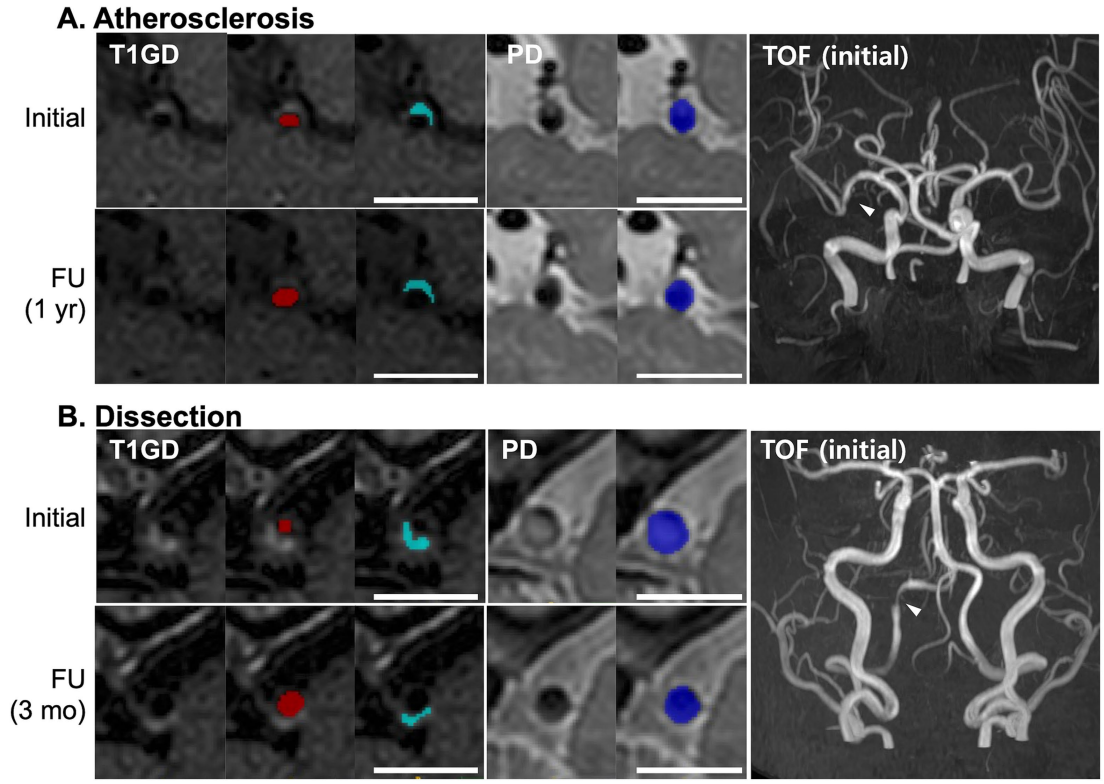

FIGURE 3
Representative images of the culprit vessels in patients with atherosclerosis **(A)** and arterial dissection **(B)**. Initial and follow-up HR-VWI scans are shown. Lumen area (red), enhancing area (light blue), and total vessel area (blue) are manually segmented. Scale bars, 1 cm.

Discussion

In this study, we evaluated temporal changes in HR-VWI parameters among 208 patients who underwent serial imaging following an ischemic stroke attributable to ICAD. We observed a general decline over time in the degree of stenosis, enhancing proportion, and enhancement ratio. Notably, these changes were more pronounced in patients with arterial dissection compared to those with atherosclerosis, suggesting differing pathological processes underpin these conditions.

The pathologies associated with ICAD display significant heterogeneity, evident in the varied manifestations of luminal stenosis and contrast enhancement. These differences arise from distinct underlying pathophysiological mechanisms. In atherosclerosis, enhancement typically occurs due to inflammation related to a ruptured cap, fibrous tissues, or ingrowing vasa vasorum (23). This inflammation is particularly pronounced even in the early stages of ischemic stroke when vulnerable plaques are enhanced vividly (24). Conversely, arterial dissections, which can also precipitate stenotic lesions, may show enhancement in the presence of an intraluminal thrombus (25, 26). The evolution of blood products within the intramural hematoma following arterial dissections does not always show the strong T1 shortening typical of methemoglobin in subacute to chronic stages (13), complicating the imaging interpretation. This overlap in imaging features between atherosclerosis and arterial dissections—both displaying stenosis, enhancement and occasionally bright T1 signal – poses a significant diagnostic challenge. Serial HR-VWI may become a critical tool in this context, providing essential diagnostic information as the vascular pathologies evolve distinctly over time, as our results showed. Understanding these temporal dynamics offers valuable insights into the underlying etiology of the disease process, aiding in differentiating between these two common causes of ICAD.

The relatively rapid decrease in both the degree of stenosis and the enhancing proportion observed in patients with arterial dissection can predominantly be attributable to the natural resorption of the mural hematoma. This process reflects a unique aspect of the healing pathway in arterial dissections, differentiating it from the slower, inflammatory-driven changes seen in atherosclerosis. Supporting this observation, prior research has shown that intramural hematomas in arterial dissection typically resolve within 6 months, with significant improvement in most lesions by 12 months (9). Another study also noted that stenosis improved in 30% of patients within a median of 40 days post-dissection (27).

Our observations of gradual improvement in the degree of stenosis, enhancement ratio, and enhancing proportion in patients with atherosclerotic ICAD suggest a possible stabilization of the culprit vessel over time. These findings align with previous studies using serial HR-VWI, which have documented reductions in the degree of stenosis, contrast ratio, surface irregularities, and overall plaque burden within 6 to 12 months following the index stroke event (10, 28, 29). This stabilization likely reflects the healing process of ruptured plaques, which results in a persistent stenotic segment with

TABLE 2 Selected β coefficients (β Coeff) and 95% confidence intervals (CI) of the linear mixed effects models for each image parameters.

Variables	Model 1: Time, age, sex, etiology		Model 2: Model 1 + etiology × Time		Model 3: Model 2 + HTN, DM, DL	
	β Coeff (95% CI)	*P*-value	β Coeff (95% CI)	*P*-value	β Coeff (95% CI)	*P*-value
Degree of stenosis (%)						
Time	−0.206 (−0.290 ~ −0.121)	<0.01	−0.111 (−0.203 ~ −0.02)	0.02	−0.11 (−0.201 ~ −0.02)	0.02
Age	0.113 (−0.123 ~ 0.350)	0.35	0.107 (−0.129 ~ 0.343)	0.38	0.093 (−0.148 ~ 0.333)	0.45
Male sex	−1.327 (7.310 ~ 4.656)	0.66	−1.434 (−7.404 ~ 4.537)	0.64	−2.017 (−7.95 ~ 3.917)	0.51
Atherosclerosis × Time			Ref		Ref	
Dissection × Time			−0.593 (−0.806 ~ −0.38)	<0.01	−0.592 (−0.804 ~ −0.381)	<0.01
MMD × Time			0.599 (−0.081 ~ 1.28)	0.09	0.603 (−0.076 ~ 1.282)	0.08
Vasculitis× Time			0.089 (−0.314 ~ 0.492)	0.67	0.091 (−0.31 ~ 0.492)	0.66
Others × Time			−0.171 (−0.737 ~ 0.394)	0.55	−0.159 (−0.719 ~ 0.402)	0.58
Enhancement ratio						
Time	−0.008 (−0.011 ~ −0.005)	<0.01	−0.01 (−0.013 ~ −0.006)	<0.01	−0.01 (−0.013 ~ −0.006)	<0.01
Age	−0.003 (−0.011 ~ 0.004)	0.40	−0.003 (−0.011 ~ 0.004)	0.39	−0.003 (−0.011 ~ 0.005)	0.45
Male sex	−0.233 (−0.431 ~ −0.035)	0.02	−0.238 (−0.437 ~ −0.04)	0.02	−0.258 (−0.456 ~ −0.059)	0.01
Atherosclerosis × Time			Ref		Ref	
Dissection × Time			0.009 (0.001 ~ 0.018)	0.04	0.009 (0 ~ 0.018)	0.04
MMD × Time			0.004 (−0.026 ~ 0.034)	0.79	0.005 (−0.025 ~ 0.035)	0.77
Vasculitis× Time			0.002 (−0.017 ~ 0.021)	0.84	0.001 (−0.018 ~ 0.021)	0.9
Others × Time			−0.001 (−0.021 ~ 0.018)	0.89	−0.002 (−0.022 ~ 0.018)	0.86
Enhancing proportion (%)						
Time	−0.36 (−0.516 ~ −0.203)	<0.01	−0.306 (−0.49 ~ −0.122)	<0.01	−0.291 (−0.474 ~ −0.107)	<0.01
Age	−0.371 (−0.805 ~ 0.063)	0.1	−0.382 (−0.812 ~ 0.048)	0.08	−0.261 (−0.697 ~ 0.175)	0.24
Male sex	−14.031 (−25.03 ~ −3.035)	0.01	−13.93 (−24.86 ~ −3.01)	0.01	−15.63 (−26.41 ~ −4.852)	<0.01
Atherosclerosis × Time			Ref		Ref	
Dissection × Time			−0.803 (−1.227 ~ −0.378)	<0.01	−0.811 (−1.233 ~ −0.389)	<0.01
MMD × Time			2.768 (1.309 ~ 4.226)	<0.01	2.8 (1.343 ~ 4.258)	<0.01
Vasculitis× Time			0.833 (−0.028 ~ 1.693)	0.06	0.776 (−0.085 ~ 1.637)	0.08
Others × Time			−0.096 (−1.157 ~ 0.966)	0.86	−0.026 (−1.081 ~ 1.03)	0.96

MMD, moyamoya disease; HTN, hypertension; DM, diabetes mellitus; DL, dyslipidemia. We used '10 days' as the unit for the time variable. Coefficients for all variables are presented in Supplementary Tables 4, 5, 7.

stable plaque. However, not all findings point towards a uniform improvement in the plaque composition. Some studies, including ours, have observed that certain atherosclerotic lesions may exhibit persistent or even enhancement up to 3 months post-stroke, suggesting ongoing inflammatory processes or other pathological activities within the plaque (11, 30).

The interpretation of HR-VWI features in ICAD remains challenging in the absence of corresponding histologic evidence. Vessel wall enhancement observed in HR-VWI could represent various underlying biological processes, such as increased endothelial permeability leading to contrast leakage, the extent of the vasa vasorum, inflammatory responses, or fibrotic changes. A decrease in the enhancement ratio over time in atherosclerotic ICAD likely signifies the stabilization of an inflamed vulnerable plaque following an acute stroke event. Conversely, the persistent enhancement in arterial dissections may be attributed to the evolution from initial traumatic vessel wall injury to subsequent post-traumatic fibrosis and vascular remodelling (31).

This study, while providing valuable insights into the temporal dynamics of ICAD via HR-VWI, is subject to several limitations that must be clarified. First, this study was conducted at a single center, which follows a standardized HR-VWI protocol. This uniformity implies that our findings may not be directly generalizable to other settings where imaging protocols differ. Secondly, the study included only a small number of patients with MMD, vasculitis, and other etiologies, limiting rigorous analysis to identify trends within these other groups. Thirdly, the statistical models assumed linearity in the temporal changes of MRI parameters for ICAD. However, these changes may follow a nonlinear pattern. Fourthly, we did not define HR-VWI findings as specific vessel wall features such as fibrous cap, vascular calcification, intraplaque hemorrhage, and intramural hematoma. Instead, we identified measurable imaging features that can be followed on serial HR-VWI exams. The identification of such specific histology-related features could potentially lead to a more nuanced understanding of the disease processes in ICAD. Fifthly, the enhancing area was defined based on visual segmentation of

hyperintense regions on T1-Gd images, which may have included pre-existing T1 hyperintensities. As such, changes in enhancing area may partly reflect the resolution of baseline T1 hyperintense lesions, such as intramural hematoma, rather than a true decrease in contrast enhancement. Although we attempted to mitigate this by also measuring the enhancement ratio, future studies incorporating voxel-wise comparison between T1 and T1-Gd images may provide deeper insight into the dynamic vessel wall changes in ICAD.

In conclusion, this study has effectively documented temporal changes in HR-VWI parameters among patients with acute ischemic stroke due to ICAD. Notably, alterations were observed in the degree of stenosis, enhancing proportion and enhancement ratio, differed across the clinical diagnosis of atherosclerosis or dissection. These findings underscore the utility of serial HR-VWI in distinguishing between different stroke etiologies, such as intracranial atherosclerosis and arterial dissection, thus aiding in the accurate diagnosis and management of ICAD. Future studies should aim to elucidate the specific factors that contribute to the dynamic temporal changes of ICAD, such as genetic predispositions, the flow dynamics of vascular anatomy, and the role of specific medical interventions. Understanding these factors could lead to more personalized and effective treatment strategies for patients with ICAD.

Data availability statement

The raw data supporting the conclusions of this article will be made available by the authors, without undue reservation.

Ethics statement

The studies involving humans were approved by the Institutional Review Board of Seoul National University Bundang Hospital (Approval number: B-2102-332 667-103). The studies were conducted in accordance with the local legislation and institutional requirements. Written informed consent from the patients/participants or patients/participants' legal guardian/next of kin was not required to participate in this study in accordance with the national legislation and the institutional requirements.

Author contributions

D-WK: Data curation, Formal analysis, Methodology, Visualization, Writing – original draft, Writing – review & editing. JK: Data curation, Methodology, Writing – review & editing. DK: Data curation, Methodology, Writing – review & editing. SB: Data curation, Methodology, Writing – review & editing. CJ: Data curation, Methodology, Writing – review & editing. BM: Writing – review & editing. JS: Writing – review & editing. M-KH: Writing – review & editing. H-JB: Writing – review & editing. BK: Conceptualization, Data curation, Formal analysis, Funding acquisition, Methodology, Writing – original draft, Writing – review & editing.

Funding

The author(s) declare that financial support was received for the research and/or publication of this article. This research was supported by a grant of the Korea Health Technology R&D Project through the Korea Health Industry Development Institute, funded by the Ministry of Health & Welfare, Republic of Korea (grant number: HI22C0454). This work was also supported by grant number 02-2023-0002 from SNUBH Research Fund. Both grants were endowed to B.J. Kim. J.W. Song is supported by the American Heart Association (938082).

Conflict of interest

The authors declare that the research was conducted in the absence of any commercial or financial relationships that could be construed as a potential conflict of interest.

Generative AI statement

The authors declare that no Gen AI was used in the creation of this manuscript.

Publisher's note

All claims expressed in this article are solely those of the authors and do not necessarily represent those of their affiliated organizations, or those of the publisher, the editors and the reviewers. Any product that may be evaluated in this article, or claim that may be made by its manufacturer, is not guaranteed or endorsed by the publisher.

Supplementary material

The Supplementary material for this article can be found online at: https://www.frontiersin.org/articles/10.3389/fneur.2025.1583857/full#supplementary-material

References

1. Suri MF, Johnston SC. Epidemiology of intracranial stenosis. *J Neuroimaging.* (2009) 19:11S–6S. doi: 10.1111/j.1552-6569.2009.00415.x

2. Qureshi AI, Feldmann E, Gomez CR, Johnston SC, Kasner SE, Quick DC, et al. Intracranial atherosclerotic disease: an update. *Ann Neurol.* (2009) 66:730–8. doi: 10.1002/ana.21768

3. Gorelick PB, Wong KS, Bae HJ, Pandey DK. Large artery intracranial occlusive disease: a large worldwide burden but a relatively neglected frontier. *Stroke.* (2008) 39:2396–9. doi: 10.1161/STROKEAHA.107.505776

4. Bang OY, Toyoda K, Arenillas JF, Liu L, Kim JS. Intracranial large artery disease of non-atherosclerotic origin: recent Progress and clinical implications. *J Stroke.* (2018) 20:208–17. doi: 10.5853/jos.2018.00150

5. de Havenon A, Mossa-Basha M, Shah L, Kim SE, Park M, Parker D, et al. High-resolution vessel wall MRI for the evaluation of intracranial atherosclerotic disease. *Neuroradiology.* (2017) 59:1193–202. doi: 10.1007/s00234-017-1925-9

6. Mandell DM, Mossa-Basha M, Qiao Y, Hess CP, Hui F, Matouk C, et al. Intracranial Vessel Wall MRI: principles and expert consensus recommendations of the American

Society of Neuroradiology. *AJNR Am J Neuroradiol*. (2017) 38:218–29. doi: 10.3174/ajnr.A4893

7. Kang DW, Kim DY, Kim J, Baik SH, Jung C, Singh N, et al. Emerging concept of intracranial arterial diseases: the role of high resolution Vessel Wall MRI. *J Stroke*. (2024) 26:26–40. doi: 10.5853/jos.2023.02481

8. Tritanon O, Mataeng S, Apirakkan M, Panyaping T. Utility of high-resolution magnetic resonance vessel wall imaging in differentiating between atherosclerotic plaques, vasculitis, and arterial dissection. *Neuroradiology*. (2023) 65:441–51. doi: 10.1007/s00234-022-03093-7

9. Lee SH, Kim KY, Jung JM. High-resolution magnetic resonance imaging for the follow-up of intracranial arterial dissections. *Acta Neurol Belg*. (2021) 121:1599–605. doi: 10.1007/s13760-020-01432-0

10. Chung JW, Cha J, Lee MJ, Yu IW, Park MS, Seo WK, et al. Intensive statin treatment in acute Ischaemic stroke patients with intracranial atherosclerosis: a high-resolution magnetic resonance imaging study (STAMINA-MRI study). *J Neurol Neurosurg Psychiatry*. (2020) 91:204–11. doi: 10.1136/jnnp-2019-320893

11. Kwee RM, Qiao Y, Liu L, Zeiler SR, Wasserman BA. Temporal course and implications of intracranial atherosclerotic plaque enhancement on high-resolution vessel wall MRI. *Neuroradiology*. (2019) 61:651–7. doi: 10.1007/s00234-019-02190-4

12. Kim BJ, Park JM, Kang K, Lee SJ, Ko Y, Kim JG, et al. Case characteristics, hyperacute treatment, and outcome information from the clinical research center for stroke-fifth division registry in South Korea. *J Stroke*. (2015) 17:38–53. doi: 10.5853/jos.2015.17.1.38

13. Choi YJ, Jung SC, Lee DH. Vessel Wall imaging of the intracranial and cervical carotid arteries. *J Stroke*. (2015) 17:238–55. doi: 10.5853/jos.2015.17.3.238

14. Kuroda S, Fujimura M, Takahashi J, Kataoka H, Ogasawara K, Iwama T, et al. Diagnostic criteria for Moyamoya disease −2021 revised version. *Neurol Med Chir*. (2022) 62:307–12. doi: 10.2176/jns-nmc.2022-0072

15. Larson AS, Klaas JP, Johnson MP, Benson JC, Shlapak D, Lanzino G, et al. Vessel wall imaging features of Moyamoya disease in a north American population: patterns of negative remodelling, contrast enhancement, wall thickening, and stenosis. *BMC Med Imaging*. (2022) 22:198. doi: 10.1186/s12880-022-00930-2

16. Obusez EC, Hui F, Hajj-Ali RA, Cerejo R, Calabrese LH, Hammad T, et al. High-resolution MRI vessel wall imaging: spatial and temporal patterns of reversible cerebral vasoconstriction syndrome and central nervous system vasculitis. *AJNR Am J Neuroradiol*. (2014) 35:1527–32. doi: 10.3174/ajnr.A3909

17. Kuker W, Gaertner S, Nagele T, Dopfer C, Schoning M, Fiehler J, et al. Vessel wall contrast enhancement: a diagnostic sign of cerebral vasculitis. *Cerebrovasc Dis*. (2008) 26:23–9. doi: 10.1159/000135649

18. Pfefferkorn T, Linn J, Habs M, Opherk C, Cyran C, Ottomeyer C, et al. Black blood MRI in suspected large artery primary angiitis of the central nervous system. *J Neuroimaging*. (2013) 23:379–83. doi: 10.1111/j.1552-6569.2012.00743.x

19. Alexander MD, Yuan C, Rutman A, Tirschwell DL, Palagallo G, Gandhi D, et al. High-resolution intracranial vessel wall imaging: imaging beyond the lumen. *J Neurol Neurosurg Psychiatry*. (2016) 87:589–97. doi: 10.1136/jnnp-2015-312020

20. Qiao Y, Zeiler SR, Mirbagheri S, Leigh R, Urrutia V, Wityk R, et al. Intracranial plaque enhancement in patients with cerebrovascular events on high-spatial-resolution MR images. *Radiology*. (2014) 271:534–42. doi: 10.1148/radiol.13122812

21. Yushkevich PA, Piven J, Hazlett HC, Smith RG, Ho S, Gee JC, et al. User-guided 3D active contour segmentation of anatomical structures: significantly improved efficiency and reliability. *NeuroImage*. (2006) 31:1116–28. doi: 10.1016/j.neuroimage.2006.01.015

22. Qiao Y, Steinman DA, Qin Q, Etesami M, Schar M, Astor BC, et al. Intracranial arterial wall imaging using three-dimensional high isotropic resolution black blood MRI at 3.0 tesla. *J Magn Reson Imaging*. (2011) 34:22–30. doi: 10.1002/jmri.22592

23. Song JW, Wasserman BA. Vessel wall MR imaging of intracranial atherosclerosis. *Cardiovasc Diagn Ther*. (2020) 10:982–93. doi: 10.21037/cdt-20-470

24. Skarpathiotakis M, Mandell DM, Swartz RH, Tomlinson G, Mikulis DJ. Intracranial atherosclerotic plaque enhancement in patients with ischemic stroke. *AJNR Am J Neuroradiol*. (2013) 34:299–304. doi: 10.3174/ajnr.A3209

25. Atsina KB, Rothstein A, Messe SR, Song JW. Intracranial vessel wall MR imaging of an intradural vertebral artery dissection. *Clin Imaging*. (2020) 68:108–10. doi: 10.1016/j.clinimag.2020.06.024

26. Zhang Y, He G, Lu J, Miao G, Liang D, Wang J, et al. Thrombus enhancement sign may differentiate embolism from arteriosclerosis-related large vessel occlusion. *J Stroke*. (2023) 25:233–41. doi: 10.5853/jos.2022.03489

27. Hanim K, Jung SC, Young CJ, Kang DW, Kwon SU, Kim JS, et al. Structural changes of intra and extracranial artery dissection: a study of high-resolution magnetic resonance imaging. *J Stroke Cerebrovasc Dis*. (2022) 31:106302. doi: 10.1016/j.jstrokecerebrovasdis.2021.106302

28. Huang J, Jiao S, Chen Y, Lu J, Song Y, Zhang J, et al. Efficacy of medical treatment and balloon angioplasty for severe intracranial atherosclerosis: a high-resolution MR vessel wall imaging. *Eur Radiol*. (2023) 33:2478–88. doi: 10.1007/s00330-022-09218-z

29. Lin X, Guo W, She D, Wang F, Xing Z, Cao D. Follow-up assessment of atherosclerotic plaques in acute ischemic stroke patients using high-resolution vessel wall MR imaging. *Neuroradiology*. (2022) 64:2257–66. doi: 10.1007/s00234-022-03002-y

30. Lee HS, Jung JM, Yang HB, Lee SH. Predicting stenosis aggravation in follow-up high-resolution magnetic resonance images of patients with intracranial atherosclerosis. *Cerebrovasc Dis*. (2022) 51:608–14. doi: 10.1159/000523725

31. Sano M. Complexity of inflammation in the trajectory of vascular disease: interleukin 6 and beyond. *Ann Vasc Dis*. (2023) 16:8–16. doi: 10.3400/avd.ra.23-00003

frontiers | Frontiers in Neurology

TYPE Original Research
PUBLISHED 06 August 2025
DOI 10.3389/fneur.2025.1603869

OPEN ACCESS

EDITED BY
Mingming Lu,
Characteristic Medical Center of Chinese People's Armed Police Force, China

REVIEWED BY
David C. Lauzier,
UCLA Health System, United States
Tijana Nastasovic,
University of Belgrade, Serbia
Mingang Zou,
Ganzhou People's Hospital, China

*CORRESPONDENCE
Jiwoong Oh
✉ nsojw@yuhs.ac

†These authors have contributed equally to this work and share first authorship

RECEIVED 01 April 2025
ACCEPTED 11 July 2025
PUBLISHED 06 August 2025

CITATION
Kim J, Kim S, Jang CK, Han HJ, Park KY, Kim J-J, Kim YB and Oh J (2025) Clinical implications and prognostic value of mastoid effusion in the management of aneurysmal subarachnoid hemorrhage.
Front. Neurol. 16:1603869.
doi: 10.3389/fneur.2025.1603869

Clinical implications and prognostic value of mastoid effusion in the management of aneurysmal subarachnoid hemorrhage

Junhyung Kim[1†], Sohyun Kim[2†], Chang Ki Jang[1], Hyun Jin Han[1], Keun Young Park[1], Jung-Jae Kim[1], Yong Bae Kim[1] and Jiwoong Oh[1*]

[1]Department of Neurosurgery, Yonsei University College of Medicine, Seoul, Republic of Korea, [2]Department of Physiology, Yonsei University College of Medicine, Seoul, Republic of Korea

Background: The clinical significance of mastoid effusion (ME) in intensive care unit (ICU) patients has not been well elucidated. Recently, an association between ME and intracranial pressure (ICP) has been reported. We aimed to investigate the clinical implications of ME occurrence in the management of aneurysmal subarachnoid hemorrhage (aSAH) patients and its association with their prognosis.

Methods: Data from patients aged > 18 years who were treated for aSAH in a single institution between January 2020 and December 2022 were retrospectively reviewed. Brain CT or MRI images obtained within the first 14 days after the onset of SAH were evaluated for the presence of ME, which is defined as either opacification or an air-fluid level in the mastoid air cells. We examined the patients' demographic information, neurological and medical status at admission, aneurysm and treatment characteristics, and clinical outcomes. We then analyzed how these factors were associated with the occurrence of ME.

Results: A total of 114 patients were included in the study. ME was observed in 40 patients (34.5%) within the first 14 days, occurring at a mean of 5.0 ± 3.5 days after the onset of SAH. In multivariate analysis, patients with ME were found to have a higher incidence of tracheostomy (odds ratio [OR] 10.034, $p = 0.024$), radiologic vasospasm (OR 4.987, $p = 0.018$), a higher APACHE II score (OR 1.138, $p = 0.013$), and poor clinical outcomes (OR 4.289, $p = 0.041$), defined as modified Rankin Scale score > 2 at 90 days. Poor clinical outcomes were independently associated with ME (OR 5.003, $p = 0.006$).

Conclusion: This study demonstrated that ME was observed in 34.5% of aSAH patients and was associated with poor clinical outcomes. ME may serve as a simple and useful prognostic indicator for predicting poor outcomes in aSAH patients.

KEYWORDS

mastoid effusion, middle ear effusion, intracranial pressure, subarachnoid hemorrhage, aneurysm, vasospasm

Introduction

Mastoid effusion (ME) occurs frequently along with middle ear effusion in children as a consequence of the accumulation of transudate caused by negative pressure or inflammation in the middle ear (1). Due to the differences in the orientation, length, and function of the Eustachian tube, ME is not a common finding in healthy adults, with an incidence of approximately 1% (2, 3). However, several studies have demonstrated that the incidence of ME is higher in intensive care unit (ICU) patients than in general population. Risk factors for the development of ME in ICU patients include old age, increased mucus secretion caused by prolonged endotracheal intubation for mechanical ventilation and a nasogastric tube, prolonged ICU stay, and altered mental status, many of which can be attributed to the anatomical connection of the middle ear space and the nasopharynx via the Eustachian tube (2, 4, 5).

Anatomical continuity also exists between the subarachnoid space and the cochlear aqueduct of the middle ear, and it provides the background for the development of a non-invasive tool for monitoring intracranial pressure (ICP) by measuring the tympanic membrane pressure (6, 7). Moreover, a recent study reported that elevated levels of ICP was associated with the occurrence of ME in neuro-ICU patients (8). Therefore, it can be postulated that the occurrence of ME in patients with neurologic insults who are at a risk of ICP variation may offer additional information regarding the clinical course and outcomes.

Subarachnoid hemorrhage (SAH) due to intracranial aneurysm rupture is a disastrous event with high morbidity and mortality rates (9, 10). A rupture of an aneurysm causes an abrupt and delayed increase in ICP, resulting in impaired cerebral perfusion and temporary intracranial circulatory arrest (11). Increased ICP plays an important role in the clinical course of aneurysmal subarachnoid hemorrhage (aSAH) patients, as it is related to common complications of aSAH such as acute hydrocephalus or delayed cerebral ischemia, which mostly occur in the first 14 days after the ictus. We hypothesized that patients receiving aSAH management who developed ME in the first 14 days would demonstrate unfavorable clinical outcomes. The purpose of this study was to investigate the incidence and the clinical significance of ME in patients with aSAH.

Methods

This retrospective study was approved by our Institutional Review Board and was performed under the guidelines outlined in the Declaration of Helsinki. The diagnosis of ME was based on the criteria proposed by J. Gossner, and only cases classified as "marked" (i.e., fluid signal involving more than half of the mastoid air cells) were considered ME-positive. By including only clearly defined cases, we minimized subjectivity in the interpretation. Accordingly, there was no interobserver disagreement between the neurovascular specialist and the neuro-intensivist who independently reviewed the images. This study follows the STROBE guidelines for retrospective studies.

Abbreviations: APACHE II, Initial Acute Physiology and Chronic Health Evaluation II; aSAH, aneurysmal subarachnoid hemorrhage; CI, confidence interval; GCS, Glasgow Coma Scale; ICP, intracranial pressure; ICU, intensive care unit; ME, mastoid effusion; mRS, modified Rankin Scale; OR, odds ratio.

Study population

Patient data between January 2020 and December 2022 were obtained from our institution's prospectively maintained aSAH database. Adult patients over the age of 18 who were admitted to the neuro-ICU of our institution for the treatment and management of aSAH were included. The exclusion criteria were as follows: (1) incomplete medical records, (2) transfer to our institution more than 1 day after the onset of aSAH, and (3) absence of follow-up brain computed tomography (CT) or magnetic resonance imaging (MRI) within 14 days to assess for ME.

Management of aSAH patients

We adhered to the standard treatment strategy for aSAH. All patients who presented with acute-phase aSAH were admitted to the neuro-ICU and received cerebral angiography within 24 h, unless contraindicated. Except for those who did not wish to receive surgical or endovascular treatment, patients received microsurgery or endovascular treatment to secure the ruptured aneurysm. To manage increased ICP, external ventricular drainage, lumbar drainage, or decompressive surgery was performed. Intravenous or oral nimodipine was administered to prevent post-SAH vasospasm. Brain CT, brain MRI, or magnetic resonance angiography (MRA) were conducted when necessary. Patients with a good initial Hunt–Hess grade who were expected to be at a low risk for post-SAH complications were transferred to the general ward as early as 3 to 7 days after ictus, but those at moderate to high risk were monitored in the neuro-ICU for at least 10 to 14 days.

Radiological assessment for ME and vasospasm

Non-contrast brain CT or brain CT angiography was the primary modality for radiologic evaluation of aSAH patients, with brain MRI or MRA performed as needed. The presence of ME was defined as partial or complete opacification of the mastoid air cell cavity, showing an air-fluid level in non-contrast brain CT, or high signal intensity in T2-weighted MR images on either or both sides. The images obtained within the first 14 days after the onset of SAH were independently reviewed by a neurovascular specialist and a neuro-intensivist. They assessed the presence of ME and reached consensus through discussion.

Radiologic vasospasm was evaluated using a standardized institutional protocol. Daily transcranial Doppler (TCD) monitoring was performed in all patients. If TCD findings were suggestive of vasospasm, CTA was immediately performed to confirm the diagnosis. In patients without vasospasm findings on TCD, routine CTA was performed approximately 1 to 2 weeks after the day of rupture to evaluate vascular status. Vasospasm was ultimately diagnosed when luminal narrowing of ≥30% was observed on CTA compared to baseline vascular imaging.

Clinical assessment

At admission, the Glasgow Coma Scale (GCS) and Hunt–Hess grade, as well as the Acute Physiology and Chronic Health Evaluation II (APACHE II) scores, were used to assess the initial neurological

condition. The duration of neuro-ICU stay and mechanical ventilation, ventriculoperitoneal shunt within 90 days, and modified Rankin Scale (mRS) score at 90 days were recorded. We defined poor clinical outcome as 90-day mRS > 2. Symptomatic vasospasm was diagnosed when vasospasm was radiologically confirmed and patients revealed neurological worsening with no other identifiable causes (12).

Statistical analysis

Statistical analysis was performed using SPSS Statistics 25.0 (IBM). Fisher's exact test or χ (2) test was performed for categorical variables. Mann–Whitney U-test or Student's *t*-test was performed for continuous variables of clinical outcomes and the univariate analysis of the factors associated with ME and poor clinical outcomes. All variables with clinical importance were introduced into a multivariate analysis using the binary logistic regression method. A *p*-value of < 0.05 was considered statistically significant.

Results

Patient and aneurysm characteristics

During the study period, 121 patients with ruptured intracerebral aneurysms were treated in our institution. Excluding one patient who was transferred to our institution a few days after the onset of aSAH and six patients who had not taken any follow-up brain CT or MRI images, a total of 114 patients (mean age, 59.5 ± 14.2 years; male/female ratio = 35:79) treated for aSAH were included for analysis. A total of 62 patients (54.4%) initially presented with a Hunt–Hess grade greater than 2 at admission. The majority of the aneurysms were saccular (n = 110, 96.5%) in the anterior circulation (n = 95, 83.3%). These characteristics are summarized in Table 1.

TABLE 1 Patient and aneurysm characteristics.

Variables	Values
Patients	114
Age, mean	59.5 ± 14.2
Male sex, *n* (%)	35 (31.7)
Comorbidities, *n* (%)	
Hypertension	47 (41.2)
Diabetes mellitus	9 (7.9)
Dyslipidemia	18 (15.8)
Smoking	23 (20.2)
Aneurysm location, *n* (%)	
Anterior circulation	95 (83.3)
Posterior circulation	19 (16.7)
Aneurysm type, *n* (%)	
Saccular	110 (96.5)
Mycotic	1 (0.9)
Dissecting	3 (2.6)
Initial Hunt–Hess Grade, *n* (%)	
1	0 (0)
2	52 (45.6)
3	34 (29.8)
4	24 (21.1)
5	4 (3.5)
Initial GCS, median	14 (11–15)
APACHE II score, mean	17.2 ± 7.9

Values are presented in mean ± standard deviation, median (interquartile range), or number (%).
APACHE II, Initial Acute Physiology and Chronic Health Evaluation II; GCS, Glasgow Coma Scale.

Treatment characteristics and outcomes

Endovascular treatment was the dominant modality (81.6%) for securing ruptured aneurysms. A total of 24 patients (21.1%) received ventriculoperitoneal shunt operation within 90 days, and 16 patients (14.0%) received tracheostomy. Patients were treated in the neuro-ICU for a median duration of 13 days (interquartile range [IQR] 8–19 days). ME was observed in 40 patients (34.5%) at a mean of 5.0 ± 3.5 days after the onset of aSAH. Poor clinical outcomes were demonstrated by 41 patients (36.0%). These characteristics are summarized in Table 2.

TABLE 2 Treatment characteristics and outcomes.

Variables	Values
Treatment modality, *n* (%)	
Microsurgery	21 (18.4)
Endovascular treatment	93 (81.6)
Extraventricular drainage, *n* (%)	36 (31.6)
Ventriculoperitoneal shunt, *n* (%)	24 (21.1)
Tracheostomy, *n* (%)	16 (14.0)
Neuro-ICU stay duration, median, days	13 (8–19)
ME within first 14 days (%)	40 (34.5)
Interval between aSAH and ME, mean, days	5.0 ± 3.5
Poor clinical outcome*, *n* (%)	41 (36)

Values are presented in mean ± standard deviation, median (interquartile range), or number (%).
aSAH; aneurysmal subarachnoid hemorrhage; ICU, intensive care unit; ME, mastoid effusion.
*Poor clinical outcome was defined as a 90-day modified Rankin Scale > 2.

Factors associated with the occurrence of ME

In univariate analysis, the occurrence of ME was statistically associated with older age (p = 0.002), male sex (p = 0.034), and ruptured aneurysms in the posterior circulation (p = 0.005). Patients with ME had a higher likelihood of presenting with an initial Hunt–Hess grade > 2 (80.0% vs. 40.5%, p < 0.001), higher APACHE II scores (22.2 ± 8.3 vs. 14.5 ± 6.2, p < 0.001), and longer durations of neuro-ICU stay (19 days vs. 10 days, p < 0.001) and mechanical ventilation (13 days vs. 0 days, p < 0.001) compared to those without ME. Furthermore, the rates of radiologic vasospasm and symptomatic vasospasm were significantly higher in patients with ME compared to those without ME (50.0% vs. 18.5%, p = 0.002 for radiologic vasospasm; 30.0% vs. 7.7%, p = 0.01 for symptomatic vasospasm). Terson's syndrome was

diagnosed in two patients, both of whom developed ME. ME was associated with poor clinical outcomes at 90 days ($p < 0.001$). There was no significant relationship between the occurrence of ME and the types of treatment modality for securing the aneurysms. In multivariate analysis, tracheostomy (odds ratio [OR] 10.034, $p = 0.024$), radiologic vasospasm (OR 4.987, $p = 0.018$), a higher APACHE II score (OR 1.138, $p = 0.013$), and a poor clinical outcome (OR 4.289, $p = 0.041$) were independently associated with ME occurrence. These results are summarized in Table 3 and Figure 1.

Factors associated with poor clinical outcomes

Univariate analysis revealed that a poor clinical outcome was associated with several factors that have been known as risk factors for aSAH, such as older age ($p < 0.001$), posterior circulation aneurysm ($p = 0.007$), and a higher Hunt–Hess grade ($p < 0.001$). Compared to patients who had good clinical outcomes, those with poor clinical outcomes had prolonged neuro-ICU care (10 vs. 19 days, $p < 0.001$) and mechanical ventilation (0 vs. 12 days, $p < 0.001$) and experienced a higher occurrence of ME (15.1% vs. 70.7%, $p < 0.001$). In multivariate analysis, along with older age (OR 1.081, $p = 0.001$) and Hunt–Hess grade > 2 (OR 4.515, $p = 0.014$), ME occurrence (OR 5.003, $p = 0.006$) was statistically associated with a poor clinical outcome. These results are presented in Table 4.

Subgroup analysis by neurological grade and treatment modality

To further explore the relationship between mastoid effusion (ME) and neurological severity at admission, a subgroup analysis was conducted based on the Hunt–Hess (HH) grade. Patients were categorized into two groups: HH $\leq$ 2 and HH > 2. The occurrence of ME was significantly higher in the HH > 2 group (51.6%) compared to the HH $\leq$ 2 group (15.4%) ($p < 0.001$), suggesting a strong association between a poor neurological grade and the presence of ME.

In addition, a subgroup analysis was performed among 94 patients who underwent endovascular treatment. In this subgroup, multivariate logistic regression revealed that the presence of ME was an independent predictor of poor clinical outcomes (OR, 4.079; 95% CI, 1.060–15.691; $p = 0.041$), even after adjusting for age, initial Glasgow Coma Scale (GCS) score, and HH grade (Table 5). These findings support the prognostic significance of ME in patients with aSAH, particularly those treated with endovascular intervention.

Discussion

In this retrospective study, we found that ME occurred in 34.5% of aSAH patients within the first 14 days (mean 5.0 ± 3.5 days) and was associated with radiologic vasospasm and poor clinical outcomes. Moreover, along with older age and a poor Hunt–Hess grade, ME was an independent risk factor for poor clinical outcomes in aSAH patients.

Several studies have reported a higher incidence of ME in ICU patients than in the healthy adult population, ranging between 10.3 and 53% (2, 8, 13). Risk factors for the development of ME include thickened oropharyngeal secretions due to mucosal irritation by endotracheal intubation and nasogastric tube, and decreased mentality impairing the patient's ability to clear excessive mucosal secretion and to open the Eustachian tube, which are hardly modifiable (2, 4, 13). Although ME can potentially cause acute mastoiditis and develop into intracranial complications such as meningitis, empyema, and brain abscess (14), incidentally detected MEs are rarely related to temporal bone disease (15). ME observed in ICU patients is considered benign in most cases, obscuring its clinical significance (2, 13). This study, however, showed that ME was independently associated with poor clinical outcomes in aSAH patients. Patients who suffer aSAH are usually hospitalized for 14 to 21 days due to the possible occurrence of delayed complications (16), allowing prognostication to be made at least 14 days after the ictus in most cases. In conjunction with the established risk factors for poor outcomes in aSAH patients, such as Hunt–Hess score, increasing age, and ruptured posterior circulation aneurysm, the occurrence of ME may offer an additional prognostic value.

Recently, Jung et al. suggested that increased ICP was associated with ME occurrence in patients who underwent intracranial surgery (8). The authors revealed that the prediction model for the development of ME improved when peak ICP values were included in the model. Timely recognition and proper management of increased ICP are critical for improving clinical outcomes in patients with aSAH. However, most widely used ICP monitoring tools, such as external ventricular drainage, are invasive, and it is often a dilemma whether to place invasive ICP monitoring devices due to the risks of infection or hemorrhage (17, 18). It has been recognized that ICP is transmitted to the perilymphatic space in the middle ear, and the middle ear pressure represented by tympanic membrane displacement can be utilized for the indirect measurement of ICP (6, 19). Assuming that the occurrence of ME reflects increased ICP, a clinician may conduct additional evaluations or procedures to assess the patient's ICP status, or ophthalmologic evaluation for the possibility of Terson's syndrome when ME is observed. Although this finding was not statistically significant, Terson's syndrome, a consequence of elevated ICP, was diagnosed in two patients who developed ME in this study. However, whether there is a causal relationship between elevated ICP and the development of ME is not known. A few studies attempted to explain the development of ME in patients with lateral sinus thrombosis as the result of venous congestion rather than the Eustachian tube dysfunction, as the laterality of the ME coincided with the intracranial lesions responsible for the elevated ICP (8, 20, 21). Such an explanation may not fit in other types of intracranial pathologies not involving venous congestion. From the anatomical perspective, the movement of cerebrospinal fluid from the subarachnoid space to the mastoid air cells via the middle ear due to a pressure gradient is theoretically possible. The relationship between elevated ICP and the development of ME, their mechanisms, and temporal associations should be further investigated to refine the clinical significance of ME in patients whose ICP assessments are critical.

Another finding in this study was that the occurrence of ME was associated with post-SAH vasospasm. Post-SAH vasospasm has multiple risk factors, including the amount of SAH, presence of intracranial hemorrhage and intraventricular hemorrhage, female sex, and increased ICP (22). Fukuhara et al. demonstrated that elevated

TABLE 3 Univariate and multivariate analyses for the risk factors of ME.

Variables	Univariate analysis			Multivariate analysis	
	No effusion (n = 74)	Effusion (n = 40)	p-value	OR (95% CI)	p-value
Age	56.5 ± 14.4	65.0 ± 12.2	0.002		
Male sex	18 (23.3)	17 (43.9)	0.034		
Comorbidities					
Hypertension	27 (36.5)	20 (50.0)	0.162		
Diabetes mellitus	6 (8.1)	3 (7.5)	>0.999		
Dyslipidemia	11 (14.9)	7 (17.5)	0.713		
Smoking	17 (23.0)	6 (15.0)	0.311		
Aneurysm in posterior circulation	7 (9.5)	12 (30.0)	0.005		
Initial Hunt–Hess Grade			<0.001		
≤ 2	44 (59.5)	8 (20.0)			
> 2	30 (40.5)	32 (80.0)			
Initial Intracranial pressure (mmHg)	20.9 ± 11.4 (n = 20)	19.2 ± 9.6 (n = 28)	0.107		
Initial GCS	15 (13–15)	8 (5–13)	<0.001		
Initial APACHE II	14.5 ± 6.2	22.2 ± 8.3	<0.001	1.138 (1.027–1.261)	0.013
Initial WBC	10,068 (3703)	11,888 (4439)	0.021		
Initial CRP†	3.5 (0.9–9.0)	3.3 (1.08–12.38)	0.787		
Initial DNI††	1.44 (2.96)	2.27 (3.23)	0.166		
Treatment modality for aneurysm			0.749		
Microsurgery	13 (17.6)	8 (20.0)			
Endovascular treatment	61 (82.4)	33 (82.5)	>0.999		
External ventricular drainage	13 (17.6)	23 (57.5)	<0.001		
Tracheostomy	2 (2.7)	14 (35.0)	<0.001	10.034 (1.352–74.448)	0.024
Ventriculoperitoneal shunt	9 (12.2)	15 (37.5)	0.002		
Hydrocephalus	15 (20.3)	27 (67.5)	<0.001		
Neuro-ICU stay duration (day)	10 (6–13)	19 (14–26)	<0.001		
Ventilator maintenance duration	0 (0–1)	13 (6–20)	<0.001		
Radiologic vasospasm*	12 (18.5)	15 (50.0)	0.002	4.987 (1.322–18.814)	0.018
Symptomatic vasospasm*	5 (7.7)	9 (30.0)	0.01		
Terson's syndrome	0 (0)	2 (5.0)	0.127		
Poor clinical outcome	12 (16.2)	29 (72.5)	<0.001	4.289 (1.061–17.333)	0.041

Values are presented as mean ± standard deviation, median (interquartile range), or number (%).
APACHE II, Initial Acute Physiology and Chronic Health Evaluation II; CI, confidence interval; CRP, C-reactive protein; DNI, delta neutrophil index; GCS, Glasgow Coma Scale; ICU, intensive care unit; OR, odds ratio; WBC, white blood cell.
† This variable was evaluated in 109 patients.
†† This variable was evaluated in 98 patients.
*This variable was evaluated in 95 patients.

ICP was associated with the development and the duration of vasospasm after aSAH (23). Similarly, Gambardella et al. showed that the use of osmotic diuretics to control ICP lowered the risk of developing delayed cerebral ischemia in patients with aSAH (24). On the other hand, Heuer et al. reported only a weak relationship between ICP and the development of angiographic or symptomatic vasospasm (25). The authors provided a few explanations for the weak link. They argue that patients with severely elevated ICP died before vasospasm could occur, or did not undergo follow-up angiographic evaluations. In our case, 8 patients (42.1%) out of 19 patients did not undergo follow-up angiography studies, as poor prognosis was expected.

The mean interval between the onset of aSAH and detection of ME was 5 days. Limited studies have reported the time for ME to develop in ICU patients. Jung et al. reported a mean of 11.1 days for the development of ME in patients who underwent intracranial surgery, and Huyett et al. described that ME was a late finding and prevalent in patients with a prolonged ICU stay (2, 8). Considering that elevated ICP contributes to the development of ME, it can

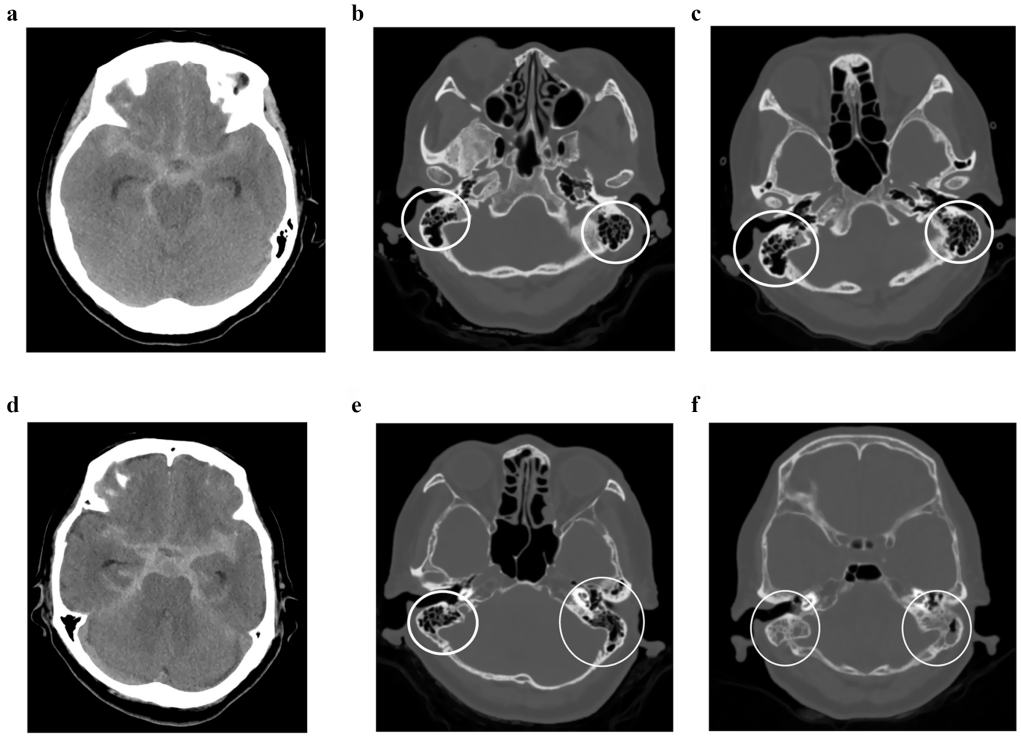

FIGURE 1
Mastoid effusion (ME) in patients with subarachnoid hemorrhage (SAH). **(a–c)** Case with absence of ME. A 66-year-old woman with an initial Fisher's grade III SAH. The initial brain CT scan showed no evidence of ME. A follow-up CT scan 2 week later also showed no signs of ME (white circle). The patient's modified Rankin Scale (mRS) score at post-operative 90 days was 0. **(d–f)** Case with the presence of ME. An 80-year-old woman with Fisher's grade III SAH on the initial CT scan, with no signs of ME. Two weeks later, a follow-up CT scan revealed bilateral ME (white circle). The patient had an mRS score of 4 at post-operative 90 days.

be postulated that ME in patients with neurological insults such as SAH would develop at an earlier period than in patients with other etiologies. Early brain injury after aSAH is known as a pathologic process that occurs in the first 72 h, and involves the elevation of ICP, reduction of cerebral blood flow, and neuronal cell death (26). SAH-induced vasospasms usually occur 4 to 14 days after the ictus, with a peak incidence at 7 days (27). The relationship between the early phase of brain injury and the development of ME should be further described in future studies.

Although our findings suggest that mastoid effusion (ME) is associated with poor outcomes and angiographic vasospasm in patients with aSAH, the exact pathophysiological mechanisms underlying ME development in neurologically injured patients remain uncertain. It has been hypothesized that elevated intracranial pressure (ICP) or impaired cerebrospinal fluid drainage may contribute to fluid accumulation within mastoid air cells. However, this mechanism has not yet been established in the existing literature.

Given the routine use of non-contrast brain CT in the acute-phase SAH, ME may serve as a readily identifiable imaging marker that reflects disease severity or elevated ICP, particularly in patients without invasive monitoring. While ME is not a direct therapeutic target, its presence may have potential implications for early risk stratification and the intensity of subsequent monitoring or intervention. Nonetheless, this study was not designed to establish a causal mechanism or to propose a clinical algorithm based on ME findings. Further prospective studies are needed to clarify the biological basis of ME in this patient population and to determine how it may be effectively incorporated into clinical decision-making processes. We acknowledge this limitation and have highlighted the need for future research in this area.

Previous studies have suggested a potential correlation between mastoid effusion (ME) and elevated intracranial pressure (ICP), implying that ME may serve as an indirect radiological marker of increased ICP in patients with acute brain injury (8). One proposed mechanism is that a pressure gradient between the subarachnoid space and the middle ear cavity could facilitate the movement of cerebrospinal fluid (CSF) into the mastoid air cells, resulting in effusion. Furthermore, elevated ICP has been linked to both the occurrence and persistence of cerebral vasospasm following aSAH, potentially explaining the association between ME and poor outcomes observed in this study.

To further explore this hypothesis, we analyzed available ICP data in relation to ME status (Table 3). The mean ICP was 20.9 ± 11.4 mmHg in the ME-negative group and 19.2 ± 9.6 mmHg in the ME-positive group, with no statistically significant difference. This finding should be interpreted cautiously for several reasons. First, the timing of ICP measurement and the detection of ME on imaging did not always coincide, limiting a temporal correlation. Second, most patients underwent intensive ICP-lowering interventions, including osmotherapy, targeted temperature management, and coma therapy,

10.3389/fneur.2025.1603869

TABLE 4 Univariate and multivariate analyses for risk factors of poor clinical outcome in aSAH patients.

Variables	Univariate analysis			Multivariate analysis	
	Good outcome (n = 73)	Poor outcome (n = 41)	p-value	OR (95% CI)	p-value
Age	55.0 ± 13.6	67.5 ± 11.4	<0.001	1.081 (1.032–1.132)	0.001
Male sex	22 (31.1)	13 (31.7)	>0.999		
Comorbidities			0.406		
Hypertension	29 (38.4)	19 (46.3)			
Diabetes mellitus	4 (5.5)	5 (12.2)	0.279		
Dyslipidemia	8 (11.0)	10 (24.4)	0.059		
Smoking	19 (26.0)	4 (9.8)	0.038		
Aneurysm in the posterior circulation	7 (9.6)	12 (29.3)	0.007		
Initial Hunt–Hess Grade			<0.001		
≤ 2	44 (60.3)	8 (19.5)			
> 2	29 (39.7)	33 (80.5)		4.515 (1.357–15.030)	0.014
Initial GCS	15 (13–15)	9 (5–13.5)	<0.001		
Initial APACHE II	14.3 ± 6.3	22.5 ± 7.8	<0.001		
Initial WBC	10,616 ± 3,823	10,914 ± 4,494	0.839		
Initial CRP†	3.5 (1.05–9.35)	3.5 (1.03–9.00)	0.905		
Initial DNI††	1.44 ± 2.81	2.29 ± 3.47	0.152		
Treatment modality for aneurysm			0.822		
Microsurgery	13 (17.8)	8 (19.5)			
Endovascular treatment	60 (82.2)	34 (82.9)			
External ventricular drainage	15 (20.5)	21 (51.2)	0.001		
Tracheostomy	3 (4.1)	13 (31.7)	<0.001		
Ventriculoperitoneal shunt	10 (13.7)	14 (34.1)	0.01		
Neuro-ICU stay duration	10 (5–13)	19 (13–26)	<0.001		
Ventilator maintenance duration	0 (0–1)	12 (2–19)	<0.001		
Radiologic vasospasm*	16 (25.0)	11 (35.5)	0.288		
Symptomatic vasospasm*	7 (10.9)	7 (22.6)	0.215		
ME	11 (15.1)	29 (70.7)	<0.001	5.003 (1.570–15.935)	0.006

Values are presented as mean ± standard deviation, median (interquartile range), or number (%).
aSAH, aneurysmal subarachnoid hemorrhage; APACHE II, Initial Acute Physiology and Chronic Health Evaluation II; CI, confidence interval; CRP, C-reactive protein; DNI, delta neutrophil index; GCS, Glasgow Coma Scale; ICU, intensive care unit; ME, mastoid effusion; OR, odds ratio; WBC, white blood cell.
† This variable was evaluated in 109 patients.
†† This variable was evaluated in 98 patients.
*This variable was evaluated in 95 patients.

which may have modified or masked actual ICP values. These factors likely contributed to the lack of observed statistical significance.

Nevertheless, we believe that ME may still reflect transient or unrecorded ICP elevations, particularly in patients without invasive monitoring. Given that non-contrast brain CT is routinely performed in the acute phase of aSAH, the detection of ME may provide a non-invasive and easily accessible clue suggesting raised ICP, especially in resource-limited settings.

Importantly, the pathophysiology of ICP elevation in aSAH differs from that of other neurological conditions such as traumatic brain injury or ischemic stroke. In aSAH, abrupt ICP elevation can occur due to aneurysmal rupture and subsequent hydrocephalus and can fluctuate rapidly with events such as rebleeding, vasospasm, or therapeutic interventions. These unique dynamics complicate the interpretation of single-timepoint ICP data but underscore the potential value of adjunctive imaging markers such as ME.

This study has several limitations. Due to its retrospective design and small sample size, selection and information bias were unavoidable, as the details of management and follow-up strategies for aSAH patients varied. For example, the follow-up non-contrast brain CT imaging intervals varied between patients, obscuring the precise timing of ME development, and only 83.3% (95/114) of the patients underwent follow-up angiography studies at irregular intervals to be evaluated for the occurrence of vasospasm. In asymptomatic patients with longstanding mastoid effusion resulting from conditions such as chronic otitis media, the absence of prior imaging may lead to

TABLE 5 Univariate and multivariate analyses of risk factors for poor clinical outcome in aSAH patients treated with endovascular treatment.

Variables	Univariate analysis			Multivariate analysis	
	Good outcome (n = 60)	Poor outcome (n = 34)	p-value	OR (95% CI)	p-value
Age	55.0 ± 14.1	67.6 ± 11.5	<0.001	1.093 (1.030–1.159)	0.003
Male sex	19 (31.7)	11 (32.4)	0.945		
Comorbidities					
Hypertension	25 (41.7)	17 (50.0)	0.435		
Diabetes mellitus	4 (6.7)	5 (14.7)	0.277		
Dyslipidemia	8 (13.3)	10 (29.4)	0.057		
Smoking	14 (23.3)	3 (8.8)	0.079		
Aneurysm in the posterior circulation	7 (11.7)	12 (35.3)	0.006		
Initial Hunt–Hess Grade > 2	24 (40.0)	29 (85.3)	<0.001	4.686 (1.032–21.279)	0.045
Initial GCS	15 (13–15)	8 (4.25–13)	<0.001	4.515 (1.357–15.030)	0.014
Initial APACHE II	14.8 ± 6.3	23.6 ± 7.9	<0.001		
Initial WBC	10,423 ± 3,766	11,176 ± 4,385	0.382		
Initial CRP	3.8 (1.1–11.7)	3.5 (1.0–9.0)	0.662		
Initial DNI	1.46 ± 2.88	1.90 ± 3.14	0.496		
External ventricular drainage	10 (16.7)	18 (52.9)	0.001		
Tracheostomy	2 (3.3)	11 (32.4)	<0.001		
Ventriculoperitoneal shunt	9 (15.0)	13 (38.2)	0.011		
Neuro-ICU stay duration	10 (5–13)	20.5 (13.25–29)	<0.001		
Ventilator maintenance duration	0 (0–1)	12.5 (3–19.75)	<0.001		
Radiologic vasospasm*	11 (20.4)	8 (32.0)	0.261		
Symptomatic vasospasm*	4 (7.4)	4 (16.0)	0.254		
ME	9 (15.0)	24 (70.6)		4.079 (1.060–15.691)	0.041

Values are presented as mean ± standard deviation, median (interquartile range), or number (%).
APACHE II, Initial Acute Physiology and Chronic Health Evaluation II; CI, confidence interval; CRP, C-reactive protein; DNI, delta neutrophil index; GCS, Glasgow Coma Scale; ICU, intensive care unit; ME, mastoid effusion; OR, odds ratio; WBC, white blood cell. *This variable was evaluated in 79 patients.

misclassification of ME as a newly developed finding. While ME could be ruled out through comparison with previous imaging in patients who underwent serial follow-up studies, this was not feasible in newly admitted patients without prior imaging. The likelihood of pre-existing mastoiditis was presumed to be comparable between the two groups. Furthermore, as mastoid effusion grade 2 or higher was defined as ME-positive in this study, cases of mild mastoiditis were likely excluded. Patients with a documented history of otitis media were also excluded based on a thorough review of medical records. In our dataset, only 5 out of the 40 patients with ME showed evidence of ME on their initial brain CT. Although it was not possible to determine whether these cases represented pre-existing ME, all five patients demonstrated progression of ME on follow-up imaging.

Another limitation is the potential subjectivity in the radiologic diagnosis of ME. To address this limitation, only clearly defined cases meeting the "marked" criteria proposed by Gossner—defined as a fluid signal involving more than half of the mastoid air cell cavity—were included (28). All imaging was independently assessed by a neurovascular specialist and a neurointensivist, and there was complete agreement between the two evaluators. Therefore, a formal consistency test was not conducted. Additionally, although a quantitative threshold such as the Hounsfield unit (HU) could be useful, variability in CT protocols and scanner calibration limited its application in this retrospective analysis. Finally, some factors that may influence the development of ME—such as the presence of nasogastric tubes or ICP values—were not included in this study. In particular, the absence of ICP data may limit the ability to fully explore the relationship between ME and elevated intracranial pressure. Despite these limitations, ME was found to be independently associated with poor outcomes and cerebral vasospasm in patients with aSAH. Further studies are warranted to clarify the underlying mechanisms linking ME with elevated levels of ICP and to validate its role as a prognostic marker.

Conclusion

This study demonstrated that the occurrence of ME in aSAH patients was independently associated with tracheostomy, vasospasm, and poor clinical outcomes. Given that ME can be easily identified on non-contrast brain CT early in the clinical course, it

may serve as an additional imaging marker for prognosis in aSAH patients.

Data availability statement

The data that support the findings of this study are available from the corresponding author upon reasonable request.

Ethics statement

The studies involving humans were approved by Yonsei University Institutional Review Board (Approval number: 4-2021-0346). The studies were conducted in accordance with the local legislation and institutional requirements. The ethics committee/institutional review board waived the requirement of written informed consent for participation from the participants or the participants' legal guardians/next of kin due to the retrospective nature of the study.

Author contributions

JK: Data curation, Writing – review & editing, Writing – original draft, Supervision. SK: Investigation, Writing – review & editing, Writing – original draft, Project administration, Software, Data curation. CKJ: Conceptualization, Writing – review & editing, Writing – original draft, Data curation, Visualization, Project administration. HJH: Writing – original draft, Data curation, Supervision, Formal analysis. KYP: Project administration, Writing – original draft, Resources, Writing – review & editing, Investigation. J-JK: Writing – review & editing, Methodology, Writing – original draft, Investigation, Formal analysis, Resources, Project administration. YBK: Validation, Supervision, Writing – review & editing, Visualization, Software, Writing – original draft. JO: Writing – original draft, Writing – review & editing.

Funding

The author(s) declare that no financial support was received for the research and/or publication of this article.

Conflict of interest

The authors declare that the research was conducted in the absence of any commercial or financial relationships that could be construed as a potential conflict of interest.

Generative AI statement

The authors declare that no Gen AI was used in the creation of this manuscript.

Publisher's note

References

1. Bluestone CD, Beery QC, Andrus WS. Mechanics of the Eustachian tube as it influences susceptibility to and persistence of middle ear effusions in children. *Ann Otol Rhinol Laryngol.* (1974) 83:Suppl 11:27–34. doi: 10.1177/0003489474083s1103

2. Huyett P, Raz Y, Hirsch BE, McCall AA. Radiographic mastoid and middle ear effusions in intensive care unit subjects. *Respir Care*. (2017) 62:350–6. doi: 10.4187/respcare.05172

3. Lee DH, Jun BC, Park JO, Yeo SW. Magnetic resonance imaging of the mastoid cavity and middle ear: prevalence and clinical significance of incidental abnormal findings in a nonotolaryngologic adult and pediatric population. *J Otolaryngol.* (2006) 35:13–8. doi: 10.2310/7070.2005.4131

4. González Pena M, Figuerola Massana E, Hernández Gutiérrez P, Rello CJ. Middle ear effusion in mechanically ventilated patients: effects of the nasogastric tube. *Respir Care*. (2013) 58:273–8. doi: 10.4187/respcare.01911

5. Lin CC, Lin CD, Cheng YK, Tsai MH, Chang CS. Middle ear effusion in intensive care unit patients with prolonged endotracheal intubation. *Am J Otolaryngol*. (2006) 27:109–11. doi: 10.1016/j.amjoto.2005.07.021

6. Gwer S, Sheward V, Birch A, Marchbanks R, Idro R, Newton CR, et al. The tympanic membrane displacement analyser for monitoring intracranial pressure in children. *Childs Nerv Syst*. (2013) 29:927–33. doi: 10.1007/s00381-013-2036-5

7. Evensen KB, Paulat K, Prieur F, Holm S, Eide PK. Utility of the tympanic membrane pressure waveform for non-invasive estimation of the intracranial pressure waveform. *Sci Rep*. (2018) 8:15776. doi: 10.1038/s41598-018-34083-6

8. Jung H, Jang KM, Ko MJ, Choi HH, Nam TK, Kwon JT, et al. Relationship between increased intracranial pressure and mastoid effusion. *J Korean Neurosurg Soc*. (2020) 63:640–8. doi: 10.3340/jkns.2020.0067

9. Macdonald RL, Diringer MN, Citerio G. Understanding the disease: aneurysmal subarachnoid hemorrhage. *Intensive Care Med*. (2014) 40:1940–3. doi: 10.1007/s00134-014-3483-5

10. Suarez JI, Tarr RW, Selman WR. Aneurysmal subarachnoid hemorrhage. *N Engl J Med*. (2006) 354:387–96. doi: 10.1056/NEJMra052732

11. Magni F, Pozzi M, Rota M, Vargiolu A, Citerio G. High-resolution intracranial pressure burden and outcome in subarachnoid hemorrhage. *Stroke*. (2015) 46:2464–9. doi: 10.1161/STROKEAHA.115.010219

12. Shirao S, Yoneda H, Ishihara H, Kajiwara K, Suzuki M. Survey study members of Japan neurosurgical S. A proposed definition of symptomatic vasospasm based on treatment of cerebral vasospasm after subarachnoid hemorrhage in Japan: consensus 2009, a project of the 25 spasm symposium. *Surg Neurol Int*. (2011) 2:74–4. doi: 10.4103/2152-7806.81968

13. Kesser BW, Woodard CR, Stowell NG, Becker SS. Middle ear effusion in adult ICU patients: a cohort study. *Ear Nose Throat J*. (2013) 92:340–6. doi: 10.1177/014556131309200807

14. Luntz M, Bartal K, Brodsky A. Shihada R (acute mastoiditis: the role of imaging for identifying intracranial complications). *Laryngoscope*. (2012) 122:2813–7. doi: 10.1002/lary.22193

15. Wilkinson SL, Sahota RS, Constable JD, Harper F, Judd O. Does incidental mastoid opacification on computerized tomography necessitate referral to ENT? *Laryngoscope*. (2017) 127:2860–5. doi: 10.1002/lary.26594

16. Diringer MN, Bleck TP, Hemphill JC III, Menon D, Shutter L, Vespa P, et al. Critical care management of patients following aneurysmal subarachnoid hemorrhage: recommendations from the Neurocritical Care Society's multidisciplinary consensus conference. *Neurocrit Care*. (2011) 15:211–240. doi: 10.1007/s12028-011-9605-9

17. Czosnyka M, Pickard JD. Monitoring and interpretation of intracranial pressure. *J Neurol Neurosurg Psychiatry*. (2004) 75:813–21. doi: 10.1136/jnnp.2003.033126

18. Nag DS, Sahu S, Swain A, Kant S. Intracranial pressure monitoring: gold standard and recent innovations. *World J Clin Cases*. (2019) 7:1535–53. doi: 10.12998/wjcc.v7.i13.1535

19. Traboulsi R, Avan P. Transmission of infrasonic pressure waves from cerebrospinal to intralabyrinthine fluids through the human cochlear aqueduct: non-invasive measurements with otoacoustic emissions. *Hear Res*. (2007) 233:30–9. doi: 10.1016/j.heares.2007.06.012

20. Agid R, Farb RI. Mastoid effusion associated with dural sinus thrombosis. *Eur Radiol*. (2005) 15:755–8. doi: 10.1007/s00330-004-2505-z

21. Fink JN, McAuley DL. Mastoid air sinus abnormalities associated with lateral venous sinus thrombosis: cause or consequence? *Stroke*. (2002) 33:290–2. doi: 10.1161/hs0102.101016

22. Inagawa T. Risk factors for cerebral vasospasm following aneurysmal subarachnoid hemorrhage: a review of the literature. *World Neurosurg*. (2016) 85:56–76. doi: 10.1016/j.wneu.2015.08.052

23. Fukuhara T, Douville CM, Eliott JP, Newell DW, Winn HR. Relationship between intracranial pressure and the development of vasospasm after aneurysmal subarachnoid hemorrhage. *Neurol Med Chir (Tokyo)*. (1998) 38:710-5. doi: 10.2176/nmc.38.710

24. Gambardella G, De Blasi F, Caruso G, Zema A, Turiano F, Collufio D. Intracranial pressure, cerebral perfusion pressure, and SPECT in the management of patients with SAH hunt and Hess grades I-II. *Acta Neurochir Suppl*. (1998) 71:215–8. doi: 10.1007/978-3-7091-6475-4_62

25. Heuer GG, Smith MJ, Elliott JP, Winn HR, Leroux PD. Relationship between intracranial pressure and other clinical variables in patients with aneurysmal subarachnoid hemorrhage. *J Neurosurg*. (2004) 101:408–16. doi: 10.3171/jns.2004.101.3.0408

26. Pluta RM, Hansen-Schwartz J, Dreier J, Vajkoczy P, Macdonald RL, Nishizawa S, et al. Cerebral vasospasm following subarachnoid hemorrhage: time for a new world of thought. *Neurol Res*. (2009) 31:151–8. doi: 10.1179/174313209X393564

27. Sviri GE, Britz GW, Lewis DH, Newell DW, Zaaroor M. Cohen W (dynamic perfusion computed tomography in the diagnosis of cerebral vasospasm). *Neurosurgery*. (2006) 59:319–25. doi: 10.1227/01.NEU.0000222819.18834.33

28. Gossner J. Fluid signal in the mastoid is a common incidental finding on MRI of the brain. *Eur Arch Otorhinolaryngol*. (2019) 276:611–2. doi: 10.1007/s00405-018-5197-8

frontiers | Frontiers in Neurology

TYPE Review
PUBLISHED 19 August 2025
DOI 10.3389/fneur.2025.1551682

OPEN ACCESS

EDITED BY
Mingming Lu,
Characteristic Medical Center of Chinese People's Armed Police Force, China

REVIEWED BY
Jiaojiao Li,
Tianjin Medical University Cancer Hospital, China
Jiayi Liu,
Capital Medical University, China

*CORRESPONDENCE
FanYin Meng
mfy19760727@163.com
Li Meng
qh_mengli@126.com

†These authors have contributed equally to this work and share first authorship

‡These authors have contributed equally to this work

RECEIVED 26 December 2024
ACCEPTED 04 August 2025
PUBLISHED 19 August 2025

CITATION
Chen L, Guo Q, Zhao J, Bao H, Meng F and Meng L (2025) Evaluation of risk factors for acute stroke using combined CTA and MR HR-VWI imaging.
Front. Neurol. 16:1551682.
doi: 10.3389/fneur.2025.1551682

Evaluation of risk factors for acute stroke using combined CTA and MR HR-VWI imaging

Lin Chen[1†], Qian Guo[1†], JiXiu Zhao[1], Haihua Bao[1], FanYin Meng[2*‡] and Li Meng[1*‡]

[1]Department of Medical Imaging Center, Affiliated Hospital of Qinghai University, Xining, Qinghai, China, [2]Department of Radiology, The First Medical Center, Chinese PLA General Hospital, Beijing, China

Objective: To investigate the correlation between the changes of peripheral carotid fat density (PFD), the occurrence of acute cerebral ischemia events and the characteristics of different dangerous plaques.

Methods: A retrospective analysis was performed on patients diagnosed with carotid plaque by head and neck CTA in the Affiliated Hospital of Qinghai University from January 2021 to March 2023. All patients received head magnetic plain scan, DWI and high resolution vascular wall imaging (MR HR-VWI). According to DWI images, the patients were divided into acute cerebral infarction group and non-acute cerebral infarction group, and the clinical data, CT features and PFD differences between the two groups were compared. Logistic regression analysis was used to adjust for confounding factors and calculate OR values. ROC curves were used to evaluate the predictive efficacy of symptomatic PFD, contralateral PFD and differential PFD for symptomatic and non-symptomatic carotid plaque. According to the CTA and MR HR-VWI, the patients were further divided into groups (calcification and non-calcification, ulcer and non-ulcer, intra-plaque bleeding and non-plaque bleeding, thin or broken fibrous cap and non-thin or broken fibrous cap, large lipid core and non-large lipid core). Multifactor linear regression equation was used to compare the differences of symptomatic side PFD, contralateral PFD and differential PFD among different groups, and to analyze the correlation between PFD and different plaque components. A retrospective analysis was conducted on patients diagnosed with carotid atherosclerotic plaques via head and neck CTA at Qinghai University Affiliated Hospital between January 2021 and March 2023. All patients underwent non-contrast brain MRI with diffusion-weighted imaging (DWI) and high-resolution vessel wall imaging (MR HR-VWI).

Results: (1) Clinical and Imaging Features: The acute stroke group demonstrated significantly elevated systolic (159.2 ± 28.35 vs. 143 ± 25.54 mmHg, $p = 0.019$) and diastolic blood pressures (93.67 ± 15.75 vs. 84.60 ± 13.21 mmHg, $p = 0.016$) compared to the non-acute group. Additionally, the acute stroke group exhibited greater plaque thickness (4.4 ± 1.4 vs. 2.9 ± 0.9 mm, $p < 0.001$), higher prevalence of severe stenosis (45.8% vs. 4.0%, $p = 0.001$), and more frequent ulcerated or irregular plaque surfaces (29.2% vs. 8.0%, $p = 0.038$). (2)Predictive Efficacy of PFD: In predictive analyses, symptomatic-side PFD showed superior performance in identifying acute ischemic events (AUC = 0.762, 95% CI: 0.653–0.870) compared to contralateral PFD (AUC = 0.672) and ΔPFD (AUC = 0.660). (3)Association with Plaque Components: Multivariate regression analysis revealed significant associations between symptomatic-side PFD and key plaque characteristics: intraplaque hemorrhage (IPH; $\beta = 0.367$, $p < 0.001$), lipid-rich necrotic core (LRNC; $\beta = 0.190$, $p = 0.046$), and plaque thickness

(β = 0.225, p = 0.027). Notably, IPH exhibited the strongest correlation with PFD values among all evaluated components.

Conclusion: Carotid perivascular fat density (PFD) can be used as a potential imaging marker to evaluate the characteristics of local vascular inflammation and high-risk plaques, providing a new direction for the early diagnosis and targeted therapy of acute cerebral ischemic events.

KEYWORDS

carotid artery, periarterial fat, stroke, dangerous patches, inflammatory index

1 Background

Stroke is a significant global health issue, characterized by high incidence, mortality, and disability rates, with a rising prevalence and a trend toward younger age groups (1–3). In China, stroke is one of the main causes of death, of which ischemic stroke accounts for the majority, and about 1/4 ischemic stroke is closely related to carotid atherosclerosis (4).

Carotid atherosclerotic plaque is the key pathological basis of stroke. Early studies focused on the degree of arterial lumen stenosis, but in recent years, studies have gradually turned to the analysis of the composition and characteristics of vulnerable plaques. Vulnerable plaques are mainly manifested as thin or ruptured fiber caps, large lipid cores, intra-plaque bleeding (IPH), plaque ulceration, inflammatory response, and neovascularization (5). The presence of these high-risk features greatly increases the likelihood of plaque rupture and stroke. Therefore, accurate identification and evaluation of these dangerous plaque components is of great clinical significance for the prevention of stroke.

Among them, inflammation plays a key role in the formation and progression of vulnerable plaques. However, compared with other plaque features, inflammation has become a research and clinical diagnosis challenge because it is difficult to be visually detected by traditional imaging methods. In recent years, detection of fluorine-18 markers based on positron emission tomography (PET-CT) has been used to assess intravascular inflammation, but its high cost and complexity have limited widespread application.

With advances in imaging technology, the coronary perivascular fat attenuation index (FAD) has emerged as a novel non-invasive biomarker for evaluating vascular inflammation (6, 7). Studies have shown that perivascular adipose tissue (PVAT) exhibits paracrine and bidirectional interactions with the vascular wall (8). During vascular inflammation, the physiological state of PVAT changes, resulting in reduced fat content and increased CT attenuation values.

Research on carotid perivascular fat density (PFD) remains limited. Some studies suggest a close association between PFD and vulnerable plaque characteristics. For example, Zhang et al. reported significantly higher PFD in patients with IPH compared to those without IPH (9). Another study indicated that PFD was elevated in patients with acute ischemic stroke, with higher values observed on the infarction side compared to the contralateral side, suggesting that changes in PFD may reflect active local inflammation (10). Despite these findings, the relationship between PFD and specific vulnerable plaque components has not been thoroughly explored, emphasizing the need for further investigation in this area.

This study aims to investigate the association between perivascular fat density (PFD) of the carotid artery and different vulnerable plaque characteristics by evaluating PFD. Its significance lies in providing a novel noninvasive imaging biomarker for early stroke warning and personalized treatment. Conventional imaging modalities are limited in directly assessing plaque inflammatory activity, whereas PFD quantifies density changes in perivascular adipose tissue to indirectly reflect the degree of local inflammation. The findings are expected to offer new insights into the in-depth research on the pathological mechanisms of carotid atherosclerosis and the development of related diagnostic and therapeutic strategies.

2 Materials and methods

2.1 General information

This study employed a retrospective analysis of data from patients diagnosed with carotid atherosclerotic plaques via head and neck CTA at Qinghai University Affiliated Hospital between January 2021 and March 2023. All patients underwent non-contrast brain MRI, diffusion-weighted imaging (DWI), and high-resolution vessel wall imaging (MR HR-VWI) after hospital admission. Ethical approval was obtained from the hospital's ethics committee, and since imaging examinations were part of routine clinical diagnostics, separate informed consent was not required.

Inclusion Criteri: Patients were included if they met both of the following conditions: (1) the time interval between head and neck CTA, MR HR-VWI, and non-contrast brain MRI examinations did not exceed 2 weeks; and (2) demonstrated carotid plaque thickness exceeding 1.5 mm on imaging.

Exclusion Criteria: Participants were excluded for any of the following reasons: (1) presence of non-atherosclerotic vascular pathologies including aneurysms or vasculitis; (2) acquisition of poor-quality CT or MRI images precluding accurate analysis; (3) previous history of carotid interventions such as stenting or endarterectomy; or (4) advanced age or physical conditions contraindicating imaging procedures.

Data Collection: Comprehensive clinical and laboratory data were systematically collected, encompassing demographic characteristics (gender, age), medical history (hypertension, diabetes, coronary artery disease), lifestyle factors (smoking status, alcohol use), and lipid profiles (total cholesterol, triglycerides, high-density lipoprotein, low-density lipoprotein). All clinical data were obtained within a two-week window surrounding the imaging studies to ensure temporal relevance.

Definitions: Symptomatic carotid artery: The carotid artery on the same side as an acute ischemic lesion in the internal carotid artery territory, as identified on DWI, or the artery associated with neurological symptoms (9).

Contralateral carotid artery: The carotid artery on the opposite side of the symptomatic carotid artery.

2.2 Imaging protocols

2.2.1 CTA imaging protocol

All examinations were performed using a 256-slice Revolution CT scanner (GE Healthcare) in spiral scanning mode, with coverage extending from the aortic arch to the cranial vault. A bolus of 60–80 mL iodinated contrast agent (Omnipaque-350; GE Healthcare) was administered intravenously at 4 mL/s, followed by a 40 mL saline flush using a power injector, with scan initiation triggered automatically 5 s after reaching an attenuation threshold of 100 HU in the aortic arch. Standard acquisition parameters included: tube voltage 100 kV, pitch 1.0, reconstruction slice thickness 0.5 mm, slice spacing 0.5 mm, and rotation time 350 ms. The effective dose (ED) was calculated as ED = DLP × K, where K represents the radiation conversion factor (0.0023 $mSv \cdot mGy^{-1} \cdot cm^{-1}$) for adult head and neck examinations.

2.2.2 High-resolution HR-VWI imaging protocol

All MR examinations were performed using 3.0 T scanners (Philips Healthcare Discovery 750 W and GE Healthcare systems). The standardized imaging protocol comprised two-dimensional time-of-flight (TOF), coronal three-dimensional T1-weighted imaging (CORONAL-3D T1WI), axial T1WI, axial T2WI, contrast-enhanced magnetic resonance angiography (CE-MRA), and contrast-enhanced three-dimensional T1-weighted imaging (CE-3D T1WI) sequences. For contrast-enhanced studies, gadopentetate dimeglumine (Gd-DTPA) was administered intravenously at a dose of 0.2 mmol/kg body weight, injected at 2.5 mL/s using a high-pressure injector (Ulrich, Germany).

2.2.3 Brain MRI + DWI

All brain MRI examinations were conducted using a Siemens Prisma 3.0 T scanner following standard diffusion-weighted imaging (DWI) protocols. The imaging protocol included four essential sequences: (1) axial T1-weighted imaging (T1WI) with TR/TE = 150/2.5 ms, (2) axial T2-weighted imaging (T2WI) with TR/TE = 5000/117 ms, (3) T2 FLAIR with TR/TE = 8000/81 ms, and (4) diffusion-weighted imaging (DWI) with b-value = 1,000 s/mm^2 and TR/TE = 3230/65 ms. All sequences shared consistent geometric parameters: field of view (FOV) 230 × 160 mm and slice thickness 5.0 mm.

2.3 Carotid perivascular fat density measurement

The PFD measurement method was based on established coronary artery fat measurement techniques, combined with semi-automated segmentation to determine perivascular fat density along the vascular narrowing region.

Definition: PFD was quantified by adjusting the technical parameters on the perivascular fat attenuation histogram within the range of −190 to −30 HU, with all fat density measurements reported in Hounsfield Units (HU), See Figure 1.

Procedure: Quantitative image analysis was performed using dedicated vascular imaging software (Shukun, version 6.21.730.3) for automated delineation of regions of interest (ROIs) and subsequent computational analysis. The perivascular fat density (PFD) difference (ΔPFD) was calculated by subtracting contralateral-side PFD values from symptomatic-side PFD values (ΔPFD = PFDsymptomatic–PFDcontralateral), with all measurements generated through the software's automated quantification algorithm.

2.4 Image interpretation

All images were independently reviewed by two radiologists with over 5 years of experience in carotid plaque analysis. In case of disagreement, a consensus was reached through discussion.

Stenosis Degree: Evaluated according to the NASCET (North American Symptomatic Carotid Endarterectomy Trial) standards (10).

The hallmark features of vulnerable plaques include: intraplaque hemorrhage (IPH), a thin or disrupted fibrous cap (<65 μm), an extensive lipid-rich necrotic core (>40% of plaque volume), prominent inflammatory cell infiltration (predominantly macrophages and T-lymphocytes), and pathological calcification patterns (particularly microcalcifications; Figure 2).

2.5 Statistical methods

Data analysis was performed using SPSS 25.0 software, with the following methods:

Continuous variables were first tested for normality using the Shapiro–Wilk test. Normally distributed data were presented as mean ± standard deviation (mean±SD), with between-group comparisons

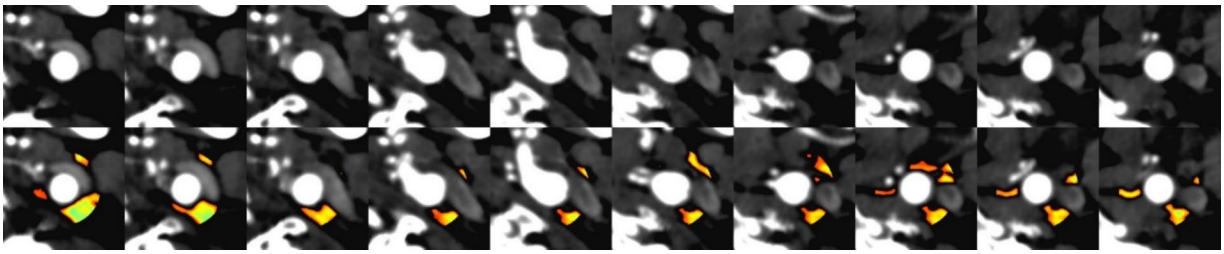

FIGURE 1
Comparison of CT angiography (CTA) imaging and automated perivascular fat density extraction: **(A)** Upper row: Conventional CTA cross-sectional images. **(B)** Lower row: Corresponding images with automated fat density extraction, where color-coded regions indicate perivascular adipose tissue (PVAT) distribution.

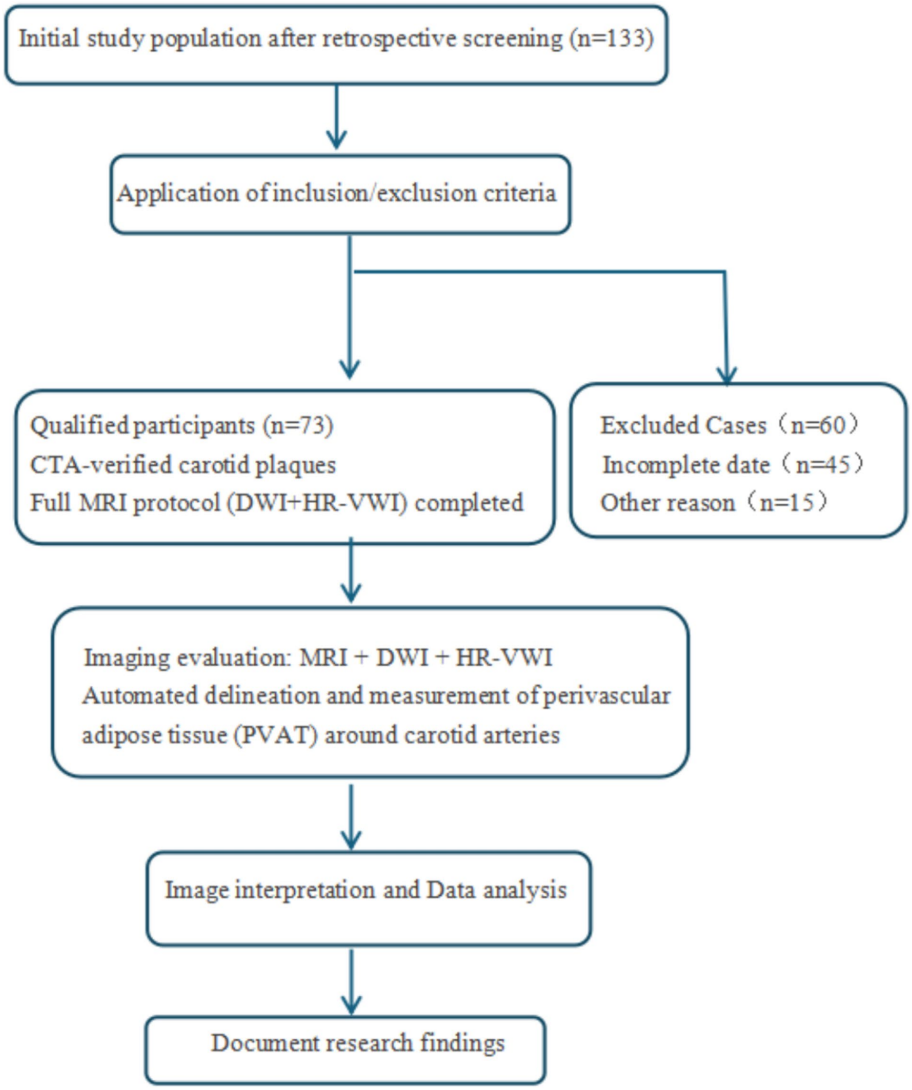

FIGURE 2
Flowchart.

performed using independent samples t-tests. Non-normally distributed data were expressed as median (interquartile range), with between-group comparisons analyzed using the Mann–Whitney U test. Paired data comparisons employed paired t-tests, For non-normally distributed paired data, the Wilcoxon signed-rank test will be used.

Categorical variables were presented as counts (percentages), with between-group differences evaluated using chi-square tests.

The following regression models were applied: (1) binary logistic regression to analyze the relationships between symptomatic-side PFD, contralateral-side PFD, ΔPFD and acute ischemic events; (2) multiple linear regression to examine associations between symptomatic-side PFD (dependent variable) and plaque characteristics (independent variables). The statistical significance level was set at $p < 0.05$.

Diagnostic performance of PFD measures was evaluated through receiver operating characteristic (ROC) curve analysis, calculating the area under the curve (AUC) and determining optimal cutoff values.

3 Results

3.1 General characteristics comparison

A total of 73 patients were included in the study, with an average age of 61 ± 12.5 years. Among them, 51 were male (69.9%) and 58 were of Han ethnicity (79.5%). The prevalence of hypertension, dyslipidemia, diabetes, and smoking was 69.9, 45.2, 27.4, and 41.1%, respectively (Table 1).

3.2 Comparison of clinical, CTA features, and carotid PFD between acute and non-acute ischemic stroke groups

Among the 73 cases, there were 48 patients with acute cerebral infarction and 25 with non-acute cerebral infarction.

The non-acute ischemic stroke group, the acute ischemic stroke group exhibited:

The acute ischemic stroke group demonstrated significantly elevated systolic blood pressure (159.2 ± 28.35 vs. 143 ± 25.54 mmHg, $p = 0.019$) and diastolic blood pressure (93.67 ± 15.75 vs. 84.60 ± 13.21 mmHg, $p = 0.016$) compared to the non-acute group. Additionally, plaque thickness was markedly greater in the acute group (4.4 ± 1.4 vs. 2.9 ± 0.9 mm, $p < 0.001$), with a higher prevalence of severe stenosis (45.8% vs. 4.0%, $p = 0.001$) and plaque surface ulceration/irregularity (29.2% vs. 8.0%, $p = 0.038$). However, no significant differences were observed in plaque length ($p = 0.067$) or calcification ($p = 0.516$) between the two groups (Table 2).

In patients with acute ischemic stroke, the symptomatic-side PFD, contralateral carotid PFD, and △PFD (HU) were (−53.63 ± 11.04) HU, (−77.16 ± 10.64) HU, and (23.53 ± 10.71) HU, respectively. In non-acute ischemic stroke patients, the symptomatic-side PFD, contralateral carotid PFD, and △PFD (HU) were (−65.40 ± 10.80) HU, (−83.08 ± 9.94) HU, and (17.68 ± 7.28) HU, respectively. The differences between the two groups were statistically significant ($p < 0.05$; see Table 2).

3.3 Perivascular fat density (PFD) comparison of symptomatic versus contralateral carotid arteries in all patients

Within the same patient, symptomatic-side PFD (−57.66 ± 12.25 HU) was significantly higher than contralateral-side PFD (−79.19 ± 10.72 HU), with an average ΔPFD of 21.53 ± 10.02 HU ($p < 0.001$; Table 3).

3.4 Comparison of PFD at different degrees of stenosis and PFD of different plaque compositions

In the study, 50 patients (68.5%) had mild-to-moderate stenosis, and 23 patients (31.5%) had severe stenosis. The symptomatic-side PFD was higher in the severe stenosis group (−50.66 ± 10.36 HU) than in the mild-to-moderate stenosis group (−60.88 ± 11.78 HU, $p = 0.001$; Table 4).

Based on plaque composition, all patients were divided into calcified and non-calcified groups, IPH and non-IPH groups, TRFC and non-TRFC groups, and LRNC and non-LRNC groups. Statistically significant differences were found between the IPH and non-IPH groups, as well as between the TRNC and non-TRNC groups ($p < 0.05$). However, no statistical differences were observed between the calcified and non-calcified groups, or between the ulcerated and non-ulcerated groups (Table 4).

3.5 Binary logistic regression analysis of risk factors for acute ischemic stroke

Symptomatic-side PFD, contralateral PFD, and ΔPFD were all significantly associated with acute ischemic events ($p < 0.05$). After adjusting for systolic blood pressure, diastolic blood pressure, antihypertensive medication use, plaque thickness, and stenosis degree, symptomatic-side PFD remained predictive (OR = 0.919, $p = 0.044$; Table 5).

TABLE 1 Clinical characteristics of the study population.

Characteristic	Value (Mean ± SD) or n (%)
Age (years)	61 ± 12.5
Gender (Male)	51 (69.9)
Ethnicity (Han)	58 (79.5)
History of Hypertension	51 (69.9)
Systolic Blood Pressure (mmHg)	153.68 ± 28.33
Diastolic Blood Pressure (mmHg)	90.56 ± 15.45
History of Dyslipidemia	33 (45.2)
Total Cholesterol (mmol/L)	4.06 ± 1.15
Triglycerides (mmol/L)	1.64 ± 0.87
High-Density Lipoprotein (HDL; mmol/L)	0.96 ± 0.24
Low-Density Lipoprotein (LDL; mmol/L)	2.53 ± 0.92
History of Diabetes	20 (27.4)
History of Coronary Artery Disease	2 (2.7)
History of Smoking	30 (41.1)
History of Alcohol Consumption	32 (43.8)

3.5.1 ROC curve analysis of symptomatic-side PFD, contralateral-side PFD, and ΔPFD in predicting acute ischemic stroke

Symptomatic-side PFD, contralateral-side PFD, and ΔPFD all demonstrated certain predictive value for acute ischemic stroke ($p < 0.05$). The predictive efficacy was ranked as follows: symptomatic-side PFD > contralateral-side PFD > ΔPFD. Among these, symptomatic-side PFD had the best predictive ability for acute ischemic stroke, with an area under the curve (AUC) of 0.762 (95% CI: 0.653–0.870; Table 6), and the optimal cutoff value is indicated in Figure 3.

3.6 Multiple linear regression analysis of the relationship between symptomatic-side PFD and different plaque components

A multiple linear regression analysis was performed with symptomatic-side PFD as the dependent variable, and IPH, TRFC, LRNC, plaque thickness, and stenosis degree as independent variables. The results showed that IPH, LRNC, and plaque thickness were significantly associated with symptomatic-side PFD ($p < 0.05$), with IPH being the most significant ($p < 0.001$; Table 7).

4 Discussion

This study investigated the association between perivascular fat density (PFD) and acute cerebral infarction events as well as vulnerable plaque characteristics. The results demonstrated that patients in the acute infarction group exhibited significantly higher PFD values in the symptomatic side, contralateral side, and ΔPFD compared to the non-acute infarction group ($p < 0.05$), consistent with recent findings (11, 27), further confirming that elevated perivascular PFD serves as an important predictor for cardiovascular risk. ROC curve analysis revealed that PFD had good predictive performance for acute cerebral ischemic

TABLE 2 Comparison of clinical, CTA features, and carotid PFD between acute and non-acute ischemic stroke patients.

Parameter	Acute ischemic stroke (n = 48)	Non-acute ischemic stroke (n = 25)	p
Age (years)	63.23 ± 13.08	58.52 ± 10.79	0.127
Gender (Male)	36 (75.0)	15 (60.0)	0.185
Ethnicity (Han)	39 (81.3)	19 (76)	0.598
History of Hypertension	35 (72.9)	15 (60.0)	0.194
Systolic Blood Pressure (mmHg)	159.2 ± 28.35	143 ± 25.54	0.019
Diastolic Blood Pressure (mmHg)	93.67 ± 15.75	84.60 ± 13.21	0.016
History of Dyslipidemia	29 (60.4)	14 (56.0)	0.453
Total Cholesterol (mmol/L)	4.11 ± 1.16	3.96 ± 1.56	0.589
Triglycerides (mmol/L)	1.67 ± 0.89	1.61 ± 0.85	0.569
High-Density Lipoprotein (HDL; mmol/L)	0.96 ± 0.23	0.97 ± 0.27	0.872
Low-Density Lipoprotein (LDL; mmol/L)	2.58 ± 0.95	2.42 ± 0.87	0.478
History of Diabetes	13 (27.1)	7 (28.0)	0.934
History of Coronary Artery Disease	2 (4.2)	0 (0.0)	0.301
History of Smoking	18 (37.5)	12 (48.0)	0.387
History of Alcohol Consumption	19 (39.6)	13 (52.0)	0.222
History of Antihypertensive Medication Use	26 (54.17)	7 (28.0)	0.029
History of Antiplatelet Medication Use	3 (6.3)	2 (8.0)	0.562
History of Statin Use	4 (8.3)	2 (8.0)	0.666
Symptomatic-side PFD (HU)	−53.63 ± 11.04	−65.40 ± 10.80	<0.001
Contralateral-side PFD (HU)	−77.16 ± 10.64	−83.08 ± 9.94	0.024
ΔPFD (HU)	23.53 ± 10.71	17.68 ± 7.28	0.017
Plaque Thickness (mm)	4.4 ± 1.4	2.9 ± 0.9	<0.001
Plaque Length (mm)	10.1 ± 5.3	7.8 ± 4.3	0.067
Degree of Stenosis (Severe)	22 (45.8)	1 (4.0)	0.001
Ulceration or Irregular Plaque Surface	14 (29.2)	2 (8.0)	0.038
Calcification	33 (68.8)	19 (76)	0.516

ΔPFD (HU), Symptomatic-side PFD–Contralateral-side PFD.

events, with the symptomatic-side PFD showing optimal predictive efficacy (AUC 0.762, 95% CI 0.653–0.870), indicating potential clinical utility. As a noninvasive imaging biomarker, PFD may play a significant role in assessing vascular inflammation and predicting high-risk plaques, serving as a novel imaging marker for vascular inflammatory activity and vulnerable plaques. This study provides preliminary evidence supporting its application in acute cerebral ischemic events. Future research should focus on: establishing standardized PFD measurement protocols; validating its predictive value through multicenter prospective cohorts; and elucidating the mechanistic relationship between PFD and molecular inflammatory markers - ultimately facilitating clinical translation of this noninvasive parameter for early identification and targeted intervention in high-risk populations.

Additionally, the study found that PFD is closely related to plaque thickness, intraplaque hemorrhage (IPH), and lipid-rich necrotic core (LRNC). Among these, IPH had the most significant effect on PFD ($p < 0.001$), which aligns with findings from Miao Yu and Zhang S (9, 12). This suggests that PFD, as an alternative imaging biomarker for local vascular inflammation and vulnerable plaques, can provide a convenient method for diagnosing and predicting high-risk ischemic events, while also offering new therapeutic targets for clinical interventions (13).

The core mechanism of atherosclerosis is the inflammatory response. The initial injury to the endothelium leads to the accumulation of macrophages and monocytes, forming different types of plaques that subsequently induce lumen narrowing. Excessive narrowing can increase distal circulation pressure and reduce metabolism, resulting in ischemia and hypoxia in brain tissue. The rupture of vulnerable plaques can also cause distal infarction.

Recent studies have suggested a bidirectional secretion effect between the vascular wall and the surrounding adipose tissue (perivascular adipose tissue, PVAT), which is considered a key protective factor in the cardiovascular system (14, 15). Inflammation can alter the composition of PVAT from a lipid phase to a water phase, increasing its CT density in the inflammatory vascular areas (16). At the same time, inflammatory factors secreted by PVAT can recruit more inflammatory cells, further exacerbating local inflammation (15). The increase in PVAT density is also independently associated with the progression of the lipid components of coronary atherosclerotic plaques (17), providing theoretical support for its use as an imaging marker.

The composition and stability of carotid plaques directly influence the risk of systemic cardiovascular events (18–20). For example, strong evidence shows that IPH and plaque ulceration are associated with an increased risk of ipsilateral ischemic stroke (19), and the size of LRNC is highly correlated with the risk of ischemic stroke (18). This study found that patients with vulnerable plaque features such as IPH, TRFC (thin or ruptured fibrous cap), and LRNC had significantly higher PFD, further supporting the potential of PFD as a predictive factor for high-risk plaques, consistent with findings from Yu et al. (12).

However, in our study, there was no statistical difference in PFD between calcified and non-calcified plaques. We speculate that this may be related to the grouping, as mixed plaques contain both calcification and other components such as IPH or TRFC. Simply classifying them as calcified and non-calcified could affect the accuracy of the results. Additionally, we believe this may be due to the small sample size and selection bias, which may be addressed in future studies by expanding the sample size and minimizing such biases. Nevertheless, the PFD value in the calcified group was slightly lower than in the non-calcified group, which aligns with previous studies where calcification was considered a protective factor (21, 22). Plaque calcification is closely related to plaque stability and inversely correlated with inflammation (21, 23, 24). Moreover, no significant difference in PFD was found between ulcerated and non-ulcerated plaques, consistent with Zhang S's

TABLE 3 Comparison of symptomatic-side PFD and contralateral-side PFD in the same patient.

Symptomatic-side PFD (HU)	Contralateral-side PFD (HU)	Difference (ΔPFD; HU)	Number of cases	*t*	*p*
−57.66 ± 12.25	−79.19 ± 10.72	21.53 ± 10.02	73	18.36	<0.001

TABLE 4 Comparison of PFD at different degrees of stenosis and PFD of different plaque compositions.

Plaque characteristics	Mild-to-moderate stenosis (*n* = 50)	Severe stenosis (*n* = 23)	*p*	Ulcerated group (*n* = 16)	Non-ulcerated group (*n* = 57)	*p*
Symptomatic-side PFD (HU)	−60.88 ± 11.78	−50.66 ± 10.36	0.001	−56.66 ± 9.91	−57.95 ± 12.89	0.713
Contralateral-side PFD (HU)	−80.39 ± 10.71	−76.59 ± 10.50	0.161	−75.76 ± 10.03	−80.15 ± 10.79	0.148
ΔPFD (HU)	19.50 ± 9.38	25.93 ± 10.15	0.010	19.09 ± 11.11	22.21 ± 9.69	0.276
	Calcified group (*n* = 50)	Non-calcified group (*n* = 23)	*p*	TRFC group (*n* = 16)	Non-TRFC group (*n* = 57)	*p*
Symptomatic-side PFD (HU)	−58.44 ± 12	−55.73 ± 12.93	0.395	−51.61 ± 9.95	−59.50 ± 12.36	0.019
Contralateral-side PFD (HU)	−80.23 ± 10.75	−76.61 ± 10.46	0.194	−74.62 ± 8.12	−80.58 ± 11.08	0.044
ΔPFD (HU)	21.79 ± 9.43	20.88 ± 11.57	0.730	−23.01 ± 9.27	21.08 ± 12.36	0.489
	LRNC group (*n* = 22)	Non-LRNC group (*n* = 51)	*p*	IPH group (*n* = 15)	Non-IPH group (*n* = 58)	*p*
Symptomatic-side PFD (HU)	−50.84 ± 11.03	−60.42 ± 11.72	0.002	−43.82 ± 7.58	−61.24 ± 10.58	<0.001
Contralateral-side PFD (HU)	−75.35 ± 8.84	−80.74 ± 11.09	0.051	−69.35 ± 8.05	−81.74 ± 9.86	<0.001
ΔPFD (HU)	24.51 ± 12.56	20.32 ± 8.64	0.172	25.53 ± 12.93	20.49 ± 8.96	0.172

TABLE 5 PFD and acute ischemic event models.

Variables	Model 1		Model 2		Model 3	
	OR(95%CI)	*p*	OR(95%CI)	*p*	OR(95%CI)	*p*
Symptomatic-side PFD	0.895(0.840–0.954)	0.001	0.889(0.831–952)	0.001	0.919(0.846–0.998)	0.044
Contralateral-side PFD	0.947(0.902–995)	0.030	0.950(0.902–1.001)	0.056	0.957(0.897–1.021)	0.185
ΔPFD	0.933(0.879–990)	0.023	0.920(0.862–0.981)	0.012	0.967(0.897–1.043)	0.387

Model 1: Regression analysis of PFD only. Model 2: Adjusted for systolic blood pressure, diastolic blood pressure, and antihypertensive medication use. Model 3: Adjusted for systolic blood pressure, diastolic blood pressure, antihypertensive medication use, plaque thickness, and degree of stenosis.

TABLE 6 Predictive values of symptomatic-side PFD, contralateral PFD, and △PFD for acute cerebral infarction.

Variables	Cut-off value	AUC	95% CI	Sensitivity (SE)	Specificity (SP)
Symptomatic-side PFD	0.449	0.762	0.653 ~ 0.870	0.729	0.64
Contralateral PFD	0.297	0.672	0.545 ~ 0.799	0.417	0.88
△PFD	0.359	0.660	0.535 ~ 0.785	0.419	0.88

Explanation: AUC, Area Under the Curve; 95% CI, 95% Confidence Interval; SE (Sensitivity), The ability to correctly identify positive cases (True Positive Rate); SP (Specificity), The ability to correctly identify negative cases (True Negative Rate).

findings (9), suggesting that the impact of ulceration on PFD might be minor.

Previous studies have indicated that an increase in carotid plaque thickness is closely related to symptomatic disease status (25), with inflammatory stimuli accelerating plaque growth, leading to lumen narrowing and thickening of the vessel wall. In a cross-sectional study involving 1,072 patients with brain ischemia, plaque thickness was found to be a better predictor of ischemic symptoms than stenosis degree (26). Another study pointed out that for every 1 mm increase in soft plaque thickness, the risk of ipsilateral ischemic events increases 3.7 times (95% CI: 1.9–7.2) (22). ROC curve analysis further supports plaque thickness as an important risk predictor, with an AUC of 0.88, a best cutoff value of 2.2 mm, sensitivity of 85%, and specificity of 83%.

4.1 Limitations

Although this study preliminarily validated the value of PFD in assessing vascular local inflammation and predicting acute cerebral ischemic events, there are still some limitations:

1. Retrospective design: The occurrence of future ischemic events cannot be predicted and needs to be verified by

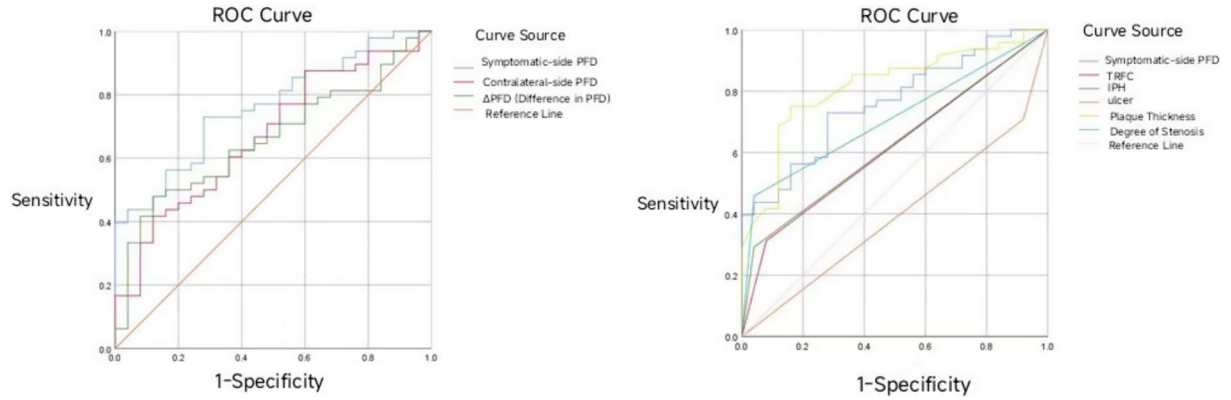

FIGURE 3
ROC curve of symptomatic-side PFD, contralateral-side PFD, and ΔPFD in predicting acute ischemic stroke.

TABLE 7 Multivariate linear regression analysis of the relationship between symptomatic side PFD and different plaque components.

Variable	B	*β*	*t*	*p*	95% CI	
					Lower limit	Upper limit
Plaque thickness	19.035	0.225	2.259	0.027	2.215	35.854
TRFC (Thin, Ruptured Fibrous Cap)	4.708	0.164	1.817	0.074	−0.463	9.879
IPH (Intraplaque Hemorrhage)	11.054	0.367	3.710	<0.001	5.107	17.001
LRNC (Lipohyalinosis)	5.102	0.190	2.034	0.046	0.095	10.109
Degree of stenosis	4.385	0.167	1.731	0.088	−0.672	9.441

prospective studies with larger sample sizes and longer follow-up periods.

2. Small sample size: There may be bias in the group results, especially in the comparison of calcified and non-calcified plaques.
3. Limitations of measurement methods: The measurement of PFD may be affected by differences in placement of ROI. This study used a coronary approach based. Although this study provides preliminary evidence for the value of PFD in assessing local vascular inflammation and predicting acute cerebral ischemic events, it has several limitations.

Author contributions

LC: Writing – original draft, Investigation. QG: Writing – original draft. JZ: Investigation, Writing – original draft. HB: Writing – review & editing. FM: Writing – review & editing. LM: Writing – review & editing.

Funding

The author(s) declare that financial support was received for the research and/or publication of this article. Qinghai Province 2023 "Kunlun Elite" Talent Program of Qinghai Province (Official Document No.: Qing Ren Cai Zi [2024] No. 1); China Red Cross Foundation Yingrui Northwest Public Welfare Program 2021 "ICON Research Fund" Sponsorship Agreement under the Yingrui Northwest Public Welfare Program, China Red Cross Foundation (Contract Archive No.: 2021-1135). All funding was allocated from the research accounts of Dr. Meng Li.

Conflict of interest

The authors declare that the research was conducted in the absence of any commercial or financial relationships that could be construed as a potential conflict of interest.

Generative AI statement

The author(s) declare that no Gen AI was used in the creation of this manuscript.

Any alternative text (alt text) provided alongside figures in this article has been generated by Frontiers with the support of artificial intelligence and reasonable efforts have been made to ensure accuracy, including review by the authors wherever possible. If you identify any issues, please contact us.

Publisher's note

References

1. Zhang DH, Jin JL, Zhu CF, Chen QY, He XW. Association between carotid artery perivascular fat density and cerebral small vessel disease. *Aging (Albany NY)*. (2021) 13:18839–51. doi: 10.18632/aging.203327

2. Saba L, Loewe C, Weikert T. State-of-the-art CT and MR imaging and assessment of atherosclerotic carotid artery disease: standardization of scanning protocols and measurements-a consensus document by the European Society of Cardiovascular Radiology (ESCR). *Eur Radiol*. (2023) 33:1063–87. doi: 10.1007/s00330-022-09024-7

3. Song P, Fang Z, Wang H, Cai Y, Rahimi K, Zhu Y, et al. Global and regional prevalence, burden, and risk factors for carotid atherosclerosis: a systematic review, meta-analysis, and modelling study. *Lancet Glob Health*. (2020) 8:e721–9. doi: 10.1016/S2214-109X(20)30117-0

4. Baradaran H, Gupta A. Carotid vessel wall imaging on CTA. *AJNR Am J Neuroradiol*. (2020) 41:380–6. doi: 10.3174/ajnr.A6403

5. McNally JS, McLaughlin MS, Hinckley PJ, Treiman SM, Stoddard GJ, Parker DL, et al. Intraluminal thrombus, intraplaque hemorrhage, plaque thickness, and current smoking optimally predict carotid stroke. *Stroke*. (2015) 46:84–90. doi: 10.1161/STROKEAHA.114.006286

6. Oikonomou EK, Marwan M, Desai MY, Mancio J, Alashi A, Hutt Centeno E, et al. Non-invasive detection of coronary inflammation using computed tomography and prediction of residual cardiovascular risk (the CRISP CT study): a post-hoc analysis of prospective outcome data. *Lancet*. (2018) 392:929–39. doi: 10.1016/S0140-6736(18)31114-0

7. Hengen PN. Methods and reagents. Is there any sense in antisense terminology? *Trends Biochem Sci*. (1996) 21:153–4.

8. Lee R, Margaritis M, Channon KM, Antoniades C. Evaluating oxidative stress in human cardiovascular disease: methodological aspects and considerations. *Curr Med Chem*. (2012) 19:2504–20. doi: 10.2174/092986712800493057

9. Zhang S, Gu H, Yu X, Kang B, Yuan X, Wang X. Association between carotid artery perivascular fat density and intraplaque hemorrhage. *Front Cardiovasc Med*. (2021) 8:735794. doi: 10.3389/fcvm.2021.735794

10. Barnett HJM, Taylor DW, Haynes RB, Sackett DL, Peerless SJ, Ferguson GG, et al. Beneficial effect of carotid endarterectomy in symptomatic patients with high-grade carotid stenosis. *N Engl J Med*. (1991) 325:445–453.

11. Yu M, Meng YK, Xu HB. Association between perivascular fat density and acute ischemic stroke events. *J Clin Radiol*. (2023) 42:910–4.

12. Yu M, Meng Y, Zhang H, Wang W, Qiu S, Wang B, et al. Associations between pericarotid fat density and image-based risk characteristics of carotid plaque. *Eur J Radiol*. (2022) 153:110364. doi: 10.1016/j.ejrad.2022.110364

13. Antoniades C, Tousoulis D, Vavlukis M, Fleming I, Duncker DJ, Eringa E, et al. Perivascular adipose tissue as a source of therapeutic targets and clinical biomarkers. *Eur Heart J*. (2023) 44:3827–44. doi: 10.1093/eurheartj/ehad484

14. Tong Y, Zuo Z, Li X, Li M, Wang Z, Guo X, et al. Protective role of perivascular adipose tissue in the cardiovascular system. *Front Endocrinol (Lausanne)*. (2023) 14:1296778. doi: 10.3389/fendo.2023.1296778

15. Margaritis M, Antonopoulos AS, Digby J, Lee R, Reilly S, Coutinho P, et al. Interactions between vascular wall and perivascular adipose tissue reveal novel roles for adiponectin in the regulation of endothelial nitric oxide synthase function in human vessels. *Circulation*. (2013) 127:2209–21. doi: 10.1161/CIRCULATIONAHA.112.001133

16. Antoniades C, Kotanidis CP, Berman DS. State-of-the-art review article. Atherosclerosis affecting fat: what can we learn by imaging perivascular adipose tissue? *J Cardiovasc Comput Tomogr*. (2019) 13:288–96. doi: 10.1016/j.jcct.2019.03.006

17. Lee SE, Sung JM, Andreini D, Al-Mallah MH, Budoff MJ, Cademartiri F, et al. Association between changes in perivascular adipose tissue density and plaque progression. *JACC Cardiovasc Imaging*. (2022) 15:1760–7. doi: 10.1016/j.jcmg.2022.04.016

18. Sun J, Zhao XQ, Balu N. Carotid plaque lipid content and fibrous cap status predict systemic CV outcomes: the MRI substudy in AIM-HIGH. *JACC Cardiovasc Imaging*. (2017) 10:241–9. doi: 10.1016/j.jcmg.2016.06.017

19. van Dam-Nolen D, Truijman M, van der Kolk AG. Carotid plaque characteristics predict recurrent ischemic stroke and TIA: the PARISK (plaque at RISK) study. *JACC Cardiovasc Imaging*. (2022) 15:1715–26. doi: 10.1016/j.jcmg.2022.04.003

20. Kolodgie FD, Yahagi K, Mori H, Romero ME, Trout HH 3rd, Finn AV, et al. High-risk carotid plaque: lessons learned from histopathology. *Semin Vasc Surg*. (2017) 30:31–43. doi: 10.1053/j.semvascsurg.2017.04.008

21. Nandalur KR, Baskurt E, Hagspiel KD, Phillips CD, Kramer CM. Calcified carotid atherosclerotic plaque is associated less with ischemic symptoms than is noncalcified plaque on MDCT. *AJR Am J Roentgenol*. (2005) 184:295–8. doi: 10.2214/ajr.184.1.01840295

22. Gupta A, Mtui EE, Baradaran H, Salama G, Pandya A, Kamel H, et al. CT angiographic features of symptom-producing plaque in moderate-grade carotid artery stenosis. *AJNR Am J Neuroradiol*. (2015) 36:349–54. doi: 10.3174/ajnr.A4098

23. Shaalan WE, Cheng H, Gewertz B, McKinsey JF, Schwartz LB, Katz D, et al. Degree of carotid plaque calcification in relation to symptomatic outcome and plaque inflammation. *J Vasc Surg*. (2004) 40:262–9. doi: 10.1016/j.jvs.2004.04.025

24. Wahlgren CM, Zheng W, Shaalan W, Tang J, Bassiouny HS. Human carotid plaque calcification and vulnerability. Relationship between degree of plaque calcification, fibrous cap inflammatory gene expression and symptomatology. *Cerebrovasc Dis*. (2009) 27:193–200. doi: 10.1159/000189204

25. Gupta A, Baradaran H, Kamel H, Pandya A, Mangla A, Dunning A, et al. Evaluation of computed tomography angiography plaque thickness measurements in high-grade carotid artery stenosis. *Stroke*. (2014) 45:740–5. doi: 10.1161/STROKEAHA.113.003882

26. Saba L, Saam T, Jager HR. Imaging biomarkers of vulnerable carotid plaques for stroke risk prediction and their potential clinical implications. *Lancet Neurol*. (2019) 18:559–72. doi: 10.1016/S1474-4422(19)30035-3

27. Antonopoulos AS, Sanna F, Sabharwal N, Thomas S, Oikonomou EK, Herdman L, et al. Detecting human coronary inflammation by imaging perivascular fat. *Sci Transl Med*. (2017) 9:eaal2658 [pii]. doi: 10.1126/scitranslmed.aal2658

Frontiers in Neurology

Explores neurological illness to improve patient care

The third most-cited clinical neurology journal explores the diagnosis, causes, treatment, and public health aspects of neurological illnesses. Its ultimate aim is to inform improvements in patient care.

Discover the latest Research Topics

See more →

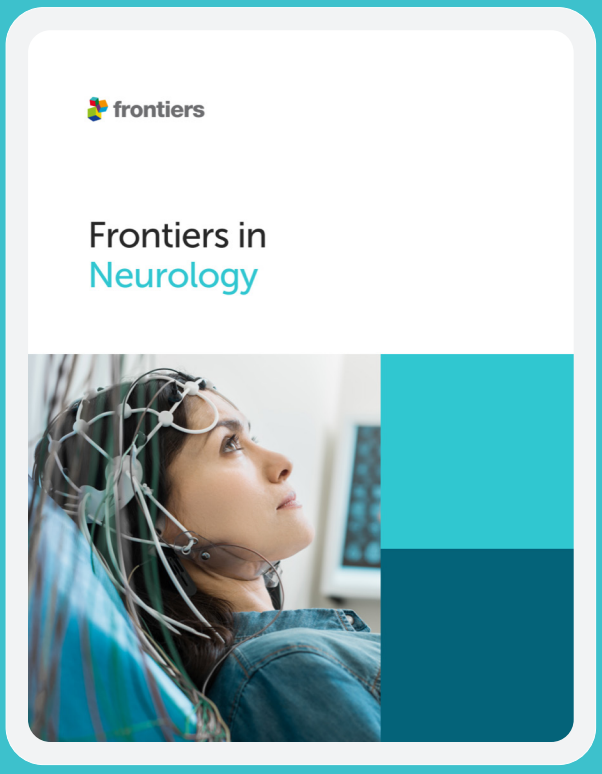

Frontiers

Avenue du Tribunal-Fédéral 34
1005 Lausanne, Switzerland
frontiersin.org

Contact us

+41 (0)21 510 17 00
frontiersin.org/about/contact